Aston University

Some pages of this thesis may have been removed for copyright restrictions.

If you have discovered material in AURA which is unlawful e.g. breaches copyright, (either yours or that of a third party) or any other law, including but not limited to those relating to patent, trademark, confidentiality, data protection, obscenity, defamation, libel, then please read our Takedown Policy and contact the service immediately

ULTRASONIC INSPECTION OF AUSTENITIC STAINLESS STEEL WELDMENTS

BY

PLATON ATHANASIOU KAPRANOS

DOCTOR OF PHILOSOPHY

THE UNIVERSITY OF ASTON IN BIRMINGHAM

MAY 1982

TITLE : ULTRASONIC INSPECTION OF AUSTENITIC STAINLESS STEEL WELDMENTS

NAME : Platon Athanasiou Kapranos

DEGREE: Doctor of Philosophy

YEAR : 1982

SUMMARY

Ultrasonic waves interact in a complex manner with the metallurgical structure of austenitic weldments resulting in ambiguity when interpreting reflections and at times in misinterpretation of defect positions.

In this work, current knowledge of the structure of austenitic welds is outlined, and the influence of this structure on the propagation of ultrasonic waves is reviewed.

Using an established and highly accurate technique, data on velocity variations as a function of the angle between the direction of soundwave propagation and the axes of preferred grain orientation existing in such welds, are experimentally obtained. These results and existing theory are used to provide quantitative evidence of (i) anisotropy factors in austenitic welds, (ii) beam skewing effects for different wave modes and polarizations, and (iii) the extent of acoustic impedance mismatch between parent and weld metals.

The existence of "false" indications is demonstrated, and suggestions are made into their nature.

The effectiveness of conventional transverse wave techniques for inspecting artificial and real defects existing in austenitic weldments is experimentally investigated, the limitations are demonstrated, and possible solutions are proposed. The possibilities offered by the use of longitudinal angle probes for ultrasonic inspection of real and artificial defects existing in austenitic weldments are experimentally investigated, and parameters such as probe angle, frequency and scanning position are evaluated.

Detailed work has been carried out on the interaction of ultrasound with fatigue and corrosion-fatigue cracks in the weld metal and the heat affected zones (HAZs) of 316 and 347 types of austenitic weldments, together with the influence of elastic compressive stresses, defect topography and defect geometry.

Practical applications of all results are discussed, and more effective means of ultrasonic inspection of austenitic weldments are suggested.

KEY WORDS : ULTRASONIC INSPECTION, LONGITUDINAL & TRANSVERSE WAVES, AUSTENITIC WELDMENTS

ACKNOWLEDGEMENTS

I would like to thank my father for providing financial support throughout my student years, and especially during the period of this research work.

I would like to extend my gratitude to Mr. V. N. Whittaker for his supervision and support at all times during this work.

The constructive discussions of Dr. J.F.W. Bell, and the interpretation of the SAECPs by Dr. W.B. Hutchinson, are gratefully acnowledged.

Thanks are also due to B.S. Gray of Risley Nuclear Power Development Laboratories, UKAEA, B.J. Lack of NEI-John Thompson Ltd., and Mr.T. Wagg of the CEGB, for providing the austenitic weldments used in this study.

I am also indebted to all personnel of the Metallurgy Department that have been involved at various stages and extents in this work ; to name but a few : Mr. P. Cox, Mr. J. Foden, Mr. E. Watson, and Mr. S. Witherington of the Dept. of Production Engineering.

Thanks are finally due to Dr. R. Halmshaw of the British Journal of NDT, and Dr. J. Blitz of Nondestructive Testing Communications for accepting various parts of this work for publication in their respective Journals.

The kind permission of J. Maybury of Wells Krautkrämer for the use of specialized equipment on a free of charge loan is gratefully acknowledged.

The assistance of the personnel of the Department of Electrical and Electronic Engineering during the joint effort described in sections 4.2 and 4.3.2, is also acknowledged.

CONTENTS

LIST OF FIGURES

LIST OF TABLES

1. INTRODUCTION

Austenitic stainless steel is an essential construction material and finds use because of its corrosion resistance and ability to withstand both high and low temperatures. These types of steel are employed for nuclear reactor vessels and in the chemical industry when the nature of the contents and reaction conditions demand the corrosion resistance and high temperature mechanical properties offered by austenitic stainless steels. At the other end of the scale, austenitic steel, because it is free of the ductile-to-brittle transition in toughness observed in ferritic steels at low temperatures, is employed in liquid gas handling and storage.

Austenitic stainless steel has found several critical applications in the nuclear industry. For example, the main vessel and most of the internal structure of Liquid Metal Fast Breeder Reactors (LMFBR) are constructed from materials such as 316 and 304 type austenitic steels. The thick piping in the Pressurized Water Reactor (PWR), and centifugal castings in the Boiling Water Reactor (BWR) are also of austenitic stainless steel.

Although these materials are inherently ductile and the stresses involved are low, reducing therefore the risks of structural failure, the consequences of failure are so severe particularly from the safety point of view, that inspection requirements are extremely demanding.

Until recently, radiography was the traditional method of detecting flaws inside metallic components; but even if a flaw was detected, its depth within the component and its dimensions parallel to the radiation path were unknown. These are essential pieces of information needed for a fracture mechanics assessment of the flaw's significance. The ability of ultrasonics to detect and locate defects in metallic components has resulted in this NDT technique being favoured. Furthermore, the potential to size defects with sufficient accuracy to permit a safety analysis based on fracture mechanics to be made, is an invaluable asset of the ultrasonic technique.

The ability of ultrasonic methods to characterize flaws has satisfied the need to discriminate between possibly insignificant defects (slag, inclusions, porosity), and potentially hazardous defects (cracks, lack of fusion) for most structural steels. However, steels with welded or cast structures are notorious for the high and variable scatter they produce, with the result that satisfactory inspection by ultrasonic methods is difficult to achieve.

This difficulty has been so pronounced in austenitic stainless steel cast components and welds, that their ultrasonic inspection has been recognized as a major NDT problem for some time. These materials exhibit markedly differing elastic properties along different crystallographic directions, so changes in grain orientation can result in variations in the

ultrasonic velocity, in the direction of propagation, in the refraction of the ultrasonic beam within grains, and in mode conversion at grain boundaries.

In austenitic welds there exists, due to epitaxial growth, a pronounced degree of grain alignment. Ultrasonic inspection of such welds is particularly difficult because of the strong attenuation and scattering of the ultrasonic beam, and the presence of large numbers of spurious signals in the A-scan data. The elastic anisotropy of this structure results in velocity variations depending on the angle of propagation direction relative to the direction of the preferred orientation of the austenitic grains existing in the weld metal. These variations appear to affect significantly the attenuation of ultrasound and depend on the propagation direction and wave mode. Due to the cyclic velocity variations observed, ultrasonic waves propagating in anisotropic austenitic weld metal, exhibit skewing or deviation from the expected wave normal direction. This effect is dependent on the angle of propagation relative to the columnar grains and can cause beam spreading or beam focusing. Grain boundary scattering is strongly dependent on the ratio D/λ of the mean grain diameter to the ultrasonic wavelength in the direction of propagation. Thus in general one would expect longitudinal waves to suffer less attenuation than transverse waves of the same frequency, due to the larger wavelength of the former.

In the light of the above problems associated with ultrasonic inspection of cast and welded austenitic structures, it is not surprising that conventional ultrasonic methods are difficult to apply.

A substantial number of papers have been published on the ultrasonic testing of these structures, but different opinions have been expressed on the effectiveness of ultrasonic examination. While the problems themselves are well documented, there has been little progress in determining in detail which aspects of these structures are responsible for the anomalies. Until the fundamental aspects of ultrasonic propagation in austenitic structures are properly understood, we can do no more than devise inspection techniques empirically. The inherent danger in such approach is that a satisfactory technique on one structure may fail completely on an apparently identical structure.

In this work, the evidence leading to our present understanding of the austenitic weld is outlined, and the consequences for ultrasonic propagation are reviewed. Using a novel technique, data on the velocity variation as a function of the angle between the direction of soundwave propagation and the axis of preferred grain orientation are experimentally obtained. These results are used in accordance with current theory in order to provide quantitative evidence on such anisotropy factors in austenitic welds, as skewing angle for different wave modes and polarizations, and the extent of the impedance

mismatch between parent plate and weld metal. The advantages and disadvantages of different wave modes, frequencies, angles, and scanning positions are demonstrated, and experimental comparisons between these variables are obtained. The interaction of ultrasound with real defects existing in a variety of austenitic weld configurations is experimentally investigated, together with the effects of compressive stresses, defect topography and defect geometry. As a result of the comprehensive test programme just completed, it is hoped that more effective ultrasonic inspection of austenitic weldments can be carried out, and that our understanding of the fundamental aspects of ultrasound propagation in austenitic weldments has been increased.

2. LITERATURE SURVEY

2.1 The Purpose of Non-Destructive Testing (NDT)

Simply stated, NDT methods are devoted to the detection of defects in material which, by their nature, might be expected to lead to an ultimate loss of function of the material or the component made from it.
Such defects include surface and subsurface cracks, inclusions, pores, delaminated or debonded regions in composites, incompletely joined regions in welds or other joints and, generally, any macro or microstructural anomaly which does not belong where it is found.
It is obviously desirable to do this in such a way as to allow a part to be used or to be restored to use undamaged by the inspection process.

2.2 NDT in the Context of Fracture Mechanics

Fracture mechanics makes an initial assumption which might horify many of us. The assumption is that flaws always exist in metals, plastics, composites or natural materials which may eventually lead to failure by growth to a critical, self-propagating size.
If, generally speaking, we define a "flaw" as an inhomogeneity, a discontinuity or a local singularity, NDT should be able to detect the presence of a flaw with complete reliability and possibly locate it geometrically and quantify it.

Fracture mechanics should be able to assess when this flaw may be technically considered as a "defect" and should indicate corrective actions, when required.

Fracture mechanics concepts allow calculations of critical sizes of cracks to be made as a function of the crack depth, the active stress intensity and stress system, and such properties of a material as its elastic modulus, its yield strength, and its fracture toughness.

The "fracture toughness" is a parameter that emerged from fracture mechanics considerations and relates in a quantitative way to the relative ability of stressed materials to resist fracture in the presence of a flaw of some given size. Thus a flawed material of high fracture toughness will operate safely at stress levels which would produce fracture in material of lower fracture toughness containing identical (sized) flaws at the same stress levels.

Fortunately most commonly used structural steels have a fracture toughness which is so large that it is difficult to measure accurately. The interrelation of fracture toughness, flaw size, yield strength and other material and shape parameters is well described in the literature [1,2,3].

The evolution of the concepts of stress intensity and fracture toughness from elasticity theory, stress concentration by shaped holes and the Griffith crack theory is neatly described in textbooks such as Knott [4]. The equations of Griffith, Inglis and Orowan all suggest that the critical

stress required to propagate a crack depends on $\sqrt{c}$ where (c) is the flaw size. These ideas were extended by Irwin [5], where once again the local stress near the root of a crack depended on the nominal stress (σ) and the $\sqrt{c}$, where here (c) is the half-flaw length. He defined the stress intensity factor :

$$k = \sigma\sqrt{\pi c}$$

for a sharp elastic crack in an infinite (wide) plate.
The central ideas behind all of this are:

(i) Flaws which act as sharp cracks (elastic discontinuities) exist in all materials and structures. These may be, as stated earlier, actual cracks, surface or sub-surface, inclusions, pores, second phase particles, etc.

(ii) The stress intensity (k), rises as the local stress (σ) rises, at a rate depending on $\sqrt{c}$ and form factors until either a critical value (k_c) is reached which spreads the crack, or the material yields if it is ductile. If yielding is restrained by elastic stresses due to the system geometry, brittle crack growth will result.

This produces a set of permissible stress levels, since $(k) \longrightarrow (k_c)$ as (σ) increases producing the schematic relation between stress, flaw size and fracture toughness shown in Figure 2.1.

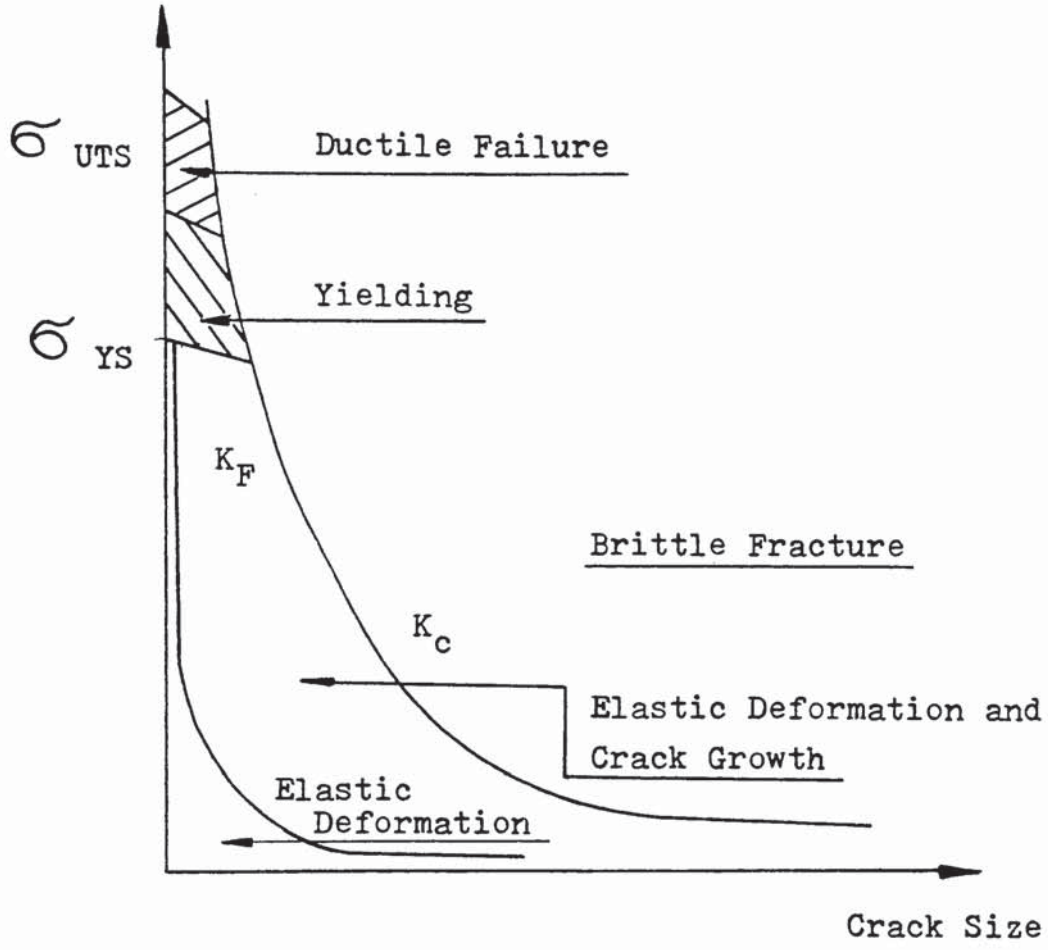

FIG. 2.1: Dependence of mechanical behaviour on crack size

All combinations of stress and flaw size in the safe zone fail to exceed a critical stress intensity level to extend the crack and thus the material does not fracture. It may yield or creep however. It should be noted that the stress intensity increases with flaw size at a given stress, and that a flaw size exists below which for a given stress (σ) the material will not fracture. Anything causing this crack to grow with time, will ultimately produce fracture when the crack reaches the size critical for this stress level.

The most important idea emphasized here is the dependence of stress intensity on flaw size. Since (k) increases as (c) increases, (Δk) will increase as the fatigue crack grows producing a corresponding increase in crack growth rate. Fatigue cracks must therefore be expected to be growing at accelerating rates. Early detection is therefore extremely important.

It is instructive to compare critical crack lengths with the detection capabilities of inspection methods. Should a crack become critical in size at a value below the detection limit, the inspection will be of no utility. If the stress level cannot be lowered, either the material or the inspection procedure must be changed.

It is now even more obvious that while sub-critically sized cracks are tolerable, they can grow with time in a dynamically stressed environment, and once critical in size can produce

catastrophic failure. So far as ultrasonic testing is concerned, the absence of sufficient experimental data results in specifications defining rather arbitrarily two or three severity classes. The class is defined in the technical specification and the criteria to apply relate to:

(a) the amplitude of the echo from the defect or the ratio of this amplitude to the amplitude of the reference echo,

(b) the nature of the defect (volumetric or non-volumetric),

(c) the decision to take (accept the defect, repair it, or reject the item).

For a steel of very high tensile strength, a critical defect size (around 1.5 mm) cannot be detected with certainty by ordinary ultrasonic testing techniques and this is a most disquieting situation. However, it is probably possible to develop suitable industrial NDT techniques using appropriately specialised ultrasonic probes. In the case of rotors of lower tensile strength ($\simeq$500-600 Nmm^{-2}), the critical dimensions of a defect amount to several centimetres and so it is possible to detect these defects when they are still small compared to the critical size and to monitor their growth with time; hence action can be taken before the rotor reaches a dangerous state. In the case of nuclear reactor vessels, such action is being taken at present.

Certain vessels are examined in-service with ordinary or focused probes which are scanned and calibrated automatically in the zones under observation. In some instances the data from successive tests are fed to a computer which classifies and interprets them.(6,7,8). If a defect can be correctly followed by ultrasonics, better surveillance will be possible and experimental evidence on the critical dimensions of defects will be obtainable.

It may be said in conclusion that ultrasonics has facilitated great progress in the construction of structures free from defects, or at least from detectable defects. Such testing is costly and must be undertaken by knowledgable personnel well trained in its application and interpretation. To expect that the NDT specialists alone could cover the complete spectrum of capabilities would be misleading and dangerous. It is clear that it is necessary to determine the definition of the maximum initial defect permitting the expected service life to be achieved, but this determination is very complex and requires close and continuous cooperation between stress engineers, fracture mechanics specialists, experts in materials technology, experimental laboratory experts and finally NDT specialists.

NDT is a link in a chain of actions and decisions and it is well known that a chain can accomplish its function only when all the links show complete integrity.

The integrated result of all the previously mentioned specialist activities will lead eventually to a sound NDT programme which must be carefully managed and continuously kept up to date.

2.3 Austenitic Stainless Steels

The austenitic stainless steel group, of which the 18/8 type is clearly the best known, is more widely used than either the martensitic or ferritic groups.

Its nickel content, which may vary from around the 7% level to as high as 20% (even more for special purposes) stabilises the austenite over a wide temperature range, and this in turn increases the corrosion resistance and provides the non-magnetic characteristics. One of the features of these austenitic grades is their superior weldability when compared with the other two grades[9]. Another advantage of these steels is their remarkably good properties at both ends of the temperature scale; a characteristic which has lead to their use in the hottest zones of power boilers and in cryogenic applications at sub-zero temperatures[10].

The common austenitic grades including type 304 and 316, stabilised versions -types 321,347 and 320- and the extra low carbon variants such as type 304L and 316L, are all readily available, which is often an important factor governing choice.

The atmospheric corrosion resistance of austenitic stainless

steels is unequalled by most other engineering materials. In rural or industrial atmospheres free from chlorides or sulphurous contaminants, grades such as type 304 can give a long service. Where slightly more aggressive media are concerned, molybdenum additions as in type 316 provide greater resistance to corrosion and should be used in heavily polluted or marine atmospheres.

Austenitic grades offer improved strength combined with oxidation resistance and at temperatures up to about 650-700 ^{o}C they are widely used in boiler applications.

The austenitic grades are considered the most weldable of the high alloy steels. Welding of most grades is straight forward provided that consumables giving deposits resistant to micro-fissuring (usually with a small amount of ferrite) are used for joints made under restraint[11].

Pre-heating of austenitic stainless steels is not helpful in general, because no structural changes, such as martensite formation, occur in the weld or the heat affected zones[11].

Heat treatment after welding is the oldest means of avoiding intergranular corrosion in the sensitized zones of welded austenitic stainless steels[12]. Customary treatment consists of a "solution" anneal which involves heating the weldment to a temperature high enough to dissolve any intergranular carbides and to restore the vital chromium to the depleted boundary areas. Disadvantages of the annealing treatment are

the high temperature required, the distortion that occurs in heating and the problems associated with the quenching operation. It is unlikely that gross defects will be encountered in plate material after manufacturers' quality control procedures have been applied.

The two most frequently encountered forms of cracking observed to occur in welded austenitic stainless steels are :

1. In the weld metal immediately following its completion,

2. In the parent metal near a weld joint[13].

Weld metal cracking in austenitic stainless steels can be separated into four types :

(i) crater cracks,

(ii) hot cracks,

(iii) star cracks, and

(iv) root cracks.

All four types of cracking are believed to be manifestations of the same basic kind of cracking; namely, "hot cracking" or, when present in its earliest stage "micro-fissuring".

Hot cracking and microfissuring gave much difficulty some years ago, but today enough is known about this form of cracking to avoid its occurence in weldments. Parent metal heat affected zone (HAZ) cracking in welded austenitic stainless steels was not recognised as a potential problem until the introduction of :

a) heavier sections, and or

b) more elaborately alloyed types of steels.

Briefly, research has shown austenitic parent metal when arc-welded to be susceptible to at least two cracking mechanisms :

(i) an intergranular form of hot shortness that occurs in the heat affected zones during welding[14], whereupon the cracking occurs because of grain-boundary segregation, or embrittlement, and

(ii) a complex phenomenon involving strain-induced precipitation in the heat affected zone during postweld heat treatment, or service at elevated temperature, wherein a change in mechanical properties results in stress-rupture failure under certain conditions[15,16].

Some difficulty has been reported with parent metal heat affected zone cracking in light sections, but only in the very complex-alloyed austenitic stainless steels[17].

The occurence of welder-induced defects, such as lack of fusion and lack of penetration, slag inclusions, and bead shape defects, applies to all materials and is well documented[18].

Defects of greater consequence are service defects :

(1) Weld decay, may occur under certain conditions, but is now not a common occurence.
Weld decay occurs when an unstabilised austenitic stainless steel containing more than 0.03 % carbon level is welded.

(2) Stress corrosion cracking, may occur in aggressive environments containing anions like Cl^- , and in sensitised structures which provide a pre-existing active path (e.g. weld heat affected zones).
The residual stresses due to welding may contribute to this.

(3) Fatigue cracks, may propagate under variable loading from stress raisers, such as , design notches, weld decay cracks, and stress corrosion cracks.

(4) Defect occurence, due to microstructural changes caused by high temperature service conditions. Delta-ferrite in weld metal accelerates these changes by providing a nucleation site, thus altering detrimentally the properties of the material and increasing susceptibility to defect occurence.
Considerations for this problem are taken into account in the design stage[19].

Fortunately, austenitic stainless steels possess high fracture toughness. Considering a pressure vessel made by such material and under steady loading conditions, the critical flaw size will in most cases be larger than a through crack in the wall of the vessel. Therefore such vessels could be designed on a "leak before break" philosophy, and Non Destructive Testing requirements will not be stringent.
Where small flaws can be enlarged by modes of failure such as fatigue, creep or stress corrosion, the NDT requirements will obviously become more critical and the size of flaws to be located will depend on the operating conditions.

2.4 In-Service Inspection of Nuclear Reactors

Ultrasonic methods of non-destructive inspection are used widely in the nuclear reactor field, where a real concern for safety exists.

Inspection procedures are applied at many stages of reactor development- when materials are selected, while the components are being fabricated, and after the elements have been in service.

Years of development and experience have produced reliable inspection methods for use during fabrication of certain components used in nuclear plants. However, after a reactor goes into service, several of these methods are no longer useful. Access to many areas of the reactor is difficult. Radiation levels prevent an individual's remaining in an area for an extended length of time, and thus remote methods of inspection are preferred.

Codes in the nuclear industry call for volumetric examination of a large percentage of the components of nuclear power plants. This means that a penetrating form of energy is required. Only two nondestructive methods are capable of practical examination of thick steel structures. These are radiography and ultrasonics. Until recent years, the traditional method of detecting flaws in metallic components was

radiography. Although radiography has proved to be a very useful quality control method, it suffers the drawback that a narrow crack will not be detected unless it is both straight and parallel to the radiation beam, in order that the contrast relative to the unflawed region is maximised. Even if the crack is detected, its depth within the component and its dimensions parallel to the radiation path are unknown. This information is essential for a fracture mechanics assessment of the crack's significance. Ultrasonic testing suffers from none of these limitations, and automatically operating ultrasonic systems have and are being developed facilitating remote inspection.

The problem is not exactly and completely solved however, because the materials used in certain components of the reactor cause scattering of ultrasonic waves generated by conventional inspection equipment. Problems exist in the use of ultrasonics even when the energy is coupled through somewhat ideal surface material such as the outer shell of the reactor vessel. In tests during fabrication of certain reactor vessels[20], inspection has been performed through cladding at normal inspection frequencies of 2.25 MHz. The cladding was weld-deposited stainless steel, and longitudinal waves at 2.25 MHz might be expected to penetrate the cladding satisfactorily. Shear waves of 2.25 MHz, using a standard 45 degree angle probe, have resulted in cracks being found during inspection from the cladding side. However, the wavelength of shear

waves, at the same frequency, in steel is approximately half of the longitudinal waves, and scattering is so excessive that the gain of the instrument must be increased by an order of magnitude above what might be considered normal; i.e. the gain setting increased to 10 times the calibration sensitivity. This practice would not be acceptable in a remote, automatic device and more reliable means of inspection should be developed.

Certain components of the reactor system are especially difficult to inspect ultrasonically. For instance, cast austenitic stainless steel pump valve bodies and thick austenitic welded components, consisting of large grain structures that are impervious to the ultrasonic energy of conventional nondestructive testing methods.

In spite of the difficulties, the development of nuclear power plants for supplying electrical power to the public is proceeding, and inspection methods must be improved to meet the demands of the codes. Certain areas can be inspected by present methods if means of access for the inspection devices can be provided.

Perhaps means of controlling grain size can be incorporated during fabrication to provide easier transmission of ultrasonic energy in those components that presently are uninspectable. If this is impractical, then lower frequency methods based upon changes in propagation characteristics indicative of developing damage may be adequate. Of course

the latter approach would probably not give the resolution and sensitivity to defects afforded by conventional methods.

2.5 Ultrasonic Inspection of Austenitic Stainless Steel Weldments

2.5.1 Outlining the Main Difficulties

Austenitic steels have become increasingly important in the last few years in the construction of power stations, particularly atomic power stations. Nondestructive evaluation plays a major role in achieving a high level of reliability for a nuclear reactor power system. For this reason, continued effort has been directed towards the development of equipment, methods, and techniques for the inspection of components throughout the life of a nuclear plant.
Ultrasonic examination of austenitic stainless steel welds is an indispensable tool for in-service work required on nuclear reactorpressure vessels, because this technique is presently the only one which is applied for the volumetric inspection of critical components in hostile radioactive environments, as has already been mentioned.
However, the methods of examination as practised on ordinary carbon steel welds are not directly applicable to welds in austenitic stainless steel, for in these welds, the microstructure dominates the wave propagation response[21,22].

When producing stainless steels, the initial austenitic phase is preserved in grains which grow along the heat dissipation lines, up to an apreciable size -several centimeters in heavy castings. Depending upon the mechanical work done on these steels, the cast structure can remain or be refined to an extent which makes the grain quite fine. In welds a similar process is observed. Even in multipass welds, the grain can be very large due to epitaxial growth between passes and usually no refinment treatment is possible. The solidification process during welding initially produces a columnar grain structure in each weld bead. Grains grow along the maximum thermal gradients in the bead along the <100> crystallographic axis[22]. Growth in this particular direction is faster than in other directions and this leads to the rapid disappearance of unfavourably oriented grains. Deposition of subsequent weld metal reheats the bead and, although in the case of a ferritic weld the columnar grain structure partially is destroyed by the austenite-ferrite phase transformation that occurs as the solid cools, no such transition occurs in the austenitic alloys considered, and consequently the columnar grain structure survives. Furthermore, each new weld bead remelts the surface of the preceding beads and the new grains grow epitaxially on the existing ones. Consequently, elongated grains can be produced as shown in Figure 2.2 ; this shows a macro-section of a single-V weldment, 25 mm thick, made by the M.M.A. process using 347

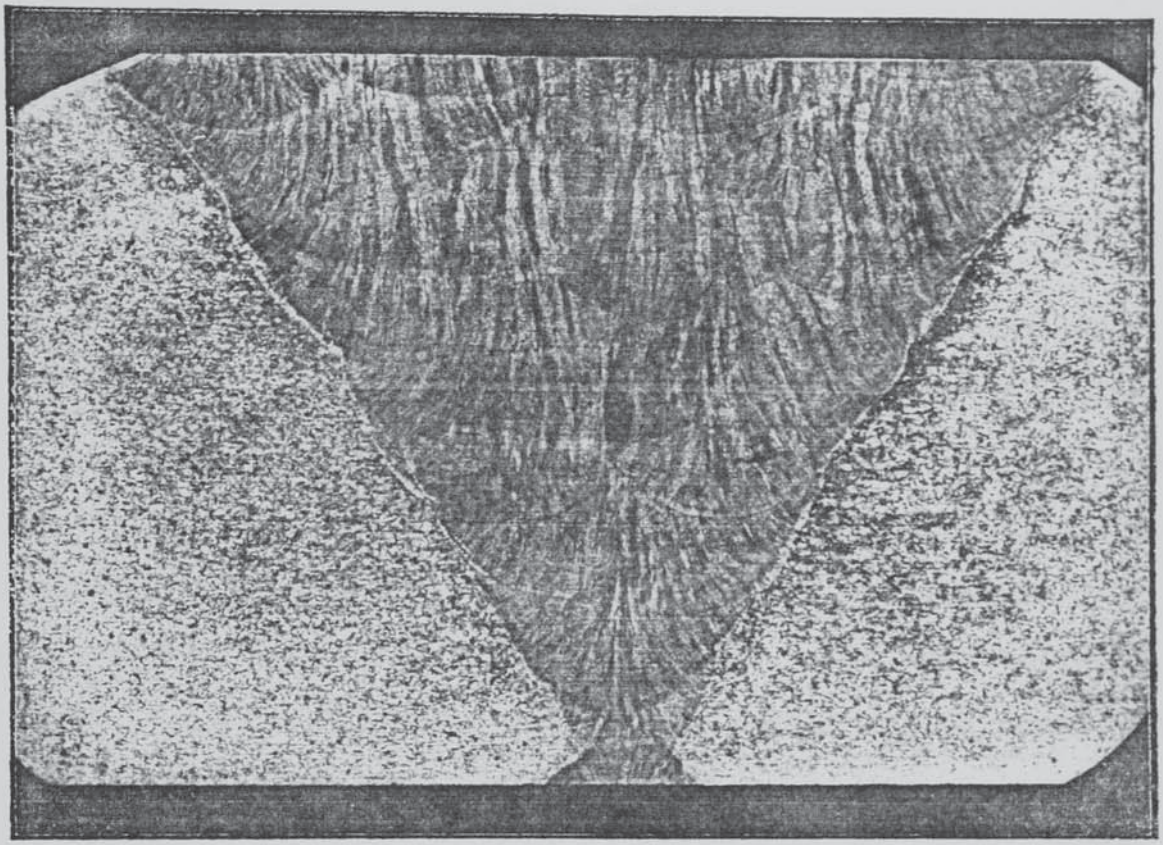

FIG. 2.2 : Single-V weldment, made by MMA process, etched in Ferric Chloride (25 mm thick), showing long columnar grains extending through successive weld runs

Nicrex NDR electrodes. This coarse and anisotropic structure of the austenitic weld metal, presents a number of difficulties to ultrasonic examination, the two most serious of these being the high level of spurious signals and the severe attenuation.

2.5.2 Effects of the Austenitic Weld Structure on Ultrasound

The Selected Area Electron Channelling Patterns technique (SAECPs) used to determine the crystallographic orientation of the austenitic weld metal (viz. Section 3.4), showed that it contained long columnar grains with a major axis along a $\langle 100 \rangle$ crystallographic direction, with near random alignment in the plane of the specimen. This substantial degree of grain alignment results in a weld region consisting of material which is anisotropic in its elastic properties and in which the laws governing the ultrasonic propagation in isotropic materials break down.

In such cases the velocity and attenuation of ultrasonic waves propagated in the material will depend on the direction of propagation relative to the crystallographic preferred orientation. The velocity of longitudinal waves propagated along the axis of preferred orientation differs from that measured perpendicular to the axis and from the velocity in an isotropic aggregate. Similarly, the velocity of ultrasonic transverse waves depends not only on the direction of propa-

gation but also on the polarization of the transverse vibration with respect to the axis of preferential grain alignment. The magnitude of the deviations is a function of the inherent aeolotropy of the grains themselves.
One of the most interesting observations is that of Baikie et al[21], which shows that the orientation of the ultrasonic beam with regard to the grain axes is extremely important in governing attenuation. Tomlinson et al[22], and Kupperman et al[23] have also come to the same conclusion; all these researchers are in agreement that minimum attenuation occurs at approximately 45° to the fibre axis and maxima occur at 0° and 90°. They also observed that velocity is a maximum in the region of 45° to the grain axes, with minima existing parallel and perpendicular to the grain axes. The range of velocities observed by Baikie et al, was from around 5,350 m/s (at 0°) to 6,050 m/s (at approx. 45°). Using the usual notations for crystallographic axes, the velocities in the major directions may be quoted as follows:

Direction	Longitudinal Wave Velocity
<100>	$(C_{11}/\rho)^{\frac{1}{2}}$
<110>	$\left[(1/2\rho)(C_{11}+C_{12}+2C_{44})\right]^{\frac{1}{2}}$
<111>	$\left[(1/3\rho)(C_{11}+2C_{12}+4C_{44})\right]^{\frac{1}{2}}$

where ρ = density of the material in (Kgm^{-3}).

If reasonable values for the elastic constants C_{11}, C_{12} and C_{44} for austenite are substituted in these expressions, variations of velocity around the values observed by Baikie et al may be predicted.

The degree of elastic anisotropy can be expressed quantitatively in terms of a parameter (A) related to the elastic constants through the relation :

$$A = 2C_{44} / (C_{11} - C_{12})$$

It can be seen that for isotropic materials (i.e. A = 1) $C_{11} - C_{12} = 2C_{44}$, and if this relationship is substituted into the velocity expressions given above, they are all reduced to the same value. This is the condition for elastic isotropy, i.e. constant velocity in all directions. The anisotropy factor (A) will provide a good estimate for the extent of velocity variations to be expected in austenitic weld metal.

Methods of determining the effective elastic constants of polycrystalline materials possessing preferred orientation are suggested by Bradfield[24].

The effect of anisotropy, appart from the anomalous refraction or skewing of ultrasonic rays, and velocity variations with preferred orientation direction[25,26], is to produce birefringence. By analogy with the stress dependence of optical wave velocities in solids, commonly known as the photoelastic effect, the phenomenon of ultrasonic wave

velocity variation in anisotropic solids has been called the acoustoelastic effect[27]. However, because both longitudinal and transverse elastic waves can be sustained in solids, the acoustoelastic phenomenon is more complex than the photoelastic effect. With transverse waves, the change in velocity also depends on the angle which the plane of polarization makes with the direction of stress, i.e. if two transverse waves are travelling in the same direction relative to the stress direction with their planes of polarization at different angles, they will travel with different velocities. This is analogous to optical birefringence where the ordinary light and extraordinary light rays travel with their planes of polarization at right angles, and with the velocity of the extraordinary ray depending on its angle to the optical axis of the birefringent crystal. This effect has been shown to be of sufficient magnitude for the experimental measurement of stress using ultrasonic shear waves[27].

It has been shown[27] that alteration of the ultrasonic frequency has no effect on the birefringent properties, provided that the grains of the material are randomly oriented. If, however, preferred orientation is present in a stress free material, the velocity alters linearly with a change in frequency.

Firestone and Frederick[28] have observed ultrasonic double refraction effects in cold rolled steel plates and forged

aluminium blocks. For transverse waves propagated perpendicular to the rolling direction, velocity differences of the order of 1 % were measured between the waves polarized perpendicular and parallel to the rolling axis. Similar effects were observed when shear waves were propagated perpendicular to the forging direction in an aluminium specimen, the faster shear wave being polarized parallel to the forging direction.

Kupperman and Reimann[29] have observed similar effects using 304 and 308 types of austenitic stainless steel weld metals, and Silk[30] as has in 316 austenitic weld metal, concluding that flaw detection in these weld metals may vary not only with the mode but also with polarization when transverse (shear) waves are employed (Figure 2.3).

The relative attenuation of longitudinal and transverse waves depends on the propagation direction, and effective examination of austenitic welds may require application of both wave modes. It has been shown[29,30] that minimum attenuation occurs for horizontally polarized transverse waves (orthogonal polarization to that of conventional transverse waves), suggesting that better inspectability might result from using these waves. Practical difficulties in coupling these shear waves directly into the austenitic welds present a problem, solutions to which have not been found as yet.

A random array of aeolotropic crystallites is essentially isotropic to the passage of an ultrasonic wave, but the

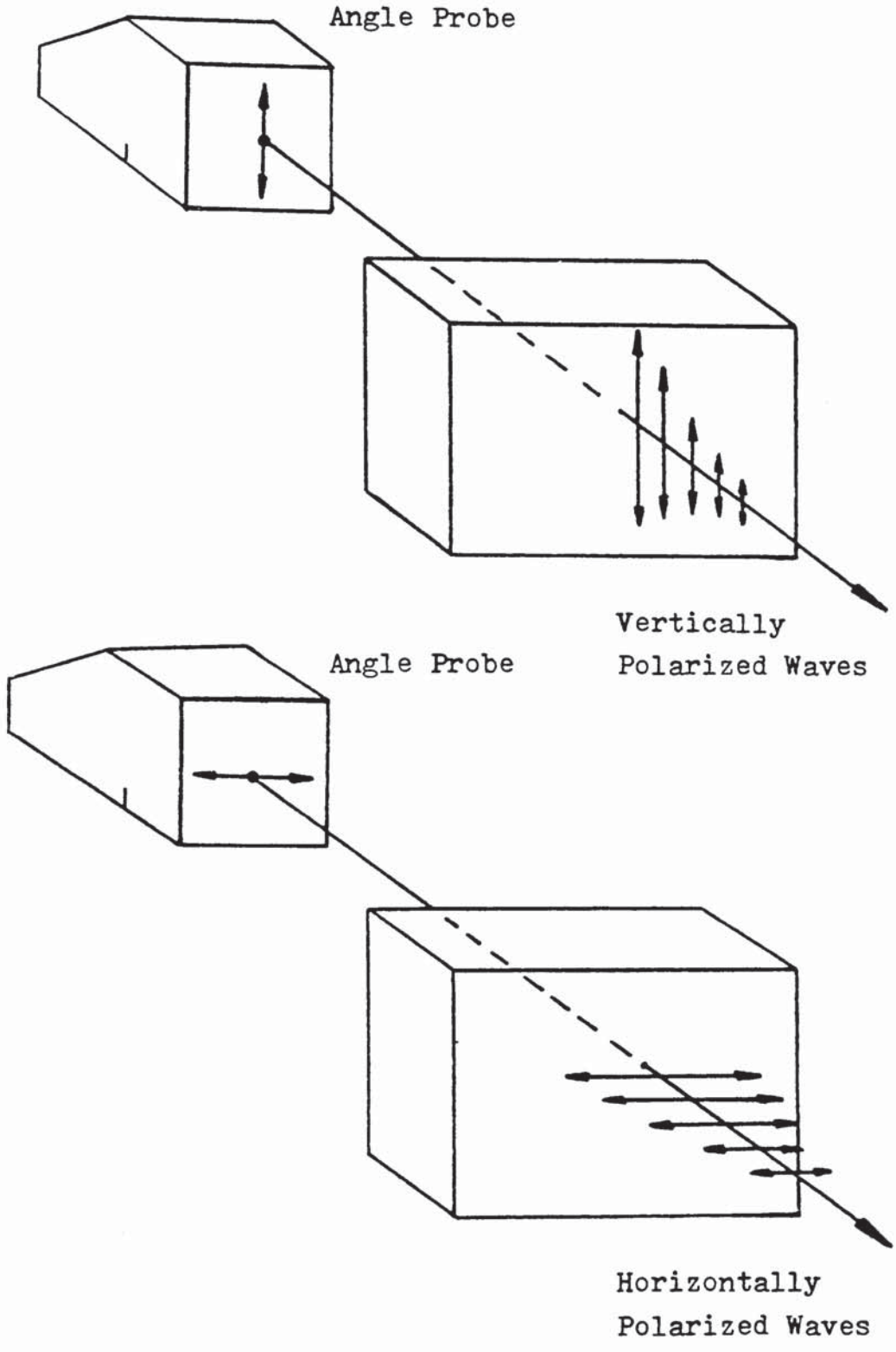

FIG 2.3 : Schematic representation of transverse wave polarization in relation to an angled transducer.

attenuation of the wave depends greatly on the magnitude of the crystallite aeolotropy. If the individual grains of a polycrystalline solid show some degree of alignment, then the bulk elastic properties become anisotropic, and structural features such as texture become the dominating factors of attenuation rather than the actual grain size.

Results by Baikie et al[21] show that attenuation is strongly orientation-dependent in anisotropic austenitic weldments. Minimum attenuation has been found to occur at the region of 45^{o} to the fibre axis, with maxima occuring at 0^{o} and 90^{o}. Results for mild steel have shown that attenuation is maximum when the ultrasonic beam travelled normal to the principal direction of grain flow[31]. This may be explained in terms of the greater number of grain boundaries encountered in such a direction with consequent enhanced scattering.

The existence of a periodic relationship between ultrasound attenuation and orientation of the ultrasonic beam direction with respect to the fibre axis is an experimental observation supported by a wide range of measurements in different austenitic welds[21,29,32]. These attenuation results are difficult to explain using existing theories, because satisfactory theories have been developed only for equiaxed grains and not for highly elongated fibrous structures.

Concluding from the work of these researchers it was found that :

1. -the dependence of the transmitted signal on beam orientation arises as a result of the anisotropy of the assembly of grains and is not related to the composition of the weld metal or the welding position.

2. -the major variation in signal to noise ratio in the austenitic welds arises from variations in signal, not in noise.

3. -with regards to the observation that the attenuation has a minimum value at the 45° direction to the fibre axis and essentially stronger in all other directions, no simplified correlation between velocity and attenuation can be given although the attenuation very often decreases with increasing velocity.

There is agreement between various researchers, that, for transverse waves attenuation is more severe than for longitudinal waves[23,33,34.35,36,37,38]. This result is not unexpected since theories of scattering in equiaxed structures show that when either transverse or longitudinal waves are propagated in a multi-grained material, the bulk of the energy scattered by the grains is in the transverse mode[39]. In fact Papadakis[39], has given formulae showing that the functional dependence of the scattering frequency (f) and the grain diameter (D) varied with the ratio of the wavelength (λ) to the grain diameter in polycrystalline materials as follows:

Type of scattering	Grain size range of behaviour	Functional dependence of scattering
Rayleigh	$D \ll \lambda$	$a = K_1 D^3/\lambda^4$
Stochastic	$\lambda/3 < D < 3\lambda$	$a = K_2 D/\lambda^2$
Diffusive	$D \gg \lambda$	$a = K_3 1/D$

where K_1, K_2 and K_3 are constants dependent on the anisotropy of the material.

Considering that the ultrasonic velocity of shear waves is approximately half of that of longitudinal waves, for any given frequency, the wavelength will also be halved. Furthermore, considering the following formulae quoted from reference (39) :

Attenuation Neper/unit length	Cubic Crystals	
	Rayleigh Scattering	Stochastic Scattering
Longitudinal waves (a_L)	$\frac{8\pi^3 \mu^2 T f^4}{375 \rho^2 V_L^3} \left\{ \frac{2}{V_L^5} + \frac{2}{V_T^5} \right\}$	$\frac{16\pi^2 \mu^2 D f^2}{525 V_L^6 \rho^2}$
Transverse waves (a_T)	$\frac{2\pi^3 \mu^2 T f^4}{125 \rho^2 V_T^3} \left\{ \frac{2}{V_L^5} + \frac{3}{V_T^5} \right\}$	$\frac{4\pi^2 \mu^2 D f^2}{210 V_T^6 \rho^2}$

where :

μ = $C_{11} - C_{12} - 2C_{44}$ (C_{ij} being the elastic **modulii** of the cubic crystallites)

T = Average crystallite volume

f = Frequency

ρ = Density

V_L = Longitudinal ultrasonic velocity

V_T = Transverse ultrasonic velocity,

it can be seen that a higher attenuation will result at a given frequency, for transverse than for longitudinal waves, e.g. for 2 MHz frequency, Rayleigh scattering is approximatelly six times more for transverse waves, and stochastic scattering is approximatelly thirtysix times more for transverse than for longitudinal waves.

The advantages of using low frequency longitudinal waves under conditions where the Rayleigh and Stochastic scattering exists are very apparent, because the frequency affects the scattering by its fourth and second power respectivelly.

Another generally accepted difficulty is the high level of spurious indications occuring in ultrasonic examination of austenitic weldments. The austenitic weld metal gives rise to local variations of the ultrasonic velocity and as a result distorts the beam geometry[33,36,37,38,40,41,42,43,44,45] and at times the fibrous grains in the welds seem to act as acoustic fibres, guiding the waves according to privileged paths[42,44].

Although the possibility of a "channelling" effect cannot be ignored, the unusual beam behaviour encountered could possibly be explained by the fact that in an anisotropic medium the direction of propagation is not, in general, normal to the wavefront and deviates by an angle (Δ). The magnitude of this deviation (skewing) has been calculated by Tomlinson et al[22] as a function of beam orientation to the grain axes. This beam skewing taking place in austenitic welds can give rise to false indications, because if a short-cut path is taken by the waves when the beam is believed to have taken the path of an ordinary angled beam, this would result in a false indication, since the apparent depth of the reflector would locate it within the weld deposit, see Figure 2.4.

On occasions, indications that soundbeams were divided into two separate components in austenitic welds have been reported [22,38,40,42,46], and also refraction of the ultrasonic beam at the parent/weld metal interface, causing serious errors in predicting the location of ultrasonic echoes[33, 38 46]. The occasional splitting of ultrasonic beams propagating through austenitic weld metal could be attributed to mode conversion and to the fact that in anisotropic media, the variation of elastic constants with direction gives rise to birefringence (double refraction), that is, the formation of two waves of the same mode and frequency but which travel at different velocities.

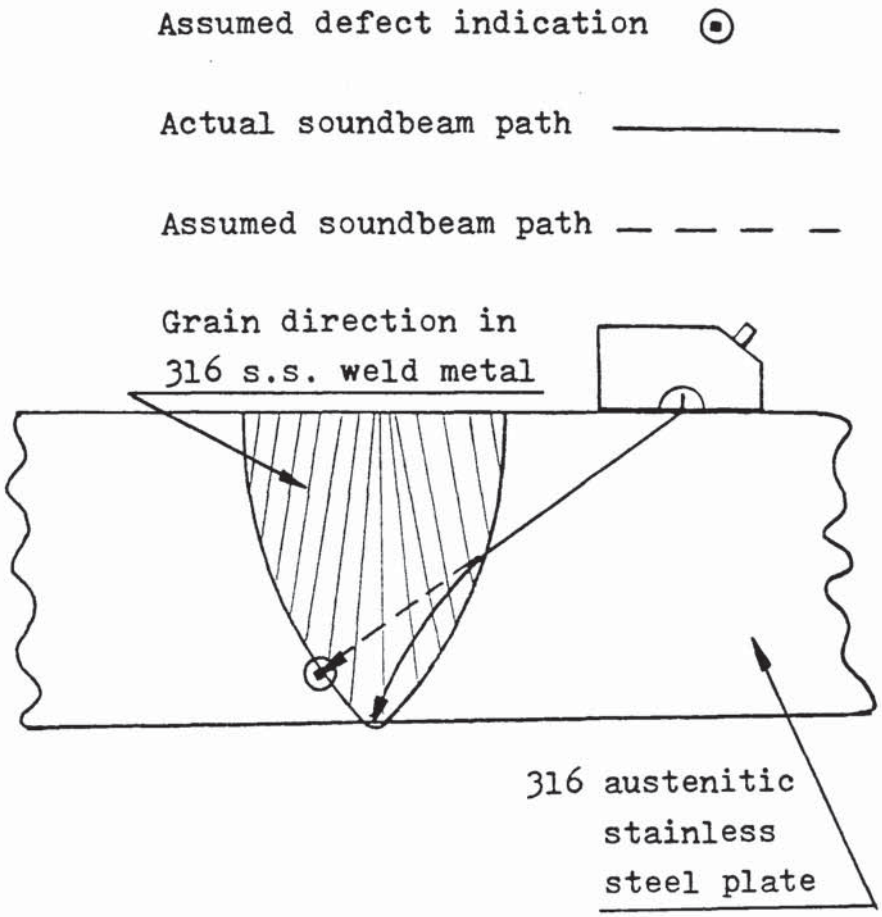

FIG. 2.4 : Occurence of false indications due to beam bending in austenitic weld metal

Large signals generated by the fusion face of austenitic weldments have been reported during shear wave examination, with smaller signals from the fusion face during longitudinal wave examination[33]. This result was qualitatively explained by two effects. First there is a difference between the velocity of shear waves in austenitic plate and in the austenitic weld metal the magnitude of which will vary depending on the angle of propagation of the waves. Gray et al[33] have shown this difference in velocities to be in the area of 25 % for shear waves and around 5 % for longitudinal waves travelling in a direction of 45° to the grain axis. Thus the acoustic impedance missmatch at the fusion boundary is larger for shear than for longitudinal waves. Secondly, longitudinal waves are weakly reflected by right angle corners as strong shear wave components are produced by mode conversion (Figure 2.5).

2.5.3 Other Microstructural Effects

The effect of grain boundary ferrite was investigated by Holmes and Beasly[42] and it was found that ferrite itself did not influence ultrasonic transmission even when present in amounts up to 30 % . Juva and Haarvisto[47] experimenting with austenitic weld metal containing 10 % δ-ferrite in this amount, being finely distributed in the weld metal, only had a minor increasing effect on the ultrasonic attenuation. They also point out that a more coarse distribution

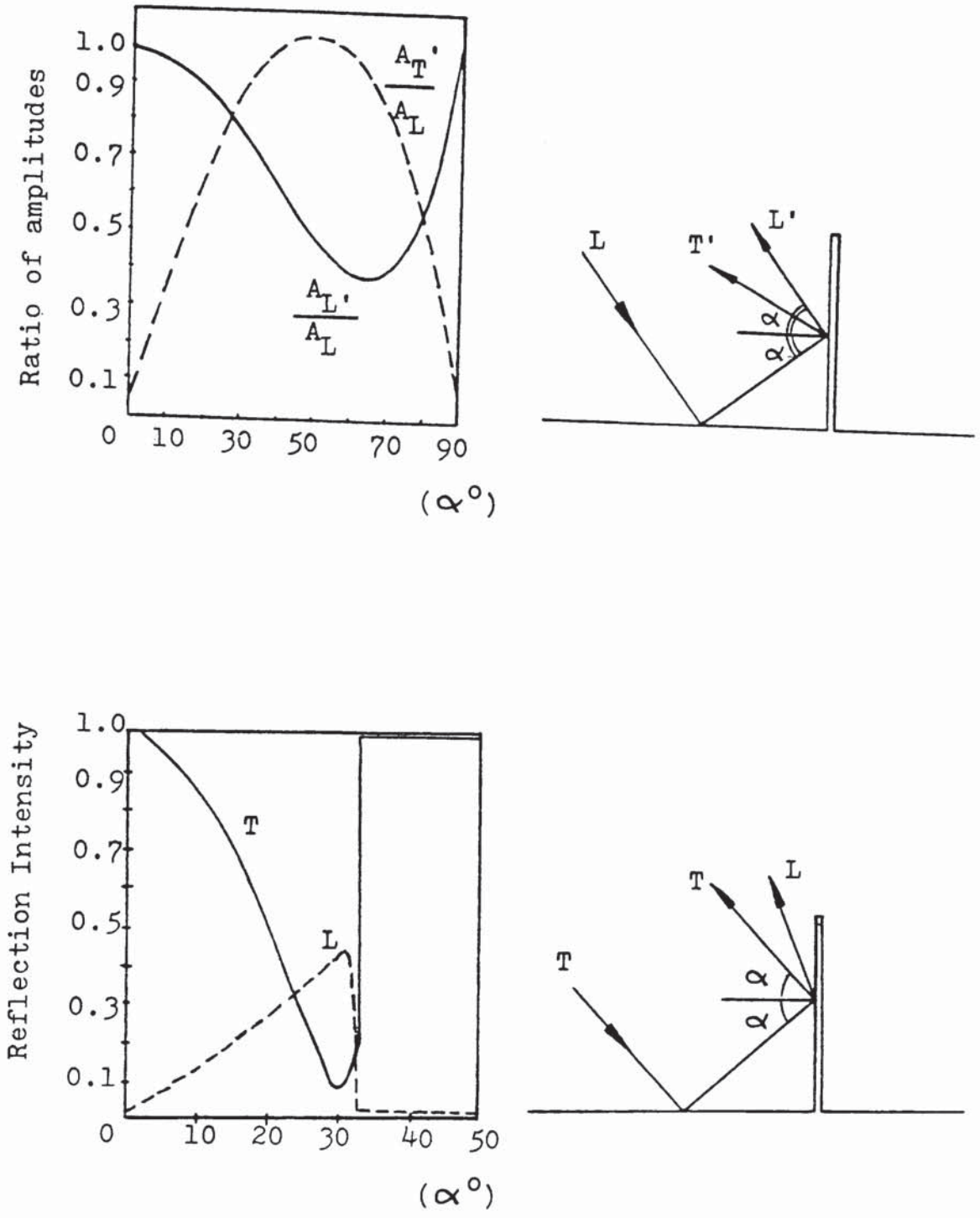

FIG. 2.5 : Longitudinal and transverse wave mode conversion from planar defect at right angles to the reflecting surface

of δ-ferrite even at lower content levels (6 %) is less favourable to ultrasound propagation.

It is probably reasonable to expect ferrite contents up to 10 % (commonly present in weld metal as fine interdendritic network) to have little influence on the factors controlling attenuation as described in section 2.5.2. The same researchers also report that the effect of carbide precipitate is such that both its content and its distribution have little effect on ultrasound behaviour. Kupperman et al[23] suggest that sensitization will not affect ultrasonic testing detrimentally. Beasley and Holmes [42] also agree that thin layers of carbide encountered in their work, did not adversly influence attenuation. On the other hand they emphasized that large grains, produced by heating the niobium-stabilized steel above 1350 °C, superimpose their own characteristics and possibly mask any effect contributed by the carbide.

2.6 Proposed Solutions to the Problem

2.6.1 Modification of the Weld Structure

The solidification process in austenitic welds, produces a columnar grain structure, with new grains growing epitaxially from existing ones, along the characteristic easy-growth direction of $\langle 100 \rangle$ for f.c.c. metals.

Since the propagation of ultrasound in these welds is determined by their columnar structure, it is highly desirable whenever economically feasible that fabrication should be such as to give predictable grain structures (if possible), with details of these procedures available to the ultrasonic inspectors.

Methods of grain refinement by nucleation and growth of equiaxed crystals ahead of the solidification front which block columnar grain growth are well established in the casting industry[48], but difficult to apply successfully in welding.

In controlling the grain structure, and particularly when aiming to produce grain refinement, it is necessary both to produce nuclei for new grains and to ensure that they survive. There are many different methods of structure control :

a) Control by Inoculants- Grain refinement in austenitic stainless steel submerged arc welds was achieved by introducing the inoculants using an auxiliary feed wire situated some distance behind the arc[49].

b) Arc Vibration and Weaving- By this method, not only was a considerable improvement in weld appearance and arc stability achieved, but also the weld metal was found to possess enhanced properties. Electrode weaving in submerged arc welding has been used on an industrial basis to achieve improved weld metal

appearance and also refine the solidification structure[50].

c) Ultrasonic Vibrations- Methods of introducing ultrasonic vibrations into the weld pool were developed for a range of processes and it was found that the most efficient and practical method was through a vibrating filler wire. It was observed that the welds formed were less prone to solidification cracking and this was associated with the quite considerable grain refinement. Industrial application would seem to substantiate the usefulness of this technique[51].

d) Weld Pool Stirring- Results of Russian work appear to have been so encouraging that the study of the grain size control in welding using electromagnetic stirring has become a major research field and equipment has been developed for industrial use applying this technique to a.c. or d.c. welding[52]. Few authors have published papers on the topic outside the USSR where the major research in this area seems to be concentrated.

e) Arc Modulation- Equiaxed solidification structure, in a modulated pulsed arc with slope-out, was obtained in stainless steel. The essence of the technique is the generation of dendrite fragmentation at the growing solid/liquid interface by forced thermal fluctuations. Pulsed arc welding is an established technique well

documented[53,54], but pulsing of the arc alone does not seem to generate effective grain or substructure refinement. If, however, current modulation is superimposed upon the pulse quite significant effects can result provided a slope-out period is used[55]. Work on arc modulation is still exploratory, but the technique has considerable promise.

Evaluation of more refined grain structure, made using the MIG welding process has been carried out by Tomlinson et al [22]. They found that instead of the long grains growing epitaxially across many weld beads with the well defined <100> orientation usually observed in the MMA welds, in this weld the grains were contained within each weld bead in a form of "fans" and only occasionally extended into the next layer of beads. It is suggested that the higher and more localized heat inputs resulting from the MIG process cause deeper remelting of the underlying beads, resulting in a more curved liquid-solid boundary than in MMA process, and consequently in a less defined grain growth direction. The effect of this less ordered grain structure was clearly seen in the ultrasonic behaviour. The attenuation observed was higher than in the more oriented structure of the MMA welds, through the plate thickness (0.55 dB / mm c.f. 0.1 dB / mm), but on the other hand there were no evidence of beam skewing.

Another method used to produce a more refined structure involved TIG welding process using fine wire and low heat input and peening of the weld between passes. If the peening introduced sufficient deformation, it would prevent the complete melting of the peened layer, and the heat of the next pass would induce recrystallisation in the deformed region. This would in turn produce a layer of equiaxed grains of more random orientations which act as nuclei for the new grains growing into the melt. The length of the resulting columnar grains is therefore limited to the dimensions of one weld bead. As in the case of the MIG process, the weld structure consisted of fine columnar grains in a fan shape in each bead. This type of structure exhibited higher attenuation than the well oriented MMA structure through the plate thickness (0.55 dB / mm c.f. 0.16 dB / mm), but did not give rise to beam skewing[19].

Gray et al[33] have carried out examination of narrow gap welds. Their study included welds made by a special Tungsten Inert Gas (TIG) and an Electron Beam welding process which yield a smaller volume of weld metal than the MMA process, and also resulted in different dendritic weld structures. They concluded that the weld metal was sufficiently short for beam skewing effects to be negligible for longitudinal waves, while the variations in signal amplitude were such as to allow a useful distance amplitude curve (DAC) to be

constructed and facilitate automated sentencing.

Appart from the above mentioned techniques that limit the volume of the weld, in Italy , Breda Termomeccanica has developed a narrow gap welding technique using the MIG process for pressure water reactor steam generator vessel components. The equipment uses a twin gun technique, the two guns steadily fill in the 16 mm gap, Figure 2.6. The use of two guns is claimed to avoid lack of side-wall fusion defects and cracks[57].

C.A. Parsons of Newcastle had long been interested in the potential of the narrow gap welding as a production costs saver for butt welding thick walled steam pipework. The company developed its own automatic orbital TIG system : 'Parsons Narrow Gap Process', using modified Astro-Arc equipment supplied by Weld Control of Tiverton, Devon. It was first used on Cr-Mo-V pipework for a CEGB contract and involved welding 250 mm diameter pipe of 63.5 mm wall thickness. Welds were subjected to close inspection by the CEGB, including X-ray radiography and Ultrasonic inspection procedures. The pipe steel was ½ Cr-Mo-V and was welded using an Oerlicon SD2 2½ Cr-1Mo-V filler wire with closely controlled Mn and Si content. Welding speed around a 9.6 mm joint gap was 50 mm/min. All weld specimens passed inspection, and room temperature tensile strength was 655 N/mm^2 after stress relief. The HAZ was only 2 mm wide compared with 2-3 mm for MMA, and 4 mm for submerged arc.

De Altamer[58], using two pass layers submerged arc narrow gap welding, has produced high quality welded joints in alloy steels which demand controlled heat input. No repairs were found necessary due to lack of sidewall fusion or the presence of slag inclusions. No troubles were experienced with joint mechanical properties, because the correct heat input can be used in each case, as it is fully controllable through particularly flexible parameters.

The progress that has been made in this area looks certain to go some way towards mitigating the problems of inspecting austenitic welds with ultrasound.

At present another approach has yielded encouraging results, that is the production of predictable well-ordered weld grain structures in ways that would positively affect the ultrasonic inspection of austenitic welds. Tomlinson et al[22] have succeded in controlling the orientation of the <100> fibre axis by varying the weld geometry, the welding position and the run sequence, in such a way that the average departure from the optimum of the angle between the grains and the ultrasonic beam is minimised. Their work was carried out on a tube-to-tube weld in the AGR, and their results showed that the welding procedure required was both practicable and capable of producing inspectable welds. The implication of their findings are twofold :

(i) Consideration and control of the weld structure must precede attempts to improve inspection sensitivity by the use of special transducers or signal processing methods, and

(ii) Plant designers should take account of the limitations of ultrasonic inspection when applied to austenitic structures at the earliest possible stage.

2.6.2. Optimizing the Ultrasonic Variables

2.6.2.1 Frequency

Defining the grain size of austenitic welds as the maximum structural dimension occuring in their complex structures, the Rayleigh and Stochastic laws are not directly applicable. It is reasonable though, from practical experience, that increasing attenuation will occur with increases in the D/λ ratio. Research results, generally recommend the use of low frequencies in testing austenitic welds[35, 41, 59, 60, 61]. By taking recourse to lower frequencies, the attenuation can be reduced considerably, but this step is promising only as long as the smallest flaws to be detected are still large compared with the grain size, or the factor of reflection of the flaws is large compared with the scatter factor of the structure, i.e. the size of minimum defect detectable is increased.

Results of spectral analyses[23] indicate that, for ultrasonic inspection of austenitic stainless steel weldments, frequencies about or below 2MHz may be most effective, although it is not uncommon practice to employ frequencies in excess of this value.

2.6.2.2 Wave Mode

The statement "attenuation is more severe for transverse than for longitudinal waves" is very often encountered in the literature[23,33,34,35,36,37,38], and it appears that this should be the case, if a comparison between the two modes is made in terms of wavelengths rather than frequencies.

The ultrasonic velocity for transverse waves, for a given frequency, is approximately half that of longitudinal waves, and consequently their wavelength is also approximately halved. Neumann et al[35] have carried out a comparison of the attenuation characteristics of the two modes on the basis of wavelenght in both weld and parent metals, and showed that transverse waves were slightly higher attenuated than longitudinal waves.

Theories of scattering in equiaxed structures show that when either transverse or longitudinal waves are propagated in a multi-grained material, the bulk of the energy scattered by the grains is in the transverse mode[39]. Consequently, in pulse-echo ultrasonic inspection, the signal to back-scatter (noise) ratio from defects will be higher for longitudinal wave transducers, since they are unable to respond to the larger part of the scattered energy which is in the transverse mode.

A further advantage of using longitudinal waves is that beam

skewing effects, associated with austenitic weld metal ultrasonic inspection, are less pronounced than for transverse waves[23,33]. Tomlinson et al[22] have experimentaly established quantitative estimates of beam skewing for both wave modes, and the largest angle of skew observed for longitudinal waves was about 15°, whilst for transverse waves, beams were found to deviate up to 50° from the expected direction of propagation. It is apparent that due to the magnitude of the deviations involved, conventional transverse wave inspection becomes extremely difficult, whilst longitudinal wave is easier, but still requires extra care in flaw position interpretations.
The variation of the skewing angle with direction leads to variations in beam width. It has been shown experimentally[37] that angled longitudinal waves follow preferred paths through austenitic welds at angles in the region of 45° beam to grain direction. It was observed that there was a positive deviation of the wavefront which increases the beam angle, for beam to columnar grain angles between 17° to 44°, the deviation became zero at 45°, and for angles between 46° and 75° there is a negative deviation which reduces the beam angle.
As expected from the theory of propagation of elastic waves in a general anisotropic medium[25,30], three propagational waves are possible, i.e. one longitudinal and two transverse at mutually perpendicular polarizations. Recently it was

demonstrated that transverse waves polarized parallel to the major interfaces existing in a weldment (fusion lines, grain boundaries) can be less attenuated than longitudinal waves of equal wavelengths[29,30].

This result might seem to contradict the previously described situation, but considering that mode conversion is another component contributing to the overall attenuation (of the transverse waves at solid interfaces, and longitudinal waves on reflection and refraction at grain boundaries), it can be seen that parallel polarized transverse waves cannot give rise to longitudinal waves by mode conversion[30]. The reason for this is that the transverse waves generated by mode conversion from a longitudinal wave beam are strongly polarized in the vertical direction, with no resolved component in the direction of vibration of the horizontally polarized transverse wave.

Although the concept of a parallel polarized transverse wave, providing a mode of propagation free of mode conversion is attractive, practical difficulties in coupling these waves into the weld present a problem, a satisfactory solution to which has not been found as yet.

When considering theoretical values[25], and values computed from experimental results[30] of the skewing for all three modes of propagation in the austenitic weld metal, there is agreement that transverse waves vertically polarized exhibit more distortion due to skewing than either of the other modes, with parallel polarized waves exhibiting the least amount of

skewing. There is experimental evidence[26,27], that parallel polarized waves have increased the inspectability of austenitic welds, and comparisons of this wave mode with longitudinal wave testing have been favourable.

The advantages of using longitudinal waves in inspecting these welds outlined above would seem to be a panacea, but this mode of propagation has its own inherent problems. The existence of two separate wave modes when using longitudinal angle probes produce at times complicated patterns on the CRT screen of an Ultrasonic Flaw Detector, and extra care must be taken in interpreting such indications.

With transverse waves, testing is usually carried out between a half and a full skip scanning positions or multiples of a skip distance. Generally, with longitudinal waves this is not possible because, as shown in Figure 2.7, the longitudinal waves when reflected at the underside of the plate will exhibit mode conversion and therefore energy loss. Consequently, when using longitudinal waves at an angle, testing has to be done between the sound entry point up to a maximum distance of a half skip. This last limitation has a twofold effect :

a) In order that flaws located near the top of welds be detected, the probes must travel over the weld metal, i.e. the top layer of the weld has to be machined level with the plate surface. This is generally the case in reactor fabrication. If the top is not machined or sufficiently ground to allow a smooth contact surface

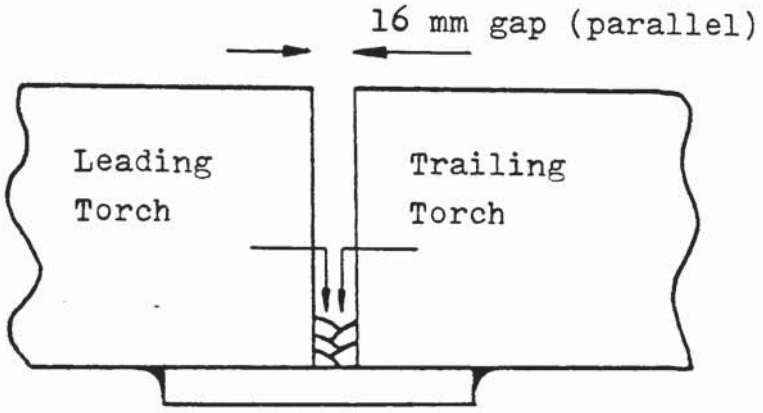

FIG. 2.6 : Breda Termomeccanica's Twin Gun MIG Narrow Gap Process

Typical scanning positions (1) and (2) used in longitudinal angle beam inspection

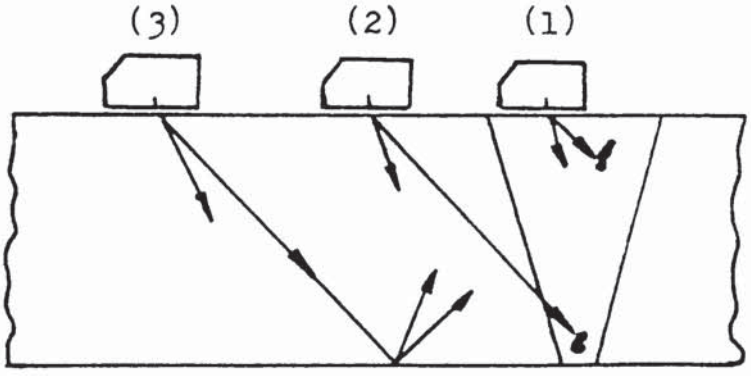

Scanning position (3), not recommended

FIG. 2.7 : Longitudinal wave testing at an angle

for the probes used, the top part of the weld will have to be tested in an additional testing sequence with a probe from the underside.

b) As reflectors immediately below the surface have to be detected, the probes used have to have an exceptional resolving power near to the probe[60].

Although ultrasonic inspection of austenitic weldments is difficult using conventional transverse wave techniques, they should be considered as first choice, especially in weldments less than 25 mm thick.

Juva and Lieto[61] conclude in their work on examination of thin austenitic stainless steel butt-welds (2-10 mm thick) that the attenuation of ultrasound is not a problem when dealing with such thicknesses, and that transverse waves give better results than longitudinal waves.

On a similar line, Reinhart[62], involved in a recent research programme formulated by the Electric Power Research Institute (EPRI-USA), concludes that pulse-echo transverse wave ultrasonics is a viable technique for volumetric inspection in 300 series core spray lines of BWR reactors, for detecting stress corrosion cracks for material thickness up to 15 mm.

Abrahams[63] working with austenitic steel tubing, expresses the view that provided the ultrasonic characteristics of the parent tubes are measured and taken into account when calibrating the equipment, a useful examination of the weld, particularly for root defects, could be made using conventional

transverse wave techniques. Edelman[64] summarises the situation of ultrasonic inspection of austenitic weldments very clearly by stating that each examination problem must be considered and tackled anew. For the development of an examination method, the most important step is the fabrication of a number of reference blocks, these blocks being made using the same base and welding materials and procedures must be kept practically identical as the object to be examined. When choosing a suitable probe for a certain examination problem, transverse waves should be the first choice, and if not succesful, the most suitable longitudinal probe should be selected on tests using the manufactured reference blocks. The main criteria for the choice being the signal-to-noise ratio, the beam angle, and the contact surface area.

2.6.2.3 Noise Reduction

In a material with very coarse grain compared with the wavelength, incident sound waves on an oblique boundary may be split into various reflected and transmitted wave types. This process repeats itself for each wave at the next boundary, and the original sound beam is constantly divided into separate waves. In the case of grain sizes of $1/100^{th}$ to $1/1000^{th}$ of the wavelength, scatter for all practical purposes is negligible. It increases very rapidly, however, approximately as the third power of the grain size, to make

itself felt at sizes from $1/10^{th}$ to the full value of the wavelength, to such an extent that testing may become impossible if the material concerned is anisotropic[66].
In such a material possessing coarse and anisotropic grain structure (viz. austenitic weld metal), scattering not only reduces the strength of signals from defects, but in addition produces numerous echoes with different transit times, the so-called noise, in which the true echoes may be lost.
Apparently this disturbance cannot be counteracted by stepping up the transmitter voltage or the amplification because the noise increases simultaneously. One remedy is to use lower frequencies, which due to the reduced beaming effect of the sound and the increasing length of the pulses sets a natural limit to the detectability of small flaws.
In order that flaws in any material be detected the following two conditions must be met[66], the signal produced by the flaw (V_f) must be stronger than the minimum signal (V_{min}) sensed by the amplifier of the flaw detector; and the flaw signal must be stronger than the noise signal (V_n). That is :

$$V_f > V_{min} \quad , \text{ and}$$

$$V_f > V_n \quad .$$

In the case of austenitic welds the second condition is difficult to meet because of the high level of structural

noise. To improve the ratio between the flaw and scatter echoes originating from the austenitic weld structure, Neumann et al[35] constructed tranceiver angle probes, with the directional lobes of the two crystals inclined towards one another resulting in a focal area. The advantage of this method over normal pulse-echo techniques is that the structural scatter echoes from the entire material region penetrated by the soundbeam are not registered, but those coming from the focal area are, whereas the echo from a defect in the focal area remains constant. Based on this principle, ultrasonic probes for the determination of sub-cladding cracks of reactor pressure vessels have been developed[67]. The construction and use of these probes is described extensively in the literature[33,35,60,62,66,67], and they are commercially available[68,69].

Focused probes have only a limited range of sensitivity, and this usually means that a combination of probes with various focal lengths is required for depth coverage.

The analytical relationship between structural noise and signals produced by various flaws is given by Ermolov and Pilin[70]. From their results it can be seen that, if a flaw is in the far field of a probe, the probe area should be increased to enhance the signal to noise ratio; in this way the probe directivity is improved (Fig. 2.8 a & b), but when a flaw is detected in the near zone, the probe area should be decreased (Fig. 2.8 c). In practical terms this

(a) Flaw in the distant zone

(b) Improvement in the directivity pattern through enlargement of the probes

(c) Flaw in the near zone

(d) Flaw in the focal plane of a focusing probe

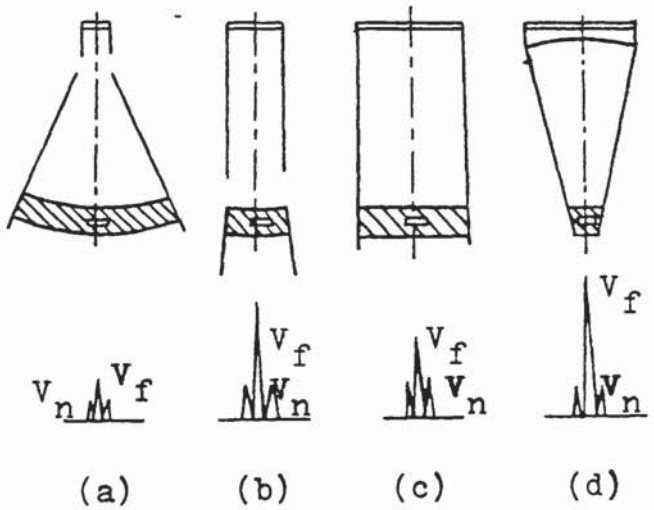

FIG. 2.8 : Relationship between amplitudes of flaw signals (V_f) versus that of structural noise (After Ermolov and Pilin[70])

means that the detection of flaws against a background of structural noise increases with the ratio of the reflecting surface of a flaw to the area of columnar grains which are exposed to ultrasound and are responsible for the structural noise. Further increases in this ratio are possible by means of focused probes (Fig. 2.8.d). It can also be seen from their results that the shorter the duration of the probing pulse, the better the conditions for discriminating the flaw signal against the noise background.

The use of wide-band ultrasonic pulses for testing strongly scattering materials has been known for a long time[71,72]. Neumann et al[35] by employing Li SO_4 transducers with their wide-band ultrasonic pulses, found that grain noise from a 50 mm double-U butt welded austenitic joint could be reduced and a signal to noise ratio of 10 dB obtained, though not many quantitative results are reported.

Another method of enhancing the signal to noise ratio is by the use of differences in the statistical characteristics of flaw signals and structural noise. Devices based on the analysis of statistical characteristics of signals and noise make it possible (with the signal to noise ratio being invariable at the input of the receiving channel) either to increase this ratio at the device output or to raise the probability of determining the presence or absence of a flaw signal against the background of noise; this latter leads to more reliable results[70].

An accumulation of the statistical reflected signals, with the search unit moving uniformly relative to the part under inspection, has been carried out by Ermolov and Pilin[66]. The variation of the noise, and the strength of the structural reverberation at each point along the ultrasonic pulse propagation axis is of a random nature. The signals from defects follow a law determined by the directional diagrams of the search unit (probe) and defect. It was observed that the envelope of reflected signal amplitudes extends in the direction of the probe travel more than that of structural noise amplitude, even if the maximum values of these signals are commensurable[66] (Figure 2.9). Thus, accumulating the signals for equal distances of uniform probe motion and comparing the resulting signals, it will be found that the total signal for the section containing a defect is larger than the total signal obtained for the same distance in a section without a defect but with structural noise. Thus, the accumulation enables the signal-to-noise ratio to be increased and the useful signal to be separated.
On the basis of this method of improving the sensitivity of flaw detection by statistical processing of information gathered by a uniformly moving search unit, a prototype device was developed[66]. Although the efficiency of accumulation increases precisely when the conditions of detecting a flaw against the backgr ound of noise by conventional methods deteriorate, there are disadvantages. It is not possible to

locate a flaw precisely; only the area where the flaw is located can be defined. When the signals are accumulated, there is loss of information on the value of the amplitude of the echo signal and its variation in the course of the probe movement. The accumulation method permits on the spot checks and lends itself to automation; a number of uses have been proposed: addition of several A-scans[69,72], B-scans[69], and a flaw detector for differential layer-by-layer checks[32].

On similar lines, a cross correlation technique has been used by Mech and Michaels[73] to locate notches placed in austenitic stainless steel pipes. In essence their technique uses an automatic data processing system to gather waveforms for analysis. The waveforms obtained are compared with waveforms containing reference signals, and when the two waveforms are slid past each other enhancement occurs where the reference and defect signals coincide. Their technique has the additional advantage that data files permit reinterogation of previously examined samples, without the necessity of repeating the tests. This is an extremely important feature allowing data from pre-service inspection to be compared later with in-service inspection data.

Another promising way of improving the sensitivity of ultrasonic inspection of high noise materials is to vary the frequency of probing pulses when the frequency of ultrasonic vibration of one emitted pulse differs from that of another

pulse by a certain value[74]. This frequency variation will bring about a considerable change in the structural noise amplitude. At the same time, the flaw signal amplitude depends on the frequency variation to a lesser degree, which makes it statistically possible to discriminate it against the background of varying signals. Using this principle a flaw detector emitting frequency-modulated pulses into the item under inspection and processing them upon reception has been developed[75]. Improvements of 15 dB in the signal to noise ratio from a submerged arc welded tube of 8 mm thick austenitic steel have been reported[76], by means of narrow-band transmitter pulses of continuously variable frequency. The same researchers have shown improvements of 12 dB, using a 2.25 MHz broad band probe.

Another means of enhancing the signal to noise ratio in ultrasonic inspection of austenitic welds is offered by using multi-frequency testing[76]. The detection of a flaw is indicated by the coincidence of the co-ordinates of pulse reflectors with two or three frequencies being used respectively. This method of inspection does not require the use of special equipment and can be easily performed using standard ultrasonic flaw detection equipment. Only one condition should be met, namely that at all frequencies used, the directivity patterns of the probes must be of the same width.

From this latest condition springs yet another promising method of obviating the effect of structural noise. This is one which uses the periodical variations of the probe directivity pattern width, the ultrasonic power being kept constant[74]. The variation in the directivity pattern is attained by varying the probe diameter. Having the probe area periodically varied with the emission power kept constant, the average noise level will also be constant, and the flaw signal will be amplitude modulated with the frequency of probe area variation. Processing the received echo signals by means of filters, the flaw signal could be easily differentiated from the structural noise.

2.6.3. Novel Ultrasonic Techniques

2.6.3.1 Ultrasonic Diffraction

In order to move away from the reliance on echo amplitude as an indication of defect size, tests have been performed using a time-of-flight approach to defect sizing. The two probe ultrasonic time-delay method, already developed for sizing surface breaking fatigue cracks[77] has been adapted for measuring the size and through thickness extent of embedded volumetric defects in welds[78]. Two angle beam longitudinal wave probes are placed on the parent metal on opposite sides of the weld, so that their beam cones intersect in the weld

region. A pulse of ultrasound transmitted by one probe produces reflected beams from the upper surface of defects and diffracted beams from their undersides which are received by the other probe (Fig. 2.10). The received signal is processed and recorded to show the changes in signal response as a function of position along the plate. Interpretation of these records reveals information on size and location of defects in the weld. This approach has been especially successful in ferritic materials and an accuracy of crack depth estimation better than $\pm$ 0.5 mm has been demonstrated [77]. Although accuracy as demonstrated above could be reason alone for using the technique in austenitic weld examination, there are more specific reasons which may be put forward in support of this technique over the alternatives for both defect location and sizing.

a) The technique normally employs bulk longitudinal waves. It has been established that this wave mode is less prone to the adverse effects produced by the austentic weld structure.

b) The technique is based on the transmission of energy, thus reducing the masking effect of scattered energy.

c) The technique is insensitive to the angle of the ultrasonic beam, and thus the choice of an angle that optimizes transmissivity, will rarely be in conflict with the efficiency of the technique.

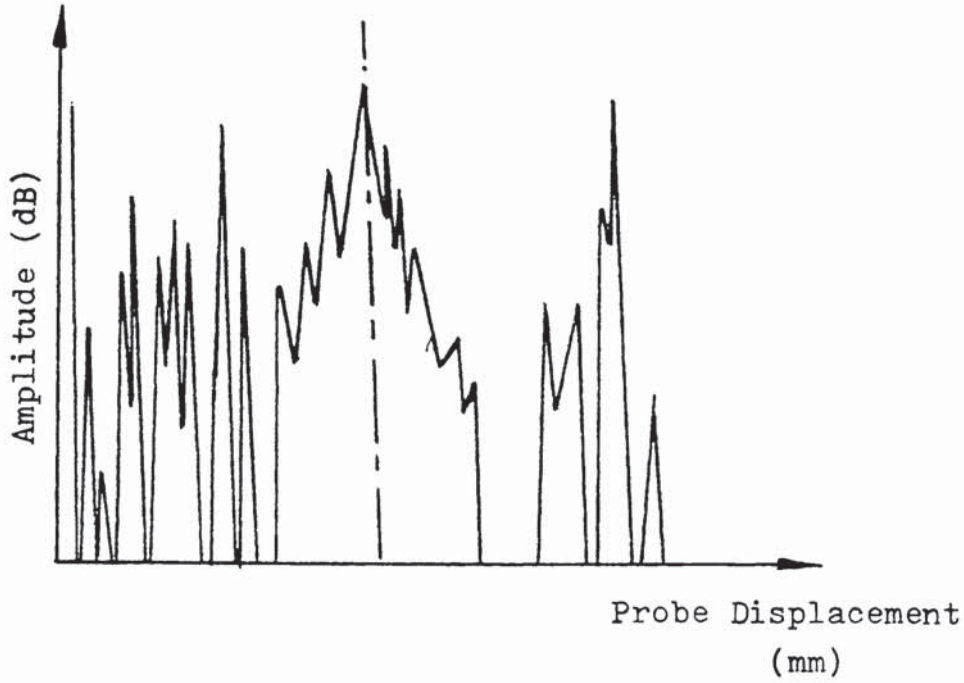

FIG. 2.9 : Distribution of signal amplitudes reflected from a defect and due to structural noise, as functions of probe displacements (after Ermolov et al[66])

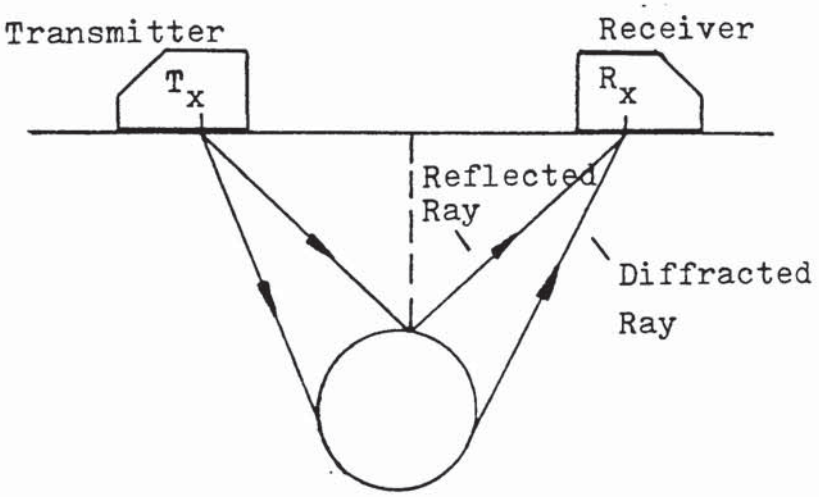

FIG. 2.10 : Schematic representation of time delay sizing applied to a volumetric defect of circular cross section (after Charlesworth, NDT Centre Harwell)

Some experimental data obtained using the diffraction technique to inspect an austenitic weld have already been published[77]. The results were obtained using a slit cut into a double-V preparation weld in 39 mm thick plate. From these, the mean error was found to be ± 0.3 mm which compares favourably with an error of ± 0.2 mm on ferritic materials under the same conditions.

There is only one example, at the present time, of a fatigue crack in austenitic weldment examined by this technique[27], and comparison with the actual cracks' depth found by sectioning the specimen is favourable with a mean error of less than ± 0.4 mm.

2.6.3.2 Ultrasonic Holography

This imaging system offers advantages in resolution which cannot be achieved with conventional techniques already mentioned. Where the resolution of more conventional techniques is governed by the ultrasonic pulse length, in holography the wavelength determines the limit of resolution[79]. The holographic technique appears to be most advantageous in the examination of thick sections in which the effects of beam spread would otherwise be troublesome.

Again, this equipment is in the laboratory stage and is particularly time consuming to apply since it involves the manufacture of a hologram in the first instance, and subsequent reconstruction on an optical bench. The system has

been described in detail by Aldridge[80].

2.6.3.3 B-Scan and C-Scan

The B-scan display provides immediate information on the cross sectional position of a reflector and with detailed measurement and proper interpretation can provide additional information on the size and character of the defect under test. The equipment used in this technique is described in detail by Harper[81]. It has been employed for site work and is portable and easy to apply. The basic ultrasonic data are derived from a conventional A-scan flaw detector and are combined with probe position and beam angle data to produce a B-scan display in the form of a trace on a bi-stable storage oscilloscope. This can be photographed to provide a permanent record. Various modes of scan using compression wave and shear wave probes can be used to build up a comprehensive picture of a defect. Conventional contact probes are employed.

A C-scan is a view in plan of the ultrasonic echo amplitudes received by the probe from reflections within a pre-selected volume of the specimen. The C-scans are contour maps of the echo amplitudes received by the probe as it scans over the surface of the component under test. Conventional probes and flaw detection equipment are employed. This system is regarded as a research tool in that the scans produced are permanent records of the ultrasonic data which can be compared

with the actual topography of the defects. In this way, the understanding of the interaction of ultrasonic pulses with defects can be improved. C-scans contain good amplitude information which may be complemented by the range of information available from B-scans.

2.6.3.4 Ultrasonic Scatter Technique

This method employs two longitudinal wave probes, which are constructed so as to generate an ultrasonic beam at an angle, placed on the surface of the material under inspection. They are placed facing one another, with such a separation as to avoid a large backwall echo. An observable ultrasonic pulse can nevertheless be transmitted between the probes. This has been studied by Wustenberg et al[82] and the transmitted energy is attributed to grain boundary scatter in the region where the ultrasonic beams are broadly focused. This explanation seems to be confirmed by other experimental work[83].

Thus when a surface opening slit or crack is present between the probes it can be shown that changing the probe separation produces a variation in signal height (Figure 2.11). This can then be explained by the progressive blocking of the paths available for scattered energy as the region of focus is brought nearer to the surface. This approach can be used as means of estimating crack depth, and by keeping the probes at a fixed distance, crack growth could be monitored as change

in signal height. The crack as it grows will obscure more and more of the paths taken by the scattered energy and therefore a fall in signal height would be expected. The technique need not to be confined to surface opening cracks and could be envisaged as sizing internal defects within the limits of resolution. An accuracy of better than ± 1 mm is reported in defect sizing. The technique has been used to size defects under cladding, but no details of the work have been published.

2.6.3.5 Adaptive Learning Networks (ALNs)

The aim of this approach is to find signal analysis algorithms which are sensitive to defects but not to metallurgical structure. The technique involves data acquisition (ultrasonic signal capture, digitization and mass storage); data analysis (peak amplitude deconvolution, cross correlation analysis and frequency domain analysis); and finally training and testing an ALN using the analysed data. Training is accomplished by stating the desired output from the defects under consideration and then combining the input data in such a way as to achieve a result as close as possible to the one desired. The ALN approach is receiving most attention in the USA, not only as applied to ultrasonic testing of austenitic steel[84], but for other materials[85] and eddy current testing[86].

2.6.3.6 Accuscan Tests (CEGB)

The NDTA Centre of the CEGB has developed a new equipment, known as "Accuscan", to record the salient features of the A-scan display at each probe position. This objective collection of the ultrasonic information allows B and C-scans to be generated, together with other related displays from the same body of data. This facilitates the comparison of different plots allowing better interpretation and diagnosis of weld defects. In addition, it gives a more complete ultrasonic record which can be compared with the actual form of the defects revealed by destructive examination.
The system consists of a motorised precision scanner, a microprocessor controlled flaw detector unit and a cassette tape drive. The unit controls probe positioning and energises the transducer. Incoming signals are digitised and passed to a magnetic tape for storage. This tape can be used in a remote microcomputer, where the information can be analysed to produce the desired defect image[87].

2.6.3.7. Search Unit Tracking and Recording System (SUTARS)

On similar lines to the "Accuscan", Southwest Research Institute (SWRI/USA) developed a system that automatically records the position of the search unit together with the ultrasonic data[6]. The search unit tracking and recording

system (SUTARS)has the following features:

1. Automatically positioned search unit.
2. Automatic recording of ultrasonic data acquired at each search unit position.
3. The entire A-scan trace is recorded and is available for computer analysis.
4. All data are recorded on tape for maximum system portability.
5. Computer printout of the data provides information identical to that recorded by manual ultrasonic methods plus other analysis tools such as B and C-scan plots.

SUTARS has proved to be a reliable, effective method of performing ultrasonic examinations during pre-service and in-service inspections. Field tests indicate significant saving in the time to perform a high technology task in a difficult work environment. Furthermore, data processing provides significant improvement in records and flexibility for analysis. Reproducability has been demonstrated to be outstanding.

2.6.3.8 P-Scan (Projection Image Scanning Technique)

This system has been developed by the Danish Welding Institute and is based on an advanced fully microprocessor-controlled

ultrasonic equipment that measures, analyses and records all echo signals from the area under inspection. In this technique echoes from defects are measured and recorded together with the corresponding defect positions. Defect positions are then visualised as a projection of the defects on one or more projection planes (Figure 2.12).
Usually two projection planes are used; one parallel and another normal to the surface of the weld, so defects appear as seen from a top view and a side view. By using two projection planes, a complete three-dimensional location of defects is obtained. In addition, all the maximum echo amplitudes along the weld are displayed in a logarithmic scale. The inspection can be carried out manually by means of a small light-weight weld scanner, which allows one to move the ultrasonic probe freely within a certain area and to inspect the weld from both sides. The indications from the two sides of the weld are shown superimposed in the P-scan image. This feature is extremely valuable, because it allows one to differentiate between real flaw indications and indications occuring from the weld geometry or structure. The P-scan technique is suited for automatic weld inspection with a very high degree of reproducibility. These possibilities of the system make it suitable for in-service inspection of components in nuclear power plants[88].

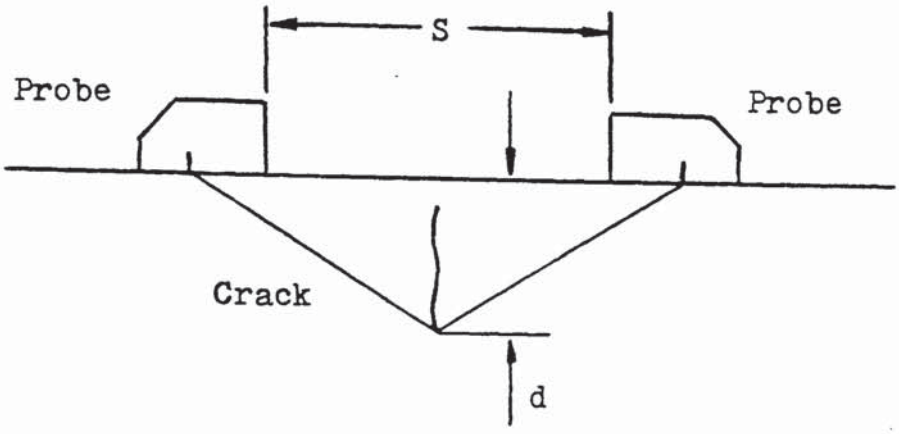

d- Flaw Depth
S- Probe Distance

FIG.2.11 : Probe geometry-Scatter technique

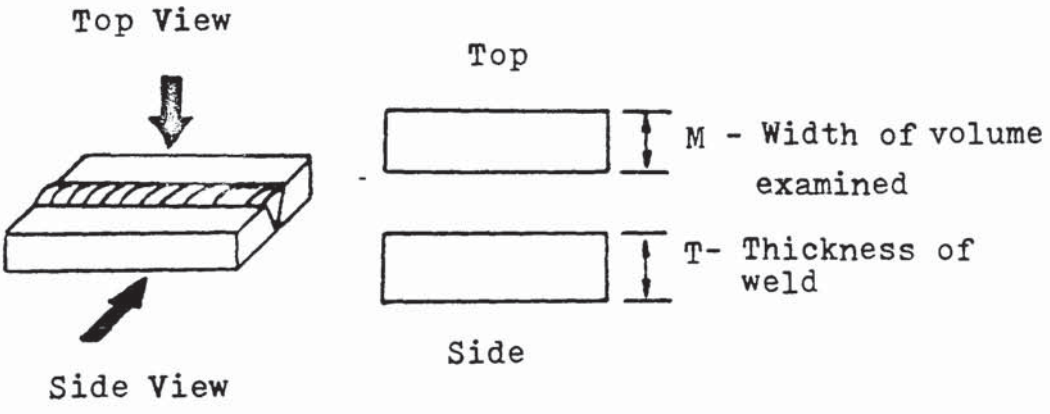

FIG. 2.12 : P-scan principle. Defect indications shown correspond to a defect in the centre of the weld and near the bottom of the plate

2.6.4 Resumé

At present, therefore, it appears that a combination of control over the metallurgical structure and of signal processing can produce improvements in the inspection of austenitic welds to the point where at least some form of inspection will be possible for most welds. It is expected that further research along both avenues will yield further benefits so that satisfactory inspection becomes generally possible. It seems unlikely, however, that the low levels of scatter and attenuation found in ferritic materials will ever be attained.

3. INITIAL EXPERIMENTAL INVESTIGATION OF THE AUSTENITIC PROBLEM

3.1 Materials and Equipment

Two austenitic materials were investigated, namely 316 and 347 type stainless steels. The dimensions and chemical compositions of the plates are given in Table 3.1.

The main aims of this investigation were to assess the characteristics and performance of the ultrasonic apparatus used, to determine the standard of examination possible on austenitic stainless steel weldments using different weld geometries and if possible, to relate the results to weld composition and microstructure.

Six test plates were welded for this part of the work, and the details of welding parameters and procedures are given in Table 3.2.

For the ultrasonic investigations, a Baugh and Weedon P.A. 1020 Ultrasonic Flaw Detector in conjunction with the probes outlined in Table 3.3, and a Krautkramer USIP 11 Ultrasonic Flaw Detector in conjunction with the probes described in Table 3.4, were used.

Velocity of sound measurements were carried out using the Interferometer technique[89].

X-ray diffraction techniques were used on a 316 austenitic plate coupon to obtain estimates of preferred orientation,

Plate Material	Thickness (mm)	C %	Cr %	Ni %	Mo %	Ti %	Nb %	Mn %
316	12.5	0.044	16.8	11.46	2.65	0.033	-	-
316	25.0	0.029	16.8	11.39	2.28	0.033	-	-
347	25.0	0.081	18.79	12.94	0.01	0.034	0.68	1.19

Table 3.1 : Details of rolled plate materials

Material & Thickness	Specimen No.	Weld Preparation	Electrode Type
347 (25 mm)	S_1	Single-V	347 Nicrex NDR
316 (25 mm)	S_2, S_3	Double-U	316 Staintrode 63.30
316 (12.5mm)	S_4, S_5	Single-U	Staintrode 316 63.30
316 (50 mm)	S_7	Single-V	-

Table 3.2 : Details of welding procedures (MMA process)

(Notes on details, see next page)

NOTES : Referred to Table 3.2.

1. Root area of single-V welds ground to sound metal, and filled using 10 swg electrodes.

2. Root area of double-U welds ground from one side to sound metal and one run made using 10 swg electrodes, then filled up according to note 3.

3. Electrode size and current for root runs and fill-up for the double-U welds were 10 swg and 100/110 amps.

4. Electrode size and current for fill-up of single-V welds were 6 swg and 190/200 amps.

5. Root area of single-U welds ground from one side to sound metal and then filled-up using 10 swg and 100/110 amps electrode size and current respectively.

6. In all welds with the exception of the single-U welds, maximum heat input was used. For the single-U welds normal heat input was used.

7. Radiographic examination of all specimens was clear.

Probe Type (B & W)	Crystal Size (mm)	Nominal Angle (degrees)	Nominal Frequency (MHz)	Actual Frequency (MHz)
3D2	15	45	2	1.88
3E2	15	60	2	1.66
3F2	15	70	2	1.94
3D5	15	45	5	5.00
3E5	15	60	5	4.00
3F5	15	70	5	4.50
2A2	10	0	2	-
2A5	10	0	5	-
AS F30 Lo	-	45	2	1.70

NOTES: All angle probes described in the above table were conventional transverse wave angle probes, with the exception of the AS F30 Lo.

AS F30 Lo. is a focused longitudinal angle probe emitting both longitudinal (at 45^{o}) and transverse (at app. 23^{o}) waves, simultaneously. The focal length of this probe is 30 mm.

Table 3.3. : Baugh and Weedon probes used in conjunction with the B & W P.A. 1020 Ultrasonic Flaw Detector.

Probe Type (Krautkramer)	Crystal Size (mm)	Nominal Angle (degrees)	Nominal Frequency (MHz)	Preferred Range of Use (mm)
WRY	24	45	2	25
WSY	8x9	45	4	25
WSY	8x9	60	4	25
WSY	8x9	70	4	25
MB2F	10	0	2	-
MB4F	10	0	4	-

NOTES: All angle probes described above were single crystal longitudinal transmitter receiver (TR) probes. The two conventional longitudinal (0^{o}) probes were used for calibration purposes.

Table 3.4 : Krautkrämer probes used in conjunction with the Krautkrämer USIP 11 Ultrasonic Flaw Detector.

using a Siemens x-ray goniometer with a 6 mm^2 beam from a CuKa tube[90].

For the location of the 316 austenitic weld grains, a scanning electron microscope (SEM)[91] was used for obtaining selected area channelling patterns (SACPs)[92]. From the SACPs, orientation of individual grains could be obtained by matching the individual SACPs on a composite map for comparison with the overall texture of the material[93].

3.2 Velocity Measurements

Measurements of longitudinal and transverse velocities were carried out on 316 austenitic plate and weld metal coupons shown in Figure 3.1.

The measurements were made in three mutually perpendicular directions (viz. x,y,z), using the Interferometer method. The results are graphically depicted in Figure 3.2.(a) & (b).

3.3 Attenuation Measurements

Using the 316 austenitic plate and weld coupons shown in Figure 3.1, attenuation measurements were carried out in three mutually perpendicular directions (x,y,z), using 2 MHz and 5 MHz conventional longitudinal wave probes.

The CRT screen was calibrated in the usual manner using the above probes on the IIW calibration block, then by placing each probe on the specimen side of which the attenuation

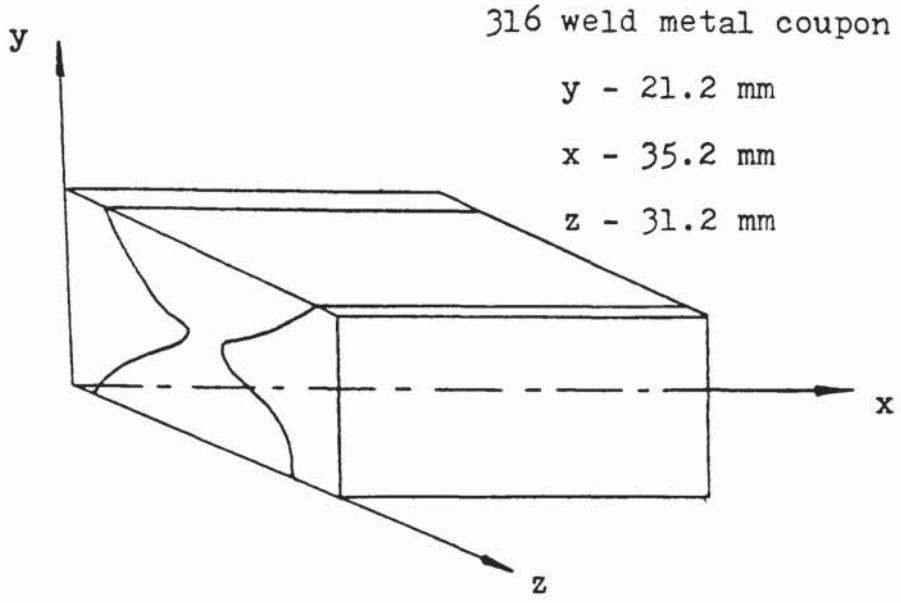

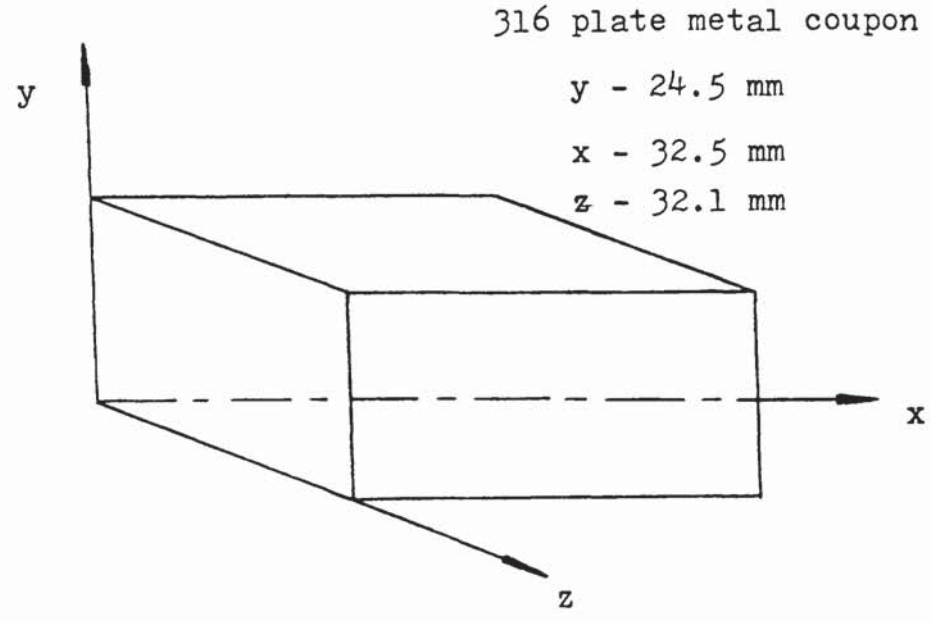

FIG. 3.1 : Austenitic weld and plate metal coupons used in velocity and attenuation measurements

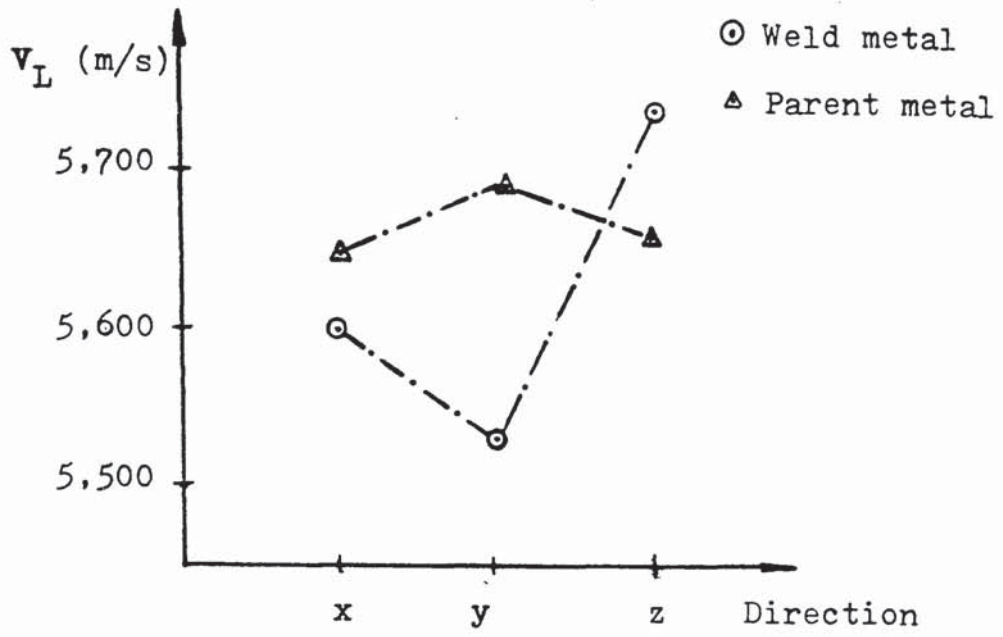

FIG. 3.2 (a) : Longitudinal velocity as a function of sound propagation direction

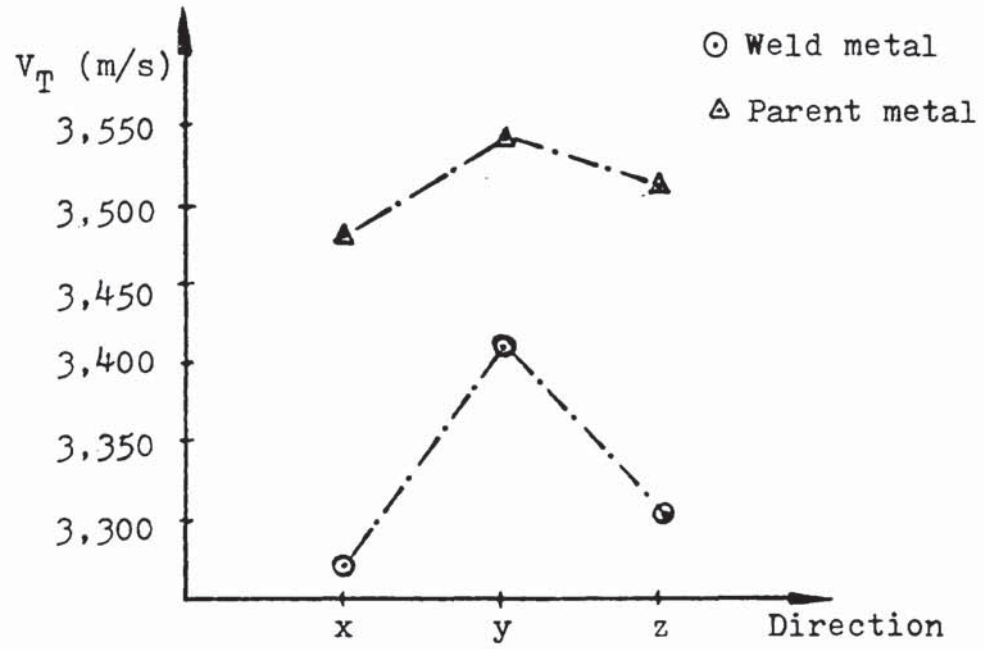

FIG. 3.2 (b) : Transverse velocity as a function of sound propagation direction

characteristics were to be measured, and using the calibrated gain switch only, the CRT screen was adjusted to show at least four backwall echoes. A convenient backwall echo was then chosen (say 2nd or 3rd) and its amplitude was recorded. Using the calibrated gain switch the first backwall echo was brought down to the level of the chosen one, and the amplitude drop in dB was recorded. Knowing the distance involved between the two echoes i.e. twice the metal thickness for the 1st and 2nd echoes, and three times the metal thickness for the 1st and 3rd echoes etc. the attenuation in dB/mm could be calculated in the chosen direction from the amplitude drop involved.
These results are shown graphically in Figure 3.3.

3.4 Preferred Orientation Measurements

A specimen was prepared from the 316 austenitic plate coupon of Figure 3.1 with dimensions 25 mm square and 3 mm thick. The specimen was mounted on a Siemens x-ray goniometer in order to establish the existence of texture in the plate material. The Schulz Reflection Method was used as described in reference (90). The specimen was found not to possess any texture.
Another specimen was prepared from the 316 weld metal coupon of Figure 3.1, together with a weld strip cut out from a 316 single-V weld (Fig.3.4), and the Electron Channelling

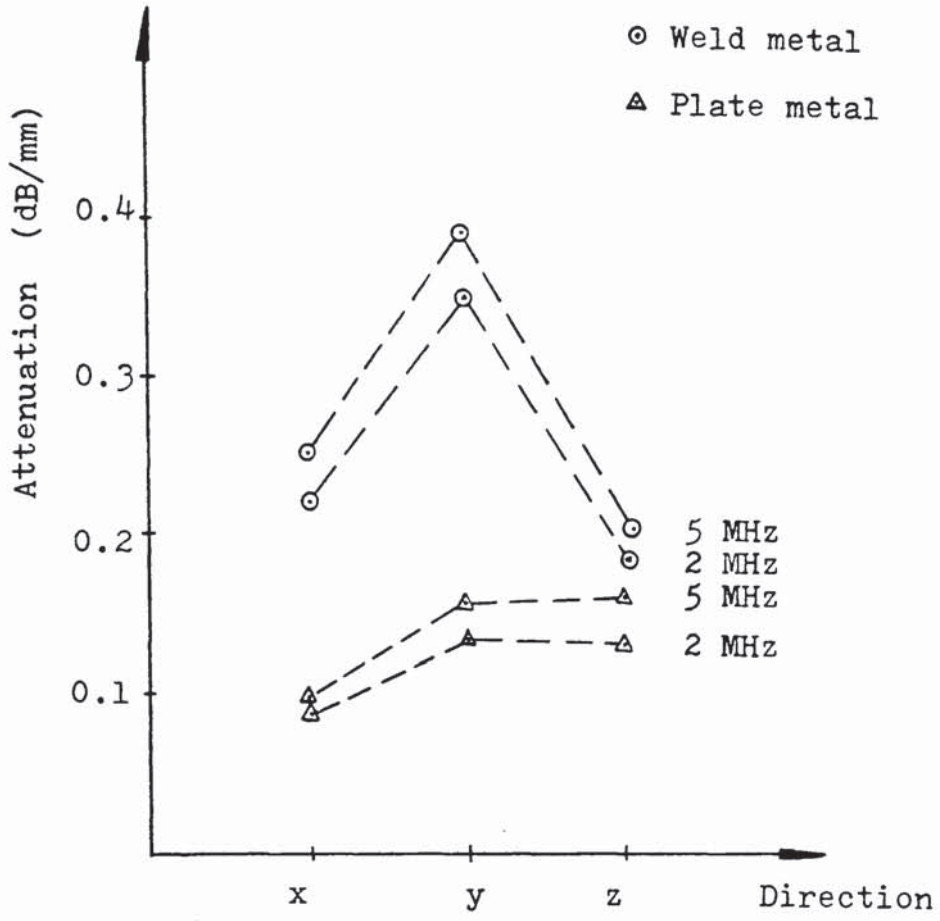

FIG. 3.3 : Attenuation as a function of propagation direction using conventional longitudinal wave probes

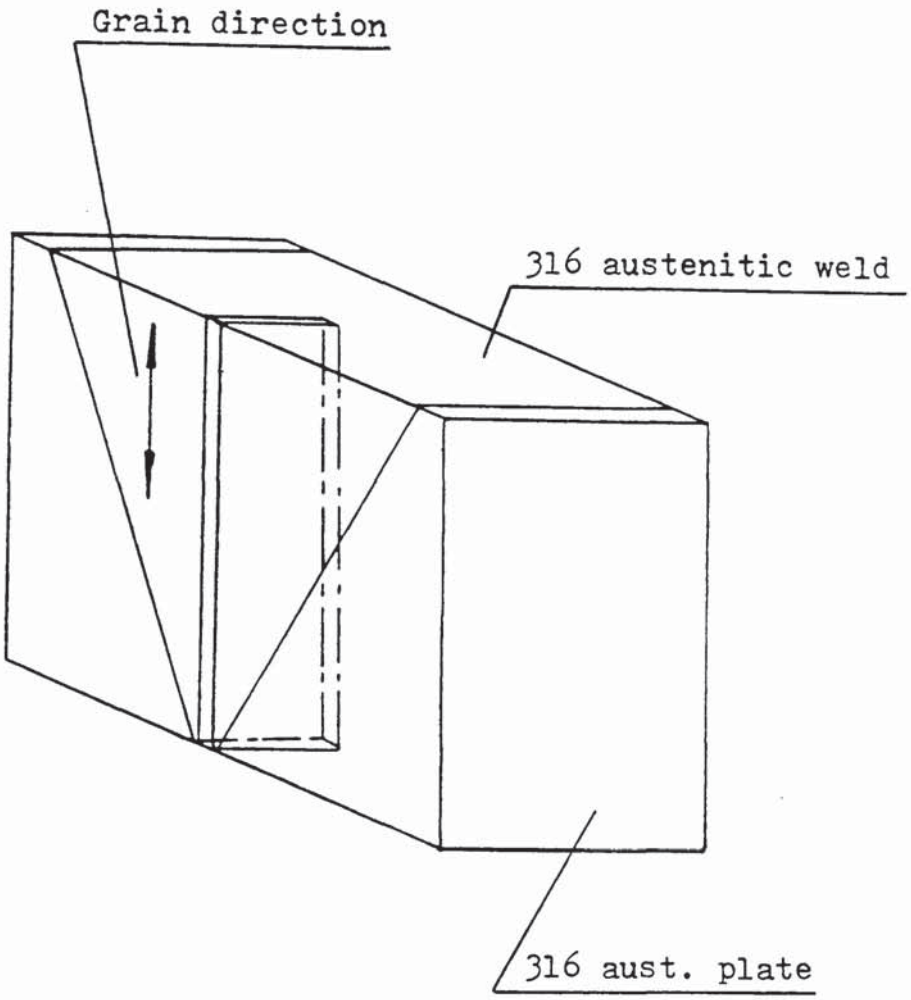

FIG. 3.4 : Strip cut from a 316 Single-V austenitic weld to be used for preferred orientation measurements by the SAECPs technique

Patterns technique (ECPs) was employed using a Scanning Electron Microscope (SEM) in order to locate the orientation of the columnar grains existing in these welds. The development of the rocking beam method in the (SEM)[94], enables ECPs to be recorded from small selected areas of strain free crystalline specimens. The ability to identify the orientation of small areas ($\geqslant 10\,\mu m$) has potential applications in many fields of metallurgy.

A convenient way of identifying the orientation from a given ECP, is to refer it to a composite map extending over one or preferably two crystallographic unit triangles[95]. The map is made by joining together a number of SAECPs from a large crystal of the same material tilted to different orientations. Figure 3.5 and 3.6 show typical SAECPs from the weld specimens used, and the composite map used for their identification. The map can be used to locate the orientations of grains and subgrains to within 2^{o}. Marking the position of each grain on an overlay on the composite map, it was established that the weld metal contained long columnar grains with a major axis along a $\langle 100 \rangle$ crystallographic direction, with a random alignment in the weld plane.

3.5 Examination of Welded Samples

Initially a block containing artificial reflectors was manufactured from 316 austenitic plate material (Fig. 3.7) and distance amplitude responses were obtained using all the probes later to be used for inspection of the welded

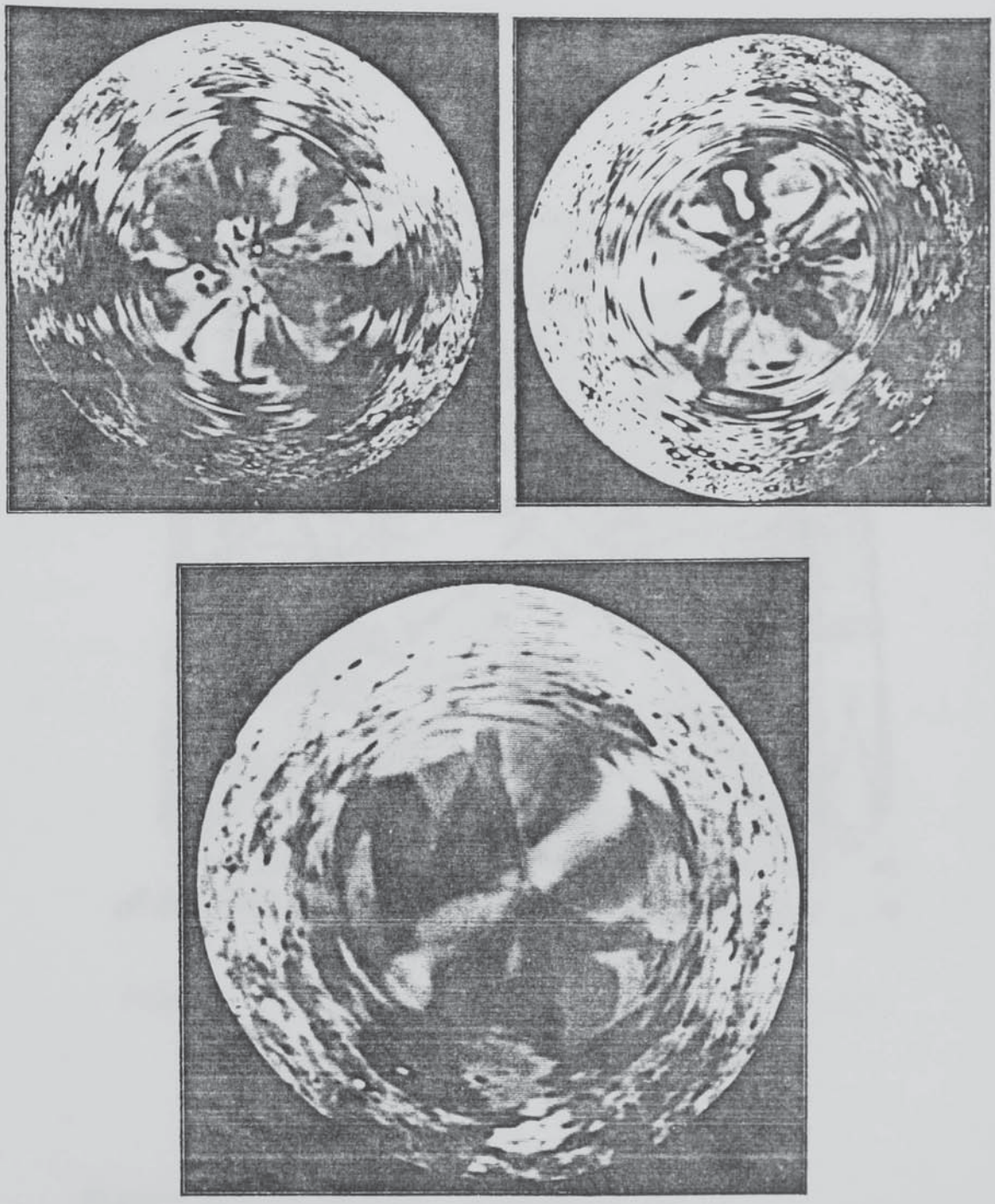

FIG. 3.5 : Typical SAECPs from 316 austenitic weld metal samples

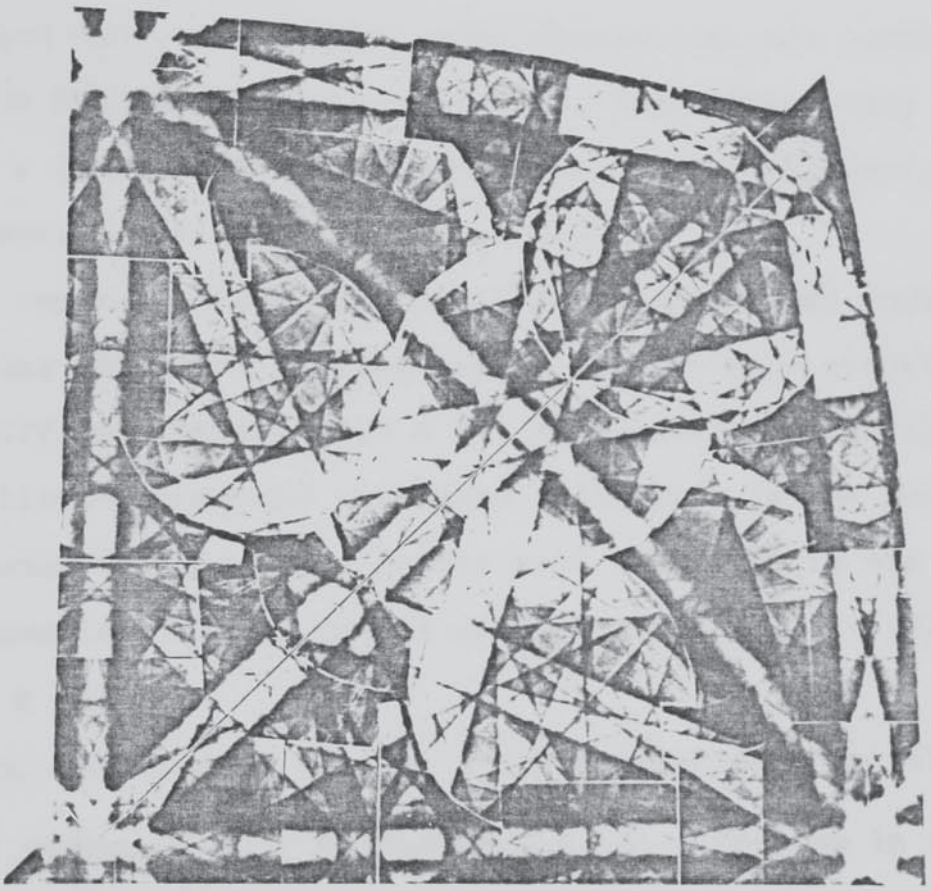

Figure 3.6 : SAECPs - composite map of two adjacent unit triangles for f.c.c. crystal symmetry

samples. These results are shown in Figure 3.8 (a) & (b). In general negligible variations were observed in any of the measured plate parameters. Noise levels for the plate material were not noticeably different than for mild steel test pieces.

A comparison between different wave frequencies was carried out using 2 MHz and 5 MHz conventional longitudinal wave probes on a 50 mm thick 316 single-V austenitic weldment, and the results are shown in Figure 3.9.

Next, the inspectability of austenitic weldments was investigated, using blocks of varying sizes, various weld geometries, and two different grades (316 & 347 austenitic materials). The test blocks contained reference reflectors in the form of horizontal drilled holes in the weld metal and in the fusion lines (weld metal/parent metal interfaces), see Fig. 3.10. (a) & (b).

The general conclusions of this investigation were as follows:

(i) The attenuation of ultrasound is not a problem in thin (less than 11 mm) austenitic steel weld. Shear waves give better results than longitudinal waves , and higher frequencies (5 MHz) should be used in thinner welds. Larger beam angles (70^{o}) should be preferred although satisfactory results were obtained by using 45^{o} and 60^{o} angle probes. Using longitudinal angle wave probes when direct scanning is possible, double crystal probes performed better than single crystal probes.

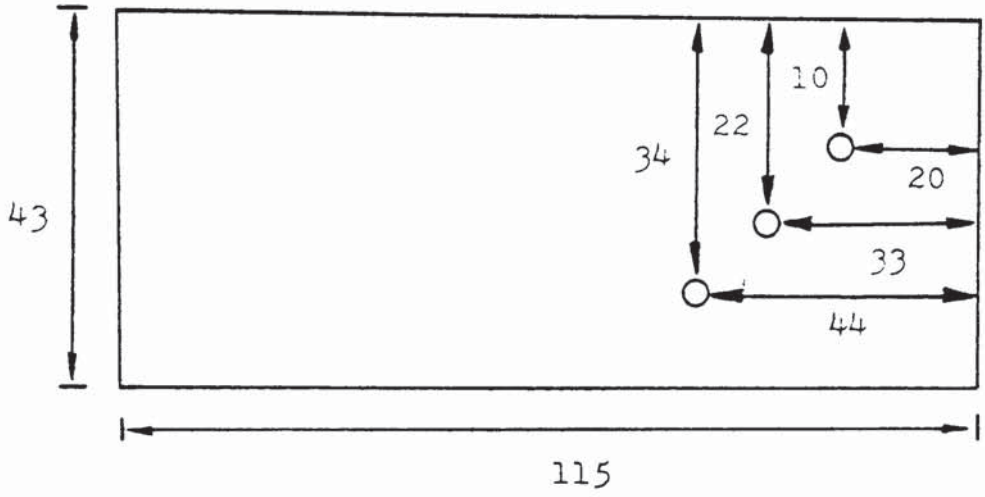

Block Material : 316 austenitic rolled plate

Block Thickness: 21 mm

Hole Diameter : 2.8 mm

All dimensions in mm

FIG. 3.7 : Test block T_1 containing artificial reflectors

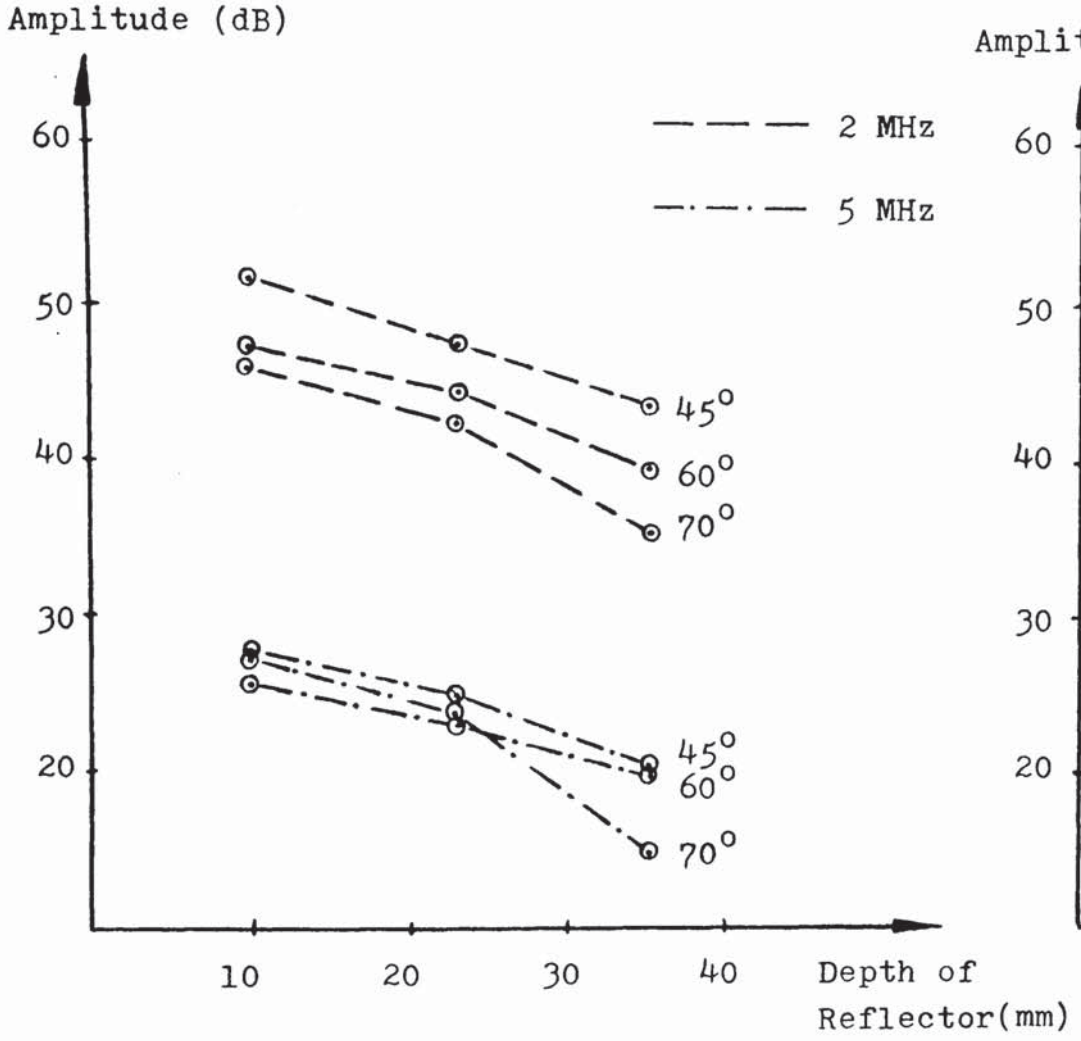

FIG. 3.8 (a) : Responses from reflectors in test block T_1, using transverse wave probes

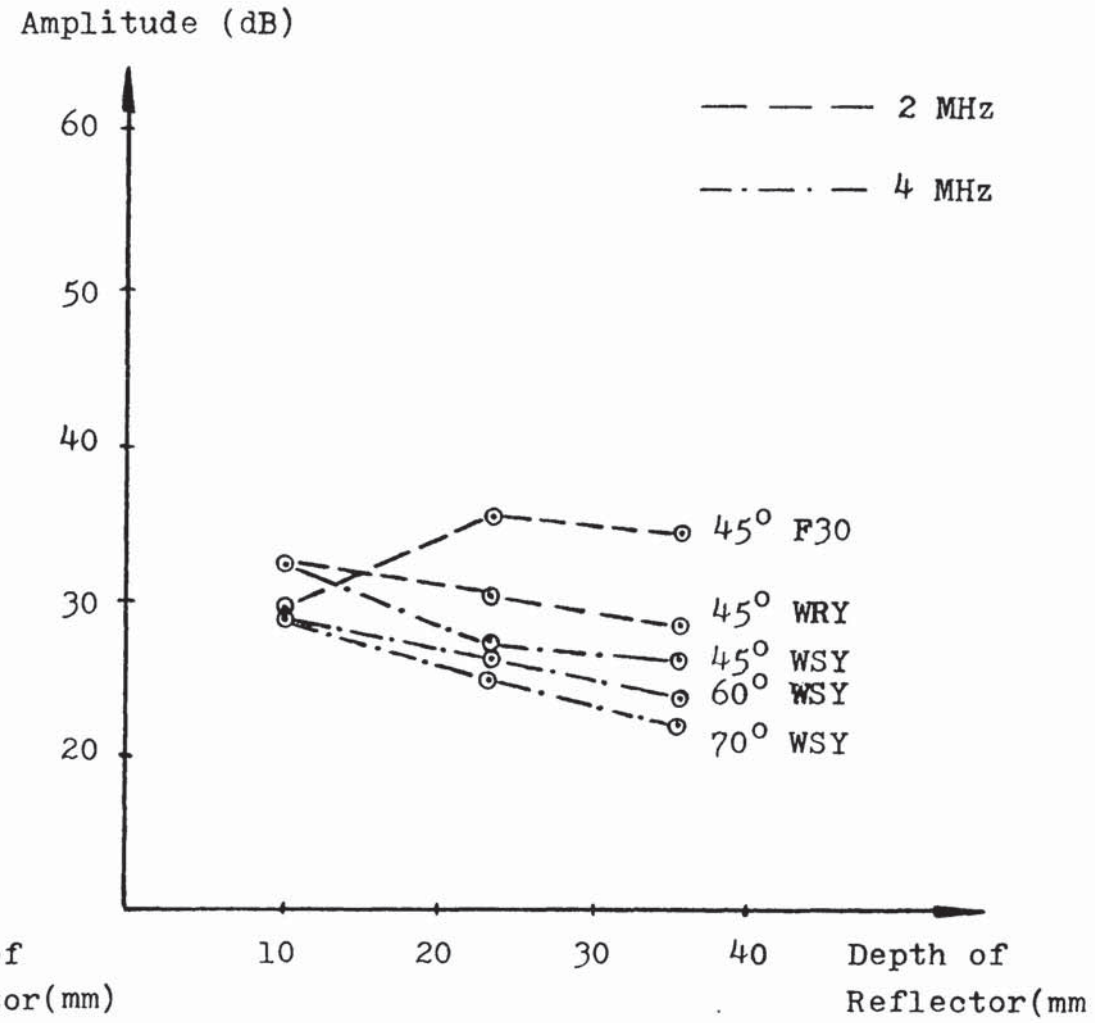

FIG. 3.8 (b) : Responses from reflectors in test block T_1, using longitudinal wave probes

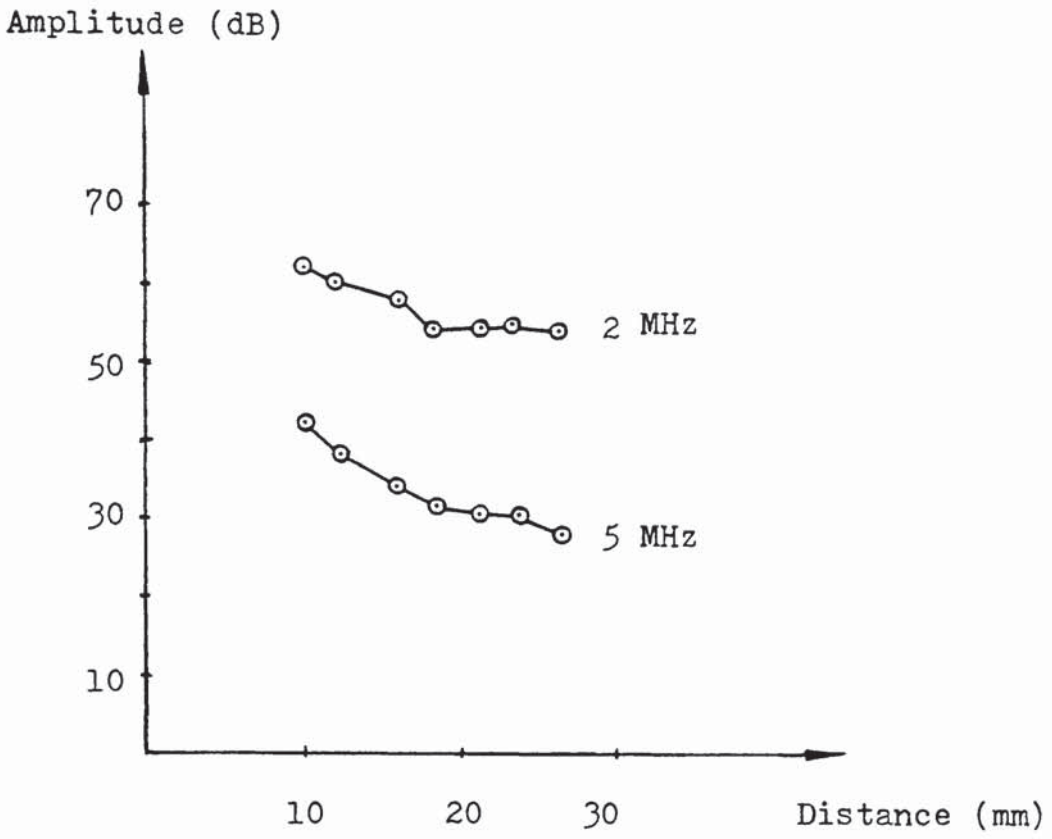

FIG. 3.9 : Comparison of 2 MHz and 5 MHz longitudinal waves travelling through various distances in 316 austenitic weld metal, using conventional longitudinal probes (0^{o}) to obtain backwall echoes at different weld depths

All dimensions in mm

Hole diameters 2.8 mm

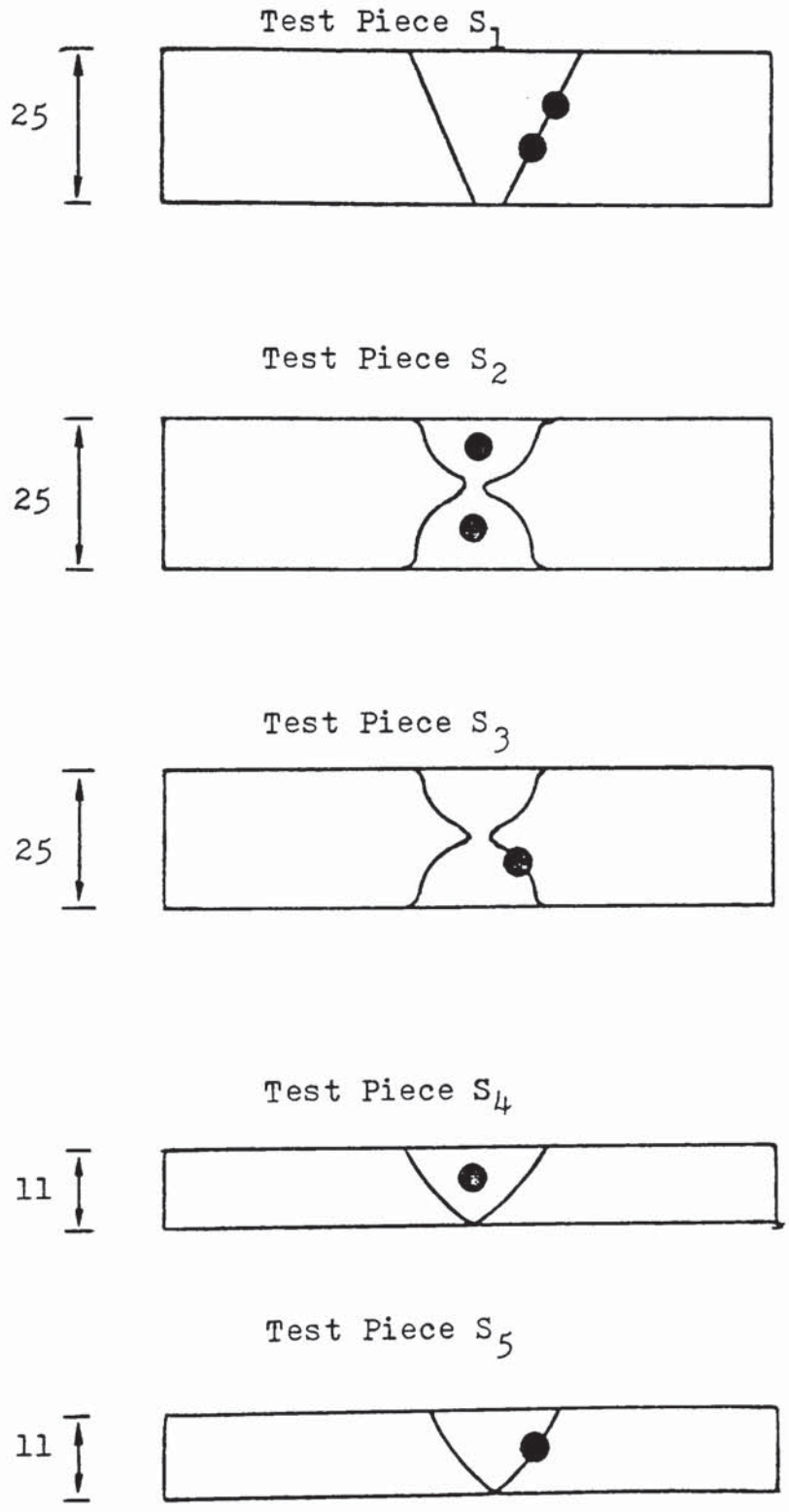

FIG. 3.10 (a) : Test pieces containing artificial reflectors

All dimensions in mm

Hole diameters 3.0mm

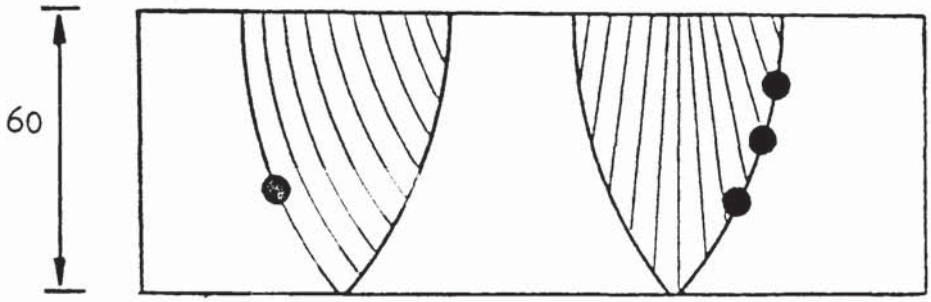

Test Piece S_6

Fine grained plate material

Coarse grained plate material

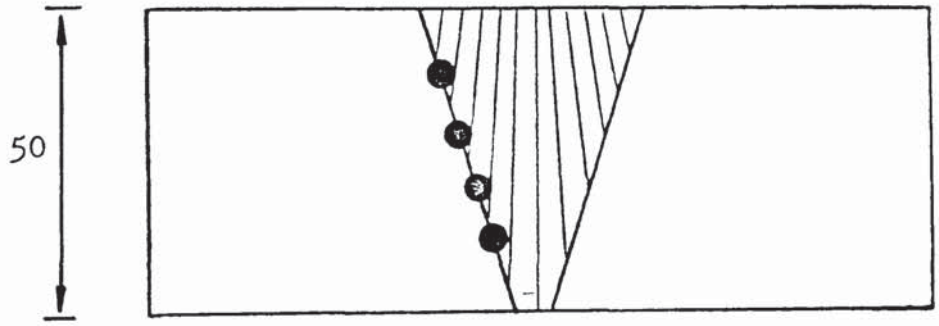

Test Piece S_7

FIG. 3.10 (b) : Thick austenitic test pieces containing artificial reflectors

(ii) Although ultrasonic inspection of austenitic weldments is difficult using conventional shear angle probes, lower frequencies and the use of 45° beam angle improve the standard of inspection. Reflectors existing in the parent/weld metal interfaces could be readily detected using both 2 MHz and 5 MHz frequencies and 45°, 60° and 70° beam angles, when the scanning involved ultrasound propagating through plate material only. When inspection involved propagation of the ultrasonic waves through the bulk of the weld metal, the weld was rendered uninspectable using higher frequency probes. The same artificial reflectors could be detected using the lower frequency probes.

(iii) Considering the response of different probe angles, frequencies and wave modes from the two different grades of austenitic weldments (viz. 316 and 347), the composition of the parent plates and weld deposits appear not to have a significant effect on the inspectability of the artificial reflectors. What appears to have significant effect on the behaviour of ultrasound is the structure of the weld itself and the size of the weld, i.e. narrower welds exhibited better inspectability than thicker welds. The effect of weld structure manifested itself as spurious indications and low signal to noise ratios.

Having established that austenitic welds contain long columnar grains with a major axis along a <100> crystallographic direction, it was proposed that this structure creates a gradual bending of the sound beam entering the weld metal, thus giving rise to false indications. These bending effects together with indications from fusion boundaries, were attributed to velocity differences existing between the plate and the weld material creating refraction, and also impedance mismatch. These two effects are demonstrated in Figures 3.11 and 3.12 respectively.

(iv) Inspecting thick weldments (between 45 and 60 mm), proved to be an impossible task for conventional transverse wave techniques even using optimum angles and frequency. Depending on the coarseness of the plate material, detecting artificial reflectors existing on the fusion boundaries was possible using conventional transverse wave 2 MHz probes with the ultrasound travelling through plate material only. Once the grains of the plate material were comparable to the wavelength used, the inspectability of the reflectors was drastically reduced.
Longitudinal wave angle probes seem to eliminate most of the problems involved in transverse wave inspection of thick austenitic weldments, so their use appears promising in achieving a realistic standard of

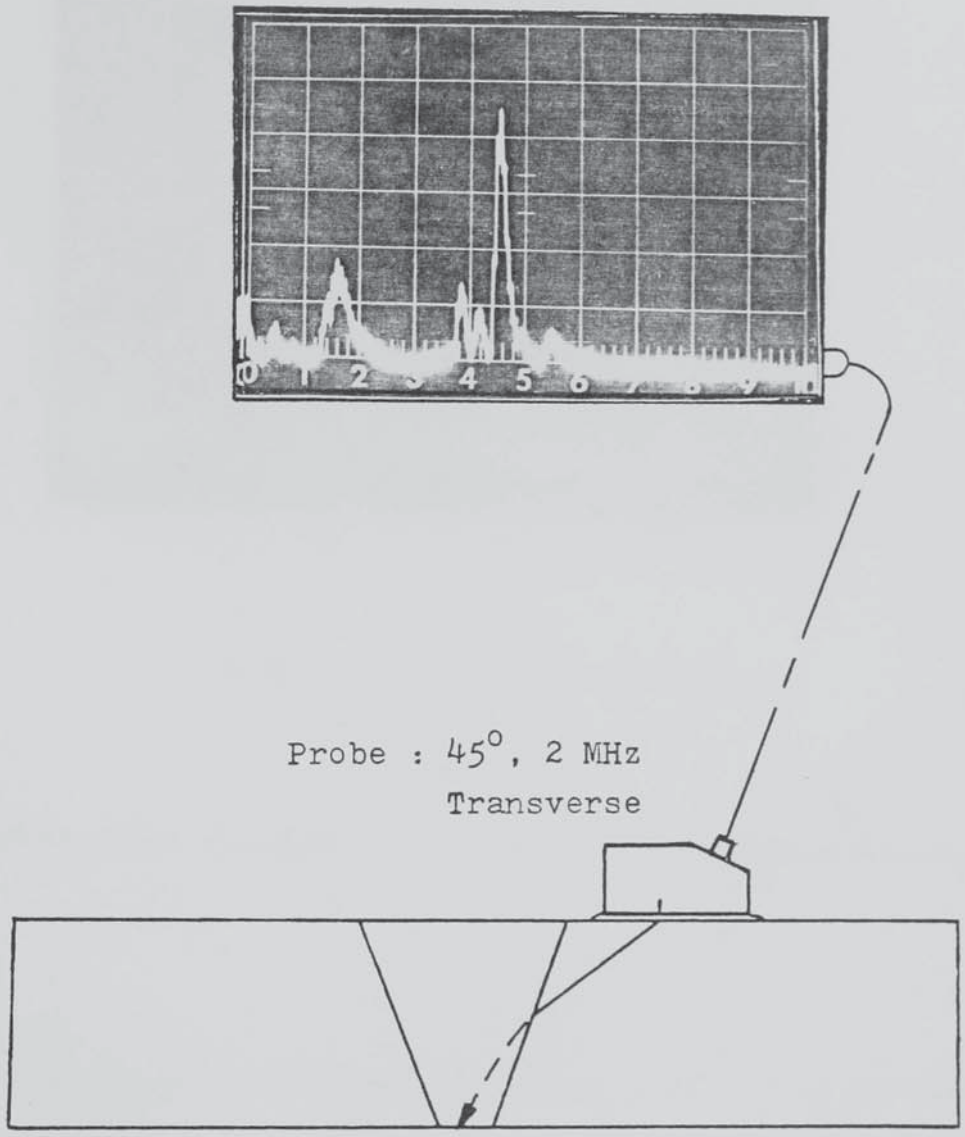

FIG. 3.11 : False indication due to beam skewing

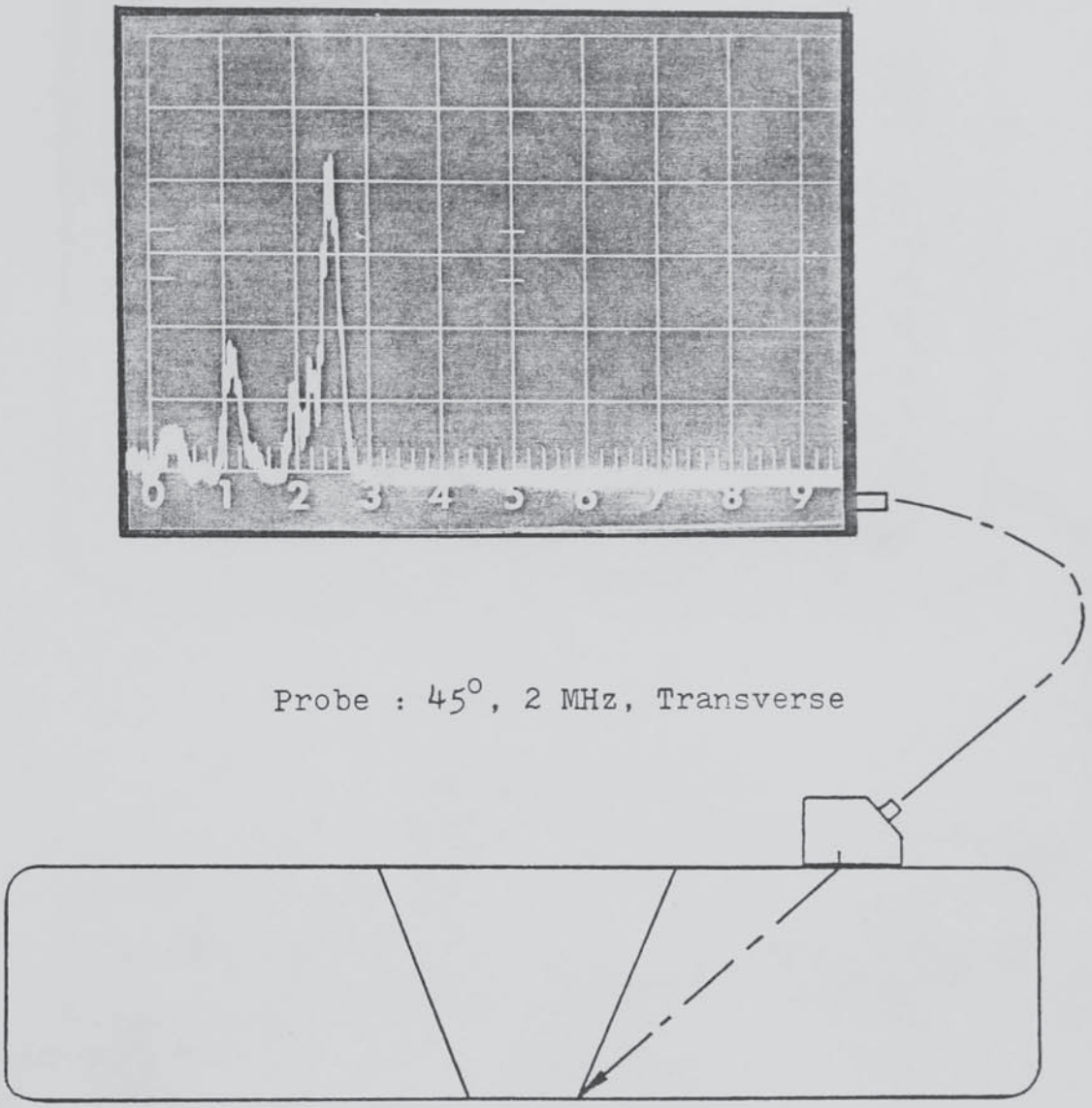

FIG. 3.12 : False indication resulting from impedance mismatch between plate and weld metals

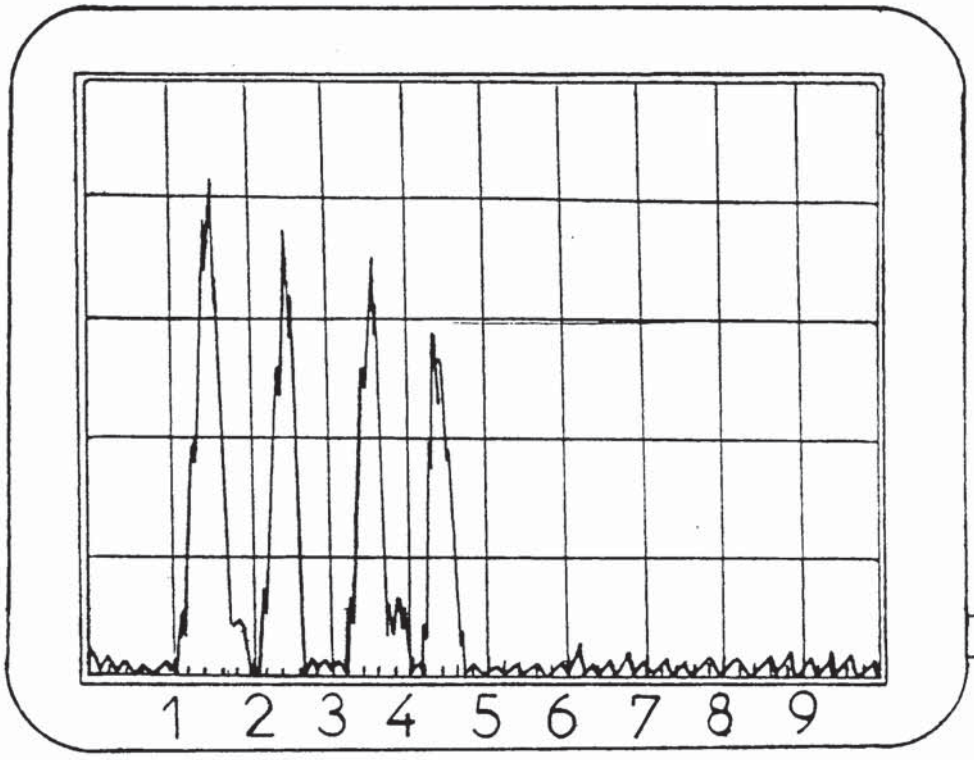

Test Piece S_7

Hole diameter 3 mm

Probe : WRY 45° Lo.

$$\cos \beta_L = \frac{d}{S + \frac{1}{2} D}$$

d (mm)	β_L (degrees)
8.5	52.6
18.5	45.7
27.5	42.0
35.5	40.2

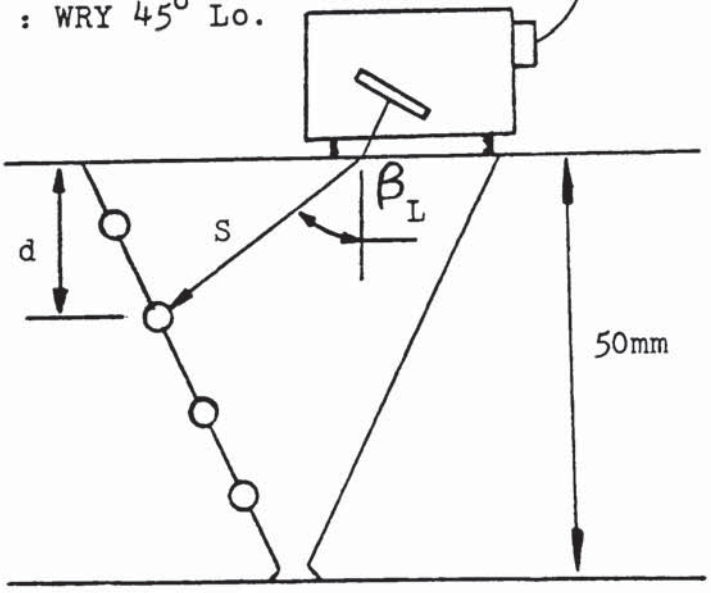

FIG. 3.13 : Establishing beam angle values in thick 316 austenitic weld material, using longitudinal wave angle probes

examination in such weldments. Using longitudinal wave angle probes better signal to noise ratios were obtained, less beam deviation was observed, and all artificial reflectors were clearly identified even when the ultrasonic waves had to travel considerable distances through austenitic weld metal (reflectors located at 34 mm depth from the surface of the weld). The main drawback in using these probes was the simultaneous emission of transverse waves, which made signal identification more complicated, and at the same time limited inspection to half skip scanning positions only.

Using the test block and conventions outlined in Fig. 3.13, it was observed that when the probe was situated to the left of the weld centre line, the sound-beam exhibited a positive deviation resulting in larger angle values. When the probe was over the weld centre line, the angle beams observed were closer to the expected values, and when the probe was to the right of the weld centre line, a negative deviation of the beam was observed in the form of reduced angles. These findings are shown schematically in Figure 3.14. Finally, using test piece S_7 and a V2 calibration block manufactured from 316 austenitic plate material, the results shown in Figures 3.15, 3.16, 3.17, 3.18, 3.19, 3.20 were obtained.

Test Piece S_7

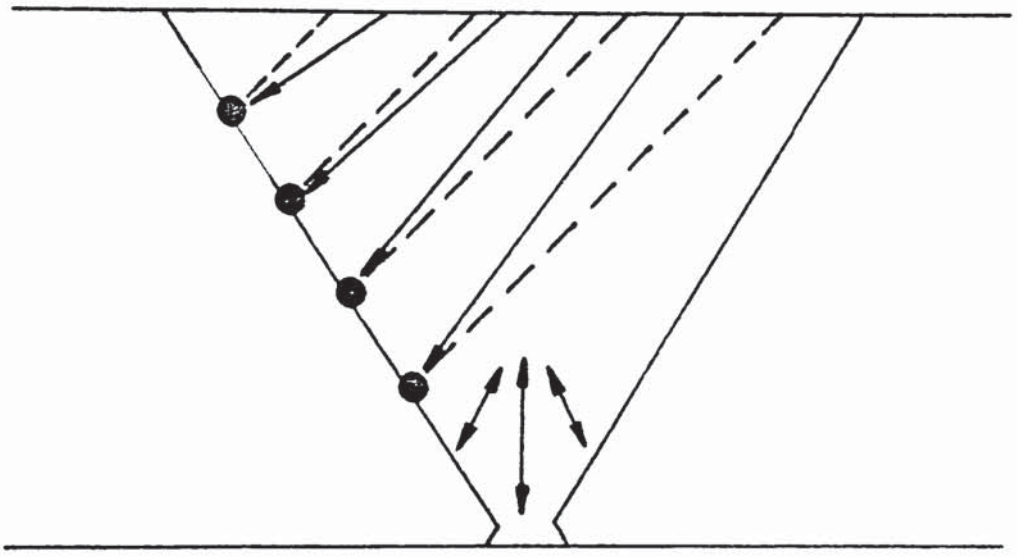

45° Direction — — — — —

Actual Beam Direction ————————

Major Grain Directions ⟵⟶

FIG. 3.14 : Schematic representation of beam skewing in thick austenitic weld material

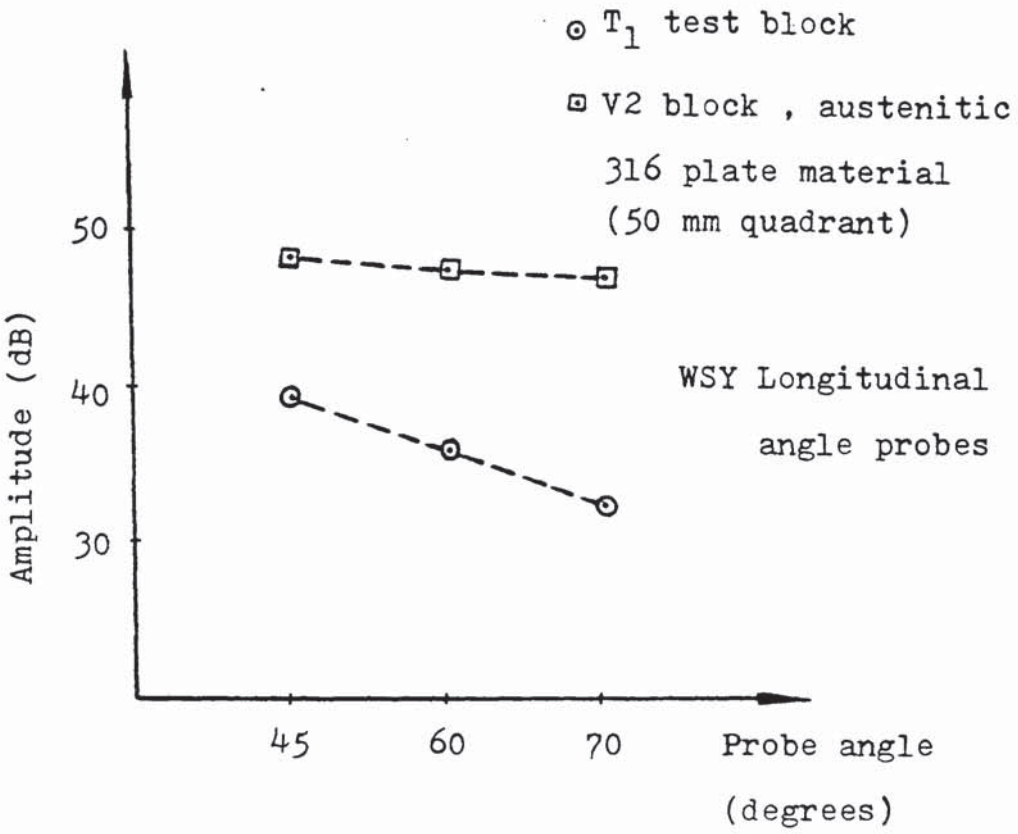

FIG. 3.15 : Amplitude response from austenitic plate material using longitudinal angle probes

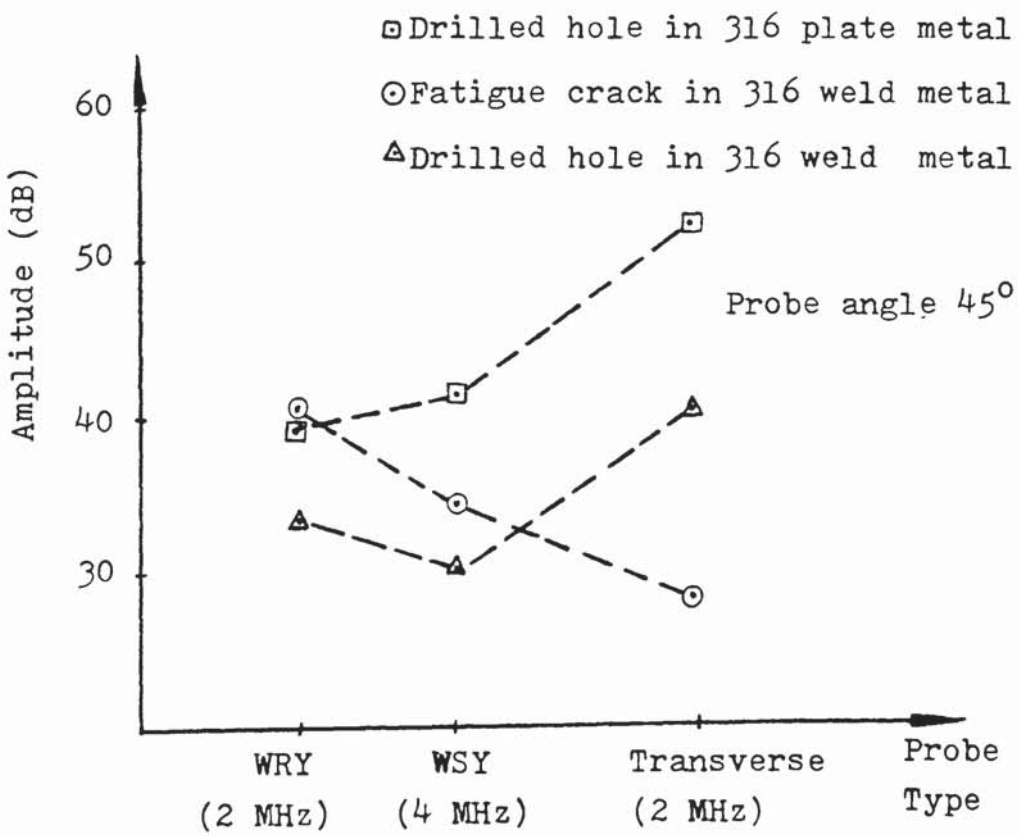

FIG. 3.16 : Amplitude responses from various reflectors using longitudinal and transverse 45° probes

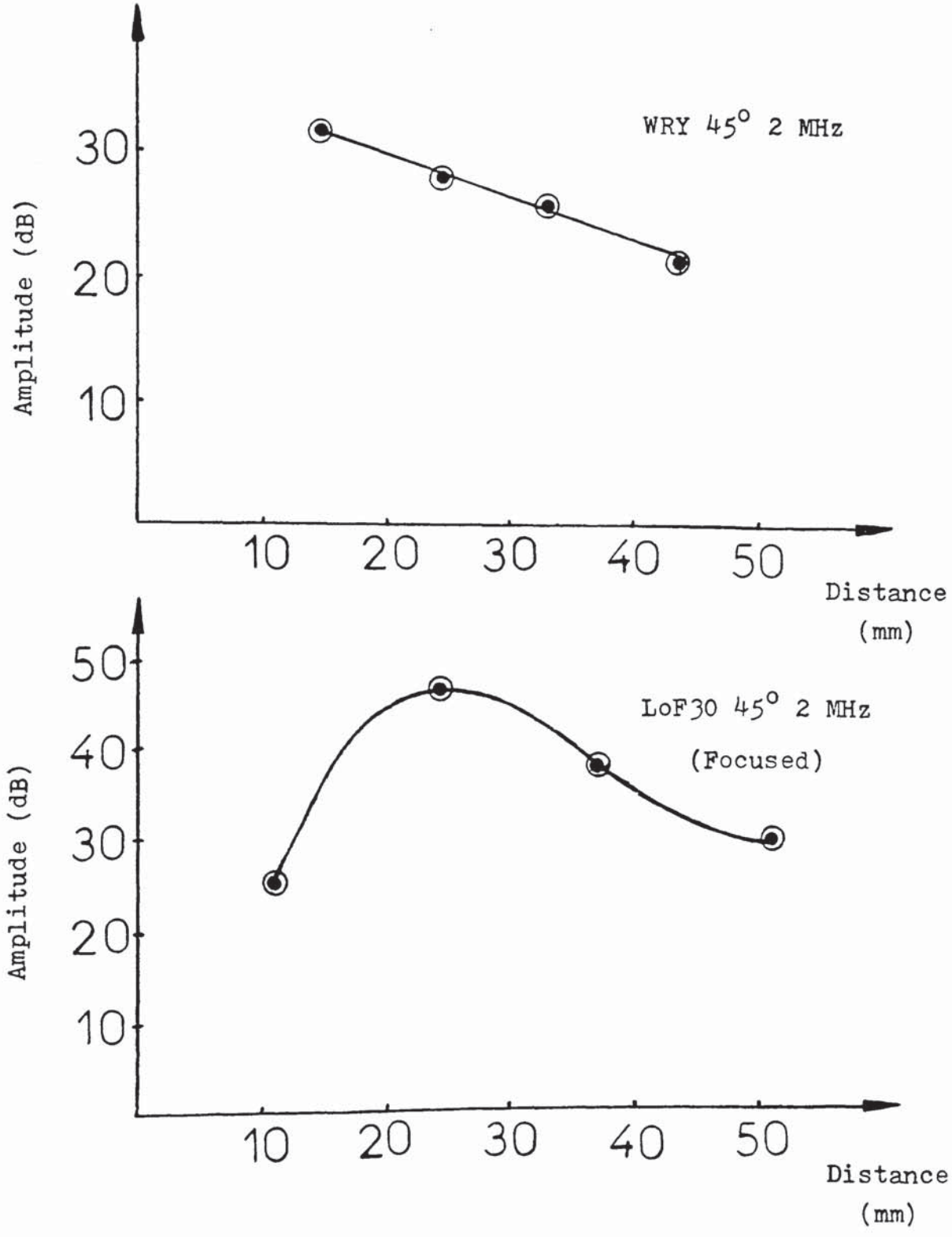

FIG. 3.17 : Amplitude response from reflectors in test piece S_7 scanning through the weld metal

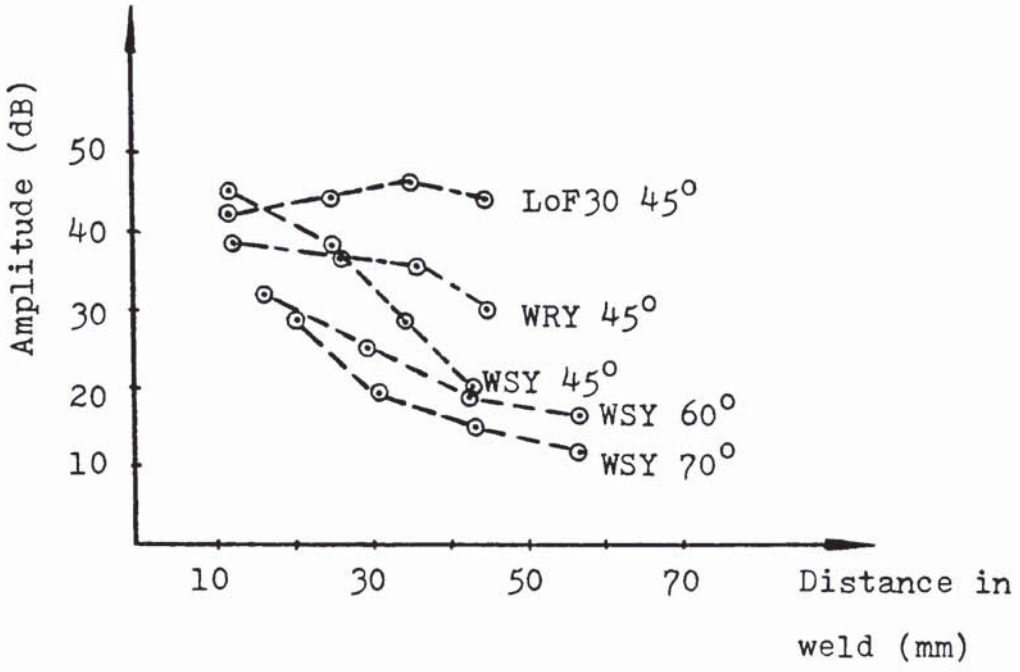

FIG. 3.18 : Amplitude responses from reflectors in test piece S_7, using various longitudinal angle probes scanning through the weld metal

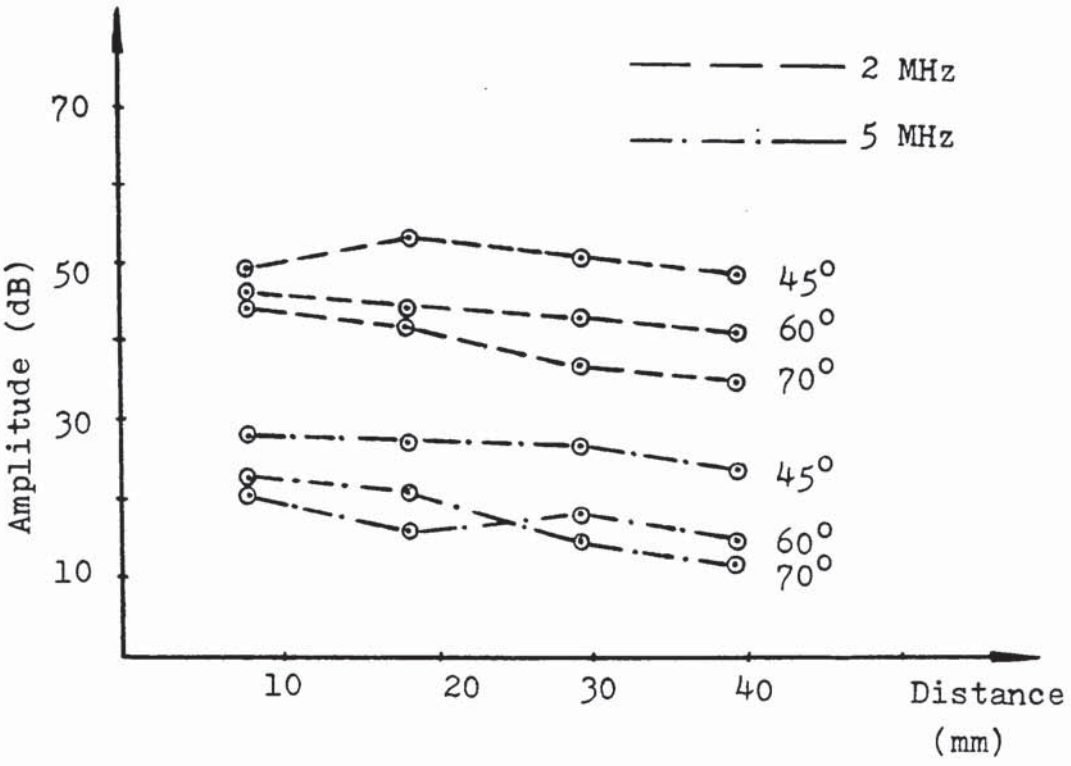

FIG. 3.19 (a) : Responses from reflectors in test piece S_7 using transverse probes scanning through plate metal only

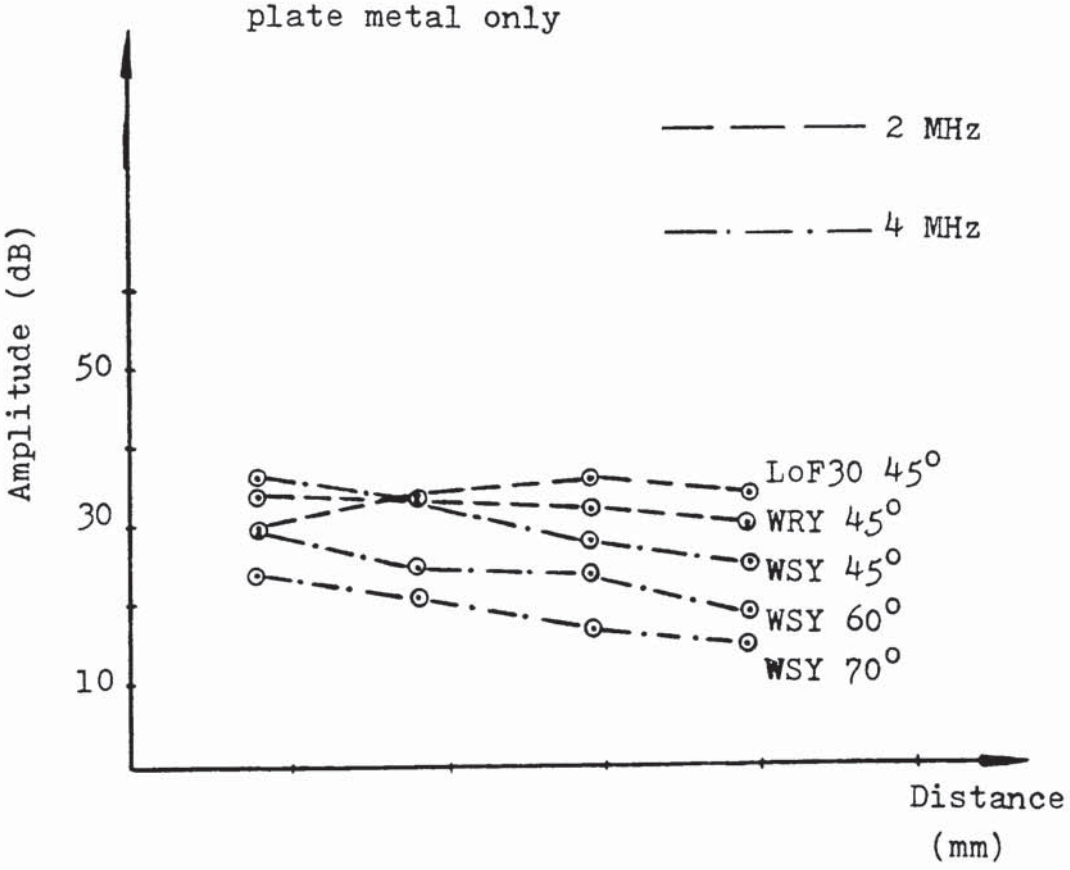

FIG. 3.19 (b) : Responses from reflectors in test piece S_7 using longitudinal angle probes and scanning through plate metal only

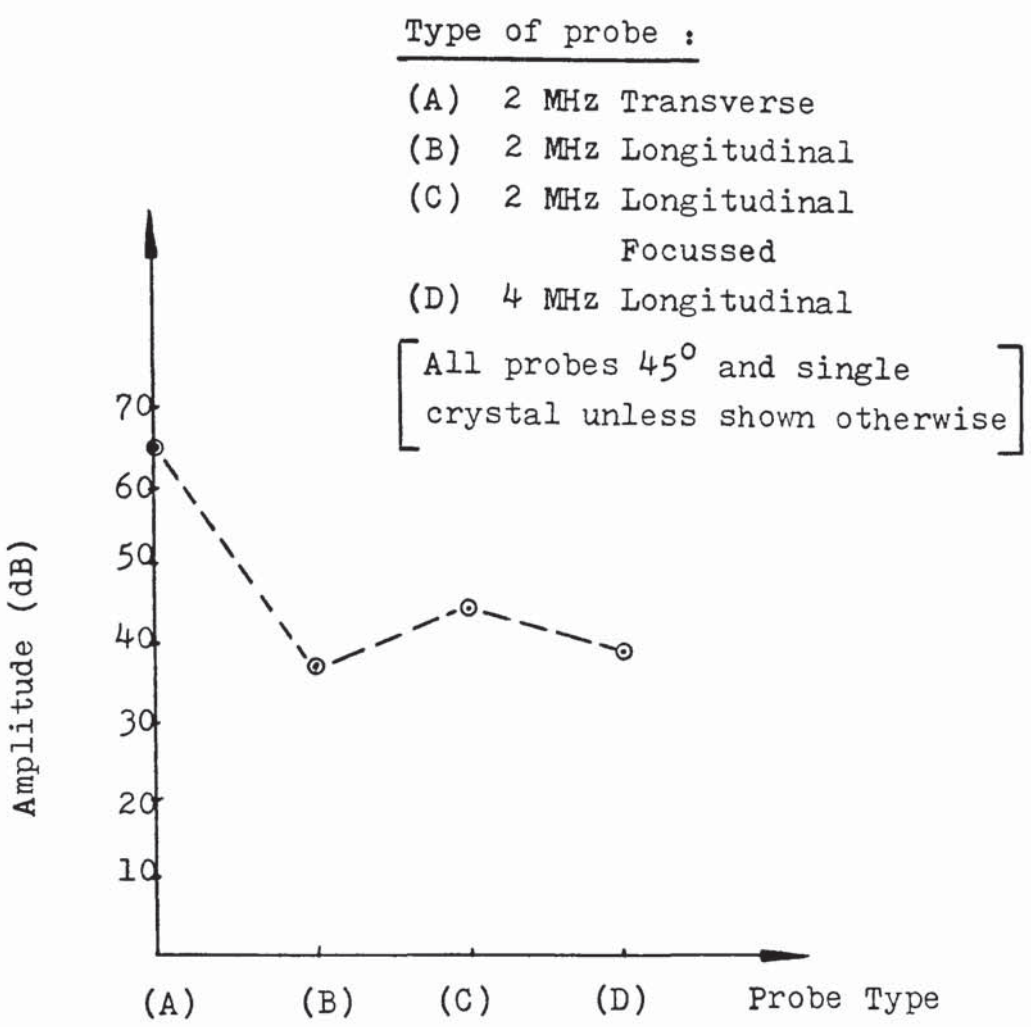

FIG. 3.20 : Amplitude responses from V_2 block manufactured from 316 austenitic plate metal, using 45° longitudinal and transverse probes

3.6 Programme of Further Work

This initial investigation led to specific conclusions which defined the programme of further work as follows:

1) The preferred texture of austenitic stainless steel weld metal leads to variations in ultrasonic velocity and attenuation when using both longitudinal and transverse waves. Assessment of the velocity variations in these welds could provide indications on the variance to be expected in flaw location within the weld metal, and would no doubt lead to a better understanding of the fundamental aspects involved in the propagation of ultrasonic waves in such welds.

2) Detecting artificial reflectors using a range of probe angles, frequencies and wave modes, resulted in useful comparisons and indications on optimization of these parameters. Repetition of these experiments using real flaws would yield particularly useful data, such as how ultrasound interacts with real defects, the effect of angle and mode choice, minimum size of detectable defect etc. The latter being very important since the minimum detectable defect size must be less than or equal to the critical defect size as defined by fracture mechanics.

3) Longitudinal wave angle probes alleviate the problems presented by transverse wave angle probe inspection of

austenitic weldments, especially when they are over 25 mm thick.

Establishing performance data of longitudinal wave probes, using various angles of incidence, through various weld structures, geometries and thicknesses, by detecting artificial and real defects, would result in useful guidelines for ultrasonic inspection of austenitic weldments using this wave mode.

4. ULTRASONIC WAVE PROPAGATION IN AUSTENITIC WELDMENTS

4.1 Introduction

The structure of welds in austenitic stainless steels has been discussed by several authors[21,96,97].
The austenitic weld grain structure is markedly different from that of ferritic welds. In both cases, the solidification process during welding initially produces a columnar grain structure in each weld bead. Grains grow along the maximum thermal gradients in the bead along a <100> crystallographic axis. Growth in this direction is faster than in others and this leads to the rapid disappearance of unfavourably oriented grains. Deposition of subsequent weld metal reheats the bead and, although in the case of a ferritic weld the columnar grain structure is destroyed by the austenite-ferrite phase transformation that occurs as the solid cools, no such transition occurs in the austenitic alloys, and consequently the columnar grain structure survives. Furthermore, each new weld bead remelts the surface of the preceding beads and the new beads grow "epitaxially" on the existing ones. Consequently, large large columnar grains are produced as shown in Figure 4.1. This shows macro-sections of a double-U and a single-V weld, made by the manual metal arc (MMA) process, using 316 Staintrode 63.30, and 347 Nicrex NDR electrodes respectively.

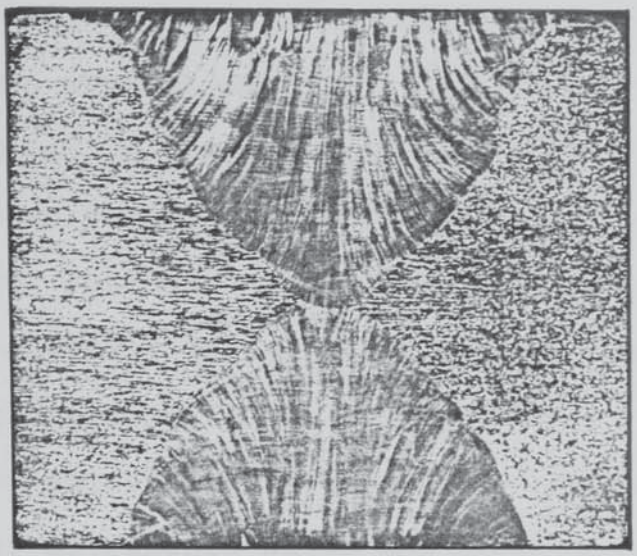

316 Austenitic Weldment, made by the MMA process, etched in Ferric Chloride, showing the long columnar grains extending through several weld runs.

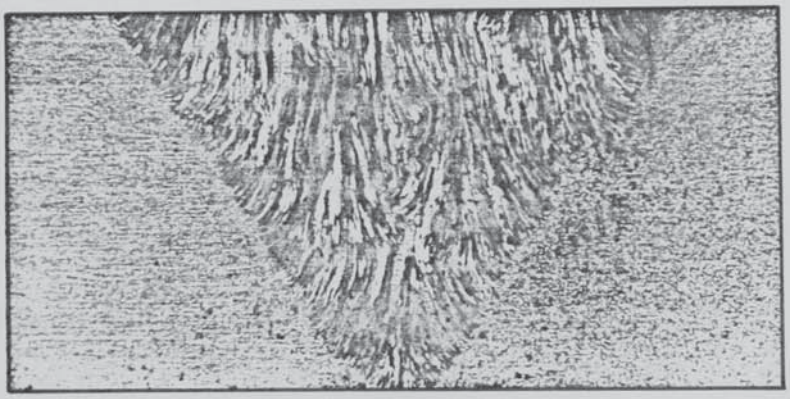

347 Austenitic Weldment, made by the MMA process, etched in Ferric Chloride, showing the long columnar grains extending through several weld runs.

Figure 4.1 : Macrographs of austenitic welds etched in Ferric Chloride.

Austenitic welds, therefore, contain long columnar grains aligned in the through thickness direction, with near random alignment in the plane of the weld. The result approximates an "orthotropic" or "uniaxial" material. Because of the elastic anisotropy of austenite and compounded with the effect of epitaxial growth, the whole weld region is anisotropic.

The effect of anisotropy is to produce anomalous refraction or skewing of ultrasonic waves and complex changes in the group velocity as a function of propagation direction[25,26,98]. It was experimentally established by Baikie et al[21] that a cyclic variation of velocity exists with respect to the grain direction in austenitic weldments, and for longitudinal waves propagated in a 316 MMA weld metal, a velocity maximum occured at approximately 45° to the grain axis, whilst minima existed parallel and perpendicular to the grain axis. The range of velocities they observed was from about 5,350 m/s (at 0°) to 6,050 m/s (at approx. 45°). Tomlinson et al[22], and Kupperman et al[29] have also obtained experimentally similar findings.

These factors affect seriously conventional NDT Ultrasonic techniques, and at the same time the velocity variations can be expected to affect more recent techniques based on time domain[83] or spectrographic analysis[99].

Having established, using the Selected Area Electron Channelling Patterns technique (SAECPs), that austenitic welds exhibit long columnar grains with a major axis along a $\langle 100 \rangle$

crystallographic direction (sec. 3.4), with a random alignment in the weld plane, accurate experimental data of velocity variations in austenitic weld metals related to this preferred texture had to be established.

4.2 Ultrasonic Velocity Measurements

4.2.1 Technique and Equipment Used

The pulse-echo technique used, was originally developed by Bell[100] and used for ultrasonic thermometry. Slight modifications allowed the resonance frequency spectra for the longitudinal modes of thin strips to be obtained. The experimental arrangement used for this investigation is shown in Figure 4.2. The system consisted of a magnetostrictive transducer used to transmit and receive a burst of longitudinal stress waves along an acoustic line. The line was made out of nickel wire of 0.35 mm diameter, and was coupled to the resonator (strip) by a cementing agent (araldite). The line was sufficiently long to accomodate the number of waves needed to obtain the required echo pattern without signal overlap, and was annealed and then stretched in order to minimize the attenuation in the line material and the scattering from the grain boundaries. Resonance occurs when the transmitted wave frequency is exactly equal or a multiple of the mode frequency of the

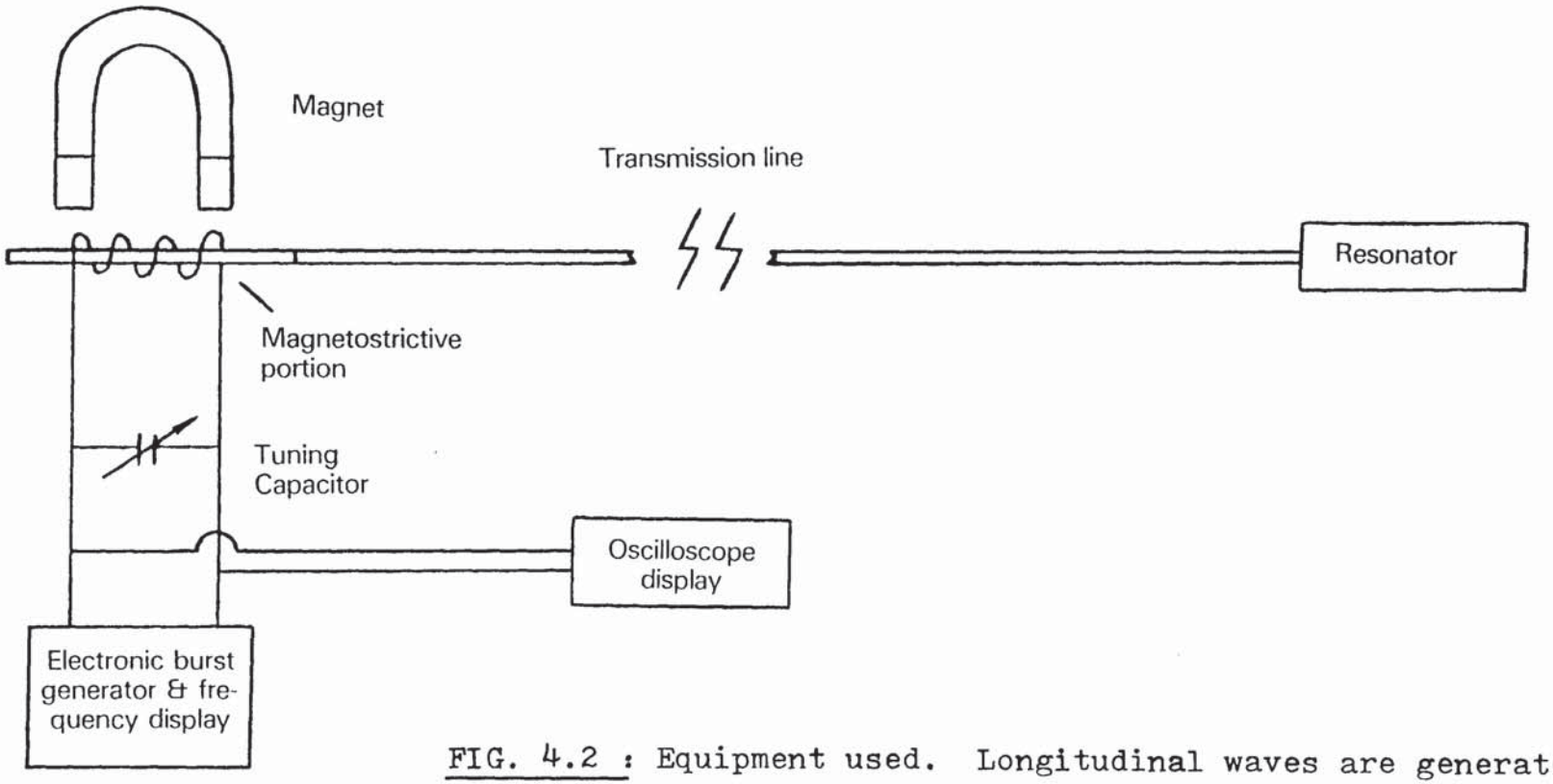

FIG. 4.2 : Equipment used. Longitudinal waves are generated and received by the magnetostrictive transducer, through the transmission line(wire). The ultrasonic velocity is measured by exciting longitudinal vibrations of the resonator

resonator, and measurements are carried out by displaying the signal returned from the resonator on an oscilloscope. In all applications only the first reflection of the transmitted signal is looked at in detail. This will be called the "echo". A typical echo, shown in Figure 4.3, consists essentially of two components; the echo-signal, and the echo-decrement. The echo signal is the direct return of the waves incident on the resonator, and is at the transmitted frequency. The echo decrement which follows is the exponential re-radiation of the energy stored, and is always at the natural frequency of the resonator.

To analyse the echo pattern, a mathematical model of a simple lossless line resonator has been developed by Sharp [101]. The echo in this situation produces a distinctive cross-over "null", providing a precise setting of frequency. The number of oscillations to the cross-over, is a function of the delay line cross-section and the properties of the resonating material. The samples to be used could be of a variety of geometrical forms depending upon the parameters to be measured and also on the availability of the theoretical solutions of the modes excited.

The samples used were manufactured as thin narrow strips because :

(i) the frequencies for different modes of vibration are proportional to each other, and this form of resonator would give a reasonable and measurable figure for the

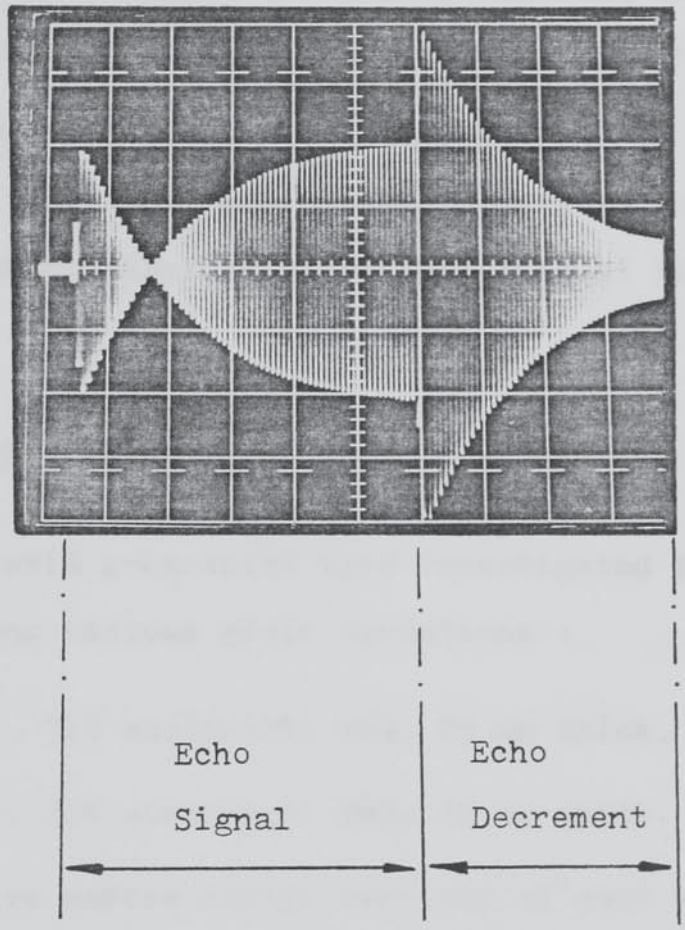

FIG. 4.3 : Typical echo pattern obtained from strip cut out of the single-V 316 austenitic weld. The crossover indicates that the frequency of the transmitted waves (drive frequency) is equal to the strip resonance. The two components of the echo are shown; the echo signal which has the same duration as the transmitted burst, and the echo decrement which is the re-radiation of the energy stored

frequency of the waves,

(ii) this form of resonator could effectivelly be cut-out from the weld metal containing long columnar grains at various angles as shown in Figure 4.4.

The method described above was successfully used by Bell et al[102,103] for measuring elastic constants and for ultrasonic characterisation of refractories at high temperatures.

4.2.2 Materials Used

Two different weld geometries were investigated for velocity variations along various grain directions :

a) A double-U, 316 austenitic MMA, 25 mm thick, and

b) A single-V, 316 austenitic MMA, 50 mm thick.

Originally, five narrow strips were cut of each weld, in such a way as to contain grains oriented at 0^{o}, 22^{o}, 45^{o}, 67^{o}, and 90^{o} with respect to their length direction as shown in Figure 4.5. The sizes of these strips were limited by the weld geometries and the physical size of the welds. Details of the resonators (strips) are shown in Table 4.1. The velocity measurements obtained using these resonators have been published in reference (104), but in order to increase the accuracy of these results, a second set of strips was machined from the same welds, details of which are given in Table 4.2.

Weld Geometry	Double-U_1					Single-V_1				
Grain Direction (degrees)	0	22	45	67	90	0	22	45	67	90
Length of strip (mm)	21.4	21.2	19.3	9.3	17	66.6	53.6	58	49.7	60.6
Width of strip (mm)	4.7	4.0	4.3	3.2	4.1	5.8	5.9	6.3	6.0	5.8

Table 4.1 : Details of resonators (strips) cut from the double- U_1 and the single-V_1 welds.

Weld Geometry	Double-U_2					Single-V_2				
Grain Direction (degrees)	0	22	45	67	90	0	22	45	67	90
Length of strip (mm)	21.0	21.2	18.5	10	18	65	55	60	50	59
Width of strip (mm)	4.5	4.2	4.0	3.5	4.0	6	6	6.2	6.1	5.9

Table 4.2 : Details of resonators from the (U_2) & (V_2) welds.

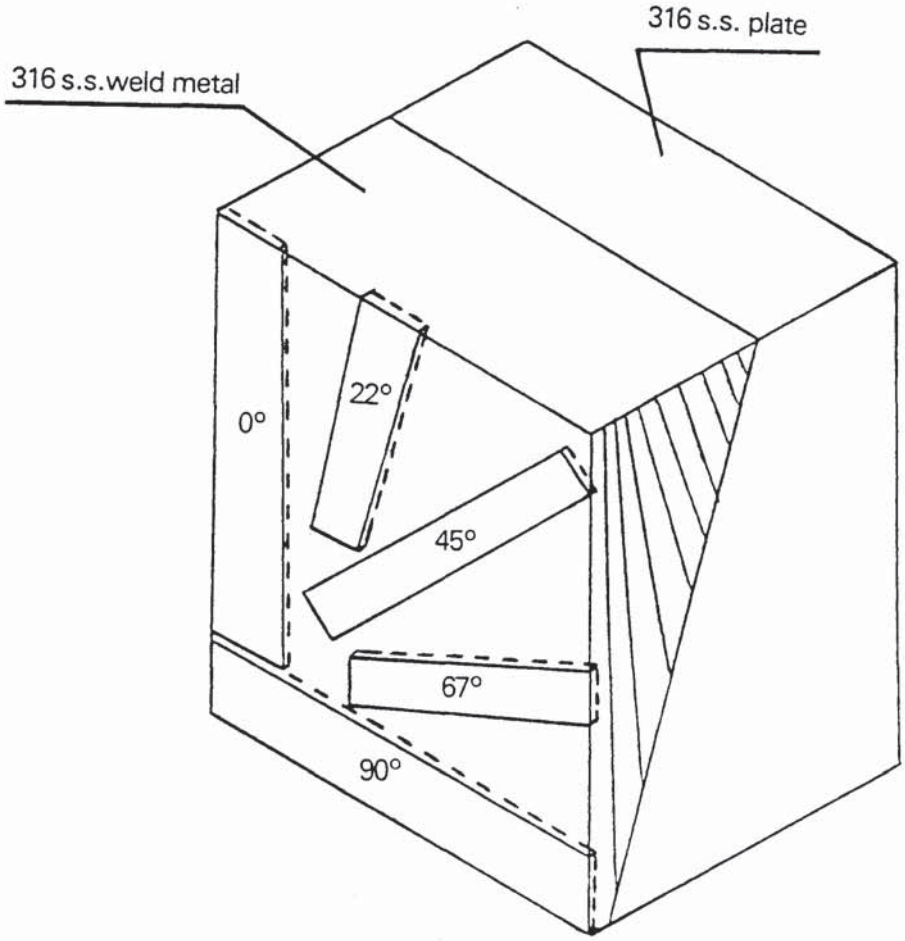

FIG. 4.4 : Position of strips (resonators) cut out from the 316 single-V austenitic weld in relation to the weld metal

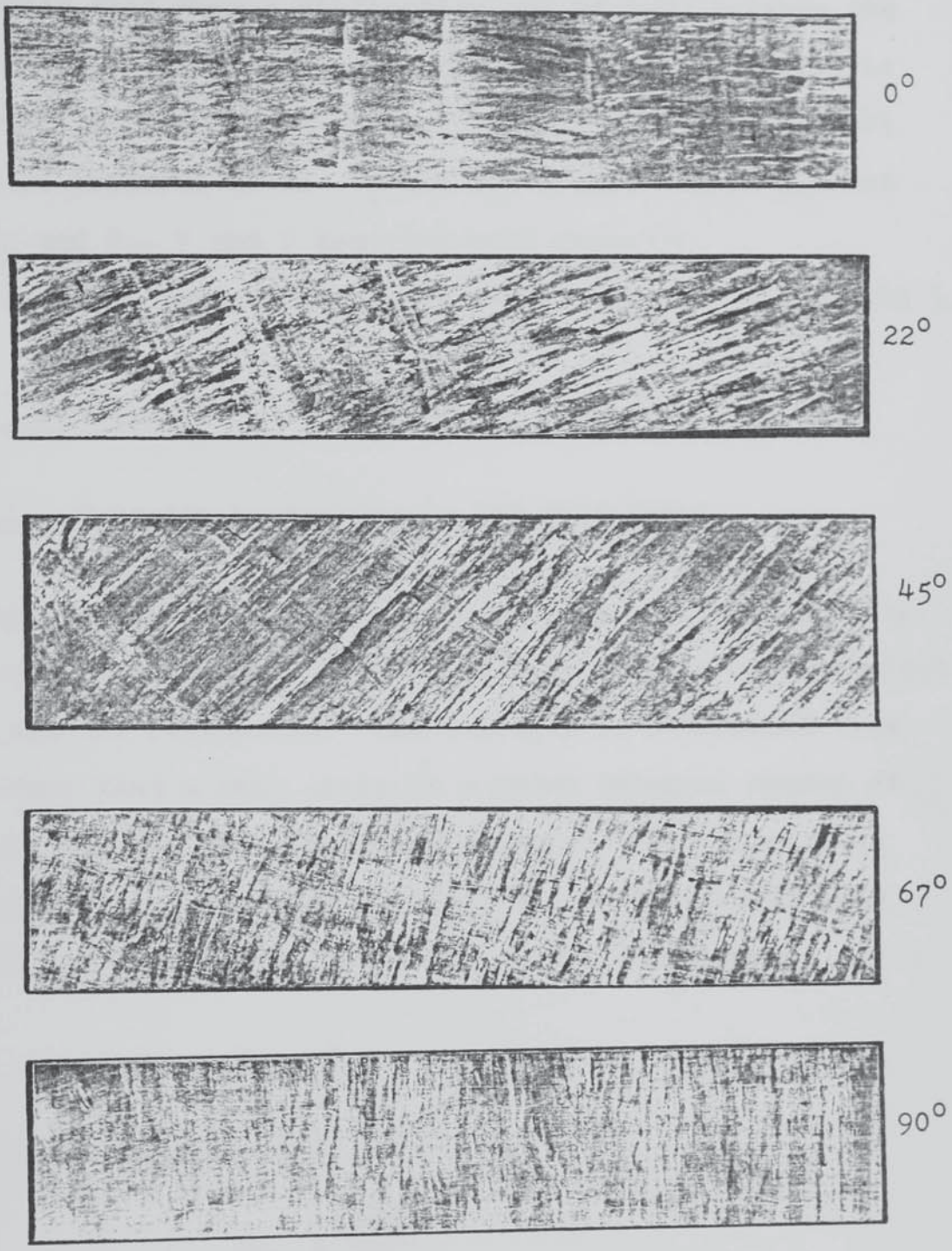

FIG. 4.5 : Resonators cut out of the 316 single-V austenitic weld, etched in Ferric Chloride showing grains at various angles to the length direction

In order that that a distinction can be made between the two sets of resonators used, the following convention is adopted :- the original samples used in reference (104) will be referred to as V_1 and U_1, whilst the second set as V_2 and U_2, V and U denoting weld geometry.
The complete text of reference (104) appears in Appendix 1.

4.3 Results

4.3.1 Velocity Variations in 316 Weld Metal

Using the technique outlined in section 4.2.1, values for the resonant frequency (f) at different modes were obtained for all the resonators. The velocity is determined from the fact that a thin strip is a known integral number of wavelengths at the resonant frequency. The velocity of sound (C) in a material is equal to the wavelength (λ) multiplied by the frequency (f) of the soundwaves.

$$C = \lambda f \quad \ldots\ldots (1)$$

For a thin narrow strip :

$$C_\phi = \frac{2\ell f}{n} \quad \ldots (2)$$

where, (n) is the mode number (i.e. 1,2,3,...), (ℓ) is the length of the resonator (strip), and (C_ϕ) is the phase velocity.

From (1) and (2) :-

$$\lambda = \frac{2\ell}{n} \quad \ldots\ldots \quad (3)$$

Dividing both sides of equation (3) by the width of the resonator (w) :-

$$\frac{nw}{2\ell} = \frac{w}{\lambda} \quad \text{, and since } w/2\ell \text{ is constant,}$$

$$\boxed{n \propto \frac{w}{\lambda}}$$

When (n) tends to zero, w/λ will also tend to zero; this is the condition for $(C_\phi) = (C_o)$, where (C_o) is the rod velocity.

Plotting graphs of (C_ϕ) against w/λ, values of (C_o) were obtained by extrapolation for all resonators.

Figure 4.6 shows a typical plot of (C_ϕ) versus w/λ for a strip (resonator) cut out from the 316 single-V_1 weld metal, having its grain axis direction at 90^o to the direction of the soundwave propagation.

Values for longitudinal velocity were calculated for all resonators using :-

$$C_L = C_o \left[(1-\nu) \,/\, (1+\nu)(1-2\nu) \right]^{\frac{1}{2}} \quad \ldots \quad (4)$$

where C_L is the longitudinal wave velocity, and (ν) is the Poisson's ratio for the material (ν=0.3 was used in the velocity computations unless otherwise stated).

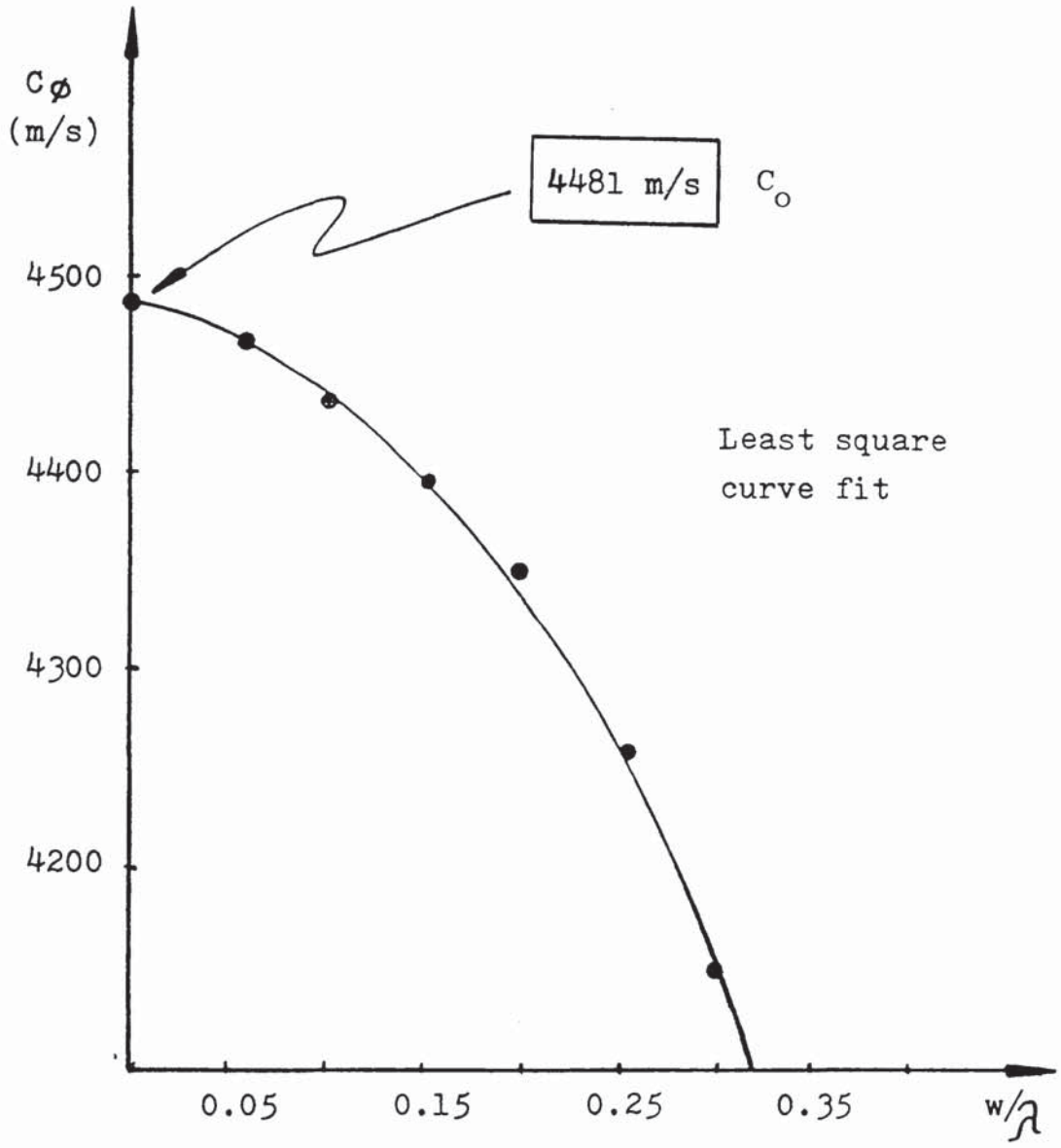

FIG. 4.6 : Typical plot of (C_ϕ) vs. (w/λ) for a strip cut out of the 316 single-V weld, with grain axes at 90° to the direction of sound propagation

Figure 4.7 shows a typical plot of (C_ϕ) against the angle of the grain axes with respect to the soundwave direction of propagation, for various frequency modes for the 316 single-V_1 weld resonators.

Figure 4.8 shows velocity variations with respect to the direction of propagation relative to the grain axis for the single-V_1 and double-U_1 austenitic welds as compared with results by Baikie et al[21]. Figure 4.9 shows velocity variations for the single-V_2 and double-U_2 austenitic weld metals as compared with results by Baikie et al. Table 4.3 gives the experimental values of longitudinal velocity (C_L) for the single-V_1,V_2 and double-U_1,U_2 weld metals, and Table 4.4 gives the computed values for (C_L) using equation (5).

The equation relating longitudinal velocity as a function of the angle (θ) made by the direction of soundwave propagation and the direction of the grain axis, was found to be :-

$$C_L = A_o + A_1\cos2\theta + A_2\cos4\theta + A_3\cos6\theta + A_4\cos8\theta \quad \ldots (5)$$

The derivation of equation (5), together with the computer programme used to obtain the longitudinal velocity variations through 360^o , and with the computed results in polar form are given in Appendix 2.

The technique used to obtain the frequency values that provided the basis for the longitudinal velocity calculations is claimed to be accurate within $\pm$ 0.1 %, allowing precise

Weld Sample	Experimental Velocity Values (C_L) m/s				
	Grain Direction Along Specimen (degrees)				
	0	22	45	67	90
U_1	4930	5570	5775	5500	5200
U_2	5050	5550	5870	5475	5415
V_1	5000	5580	6500	6150	5200
V_2	5040	5580	6260	6140	5230

Table 4.3 : Experimental Values of Velocity Variations for longitudinal waves.

Angle (θ)	Longitudinal Velocity Values (m/s)			
	U_1	V_1	U_2	V_2
0	5000	4998	5040	5050
10	5220	5204	5249	5214
20	5705	5612	5678	5577
30	6150	5855	6009	5874
40	6423	5834	6189	5930
50	6536	5714	6323	5776
60	6424	5604	6329	5574
70	6005	5446	6014	5450
80	5459	5237	5494	5415
90	5200	5133	5230	5415

Table 4.4 : Computed velocity values using equation (5).

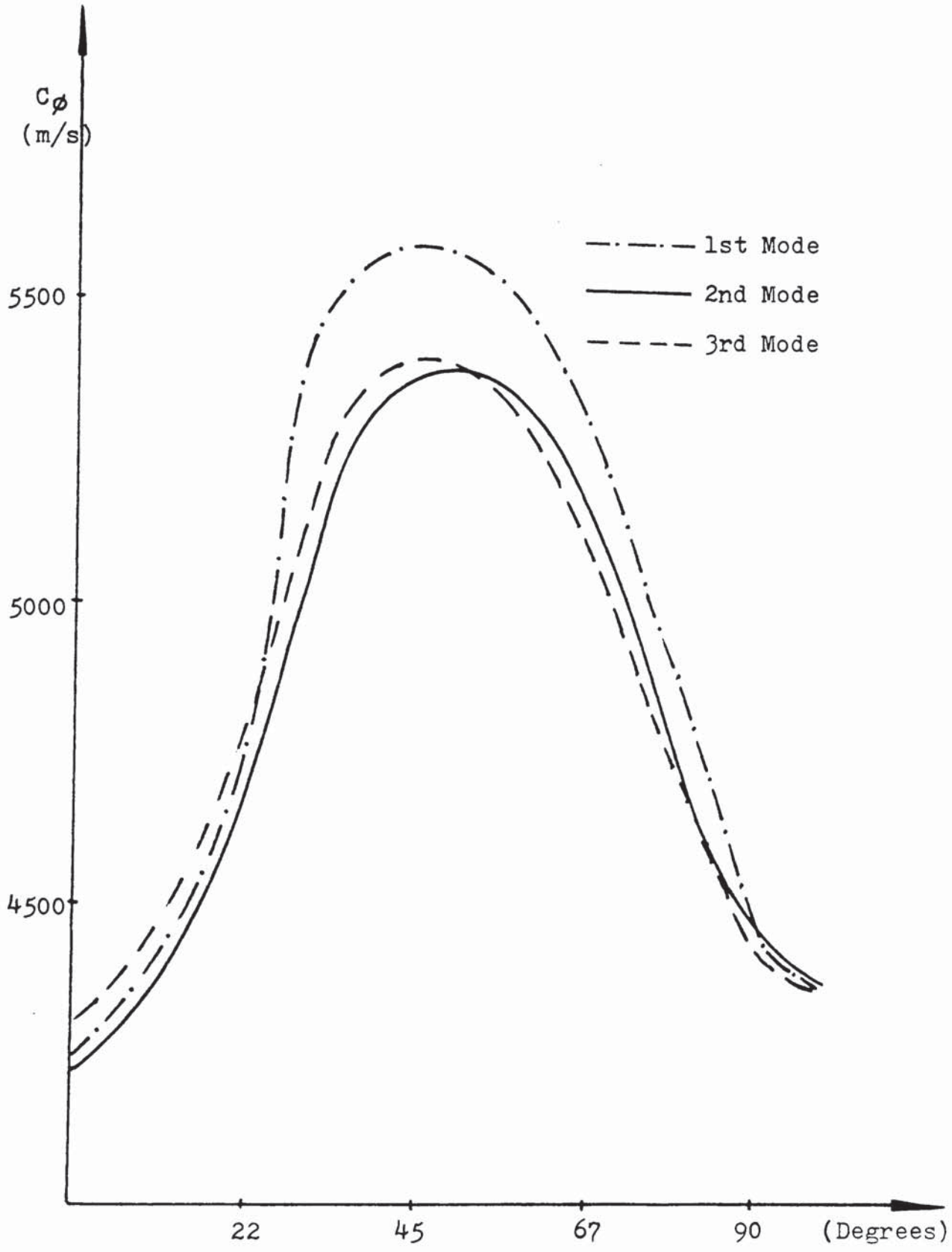

FIG. 4.7 : Plot of (C_ϕ) vs. angle between grain axes and sound propagation direction, for various frequency modes, using the strips from the 316 single-V weld

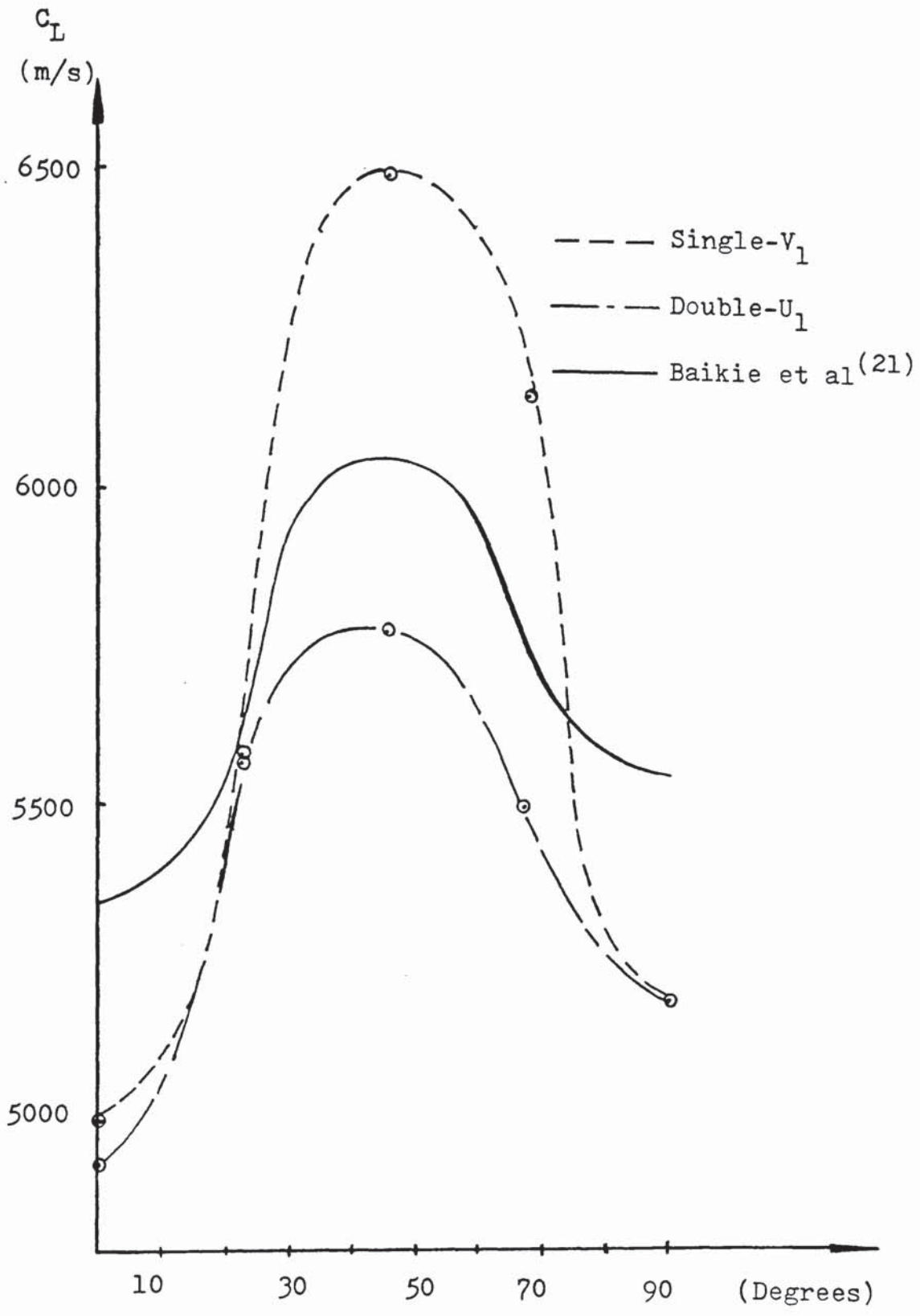

FIG. 4.8 : Velocity variation with respect to the angle made between the propagation direction and the grain axes. Experimental results as compared with results by Baikie et al

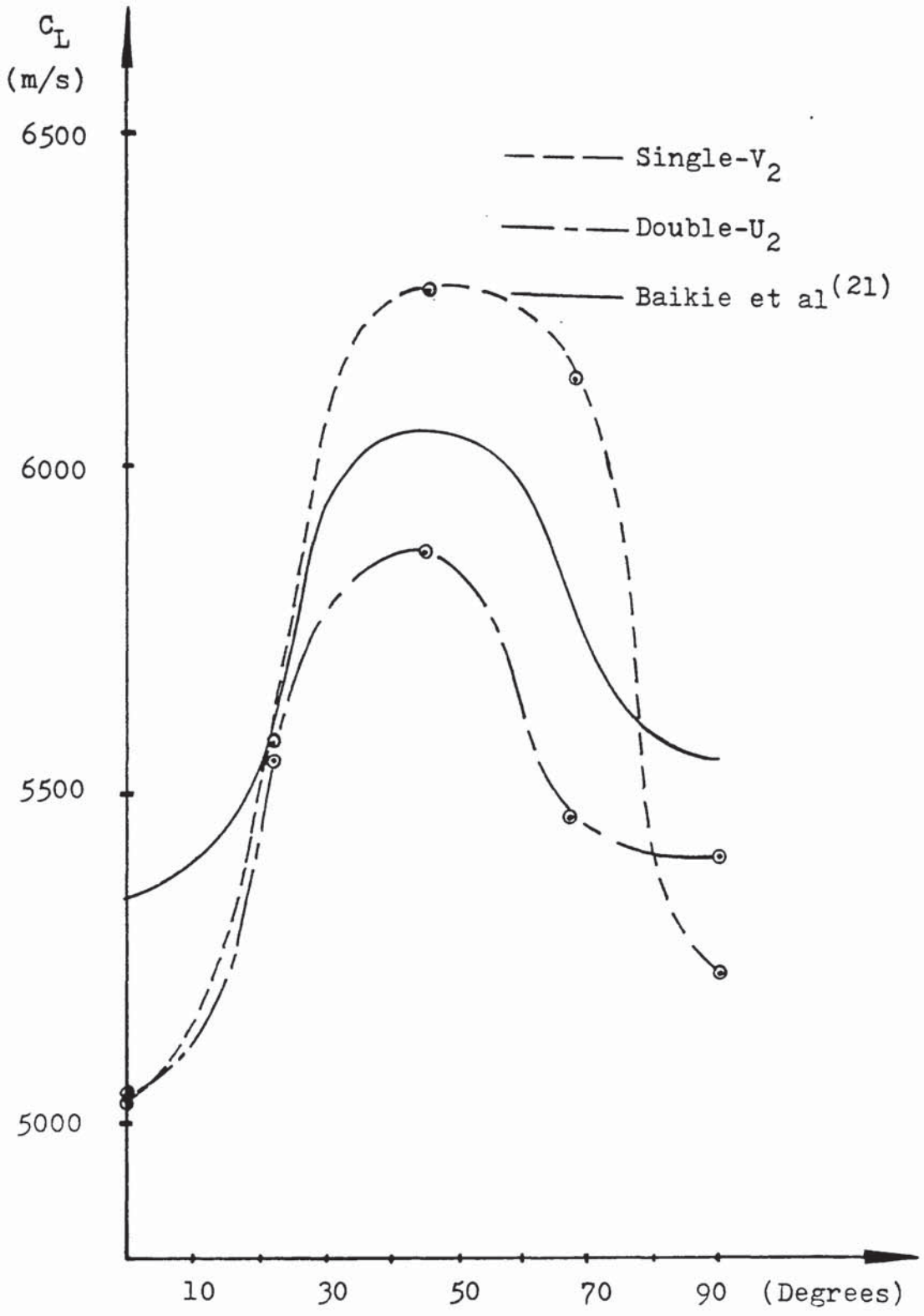

FIG. 4.9 : Velocity variation with respect to the angle made between the propagation direction and the grain axes. Experimental results as compared with results by Baikie et al

settings for frequency to be obtained. The main sources of error involved in the velocity measurements were :-

a) in extrapolating the values of (C_o), and when

b) measuring the dimensions of the resonators.

In order that the errors involved in extrapolating the (C_o) values be reduced, the least square method was used for a second order polynomial fit, since theory predicts the results to have such a form[105].
The computer programme used for the curve fitting together with the computed values of (C_o) for all resonators are given in Appendix 3.

The errors involved in measuring the dimensions of the resonators where considered to be negligible since the accuracy of the micrometer used for obtaining them is $\pm$ 0.1%, and therefore no statistical analysis of these measurements was felt necessary.

4.3.2 Velocity Measurements in Austenitic Plate Metal

Using the technique outlined in section 4.2.1, measurements were carried out to determine the ultrasonic velocity of longitudinal waves in the austenitic plate material.
Two samples were cut-out from the 316 austenitic plate at right angles to each other (Figure 4.10). Figures 4.11 and 4.12 show plots of (C_ϕ) against w/λ for the two samples,

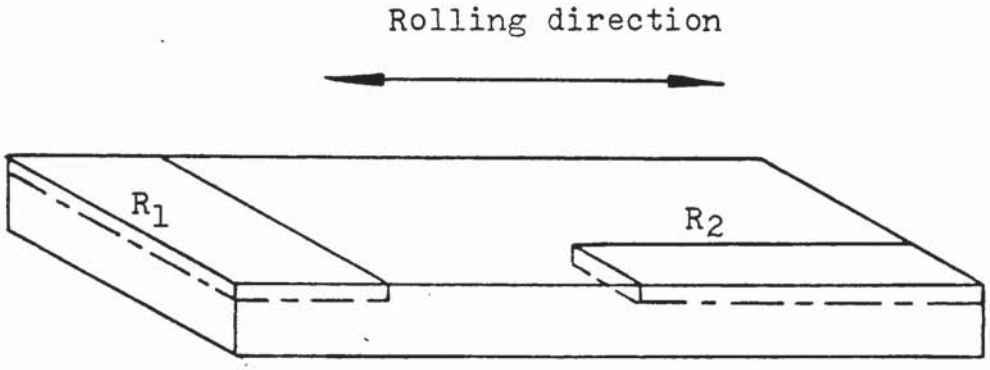

FIG. 4.10 : Strip resonators cut out from the 316 austenitic plate

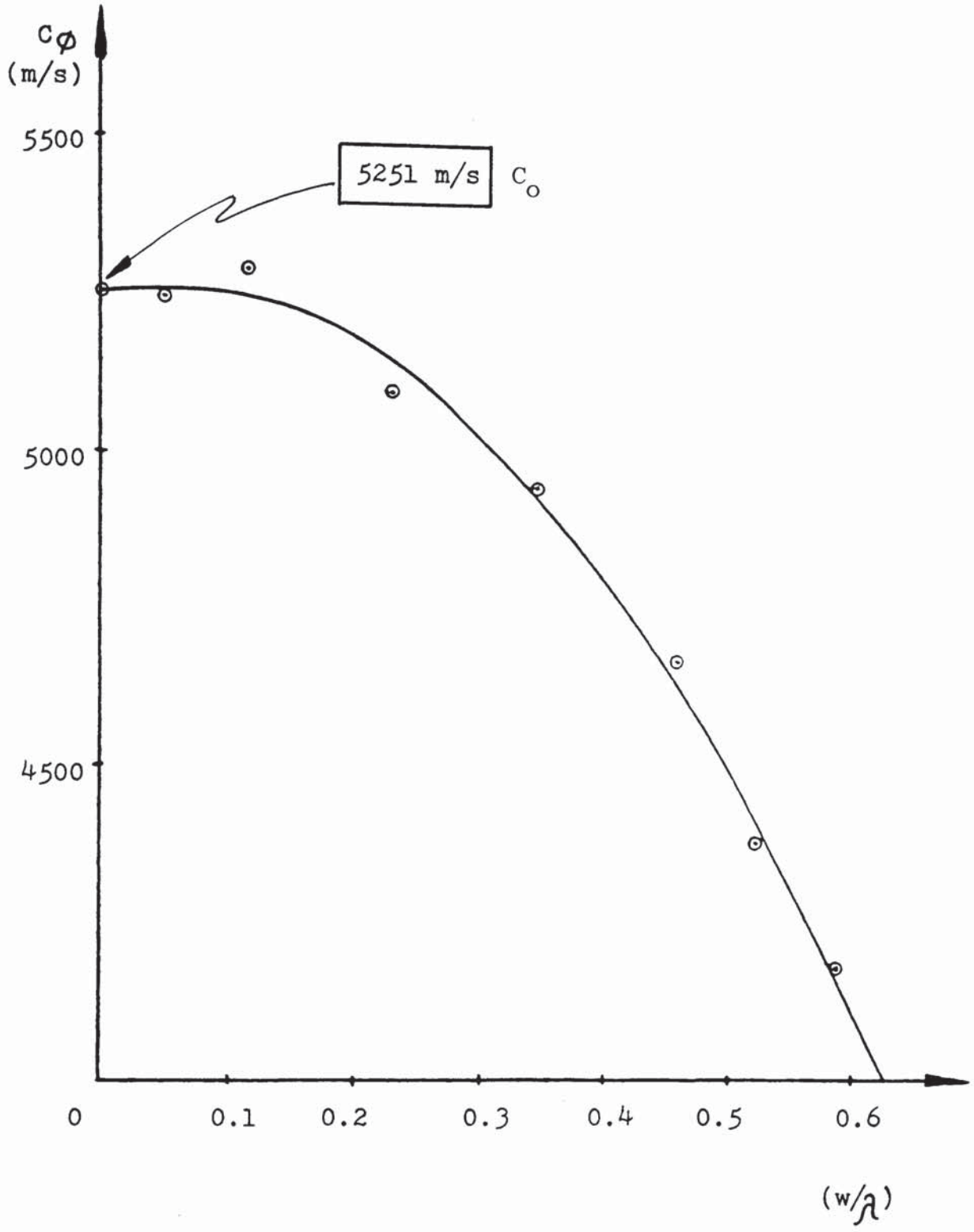

Figure 4.11 : Plot of (C_ϕ) vs. (w/λ) for strip R_1.

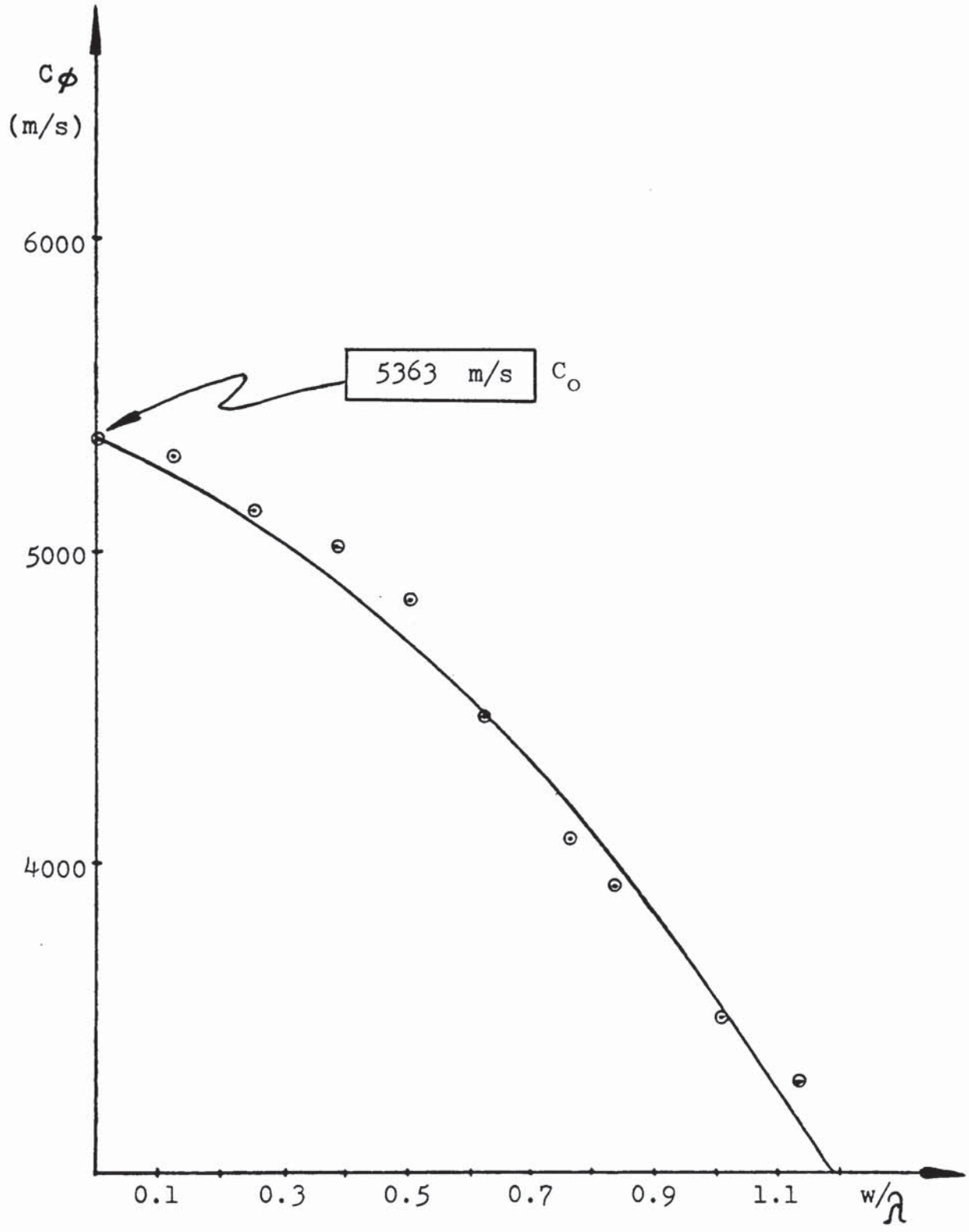

Figure 4.12 : Plot of ($C\phi$) vs. (w/λ) for strip R_2.

obtained using the least square curve fit. The computed values of longitudinal velocity along the length direction of the resonators, (C_L), are given in Table 4.5.
In order that values for the transverse velocity of ultrasound propagated in the 316 austenitic plate material were obtained, the system of excitation described previously was once more employed, but this time the resonator was machined from the plate in the form of a disc (Figure 4.13). This form of resonator was employed because it enables precise measurements of elastic constants, longitudinal and transverse velocities, and Poisson's ratios of a variety of materials to be determined[106,107]. The longitudinal and transverse velocity values together with Poisson's ratio for the plate material are given in Table 4.6.

4.4 Theoretical Considerations

4.4.1 Cubic Media

Austenite crystallizes in the face-centred cubic form (f.c.c.) and as has been shown, the ultrasonic velocity is a strong function of direction within the crystal structure.
Using the usual notations for crystallographic axes, the velocities in the major directions may be quoted as shown in Table 4.7. If reasonable values for the elastic constants

Resonator	Experimental Velocity Values (m/s)
R_1	6172
R_2	6219

Table 4.5 : Longitudinal velocity along the length of resonators R_1 and R_2 cut from the 316 austenitic plate.

Longitudinal Velocity (m/s)	Transverse Velocity (m/s)	Poisson's Ratio (ν)
6160	3248	0.285

Table 4.6 : Experimental values of longitudinal, and transverse velocities, together with Poisson's ratio for the austenitic plate material (316), using the disc resonator.

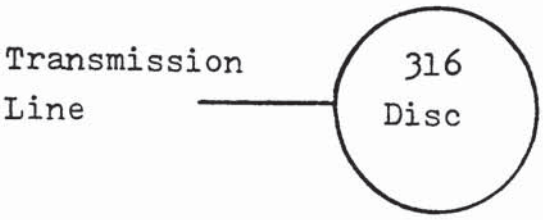

FIG. 4.13 : Disc resonator cut from 316 austenitic plate, used for transverse velocity measurements

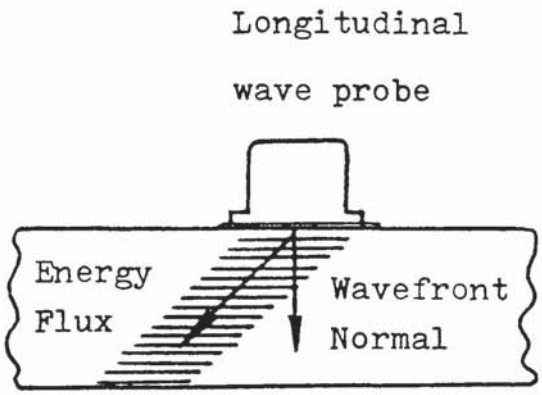

FIG. 4.14 : Schematic representation of the wavefront normal and the direction of energy flux i.e. "propagation direction"

C_{11}, C_{12}, C_{44}, of the austenite are substituted in these expressions, variations of velocity around the observed values may be predicted.

Direction	Longitudinal Wave Velocity
⟨100⟩	$\left[C_{11}/\rho \right]^{\frac{1}{2}}$
⟨110⟩	$\left[(\frac{1}{2}\rho)(C_{11} + C_{12} + 2\,C_{44}) \right]^{\frac{1}{2}}$
⟨111⟩	$\left[(\frac{1}{3}\rho)(C_{11} + 2C_{12} + 4\,C_{44}) \right]^{\frac{1}{2}}$
ρ = density of material (Kgm^{-3})	

TABLE 4.7 : Expressions relating Longitudinal Wave Velocities to major crystallographic directions

The problem of propagation of elastic waves in cubic media has been studied in detail by Miller and Musgrave[108], and treatments dealing with the case of austenitic weldments have been also published[30,109,110]. Following Silk[30], in general for a completely anisotropic medium, the relationship between stresses and strains will be written as follows :-

$$\begin{bmatrix} \sigma_{xx} \\ \sigma_{yy} \\ \sigma_{zz} \\ \sigma_{yz} \\ \sigma_{zx} \\ \sigma_{xy} \end{bmatrix} = \begin{bmatrix} c_{11} & c_{21} & c_{31} & c_{41} & c_{51} & c_{61} \\ c_{12} & c_{22} & c_{32} & c_{42} & c_{52} & c_{62} \\ c_{13} & c_{23} & c_{33} & c_{43} & c_{53} & c_{63} \\ c_{14} & c_{24} & c_{34} & c_{44} & c_{54} & c_{64} \\ c_{15} & c_{25} & c_{35} & c_{45} & c_{55} & c_{65} \\ c_{16} & c_{26} & c_{36} & c_{46} & c_{56} & c_{66} \end{bmatrix} \times \begin{bmatrix} \varepsilon_{xx} \\ \varepsilon_{yy} \\ \varepsilon_{zz} \\ \varepsilon_{yz} \\ \varepsilon_{zx} \\ \varepsilon_{xy} \end{bmatrix}$$

where (C_{ij}) are the appropriate elastic constants.

It is appropriate at this point to distinguish between the use of terms such as "anisotropic" and "aeolotropic". These two terms are often used synonymously in the literature, to denote homogeneous materials whose physical properties depend on the direction of observation. More specifically the term aeolotropic is used in connection with materials possessing no internal boundaries such as single crystals, while the term anisotropic is concerned with bulk properties.

The propagation of elastic waves in a general anisotropic medium has the following characteristics. Three propagational velocities, i.e. separate waves are possible, but these are not true longitudinal or true transverse waves. In general there is one quasi-longitudinal wave and two quasi-transverse waves, but under specific circumstances

a given wavefront may have quasi-longitudinal properties in some directions and quasi-transverse properties in others. It will be normally found that the three elastic wave beams which might be generated by surface modulation are not co-planar. The direction of propagation is not, in general, normal to the wavefront and deviates from this by an angle (Δ).

Considering the specific case of materials with cubic symmetry, the above relationship is simplified to :

$$\begin{bmatrix} \sigma_{xx} \\ \sigma_{yy} \\ \sigma_{zz} \\ \sigma_{yz} \\ \sigma_{zx} \\ \sigma_{xy} \end{bmatrix} \begin{bmatrix} C_{11} & C_{12} & C_{12} & 0 & 0 & 0 \\ C_{12} & C_{11} & C_{12} & 0 & 0 & 0 \\ C_{12} & C_{12} & C_{11} & 0 & 0 & 0 \\ 0 & 0 & 0 & C_{44} & 0 & 0 \\ 0 & 0 & 0 & 0 & C_{44} & 0 \\ 0 & 0 & 0 & 0 & 0 & C_{44} \end{bmatrix} \begin{bmatrix} \varepsilon_{xx} \\ \varepsilon_{yy} \\ \varepsilon_{zz} \\ \varepsilon_{yz} \\ \varepsilon_{zx} \\ \varepsilon_{xy} \end{bmatrix}$$

Defining the following relationships:

$$a = C_{11} - C_{44}$$

$$b = C_{12} - C_{44}$$

$$c = (a-b) = C_{11} - C_{12} - 2C_{44}$$

and if the material density is (ρ), following Silk[30],

three velocity equations are obtained :

$$V_1 = \left(C_{44} / \rho\right)^{\frac{1}{2}} \qquad \ldots\ldots\ldots (6)$$

$$\rho V_2^2 = C_{44} + \tfrac{1}{2}a - \tfrac{1}{2}\left[a^2 - 4(a^2-b^2)\, n^2\, l^2\right]^{\frac{1}{2}} \qquad \ldots\ldots (7)$$

$$\rho V_3^2 = C_{44} + \tfrac{1}{2}a + \tfrac{1}{2}\left[a^2 - 4(a^2-b^2)\, n^2\, l^2\right]^{\frac{1}{2}} \qquad \ldots\ldots (8)$$

Equation (6) represents a truly transverse wave and does not deviate from its expected path ($\Delta_i = 0$).
Equations (7) and (8) represent a quasi-transverse and a quasi-longitudinal wave respectively. These waves only become truly longitudinal or transverse in certain directions and also, in general, deviate from their expected direction, the wave normal (Figure 4.14).
This deviation can be quantified in angular terms Δ_i (i= 2,3), where :

$$\cos \Delta_i = \frac{l \lambda_i + n V_i}{(\lambda_i^2 + V_i^2)^{\frac{1}{2}}} \qquad \ldots\ldots (9)$$

$$\frac{\lambda_i}{V_i} = \frac{\left[(P_i^2 / l) H_i + l C_{44}\right]}{\left[(R_i^2 / l) H_i + n C_{44}\right]} \qquad \ldots\ldots (10)$$

and $$\frac{P_i}{R_i} = \frac{lnd}{H_i - l^2 a} \qquad \ldots\ldots (11)$$

with the additional relationship ($H_i = \rho V^2 - C_{44}$) having been introduced.

Juva and Lenkkeri[110], using velocity measurements obtained from austenitic cubic single crystals, have proceeded to derive effective elastic constants C_{11} , C_{12} and C_{44} , which they used to calculate the orientation dependence of velocities in austenitic metal.

In order to determine Δ_i for the quasi-transverse and quasi-longitudinal wave modes in austenitic weld materials, a computer programme is required to solve the complex relationships involved, utilizing experimentally obtained values for the elastic constants in the austenitic weld metal.

4.4.2 Orthotropic Media

It was established in Sect. 3.4, that within the austenitic weld metal the crystal alignment is mainly in the through thickness direction, with near random alignment in the weld plane. This means that the material properties will be orthotropic (uniaxial) rather than cubic.

Assuming the latter model, Tomlinson et al[22] calculated the expected angular variation in the velocity of longitudinal waves and obtained acceptable agreement with experimental data (Figure 4.15).

Since both for cubic and orthotropic media :

$$\rho V_{min}^2 = C_{11} \quad \ldots\ldots (12)$$

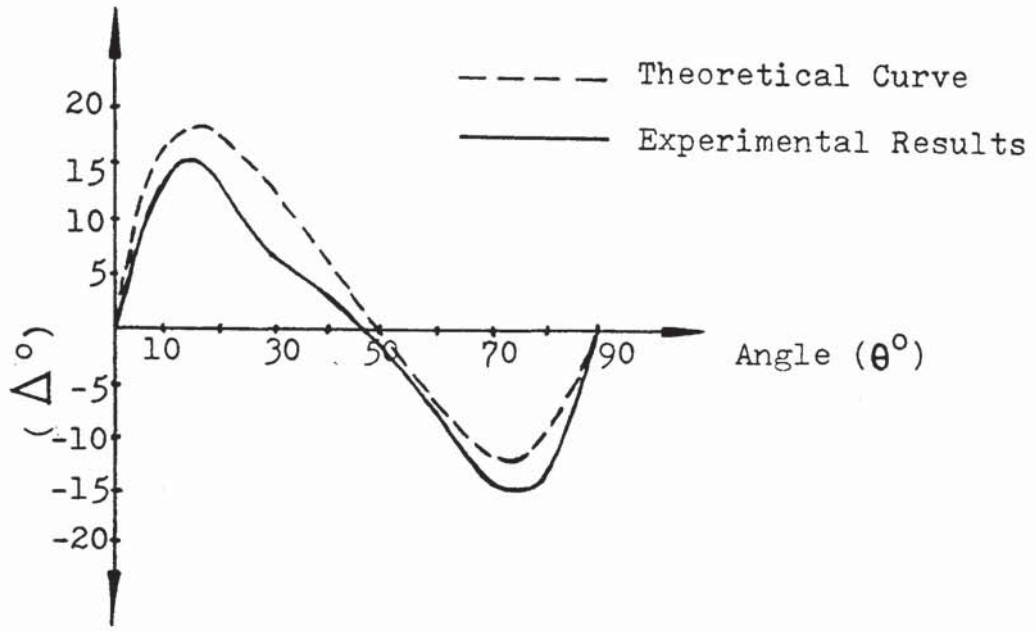

Constants assumed in calculation :

C_{11}= 239 GNm^{-2}

C_{12}= 168 GNm^{-2}

C_{44}= 123 GNm^{-2}

FIG. 4.15 : Skewing angle (Δ) as a function of the angle (θ) between the normal to the wavefront and the columnar grain axes (after Tomlinson et al [22])

one could arrive at an estimate of C_{11} using experimental data of velocity variations in austenitic weld metal. In the case of a cubic model being assumed to represent the austenitic weld metal, data on the other elastic constants could be obtained from :

$$2\rho V_{max}^2 = 2C_{44} + C_{11} + C_{12} \quad \ldots\ldots (13)$$

The calculations become more difficult in the case of the orthotropic model being assumed, since the maximum velocity is an integral over the velocities in the $\langle 110 \rangle$, $\langle 111 \rangle$ and intermediate directions (Table 4.7).
Following Silk's approach [30], it is an acceptable approximation to define that :

$$2\rho^{\frac{1}{2}} V_{max} = \left\{ \frac{2C_{44} + C_{11} + C_{12}}{2} \right\}^{\frac{1}{2}} + \left\{ \frac{4C_{44} + 2C_{12} + C_{11}}{3} \right\}^{\frac{1}{2}} \quad ..(14)$$

and similarly, since the subsidiary minimum velocity at 90° (V_{90}) is also the result of an integral over velocities in the $\langle 110 \rangle$, $\langle 100 \rangle$ and intermediate directions, accepting the same degree of approximation :

$$2\rho^{\frac{1}{2}} V_{90} = \left\{ \frac{2C_{44} + C_{12} + C_{11}}{2} \right\}^{\frac{1}{2}} + (C_{11})^{\frac{1}{2}} \quad ..... (15)$$

A solution of equations (12), (14) and (15), provides approximate data on the elastic constants for 316 austenitic weld metal.

In order that reasonable values for the elastic constants of the 316 austenitic weld metal were obtained, it was considered appropriate to average the velocity values experimentally obtained for the 316 single-V and 316 double-U weld samples.

Using the above equations and the "averaged" velocity values for the 316 weld metal, the elastic constants given in Table 4.8 were calculated.

Elastic Constants (Nm^{-2})	316 weld metal Silk[30]	316 single crystal Juva et al[110]	316 weld metal Kapranos et al[104]
C_{11}	21.9×10^{10}	20.36×10^{10}	20.0×10^{10}
C_{12}	17.3×10^{10}	13.35×10^{10}	16.7×10^{10}
C_{44}	8.35×10^{10}	12.98×10^{10}	6.0×10^{10}

TABLE 4.8 : Elastic constants of austenitic material derived from experimental data on velocity variations as a function of propagation direction.

Using the values of the elastic constants given in the above table, the degree of elastic anisotropy can be expressed

quantitatively in terms of a parameter (A) that is related to these constants via the relation :

$$A = \frac{2C_{44}}{C_{11} - C_{12}} \qquad \ldots\ldots (16)$$

For elastically isotropic materials, A = 1.
Using the values of the elastic constants given in Table 4.8, and equation (16), the following anisotropy factors for austenitic 316 materials are obtained :

	Data by Silk[30]	Data by Juva et al[110]	Data by Kapranos et al[104]
(A)	3.63	3.7	3.66

TABLE 4.9 : Anisotropy factors for austenite

4.4.3 Application to 316 Type Austenitic Weld Metal

All three modes of propagation described above have both advantages and disadvantages for ultrasonic inspection; longitudinal waves are easily generated, but when used for angled inspection, a shear wave component is also present creating difficulties of signal interpretation. Vertically polarized transverse waves (S_V) are usually

generated from longitudinal waves by mode conversion (viz. conventional shear wave probes), though both they and the horizontally polarized transverse waves (S_h) may be generated by transverse wave transducers. Recently Kupperman and Reimann[29] have shown that horizontally polarized transverse waves exhibit less attenuation than vertically polarized transverse waves, when used in austenitic weld inspection. As compared to longitudinal waves, transverse waves when used in inspecting coarse grained materials exhibit lower signal to noise ratios, because most of the energy scattered from the grains is in the shear mode[39]; but transverse waves have the advantage that being slower they provide greater resolution in time domain analysis[30], a promising technique for crack size estimation in austenitic weldments. From the above considerations, there seems to be reason to study the theoretical propagation of all three modes in austenitic weld metal.

Using the "averaged" velocity measurements obtained from the 316 welds for longitudinal waves (sect.4.3.1), the elastic constants of Table 4.8 were obtained using three specified points on the velocity curve (at 0°, 45° and 90°). These results are rather sensitive to the position of the velocity maximum. To amend this, the procedure described by Gillan[98] will be adopted :-

(i) Define $C_{33} = C_{11}^c$ from the velocity along the grains at $\theta = 0$.

(ii) Assume $C_{12}^c = 1.2\, C_{44}^c$, this being a typical ratio for austenitic steels. The velocity curve is not very sensitive to the difference between C_{12}^c and C_{44}^c .

(iii) Expressing everything in terms of C_{44} $(= C_{44}^c)$, C_{44} is adjusted so that the magnitude of the maximum velocity attained is correct. Nothing will be assumed regarding the position of the maximum velocity as a function of propagation direction.

The transversly-isotropic elastic constants are obtained by averaging the constants of the grains, and then considering the properties of a material with such constants. Thus the following non-vanishing transversly isotropic elastic constants C_{ij} are obtained after averaging the cubic elastic constants of the weld metal C_{ij}^c :

$$C_{11} = C_{11}^c - \frac{c}{4}$$

$$C_{12} = C_{12}^c - \frac{c}{4}$$

$$C_{13} = C_{12}^c$$

$$C_{33} = C_{11}^c$$

$$C_{44} = C_{44}^c$$

$$C_{66} = \tfrac{1}{2}\,(C_{11} - C_{12}) = \tfrac{1}{2}\,(C_{11}^c - C_{12}^c - \frac{c}{2})$$

$$c = C_{11}^c - C_{12}^c - 2\,C_{44}^c$$

The orthotropic constants for all weld metal samples used, together with "averaged" elastic constants resulting from the combination of 316 single-V_1, V_2 and double-U_1, U_2 are given in Table 4.10.

The phase velocities of longitudinal (V_L) and transverse (V_{T_1} , V_{T_2}) waves are obtained from:

$$2\rho V_L^2 = m^2 (C_{11} + C_{44}) + n^2 (C_{33} + C_{44}) + \left[(m^2 a - n^2 h)^2 + 4m^2 n^2 d^2 \right]^{\frac{1}{2}} \quad \ldots\ldots\ldots \quad (17)$$

$$\rho V_{T_1}^2 = 2 m^2 C_{66} + n^2 C_{44} \quad \ldots\ldots\ldots \quad (18)$$

$$2\rho V_{T_2}^2 = m^2 (C_{11} + C_{44}) + n^2 (C_{33} + C_{44}) - \left[(m^2 a - n^2 h)^2 + 4m^2 n^2 d^2 \right]^{\frac{1}{2}} \quad \ldots\ldots\ldots \quad (19)$$

where : V_{T_1} = Horizontally polarized transverse waves

V_{T_2} = Vertically polarized transverse waves

$n = \cos\theta$

$m = \sin\theta$

ρ = density of the material (Kg m^{-3})

Elastic Constants $(Nm^{-2})x10^{10}$	Weld Samples						
	U_1	V_1	U_2	V_2	V_1&V_2	U_1&U_2	"Average"
C_{11}	23.02	26.86	23.96	25.8	26.33	23.46	24.91
C_{12}	9.09	10.93	9.42	10.36	10.64	9.28	9.95
C_{13}	12.71	17.82	13.00	15.87	16.84	12.85	14.85
C_{33}	19.40	19.98	20.38	20.29	20.13	19.89	20.01
C_{44}	10.59	14.85	10.84	13.23	14.04	10.71	12.38
C_{66}	3.16	1.1	3.67	2.22	1.65	3.52	3.08

Table 4.10 : Orthotropic elastic constants computed from constants of Table 4.8.

$a = C_{11} - C_{44}$

$h = C_{33} - C_{44}$

$d = C_{13} - C_{44}$

θ = angle between wave propagation direction and axis of the columnar grains in the weld metal

Using equations (17), (18) and (19) and the computer programme of Appendix 4., the results of Table 4.11 were obtained. These are shown in graphical form in Figures 4.16 to 4.18 inclusive.

The deviation (Δ_i) between propagation direction and the wavefront normal is quantitatively obtained from :

$$\tan \Delta_L = \frac{mn}{2\rho V_L^2} \left\{ (a-h) + \frac{\left[(a-h)((a+h^2)(h-a)) - (ah-d^2)(4n^2-2)\right]}{\left[((a+n^2)(h-a))^2 - 4n^2(1-n^2)(ah-d^2)\right]^{\frac{1}{2}}} \right\}$$

..... (20)

$$\tan \Delta_{T_1} = \frac{mn}{\rho V_{T_1}^2} \left(C_{66} - C_{44} \right) \quad ..... \quad (21)$$

Angle (θ)	Computed Velocity Values (m/s)		
	V_L	T_1	T_2
0	5004	3936	3936
10	5259	3906	3614
20	5663	3819	3031
30	5990	3681	2488
40	6191	3504	2179
45	6238	3406	2166
50	6249	3305	2254
60	6169	3107	2662
70	5970	2936	3210
80	5719	2819	3712
90	5584	2777	3936

Table 4.11 : Computed velocity values using the elastic "average" constants of Table 4.10 and equations (17), (18), and (19).

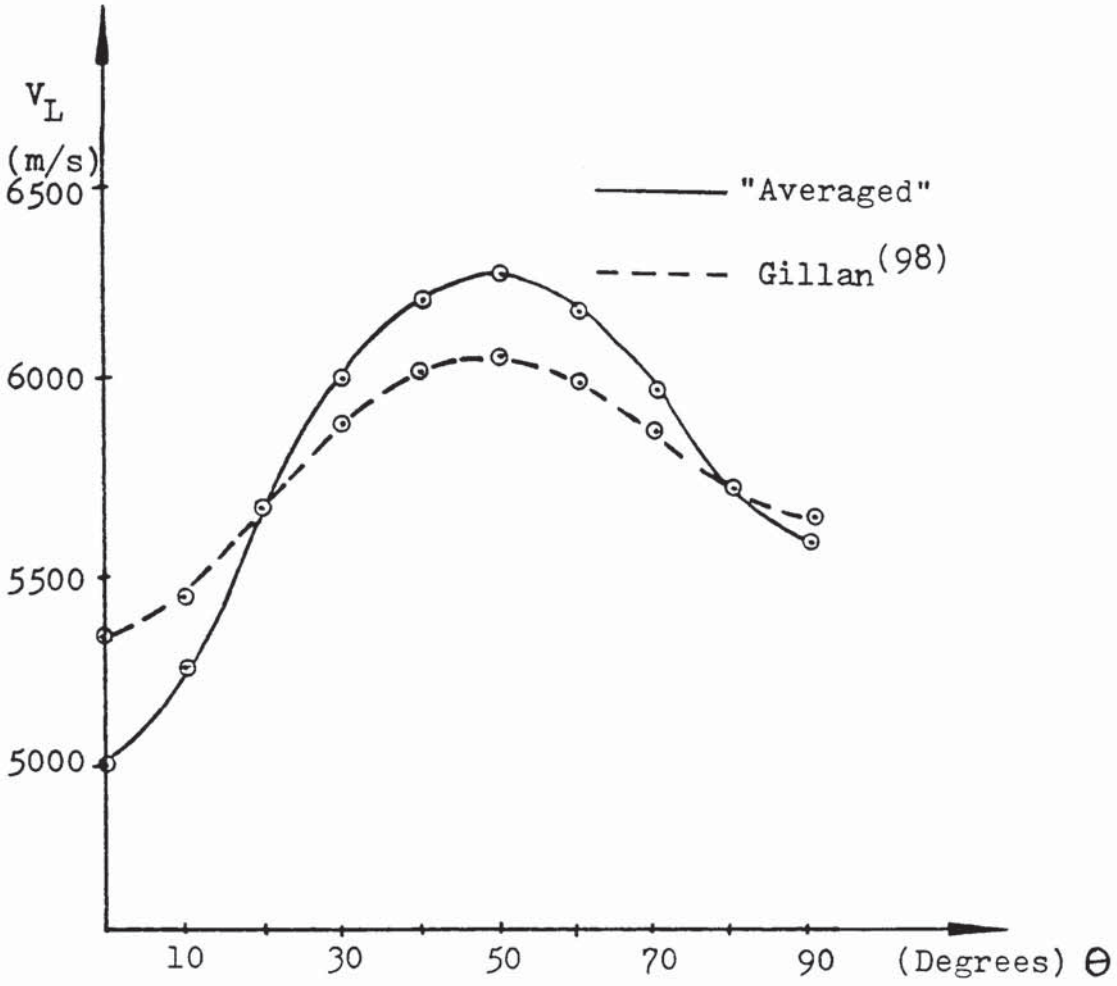

FIG. 4.16 : Computed velocity variations w.r.t. the angle (Θ) using "averaged" elasticity constants of Table 4.10, as compared with results by Gillan (Longitudinal waves)

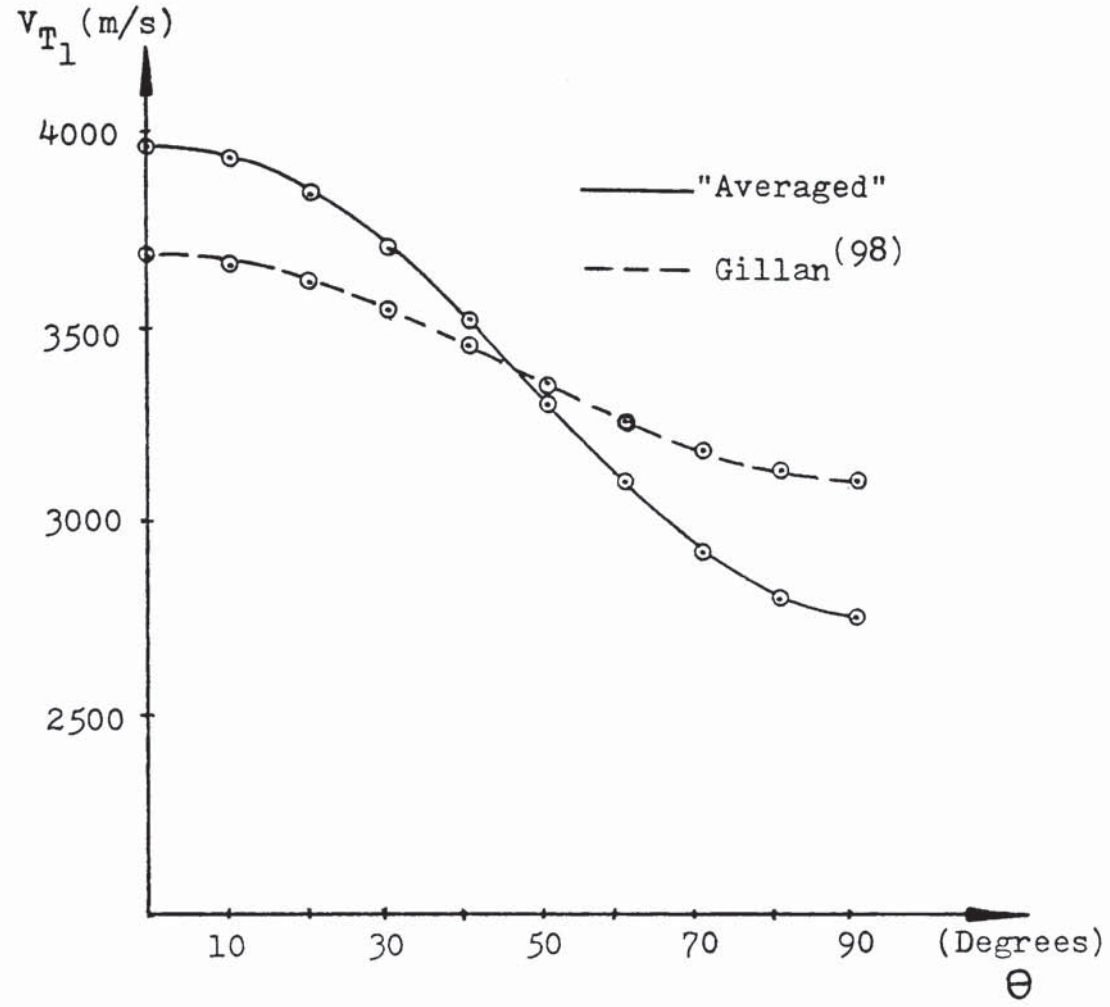

FIG. 4.17 : Computed velocity variation of horizontally polarized transverse waves w.r.t. the angle (Θ), using "averaged" elasticity constants of Table 4.10, as compared with results by Gillan

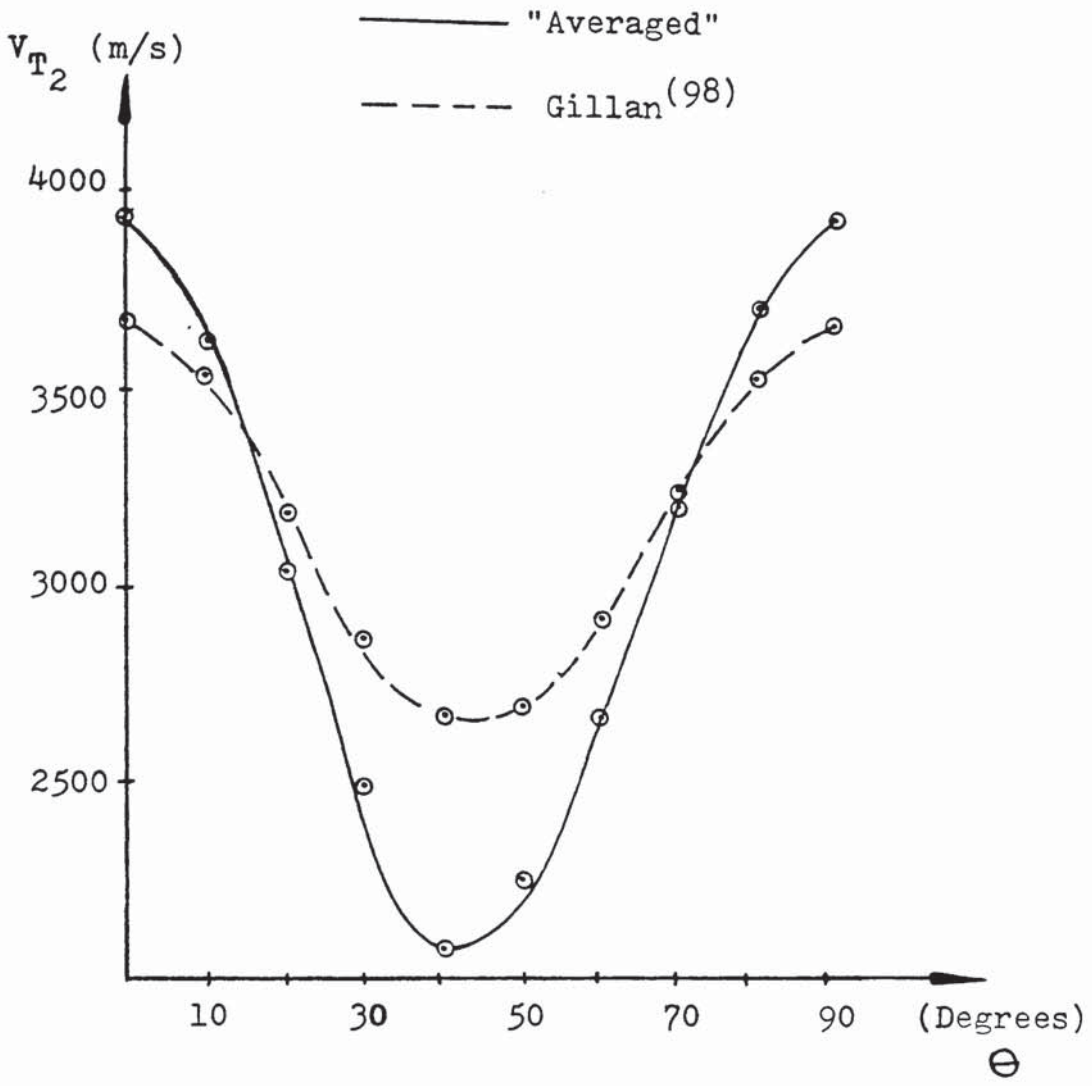

FIG. 4.18 : Computed velocity variation of vertically polarized transverse waves w.r.t. the angle (θ), using "averaged" elastic constants of Table 4.10, as compared with results by Gillan

$$\tan \Delta_{T_2} = \frac{mn}{2\rho V_{T_2}^2} \left\{ (a-h) - \frac{\left[(a-h)((a+h^2)(h-a))-(ah-d^2)(4n^2-2)\right]}{\left[((a+n^2)(h-a))^2-4n^2(1-n^2)(ah-d^2)\right]^{\frac{1}{2}}} \right\}$$

..... (22)

Using equations (20), (21) and (22) and the computer programme of Appendix 5., the results of Table 4.12 were obtained, (Figure 4.19).

Having expressed the phase velocities as homogeneous functions of (m) and (n) of the first degree, the magnitude of the group velocity (S) may be obtained from :

$$S = \frac{V_i}{\cos \Delta_i} \qquad \text{..... (23)}$$

The angle between the group and phase velocities is obtained from :

$$\Delta_i = \theta_g - \theta \qquad \text{..... (24)}$$

where (θ_g) is the angle between the group and phase velocities, (Δ_i) is the deviation angle between the propagation direction and the wavefront normal, and (θ)

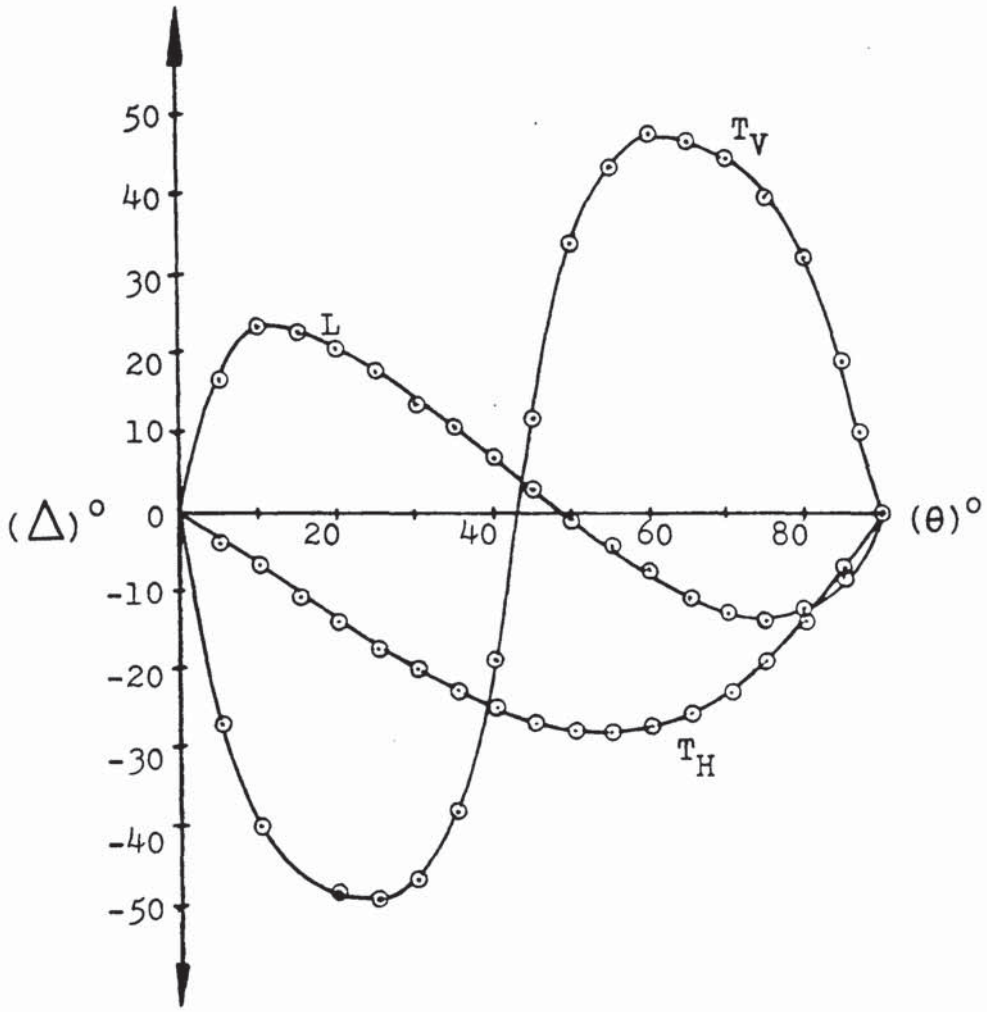

Figure 4.19 : Deviation angle (Δ) as a function of the angle (θ) for the three propagational wave modes.

Angle (θ) (degrees)	Deviation Angle (Δ) in degrees		
	(Δ_L)	(Δ_{T_1})	(Δ_{T_2})
0	0	0	0
10	23	-7	-40
20	21	-14	-48
30	14	-20	-47
40	7	-25	-19
45	3	-27	12
50	-0.6	-28	34
60	-8	-28	48
70	-13	-23	45
80	-13	-14	32
90	0	0	0

Table 4.12 : Deviation angle (Δ) as a function of the angle sustained between the direction of propagation and the columnar grain axis (θ).

Angle (θ) (degrees)	Group velocity (m/s)		
	(S_L)	(S_{T_1})	(S_{T_2})
0	5004	3936	3936
10	5734	3939	4718
20	6066	3942	4564
30	6184	3927	3621
40	6236	3867	2301
45	6247	3811	2212
50	6250	3733	2730
60	6225	3505	3957
70	6129	3201	4524
80	5873	2906	4387
90	5584	2777	3936

Table 4.13 : Group Velocities as functions of (θ).

Angle (θ) (degrees)	Angle between Group & Phase Velocities		
	(θ_{g_L})	($\theta_{g_{T_1}}$)	($\theta_{g_{T_2}}$)
0	0	0	0
10	33	3	-30
20	41	6	-28
30	44	10	-17
40	47	15	21
45	48	18	57
50	49	22	84
60	52	32	108
70	57	47	115
80	67	66	112
90	90	90	90

Table 4.14 : Angle (θ_g) as a function of angle (θ).

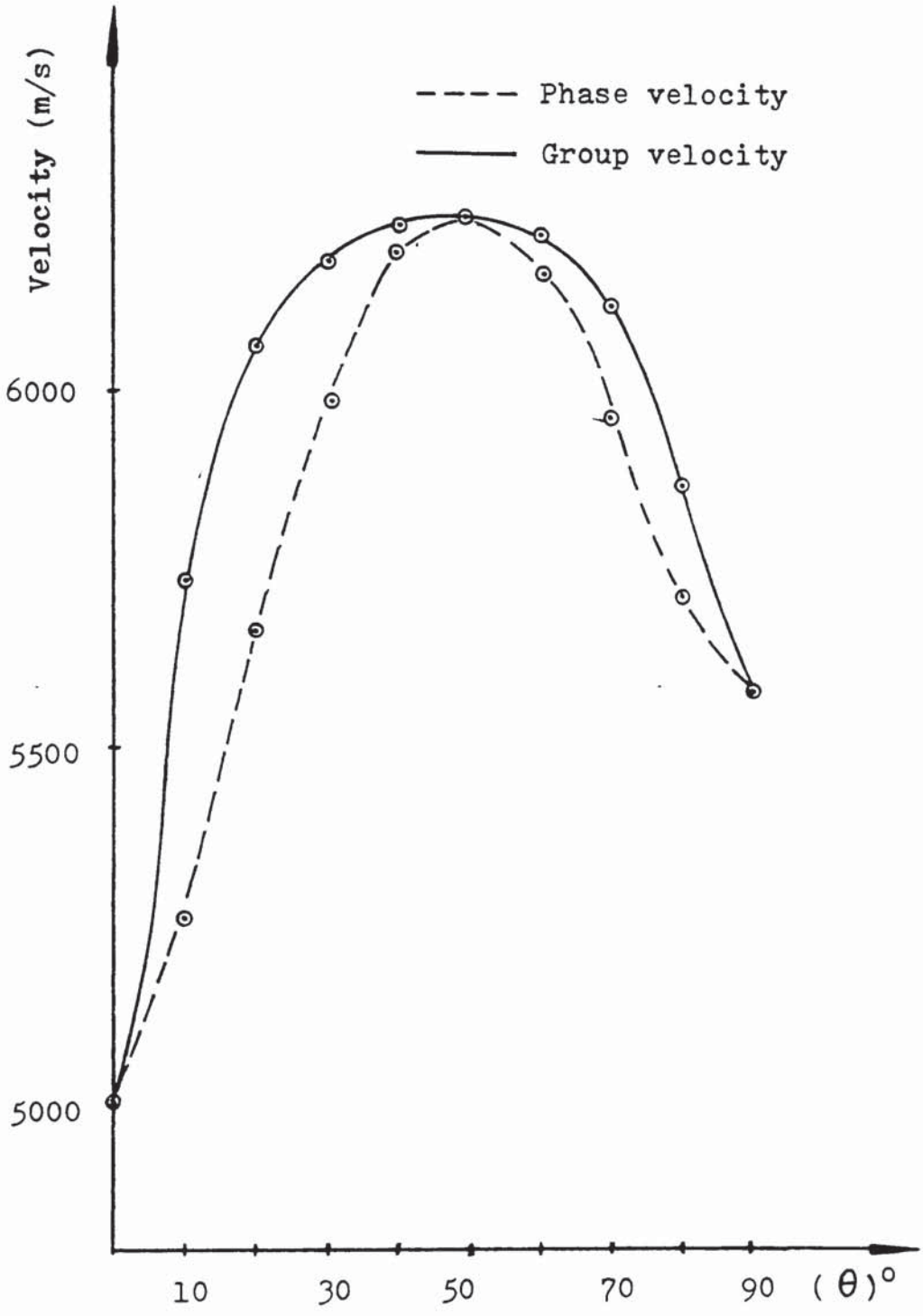

Figure 4.20 : Group and phase longitudinal velocities as functions of angle (θ).

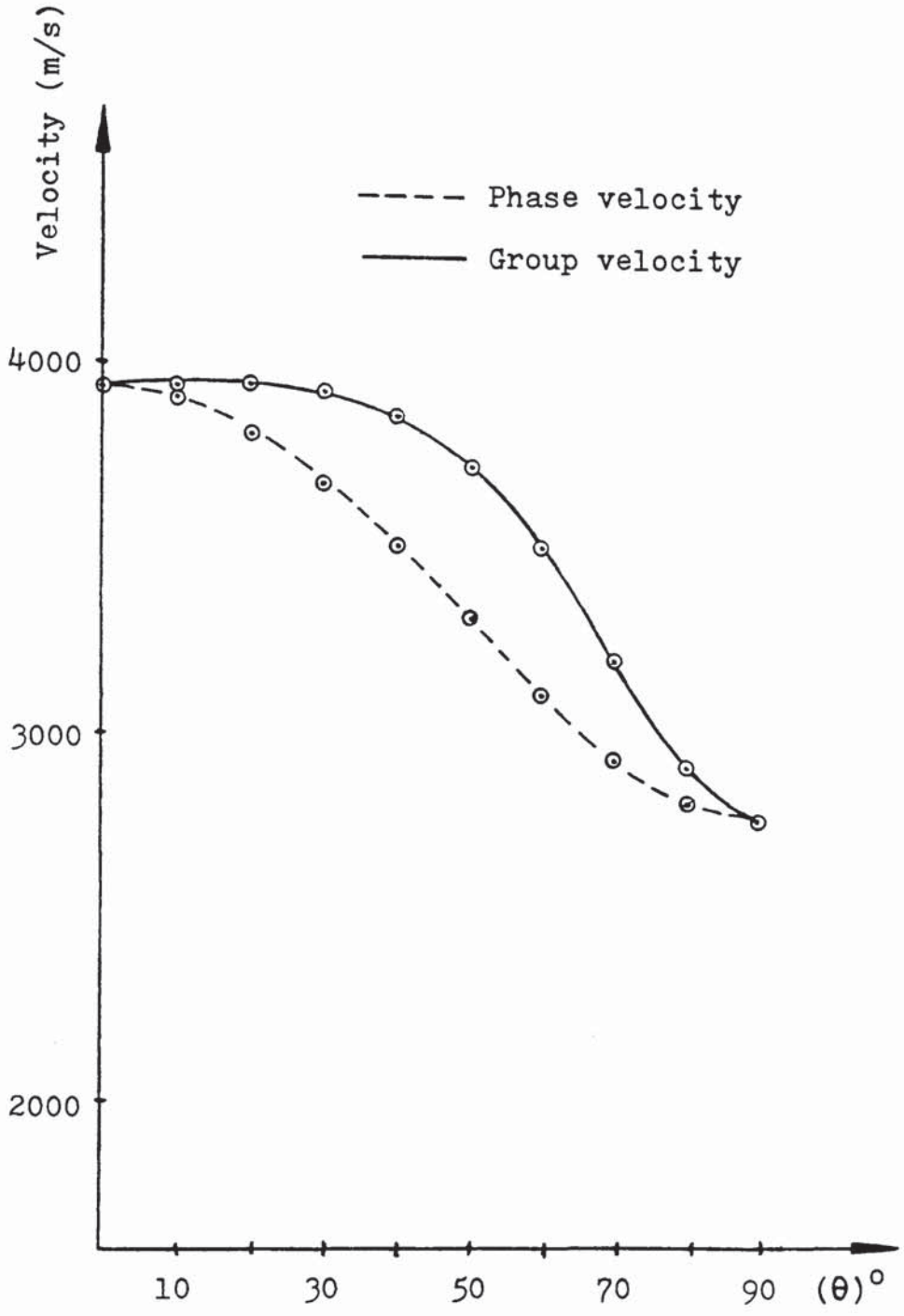

Figure 4.21 : Group and phase velocities for horizontally polarized transverse waves as functions of angle (θ).

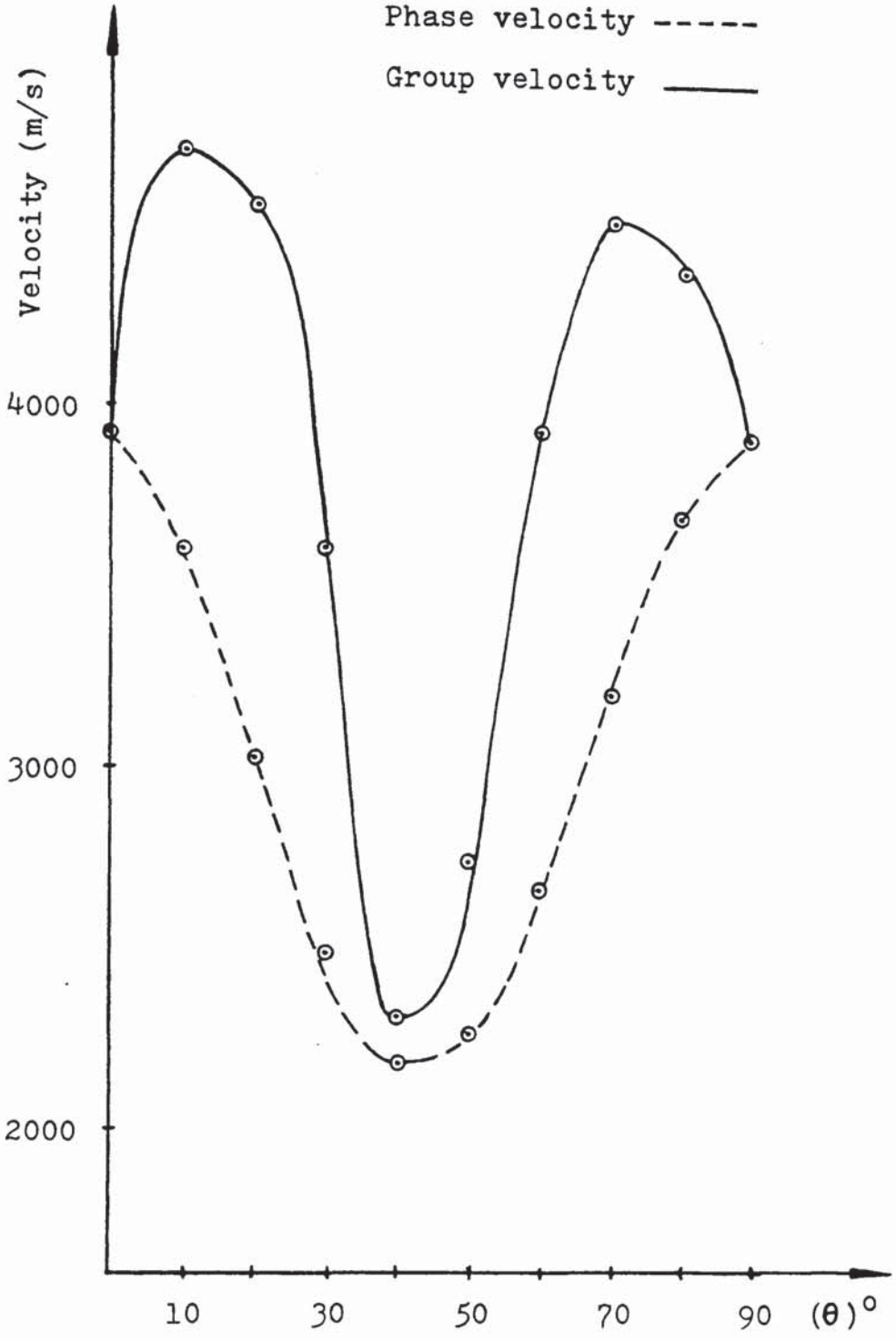

Figure 4.22 : Group and phase velocities for vertically polarized transverse waves as functions of angle (θ).

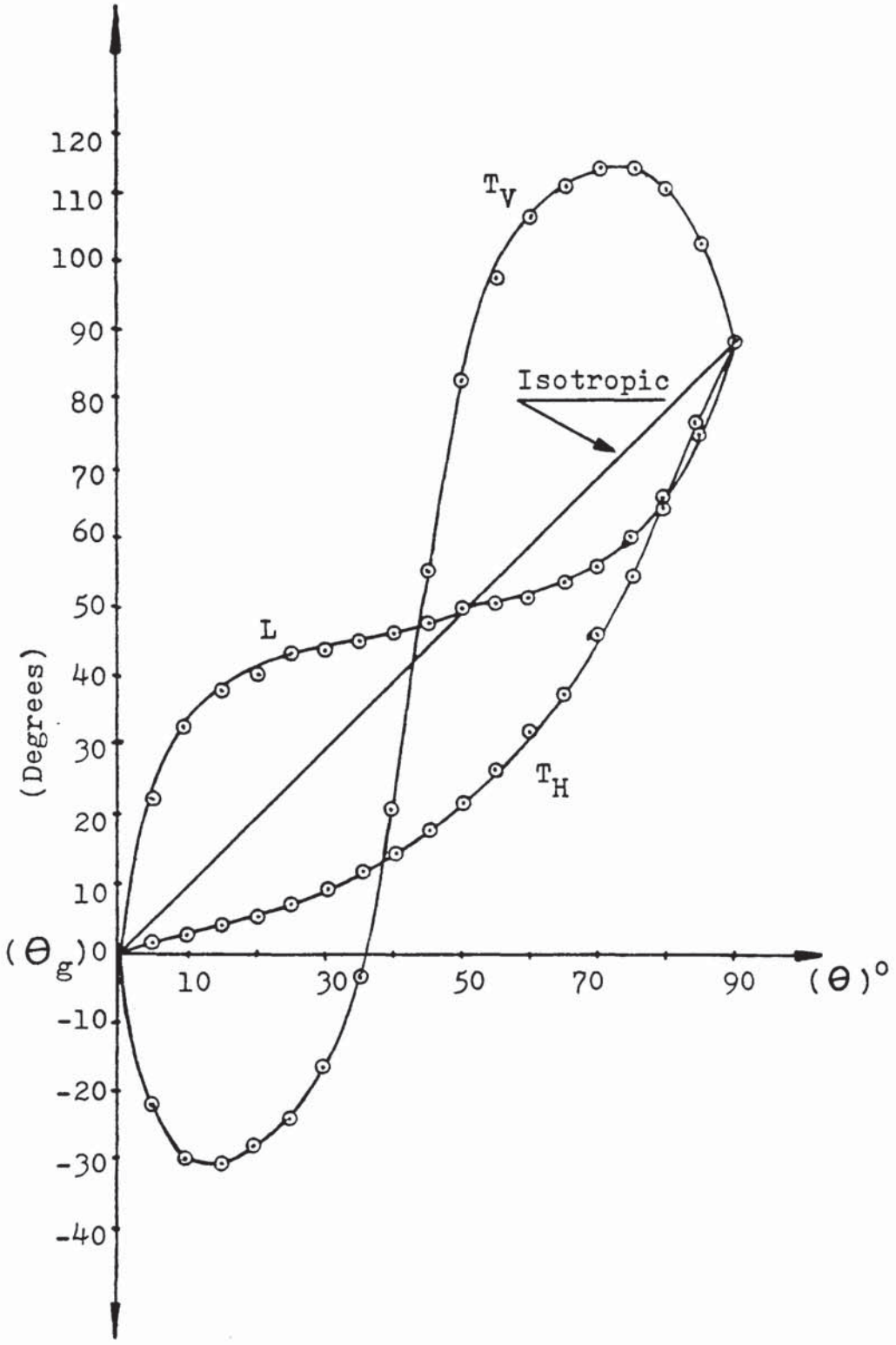

Figure 4.23 : Angle (Θ_g) between group and phase velocities as a function of angle (Θ) for the three propagational wave modes.

the angle between propagation direction and the columnar grain axis in the austenitic weld metal.

Using equations (23) and (24) and the computer programmes of Appendix 6, the results of Tables 4.13 and 4.14 were obtained. These results showing group velocity (S) and angle (θ_g) between group velocities and phase velocities as functions of the angle (θ), for the three propagational modes (L, T_1, T_2) are represented graphically by Figures 4.20, 4.21, 4.22 and 4.23, using the "average" elastic constants of Table 4.10.

The results of the velocity computations using all the elastic constants of Table 4.10, are represented in polar form in Appendix 7, for the three propagational modes.

4.4.4 Evaluation of Acoustic* Impedance Mismatch in the Austenitic Weldments

For sound propagating between two media with different elastic properties, there is a limit to the amount of energy that passes through the interface. Decisive for the amount of energy which is reflected and the amount that travels on into the second medium is a property of the media , namely their acoustic impedances.

The acoustic impedance of a medium is defined as the product of the density of the medium (ρ) and the velocity of sound in it (C) :

$$Z = \rho C \quad \ldots\ldots (25)$$

*(Characteristic acoustic impedance)

It has been established[121], that the ratio of the reflected (I_r) and incident energy (I_i) at normal incidence to a plane boundary separating two media, is related to their impedances via the relation:

$$\frac{I_r}{I_i} = \frac{(Z_2 - Z_1)^2}{(Z_1 + Z_2)^2} = R \quad \ldots\ldots\ldots (26)$$

where : $Z_1 = \rho C_1$ is the impedance of the first medium,

$Z_2 = \rho C_2$ is the impedance of the second medium,

and R is the reflection coefficient.

For the transmitted beam a similar result holds :

$$\frac{I_t}{I_i} = \frac{4 Z_1 Z_2}{(Z_1 + Z_2)^2} = T \quad \ldots\ldots\ldots (27)$$

where : I_t is the intensity of the transmitted beam,
and T is the transmission coefficient.

Large signals have been reported[33] as being generated by the interface of austenitic weldments during transverse wave examination, with lower signals when reverting to longitudinal wave examination. The effect was attributed to local impedance mismatch between the austenitic plate and weld metals.

As can be seen from equation (25), acoustic impedance is directly proportional to velocity, therefore the impedance of the austenitic weld relative to the plate impedance will vary according to the angle of approach (θ) of the waves. Having already obtained experimental values for the longitudinal velocity in the 316 austenitic plate, and velocity variations in the 316 austenitic weld metal, values of the reflection and transmission coefficients as functions of (θ) could be obtained using :

C_{L_p} = Longitudinal wave velocity in 316 austenitic plate,

C_{T_p} = Transverse wave velocity in 316 aust. plate,

Z_p = Acoustic impedance of 316 aust. plate,

Z_w = Acoustic impedance of 316 weld metal,

ρ_p = Plate density, 7990 Kgm^{-3},

ρ_W = Weld density, 8000 Kgm^{-3},

C_{L_w} = Longitudinal wave velocity in 316 weld metal,

C_{T_v} = Vertically polarized transverse velocity in weld,

C_{T_h} = Horizontally polarized transverse velocity in weld,

C_{L_p} = 6157 m/s , and C_{T_p} = 3248 m/s.

It was decided that the "average" velocity values of Table 4.11 were to be used in the calculations, in order that the results could be applied to a wider spectrum of austenitic weldments.

Table 4.15 gives the impedance values for the three propagational wave modes at various angles (θ).

Tables 4.16, and 4.17 give the reflection and transmission coefficients for the three propagational wave modes at normal incidence to the austenitic plate and weld metal interface for various angles of (θ). The results of Table 4.16 are shown in graphical form in Figure 4.24.

It is appropriate at this point to consider the relation between the sound pressure of the reflected wave (P_r) and the pressure of the incoming wave (P_i), because the electric potential generated from an ultrasonic transducer (probe), is directly proportional to the sound pressure of the impinging sound wave and vice versa.

It has been shown that[121] :

$$\frac{P_r}{P_i} = \frac{(Z_2 - Z_1)}{(Z_1 + Z_2)} \quad \ldots\ldots\ldots (28)$$

and

$$\frac{P_t}{P_i} = \frac{2\,Z_2}{(Z_1 + Z_2)} \quad \ldots\ldots\ldots (29)$$

(θ)	Z_L	Z_V	Z_H
	kg $m^{-2}s^{-1}$		
0	39981960	31448640	31448640
10	42019410	28875860	31208940
20	45247370	24217690	30513810
30	47860100	19879120	29411190
40	49466090	17410210	27996960
45	49841620	17306340	27213940
50	49929510	18009460	26406950
60	49290310	21269380	24824930
70	47700300	25655890	23458640
80	45694810	29658880	22523810
90	44616160	31448640	22188230

Table 4.15 : Acoustic impedances of 316 weld metal for the three propagational modes at various angles (θ).

(θ) Degrees	Reflection Coefficient %		
	(R_L)	(R_{T_V})	(R_{T_H})
0	1.1	0.9	0.9
10	0.63	0.3	0.8
20	0.2	0.1	0.6
30	0.02	1.8	0.4
40	0	3.9	0.1
45	0	4	0.1
50	0	3.3	0
60	0	1.0	0.1
70	0.03	0	0.3
80	0.14	0.4	0.5
90	0.24	0.9	0.6

Table 4.16 : Reflection coefficients from 316 weld metal parent metal interface for various values of (θ).

(θ) Degrees	Transmission Coefficient %		
	T_L	T_{T_V}	T_{T_H}
0	98.9	99.1	99.1
10	99.4	99.7	99.2
20	99.8	99.9	99.4
30	99.98	98.2	99.6
40	100	96.1	99.9
45	100	96	99.9
50	100	96.7	100
60	100	99	99.9
70	99.9	100	99.7
80	99.9	99.6	99.5
90	99.8	99.1	99.4

Table 4.17 : Transmission coefficients for a 316 weldment.

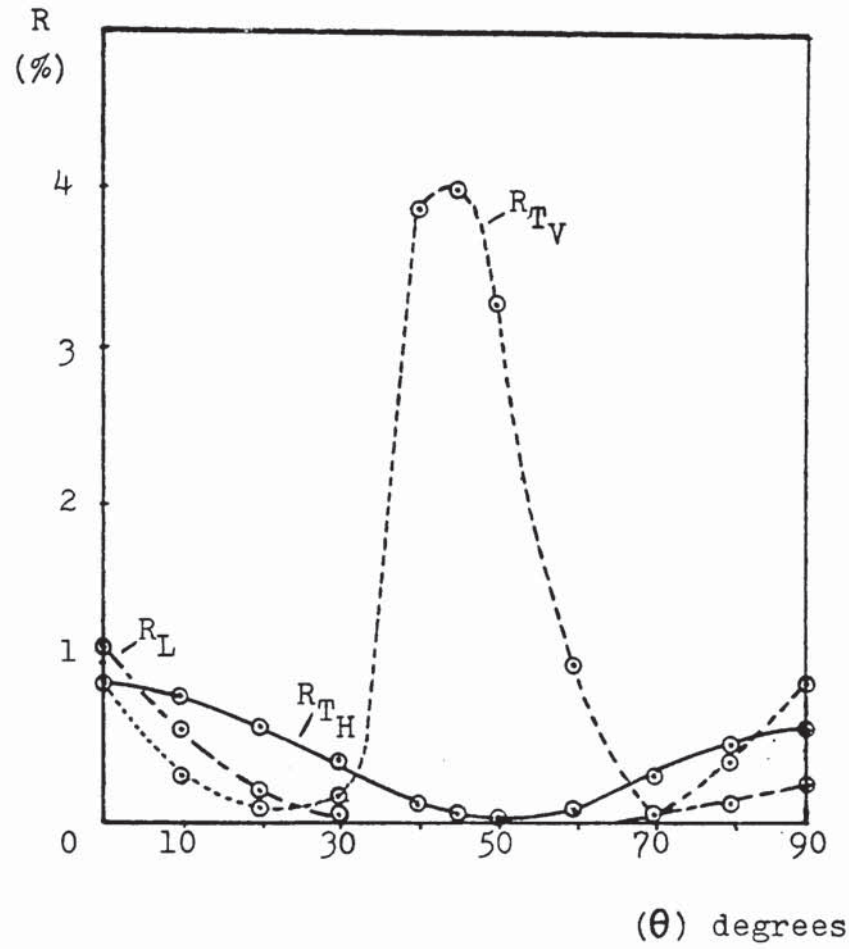

Figure 4.24 : Reflection coefficients (%) for the three propagational modes at various angles (θ).

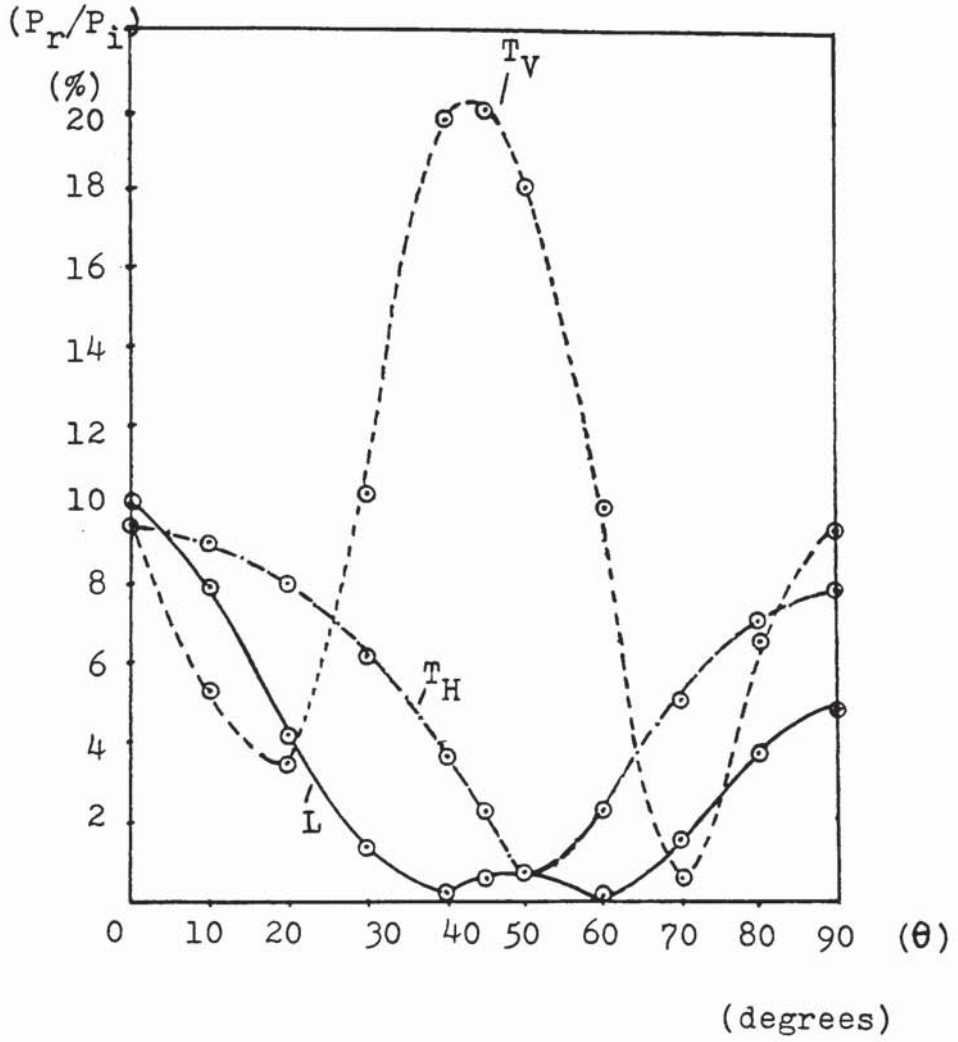

Figure 4.25 : Ratios of reflected to incident pressures for the three propagational wave modes for various angles(θ).

(θ) Degrees	Pressure Ratios %		
	$(P_r/P_i)_L$	$(P_r/P_i)_{T_V}$	$(P_r/P_i)_{T_H}$
0	-10.4	9.5	9.5
10	- 7.9	5.3	9.1
20	- 4.2	-3.5	8.0
30	- 1.4	-13.3	6.2
40	0.2	-19.8	3.7
45	0.6	-20	2.3
50	0.7	-18.1	0.8
60	0.03	-10	-2.3
70	-1.6	- 0.6	-5.1
80	-3.8	6.6	-7.1
90	-4.9	9.5	-7.9

Table 4.18 : Ratios of reflected to incident wave pressures for the three propagational wave modes on an interface of 316 weld and plate metals.

(θ)	$(P_t/P_i)_L$	$(P_t/P_i)_{T_V}$	$(P_t/P_i)_{T_H}$	%
0	89.6	109.5	109.5	
10	92.1	105.3	109.1	
20	95.8	96.5	108	
30	98.6	86.7	106.2	
40	100.2	80.2	103.7	
45	100.6	80	102.3	
50	100.7	81.9	100.8	
60	100	90	97.7	
70	98.4	99.4	94.9	
80	96.2	106.6	92.9	
90	95.1	109.5	92.1	

Table 4.19 : Ratios of transmitted to incident wave pressures for the three propagational wave modes on an interface of 316 weld and plate metals.

where : P_i is the acoustic pressure of the incident waves,

P_r is the acoustic pressure of the reflected waves,

P_t the acoustic pressure of the transmitted waves,

Z_1 is the acoustic impedance of the first medium,

and Z_2 is the acoustic impedance of the second medium.

It can be seen from equation (28) that when Z_2 is greater than Z_1, i.e. when sound travels from an acoustically less dense to an acoustically denser medium, reflection will take place without any change in phase of the acoustic pressure. However, when Z_2 is less than Z_1 , there is a phase change of 180 degrees in acoustic pressure.
Using equations (28) and (29), together with the impedances given in Table 4.15, the values of Tables 4.18 and 4.19 are obtained. The results of Table 4.18 are graphically represented in Figure 4.25.

5. Ultrasonic Detection of Real Flaws in Austenitic Weldments

5.1 Interaction of Ultrasound with Defects

The most common method of Ultrasonic testing at present, involves a skilled operator scanning a probe manually over the component under test. The probe (Ultrasonic Transducer) injects a short pulse of elastic waves into the component, and the returning signals are viewed on an oscilloscope screen, the vertical axis corresponding to the echo height and the horizontal axis to the elapsed time. A crack or other defect is an effective reflector, and some of the sound energy will be reflected back in the direction of the probe, arriving after a time interval which depends upon the distance travelled to and from the defect. Moving the probe so that the beam emitted scans across a defect enables its dimensions to be estimated, i.e. the operator interprets changes in the display as the probe is scanned in terms of defects which might be present. A detailed knowledge of the interaction of ultrasound with real defects, its propagating medium and other components is of fundamental importance in the process of defect characterization and directly affects the information available for a failure-assessment calculation.
In conventional NDT techniques defect location, sizing and

characterization are deduced from both the reflected pulse amplitude and its variation in position and magnitude as the defective volume is scanned with a transducer. It has long been recognized that many factors influence the amplitude of reflected ultrasonic signals from a defect[111,112,113,114], the most significant of these being the orientation of the reflecting surfaces of the defect with respect to the incident pulse, the shape and size of the defect, and its surface roughness. The magnitude of the last three parameters relative to the ultrasonic wavelength governs the defect reflection behaviour and hence the ultrasonic frequency of the transducer is another variable affecting the response of a defect.

On the interaction of ultrasound with defects, Wustenberg et al[112] have considered the effects of defect orientation on echo amplitude, and Haines and Langston[113] developed a model which accounts for the experimentally observed reflection of ultrasound from a variety of surfaces. Effects of a statistical surface roughness and variable reflection coefficient were included in the model. Haines on another paper[114] highlights the sensitivity to small changes of angle, to defect size, shape and surface roughness of the reflected amplitude from a crack-like defect, and outlines the limitations of present inspection codes based on reflected pulse amplitude.

The main problem arises from the fact that defects with mean surface roughness less than $\simeq \lambda/20$ tend to reflect ultrasound specularly rather than diffusely[114].
In such a case, defects larger or of the same order as the ultrasonic wavelength, will reflect energy directly back to the transducer for a limited range of angles. Surface roughness greater than $\simeq \lambda/20$ will produce significant scattering of the ultrasonic beam from the defect surface and a reduction of the received signal will take place (Figure 5.1).
A similar effect occurs when there is partial transmission of the ultrasound through a defect. For open cracks, blow holes, laminations, porosity etc. , their impedance might be vastly different from the impedance of the solid in which they occur and thus almost total reflection of ultrasound from these defects occurs. Inclusion defects, crack-like defects containing oil or water, and defects under compressive stresses might allow a significant through-transmission of ultrasound. "Ultrasonic transparency" has been reported on fatigue cracks under low levels of compressive stress (up to 20 MNm^{-2})[115,116]. Wooldridge [117] has demonstrated that for fatigue cracks under compressive stress, the reflectivities of the crack tip and the crack face can vary as much as -11 dB on application of compressive stress of 90 MNm^{-2}.

It has been demonstrated in the literature[113,114] that favourably oriented facets of a crack-like defect can give rise to echo signals of amplitude proportional to the projected area of the facet onto the incident ultrasonic wavefront plane (Figure 5.2). Thus one faceted defect can produce an echo pattern similar to that of several smaller isolated defects.

With crack-like defects, diffraction of the ultrasonic waves occurs from edges of the defect lying within the insonifying beam. For badly oriented flat defects, these diffracted signals may be the only ones returning to the transducer from the defect, giving misleading information about the defect size and character. This phenomenon has been clearly demonstrated by Nabel and Neumann[118] and by Jessop and Mudge[119].

Mode conversion of the incident ultrasonic beam at the defect can further complicate interpretation of conventional ultrasonic techniques due to the resulting reduction in intensity of the unconverted reflected signal and the production of several echoes from the defect. Silk[120], outlines the many possible wave components that might result from such an interaction with a defect, with several references to fundamental work on the theory of interaction of ultrasound with defects.

The pulse length and position of the receiver probe govern whether the various signals generated at the defect will be

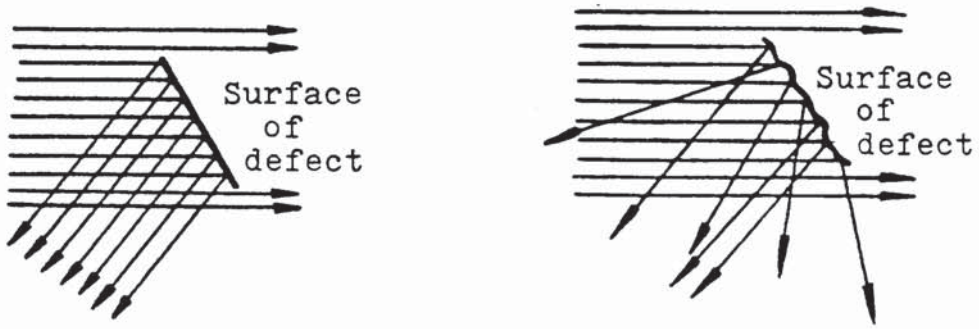

FIG. 5.1 : Reflection of waves from defects with dimensions very much greater than the wavelength having flat and rough surfaces oriented at an angle to the ultrasonic waves

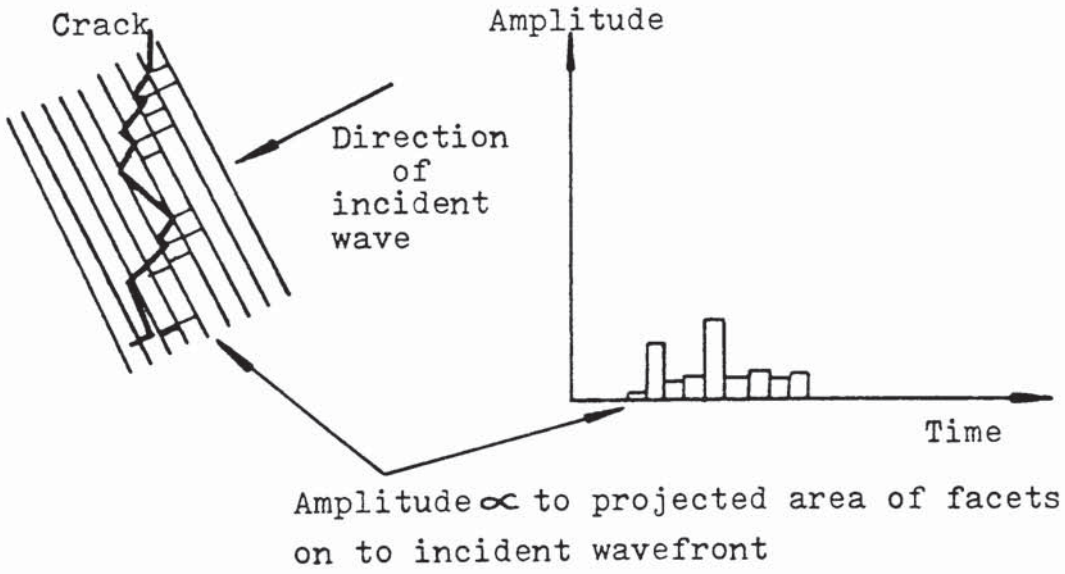

FIG. 5.2 : Ultrasonic response function from a faceted crack surface (after Haines[114])

seen as individual pulses, or as a single complex pulse formed by interference.

Another important factor that governs the ease of interpetation of received ultrasonic signals is the defect location. Signals from several defects that are close together may be difficult to separate due to overlap and interference effects. An added factor is the possibility of the receiver failing to detect a large but poorly oriented crack-like defect due to its weak signal arriving at the transducer during the dead time following the reception of a large signal from an innocuous reflector, such as slag or test piece surfaces such as front and back walls or weld metal parent metal interfaces. A similar effect could occur if the pulse length were such that the weak signal is lost in the strong.

In view of the complexity of the interaction of ultrasound with defects outlined above, the problems associated with ultrasonic propagation in austenitic weldments exacerbate an already difficult situation.

On the positive side, however, the amount of information contained in the reflected signals from defects in austenitic weldments, could be greatly enhanced if the right choice of inspection technique is made. By suitability of technique is meant, the most effective frequency, angle, scanning position, wave mode etc. The rest of this section

is concerned with establishing experimental data comparing the effectiveness of these parameters when inspecting fatigue, and corrosion-fatigue cracks in 316 and 347 type austenitic weldments.

5.2 Experimental Technique

5.2.1 Preparation of Fatigue Cracks

Two specimens from the 316 welded plate (double-U), together with one from the 347 welded plate (single-V) were machined to bars of dimensions 300 x 22.5 x 31, 300 x 22.5 x 35, and 300 x 22.5 x 31 mm respectively. The chemical compositions of the plate materials are given in Table 3.1, and the details of welding parameters and procedures in Table 3.2.

All specimens were finished by grinding. A V-notch of 60^{o} included angle and 2 mm depth was introduced in the weld metal of specimen S_1 and the HAZ's of specimens S_2 and S_3 to act as a crack initiator (Figure 5.3).

Fatigue cracks of 2 mm were then propagated in all specimens using a 2-Ton Amsler Vibrophore fatigue machine. The V-notches were then machined off and the surfaces finished by grinding. Table 5.1 gives the mechanical properties of specimens S_1 and S_2, and Table 5.2 indicates the cracking conditions both for the initiation and propagation stages for all specimens.

316 austenitic weldment

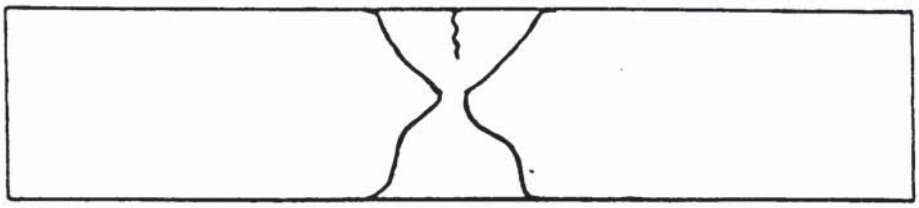

Specimen S_1

316 austenitic weldment

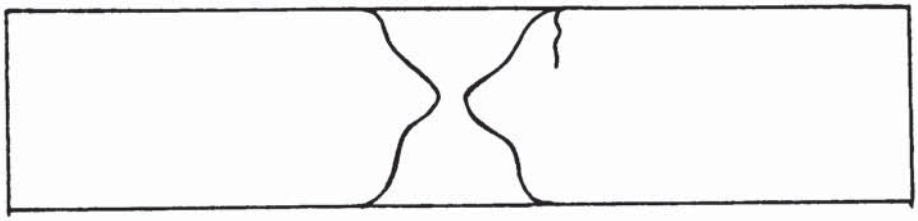

Specimen S_2

347 austenitic weldment

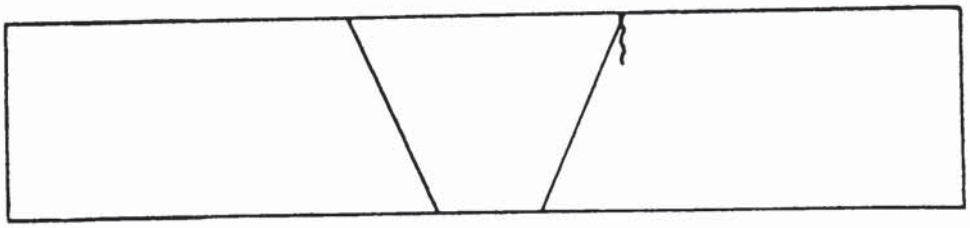

Specimen S_3

Figure 5.3 : Austenitic weldments containing fatigue cracks.

Alloy 316 s.s.	Yield Strength (MNm^{-2})	Tensile Strength (MNm^{-2})	(%) Elongation	(%) Reduction in area	Hardness (Hv)
Weld Metal	333	655	76	66	317
Parent Metal	309	605	67	58	282

Table 5.1 : Mechanical properties of 316 austenitic stainless steel plate and weld metal.

Stages	316 Austenitic Weldments and 347 a.w.			
	Main load		Resonating load	
	Tons	Newtons	Tons	Newtons
Initiation	0.76	7600	±0.70	±7000
Propagation	0.60	6000	±0.50	±5000

Table 5.2 : Fatigue crack initiation and propagation conditions in the heat affected zone and the weld metal of 316 & 347 austenitic weldments.

5.2.2 Preparation of Corrosion-Fatigue Cracks

In order that valid comparisons could be drawn, two more specimens were machined from the 316 (double-U) welded plate in the shape of bars of dimensions 250x22.5x26 , 230x22.5x25 mm respectively. For accomodating the corrosive medium in such a way that it would be allowed to act on the fatigue cracks generated in the specimens, provisions were made in the designing of the V-notch in the weld and the heat affected zone (HAZ) of the two specimes (Figure 5.4). The corrosive agent used was artificial sea water, and it consisted of :

Sodium Chloride	26.5 gms
Magnesium Chloride	2.4 gms
Magnesium Sulphate	3.3 gms
Calcium Chloride	1.1 gms
Potassium Chloride	0.7 gms
Sodium Carbonate	0.2 gms
Sodium Bromide	0.3 gms

The cracks were initiated and propagated to a size of 2 mm, and then the slotted step and the V-notch were removed. The specimens were finished by grinding.
Table 5.3 gives the initiation and propagation conditions for specimens S_4 and S_5 shown in Figure 5.5.

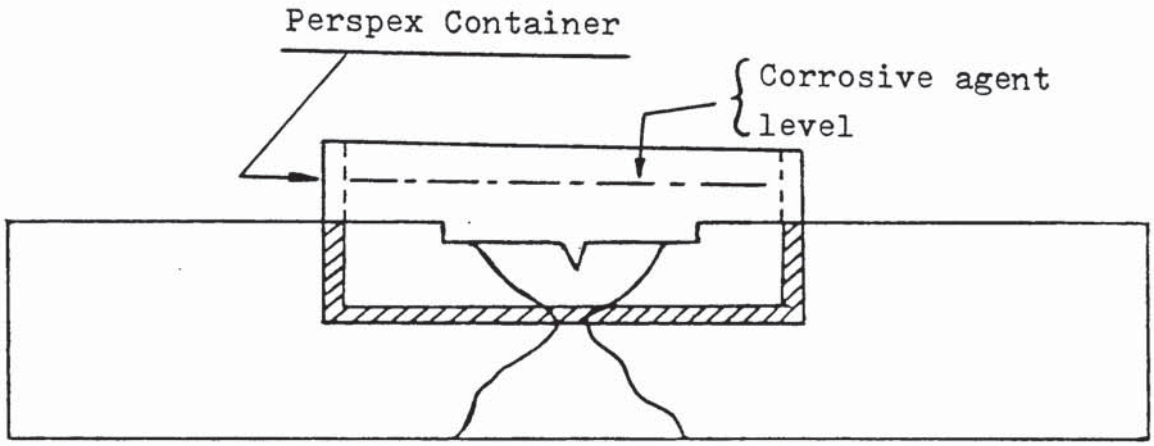

Figure 5.4 : Schematic representation of arrangement used for the propagation of corrosion-fatigue cracks in austenitic weldments.

Stages	316 Austenitic Weldments			
	Main load		Resonating load	
	Tons	Newtons	Tons	Newtons
Initiation	0.5	5000	$\pm$0.3	$\pm$3000
Propagation	0.4	4000	$\pm$0.2	$\pm$2000

Table 5.3 : Corrosion-fatigue cracks initiation and propagation conditions in the heat affected zone and the weld metal of 316 austenitic weldments.

5.2.3 Ultrasonic Inspection of Fatigue Cracks

In order that the most significant parameters, e.g. beam angle, frequency, mode and scanning position, were evaluated, and the most effective combination of these parameters established, Specimen S_2 was used as the initial guide. Cracks of 2,4,6, and 8 mm sizes were successively introduced in the heat affected zone (HAZ) of this specimen, allowing inspection to take place with the ultrasonic beam scanning through the austenitic plate only, and plate and weld metal together (Figure 5.6).

From these initial tests it was decided that half-skip scanning positions should be used throughout the experimental investigations because the poor signal to noise ratios involved and the complex indications resulting when the soundbeams travelled through the austenitic weld metal would become intolerable at full-skip scanning positions.

In a similar manner it was decided that 5 MHz transverse wave angle probes were not suitable for detecting the cracks when the ultrasonic beam travelled through the austenitic weld metal. Figure 5.7 shows the response to fatigue cracks of various sizes generated in specimen S_2, using 45°, 60° and 70°, 2 & 5 MHz transverse wave probes at half skip scanning positions. Figure 5.8 shows the response to fatigue cracks of various sizes in specimen S_3, using the above probes and parameters.

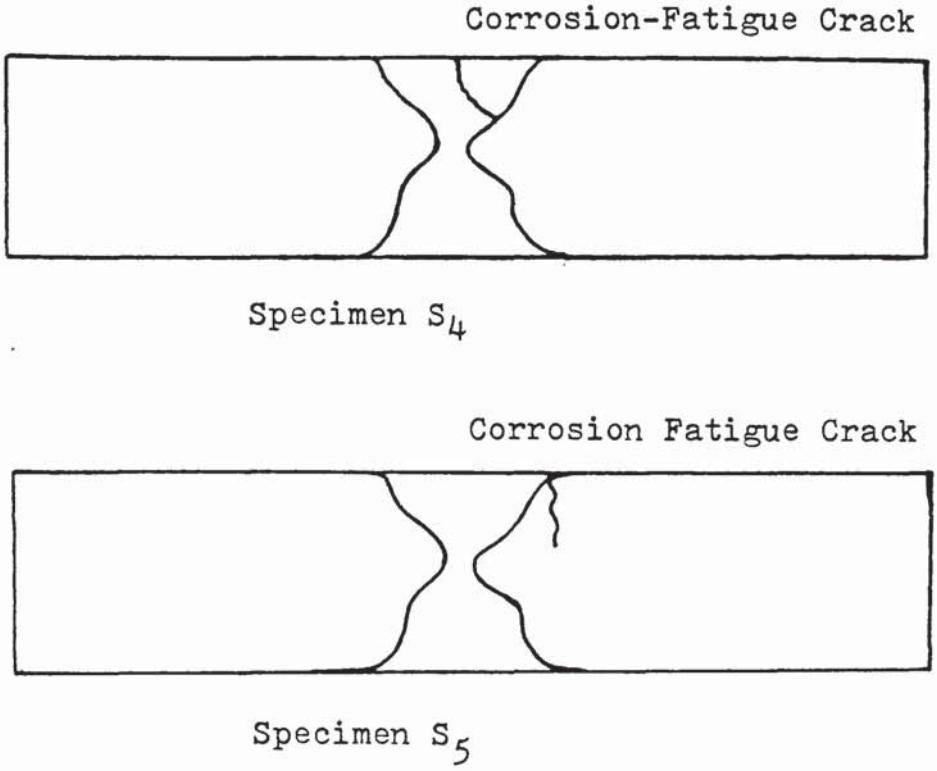

Figure 5.5 : 316 Austenitic Weldments containing Corrosion Fatigue Cracks.

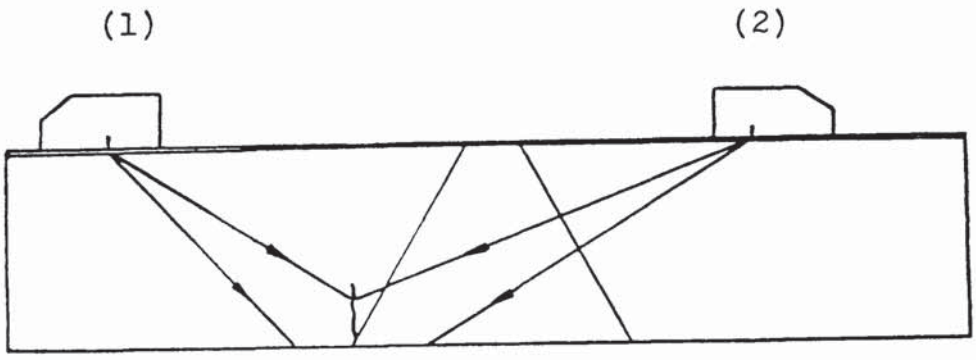

Figure 5.6 : (1) Scanning through plate metal only,
(2) Scanning through plate and weld metal together (schematic).

Figure 5.9 gives a graphical representation of the response to fatigue cracks of various sizes in specimen S_1, using 45^o, 60^o and 70^o 2 MHz transverse wave probes at half skip scanning positions.

In the case of specimen S_1, only the 2 MHz frequency probes were used, and the crack sizes were slightly larger than in specimens S_2 and S_3 (viz. 3,5,7 mm respectively).

Due to the late acquisition of longitudinal angle probes, and welded material constraints, only one sample could be manufactured from the 316 (double-U) plate in the form of a bar with dimensions 220x22.5x20 mm.

The same procedure was used for generating a fatigue crack (of size 1.8 mm) in the weld metal of sample S_6. The crack was inspected using all the longitudinal angle probes and then its size was increased to 3 mm and once again inspected, this time using all longitudinal angle probes available (see Table 3.4), and for comparison reasons with the 2 MHz 45^o, 60^o and 70^o transverse wave probes. Finally the crack was increased to a size of 4mm and inspected once more using the longitudinal angle probes. These results are shown in Figs. 5.10, 5.11 and 5.12 respectively.

5.2.4 Ultrasonic Inspection of Corrosion-Fatigue Cracks

The initial crack sizes in specimens S_4 and S_5 were 2 mm. These cracks were inspected using 2 MHz transverse wave probes,

at half skip scanning position, with the ultrasonic beam propagating both through the austenitic plate only, and through both the plate and weld metal as shown in Fig.5.13. The cracks were increased in steps of 2 mm up to a final size of 8 mm, and were inspected at each step using the 2 MHz transverse probes. For comparison, the final size of 8 mm was inspected using the longitudinal 45° focused probe that was available at the time. These results are graphically represented in Figures 5.14 and 5.15.

5.2.5 Ultrasonic Inspection of Fatigue and Corrosion-Fatigue Cracks Under Compression

The specimens containing the fatigue and corrosion-fatigue cracks of known depths were placed in the Amsler 3-point bending jig and were subjected to static compression. The specimens were mounted in such a way that the crack would tend to close under the applied compressive stresses (Figure 5.16).

In order that the effect of compressive stresses on the ultrasonic signal returning from the crack be recorded, the following steps were taken :

1. The specimen was scanned using an angle probe until the crack existing in the weldment was located.

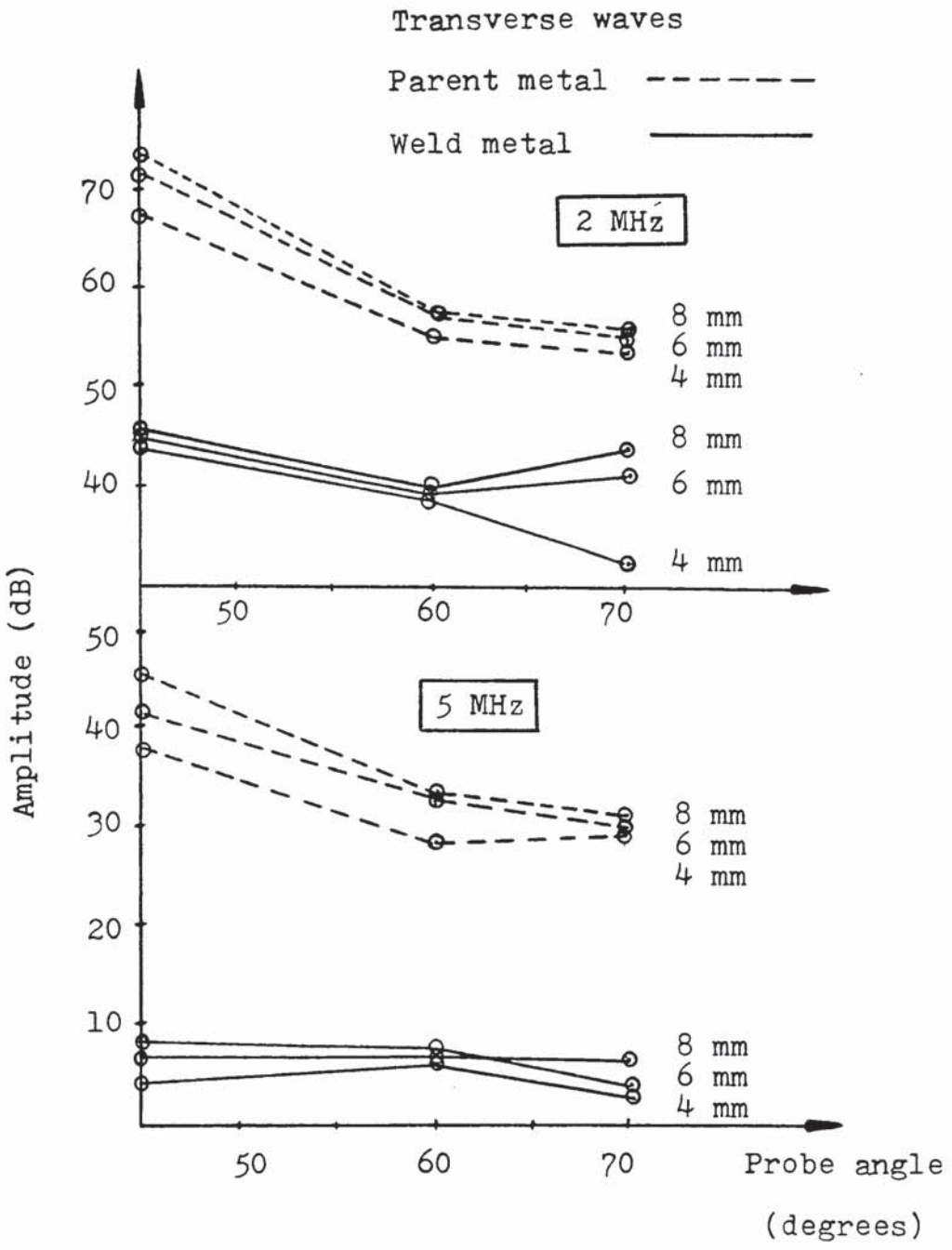

Figure 5.7 : Response to fatigue cracks in specimen S_2 using 45^{o}, 60^{o}, and 70^{o} probes at $\frac{1}{2}$ skip scanning positions.

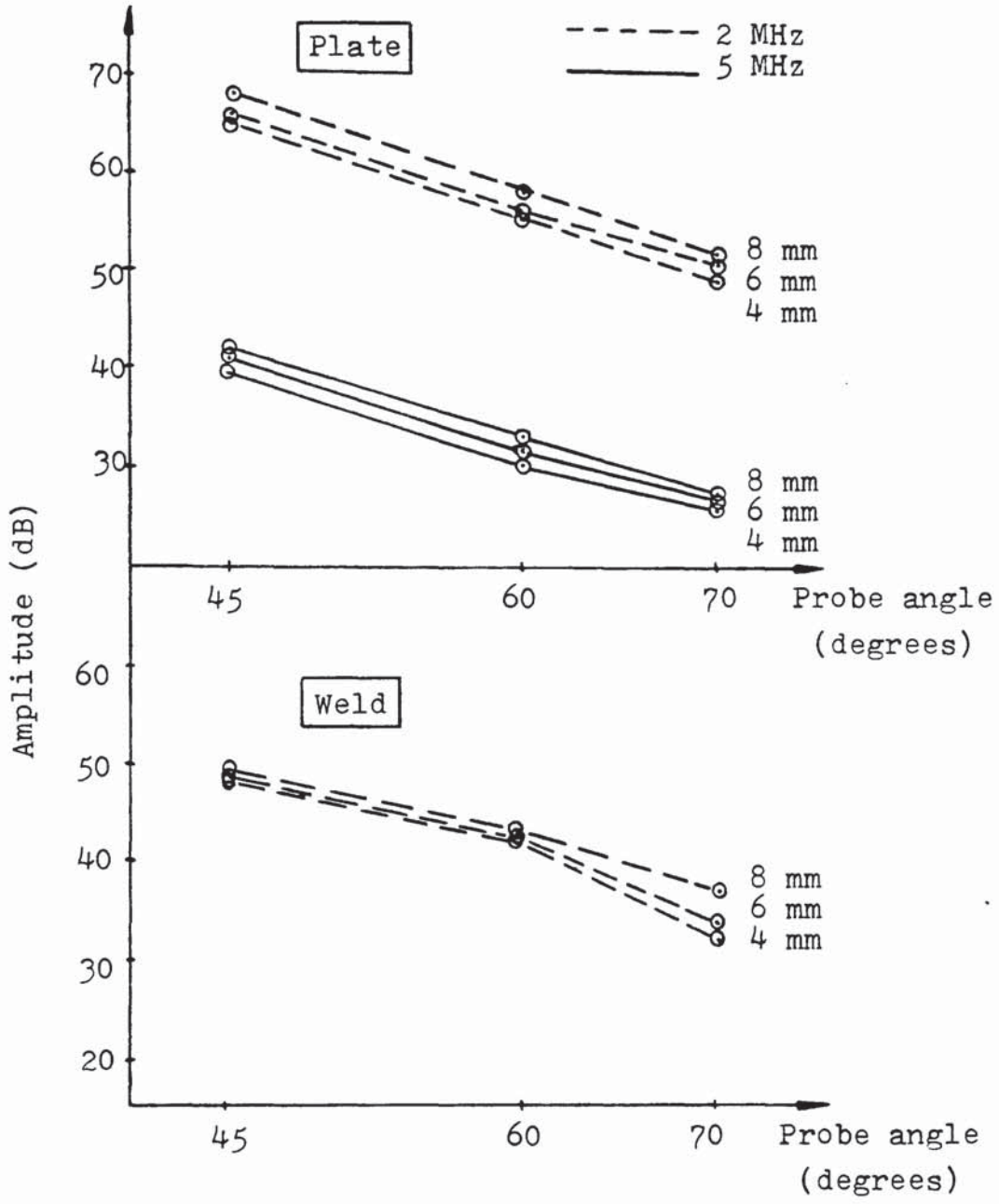

Figure 5.8 : Response to fatigue cracks in Specimen S_3 using 45°, 60° and 70° transverse probes at $\frac{1}{2}$ skip scanning positions.

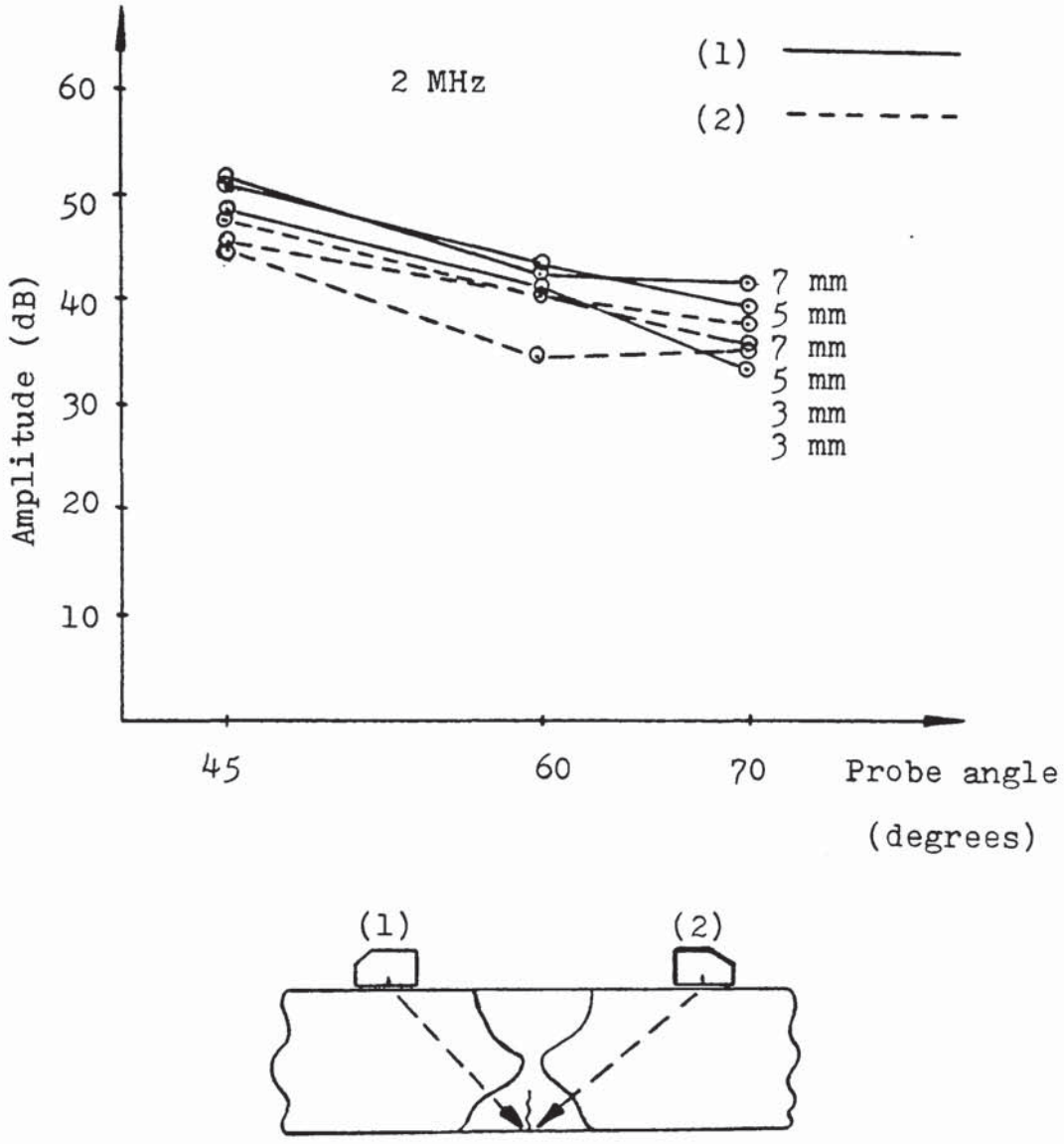

Figure 5.9 : Response to fatigue cracks in Specimen S_1 using transverse angle probes at $\frac{1}{2}$ skip scanning positions.

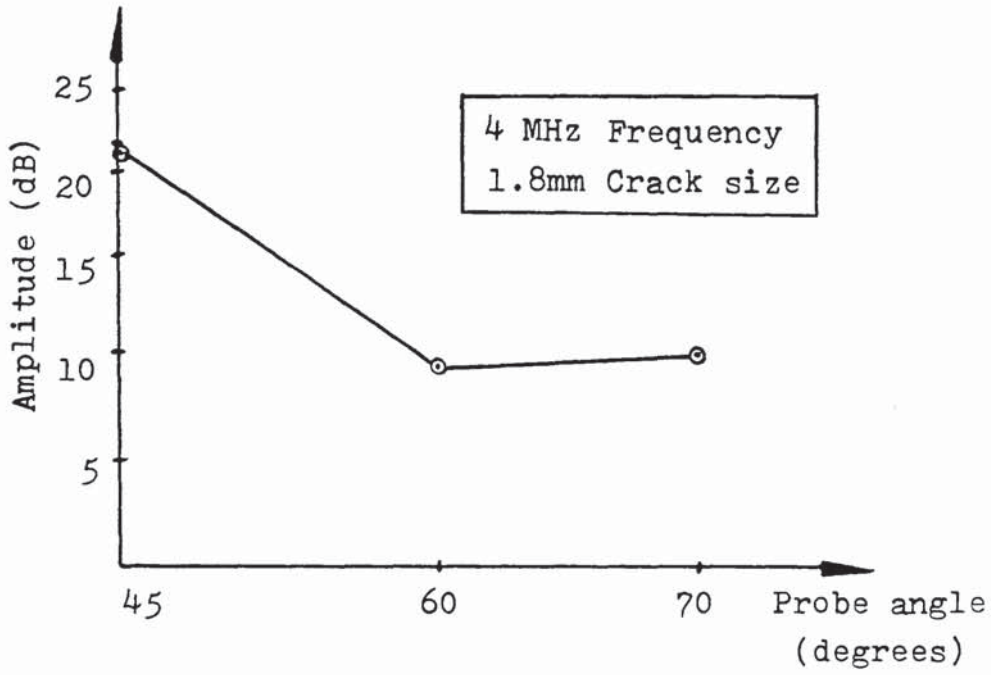

Figure 5.10 : Response to fatigue cracks in Specimen S_6 using longitudinal angle probes at $\frac{1}{2}$ skip scanning positions.

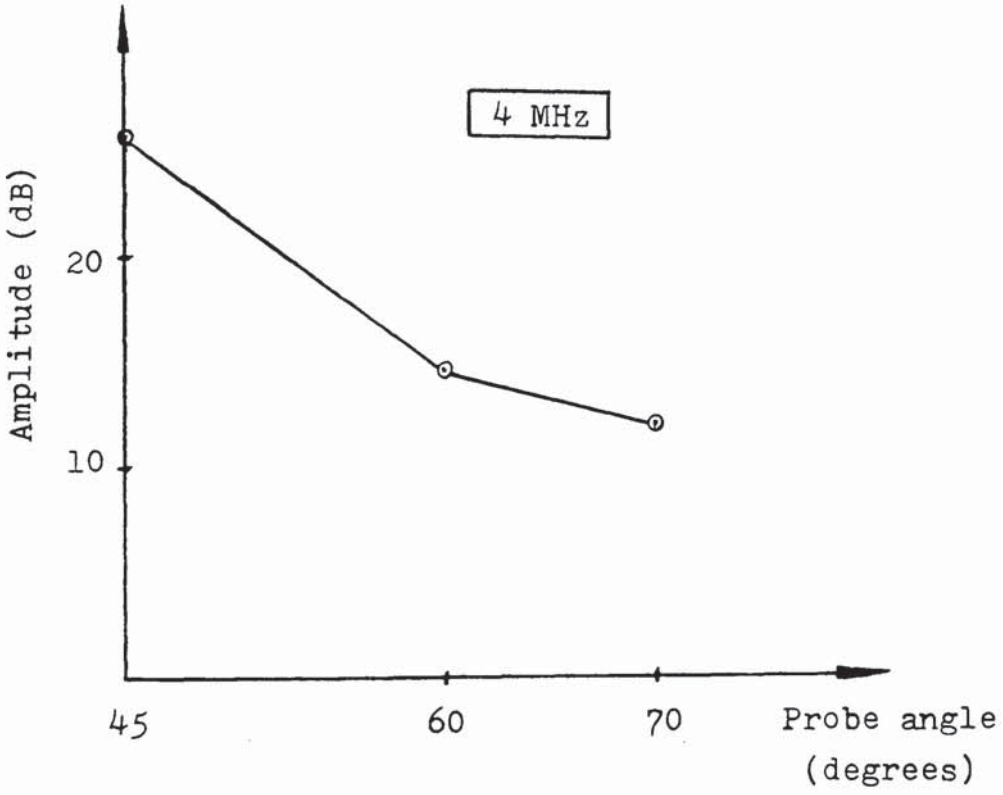

Figure 5.11 : Response to a 4 mm fatigue crack in Specimen S_6 using longitudinal angle probes.

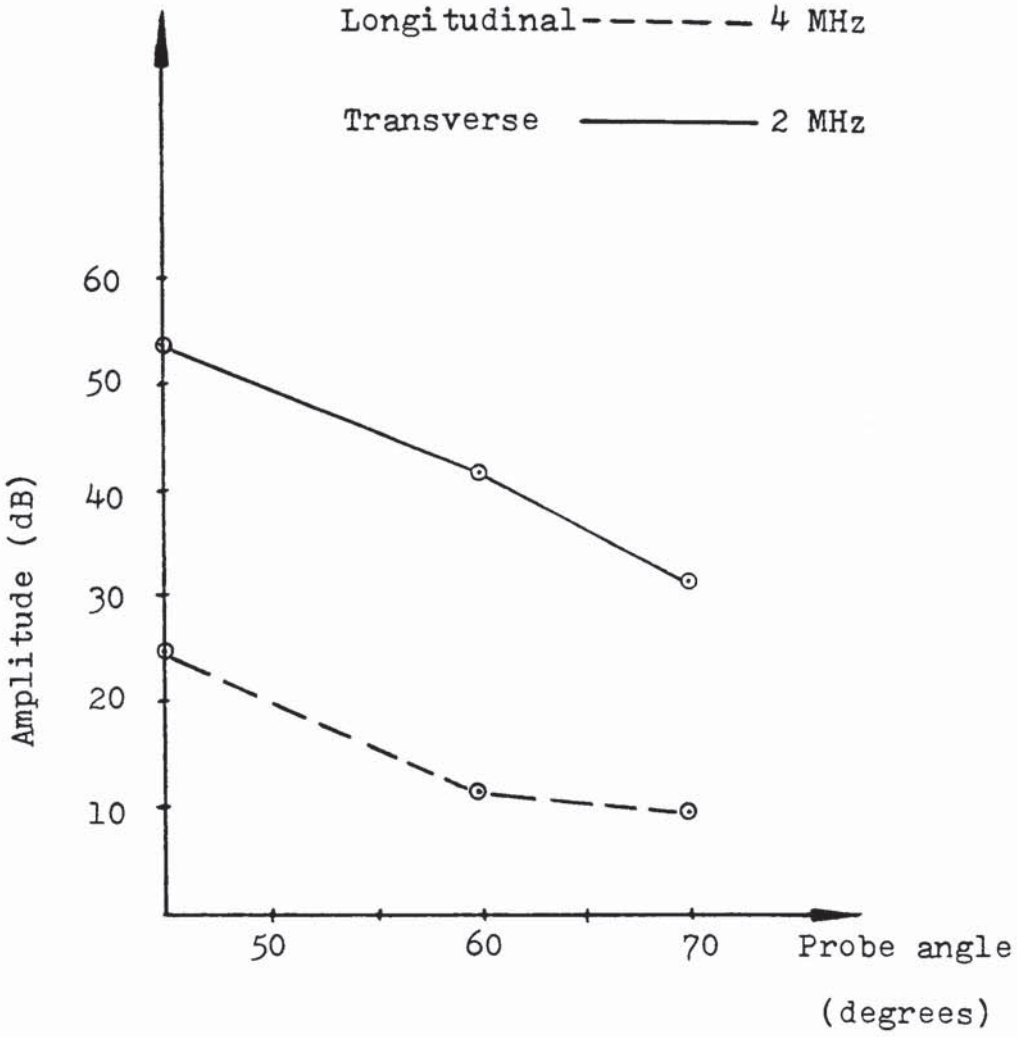

Figure 5.12 : Response to a 3 mm fatigue crack in Specimen S_6, using longitudinal and transverse angle probes at $\frac{1}{2}$ skip.

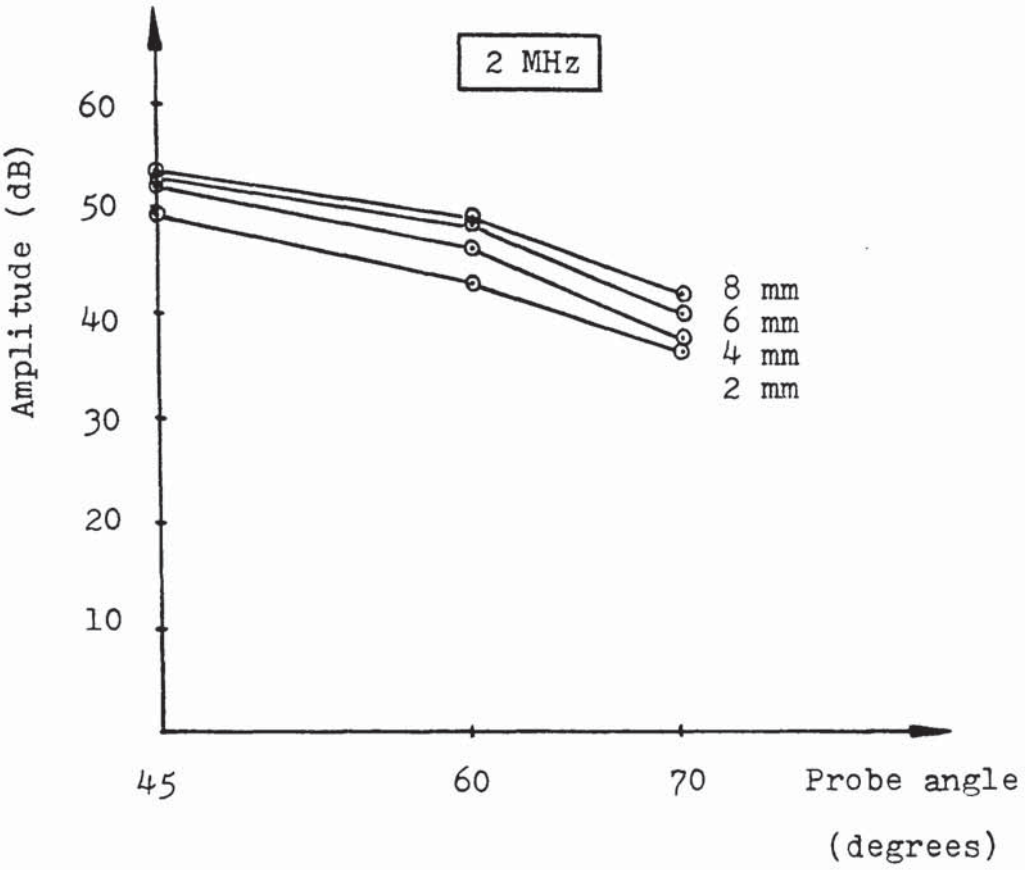

Figure 5.13 : Response to corrosion-fatigue cracks in Specimen S_4, using transverse wave angle probes at $\frac{1}{2}$ skip.

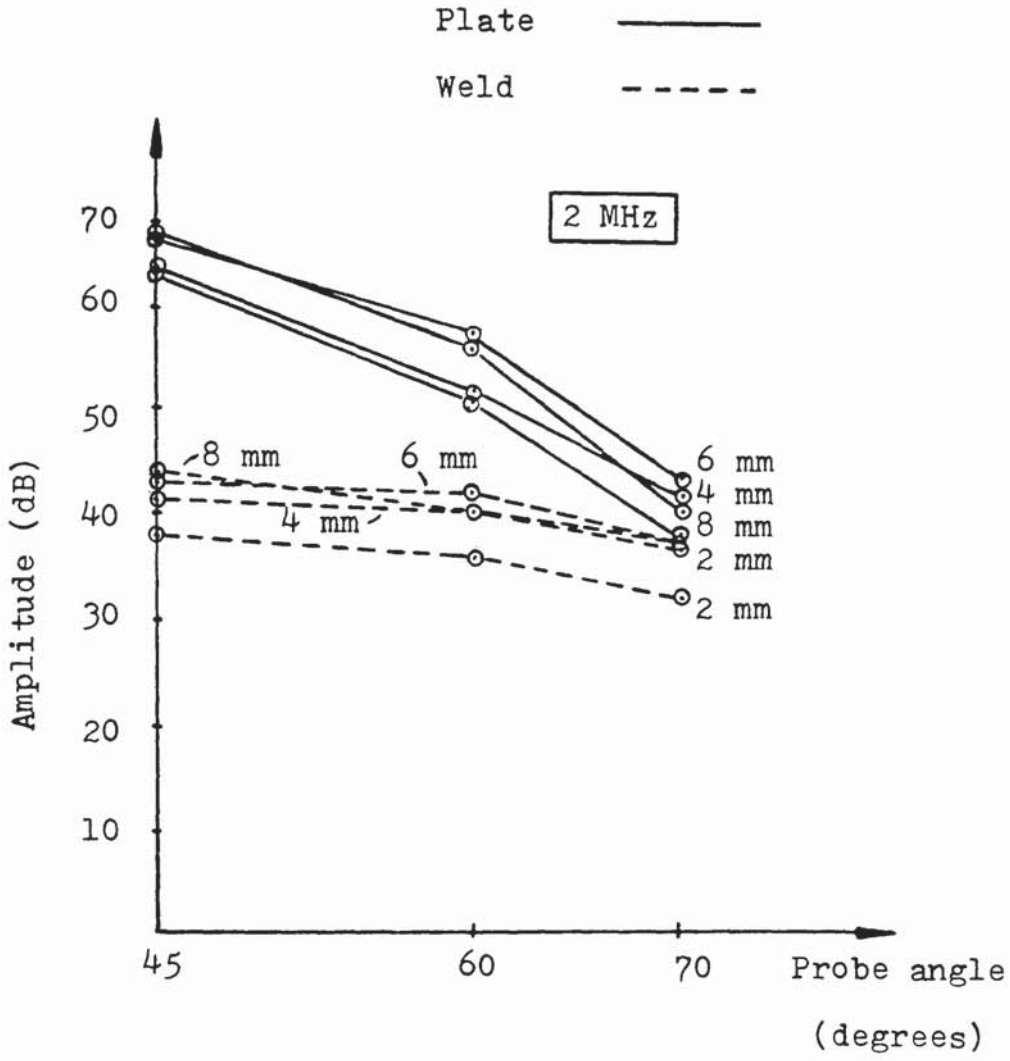

Figure 5.14. : Response to corrosion-fatigue cracks in Specimen S_5, using transverse angle probes at $\frac{1}{2}$ skip.

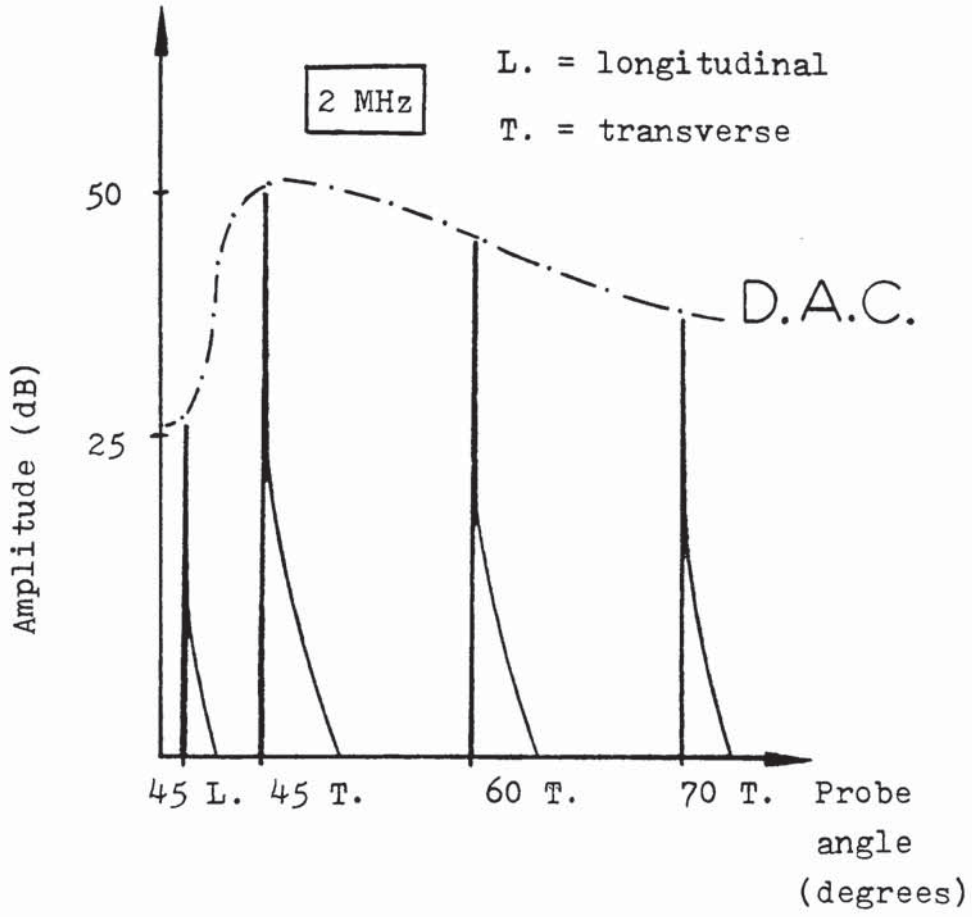

Figure 5.15 : Response from an 8 mm corrosion-fatigue crack in Specimen S_5, using transverse angle probes together with a focussed longitudinal angle probe at $\frac{1}{2}$ skip.

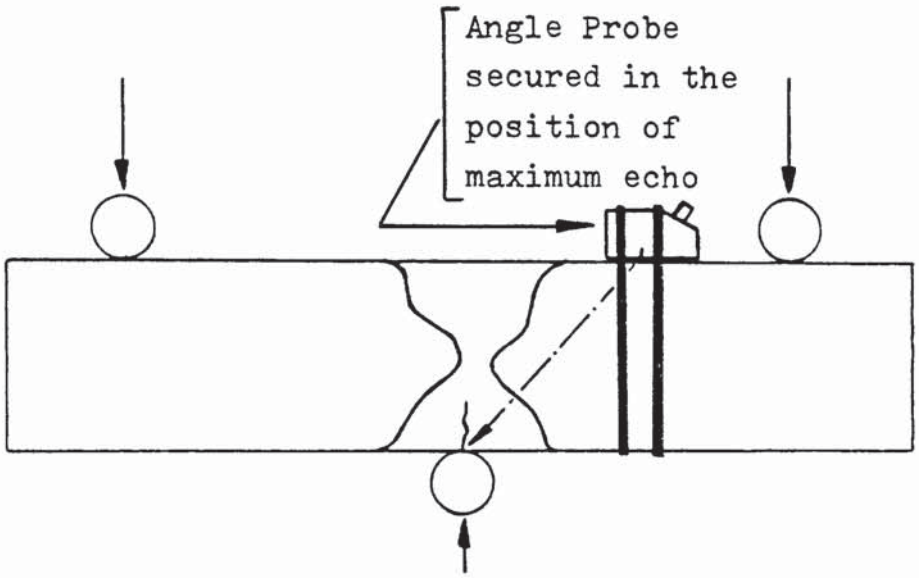

Figure 5.16 : Test piece mounted on three point bending jig for angle probe scanning of cracks under compressive loading.

2. The signal from the crack was maximised, and the probe was securely bound in position.

3. The specimen and probe arrangement was mounted on the bending jig (Figure 5.16).

4. Elastic bending loads were introduced in small increments, and the amplitude of the echo signal in dB was recorded, keeping the signal height at 80 % full-screen-height (F.S.H.) at each load increment.

This procedure was continued until a predetermined load value was reached. The resultant compressive stresses involved were kept below the yield strength of the material, because bending theory only applies up to the yield stress of the material.

Using the procedure outlined above, the results shown in Figures 5.17 to 5.31 inclusive were obtained.

Appendix 8, outlines how the elastic compressive bending stresses involved in the above procedure were determined, together with calculation samples on their determination.

Appendix 9, presents typical echo amplitude measurements from fatigue and corrosion-fatigue cracks under comressive stresses.

Finally, Appendix 10 contains two papers published in the British Journal of NDT based on the work outlined in this section.

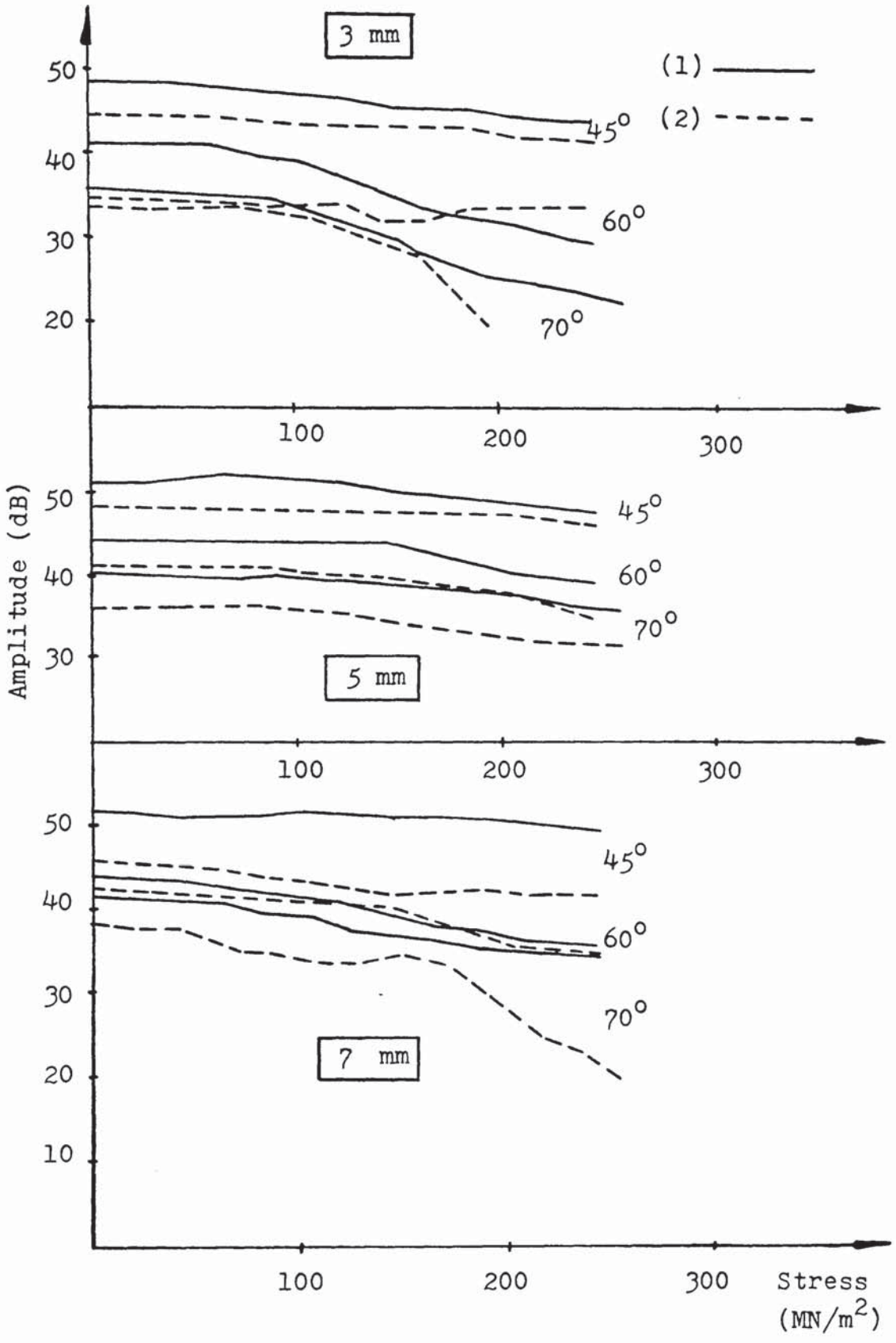

Figure 5.17 : Signal amplitude responses from fatigue cracks in specimen S_1 using 2 MHz transverse angle probes at $\frac{1}{2}$ skip.

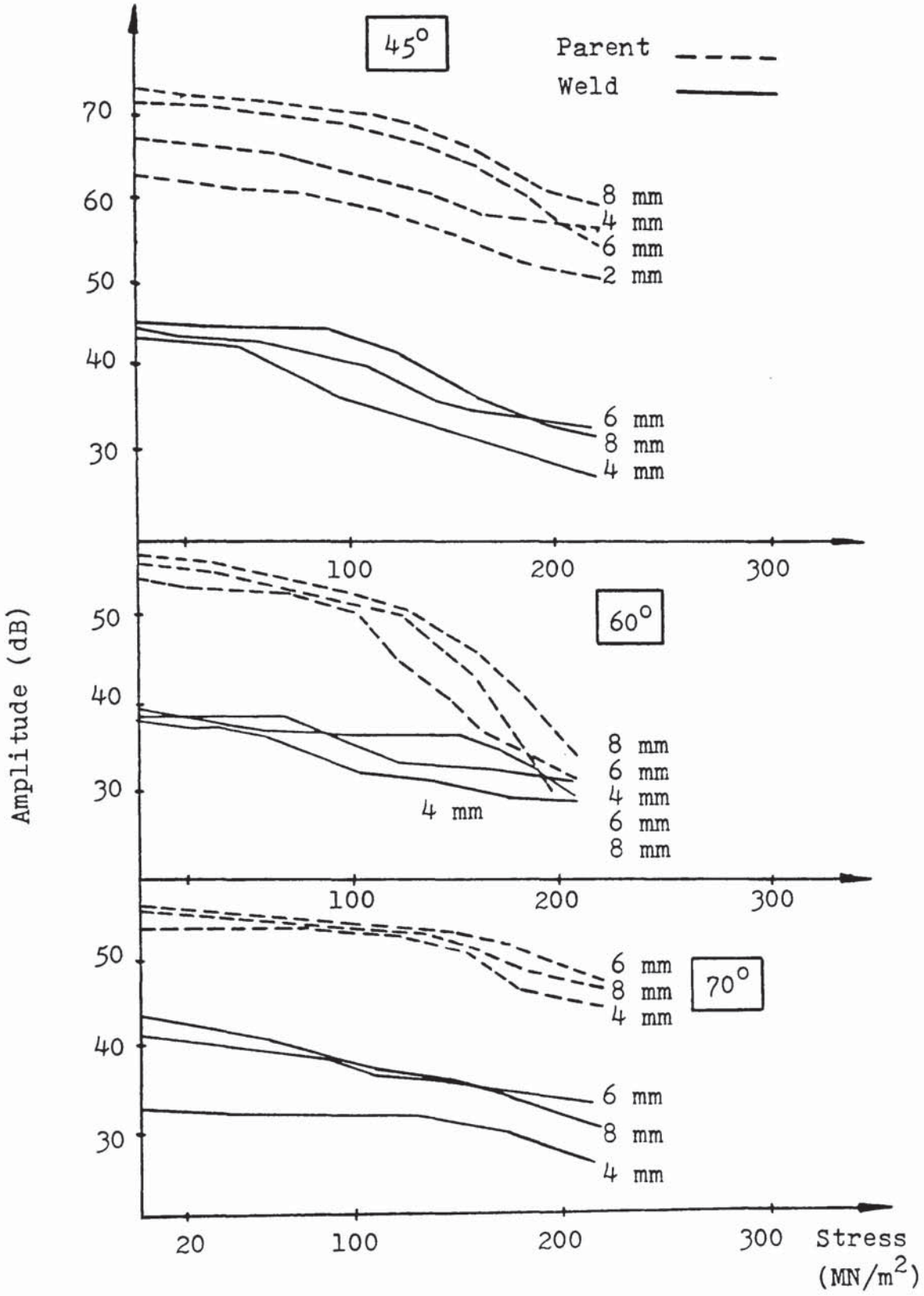

Figure 5.18 : Responses from fatigue cracks in specimen S_2, using 2 MHz transverse angle probes at $\frac{1}{2}$ skip scanning positions.

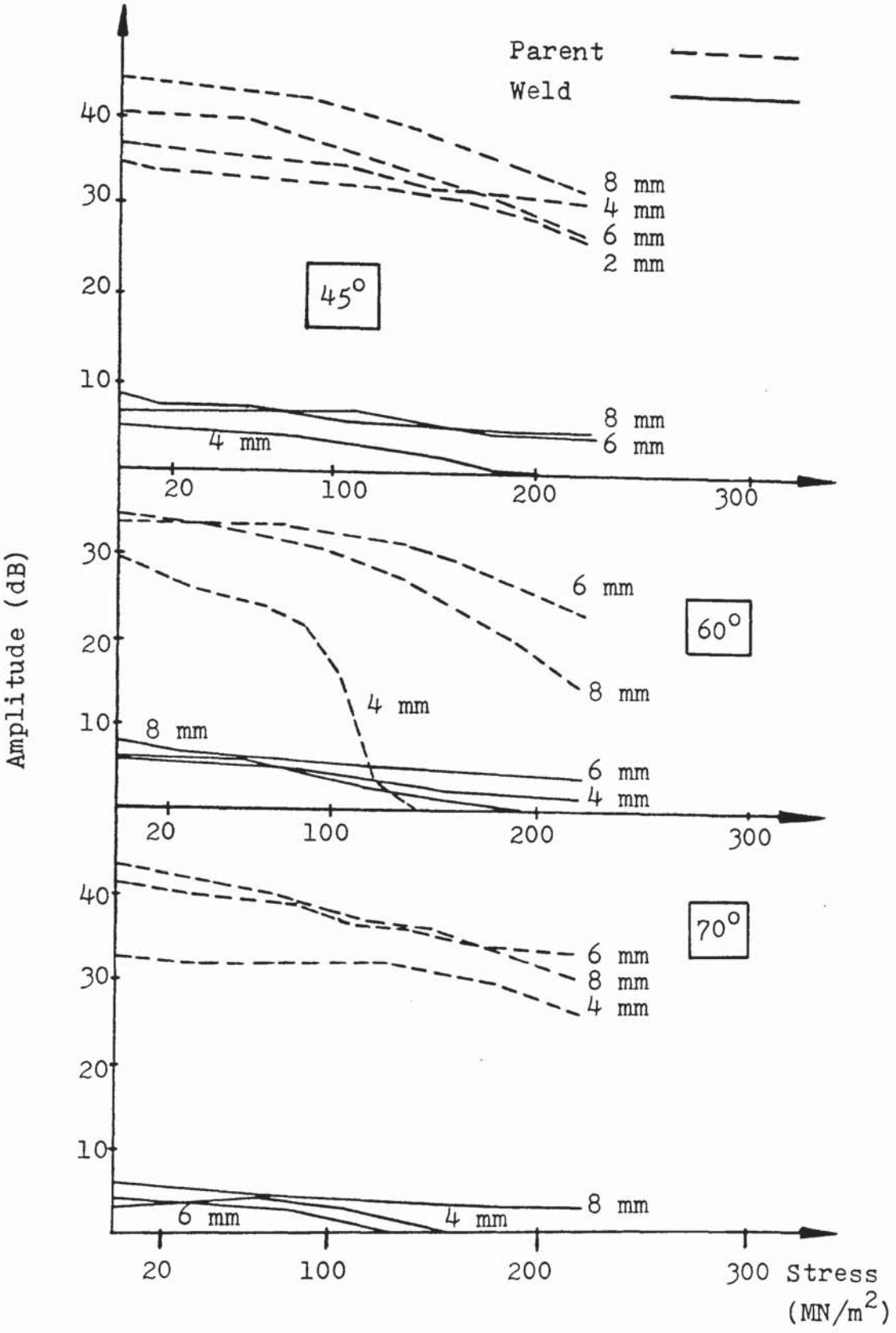

Figure 5.19 : Responses from fatigue cracks in specimen S_2, using 5 MHz transverse angle probes at $\frac{1}{2}$ skip scanning positions.

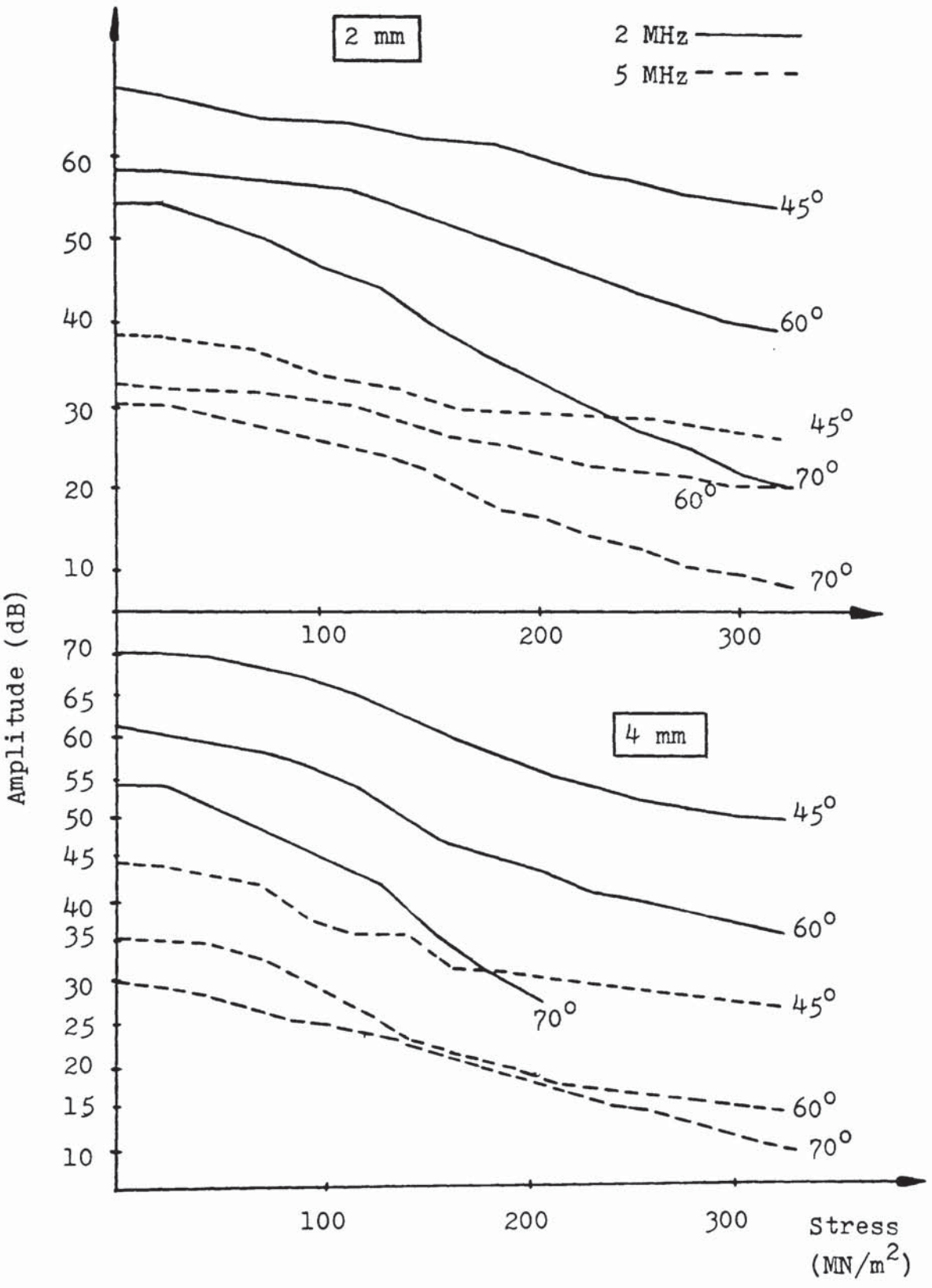

Figure 5.20 : Responses from fatigue cracks in specimen S_3, using transverse angle probes at $\frac{1}{2}$ skip scanning positions, through plate metal.

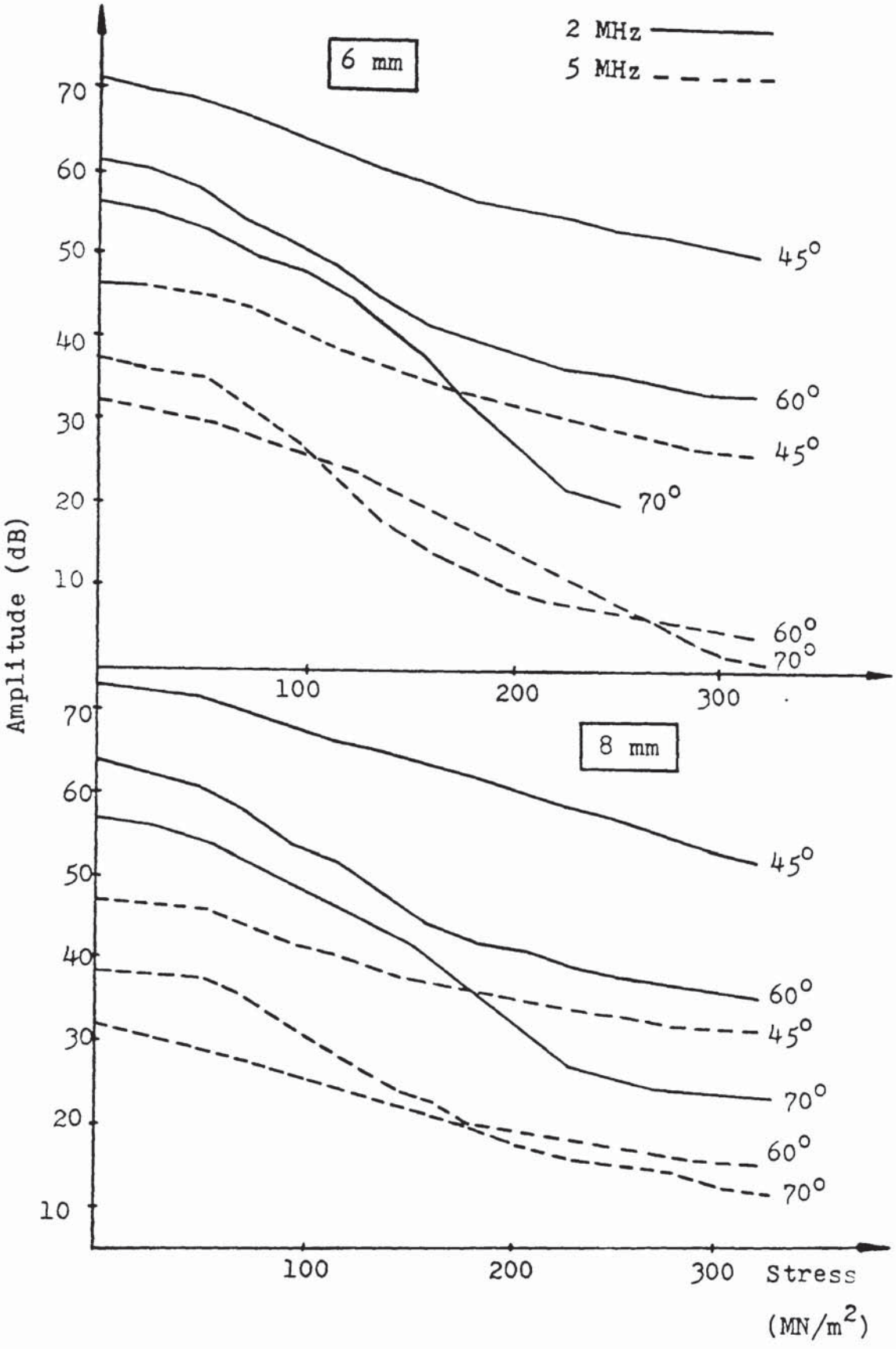

Figure 5.21 : Responses from fatigue cracks in specimen S_3, using transverse angle probes at $\frac{1}{2}$ skip scanning positions, scanning through plate metal.

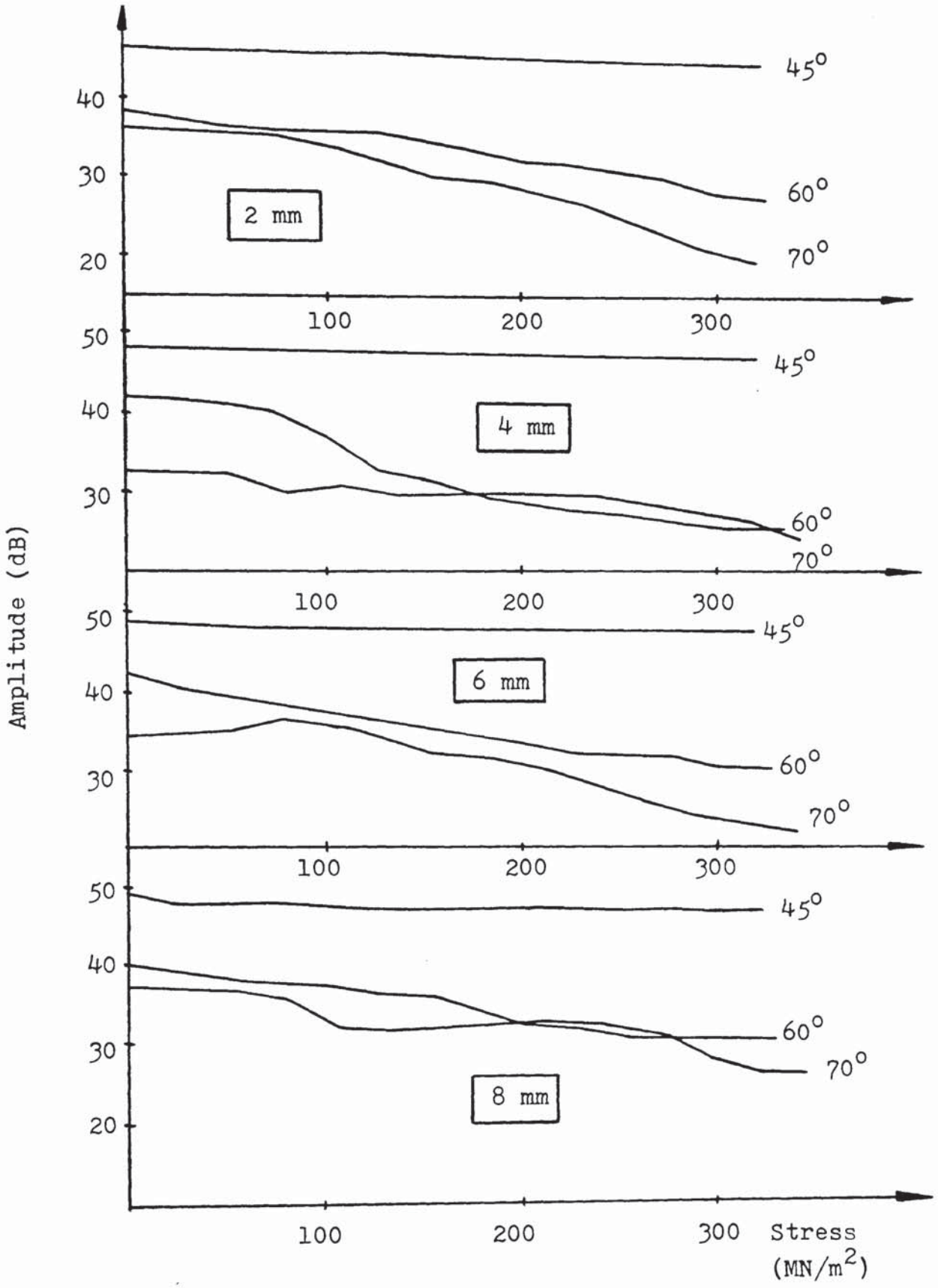

Figure 5.22 : Responses to fatigue cracks in specimen S_3, using 2 MHz transverse angle probes at $\frac{1}{2}$ skip scanning positions, scanning through the weld metal.

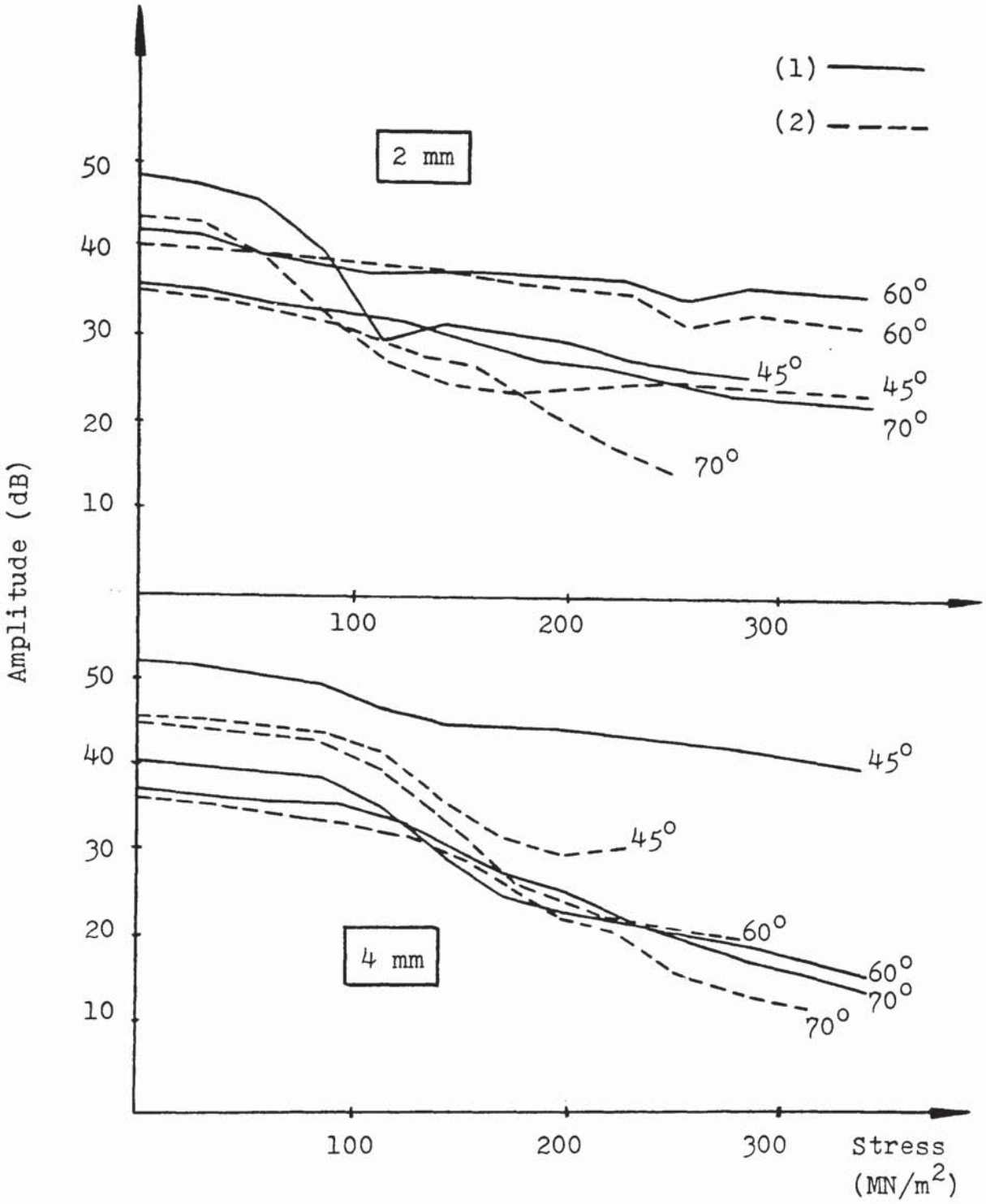

Figure 5.23 : Responses from corrosion-fatigue cracks in specimen S_{4_1} using 2 MHz transverse angle probes at $\frac{1}{2}$ skip scanning positions.

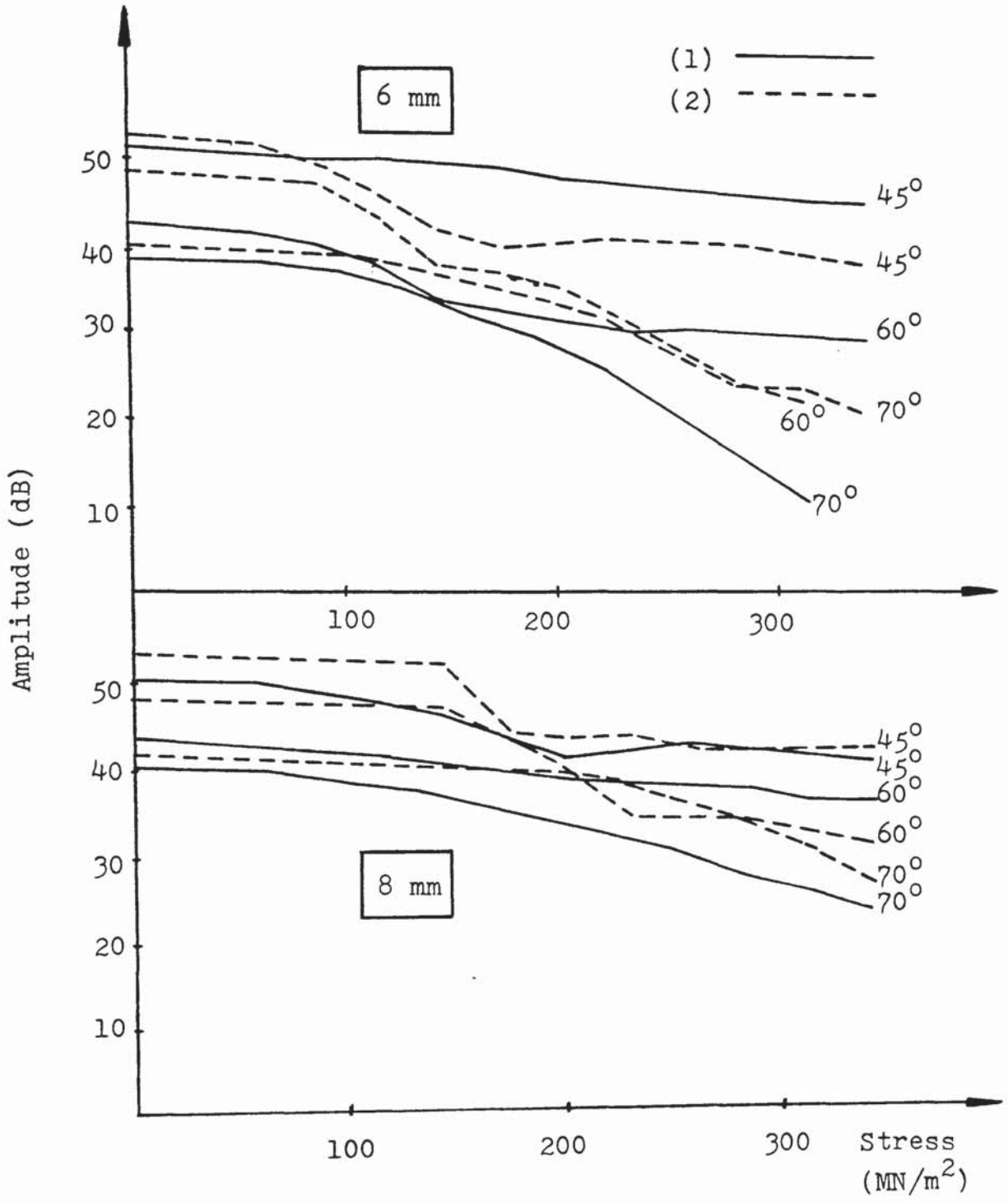

Figure 5.24 : Responses from corrosion-fatigue cracks in specimen S_4, using 2 MHz transverse angle probes at $\frac{1}{2}$ skip scanning positions.

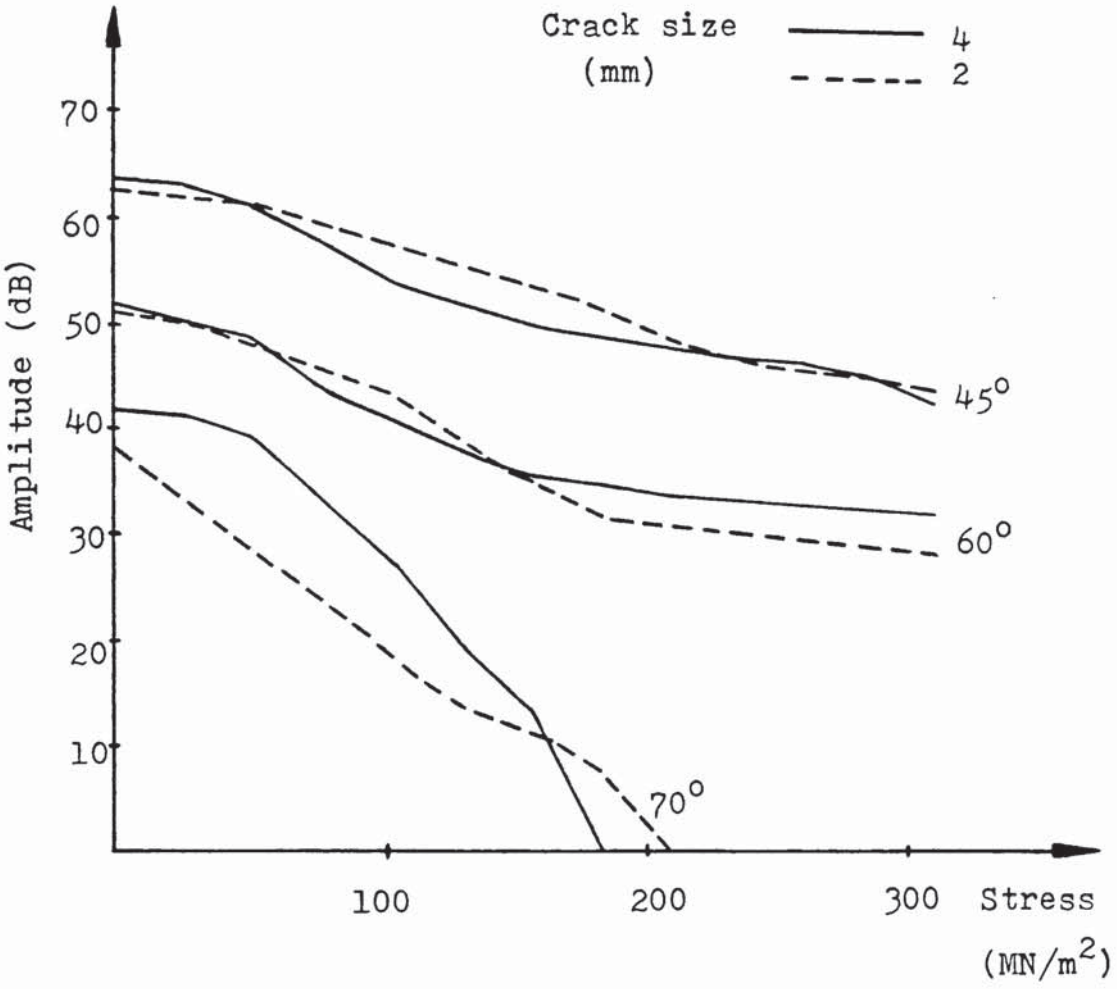

Figure 5.25 : Signal amplitude responses from corrosion-fatigue cracks in specimen S_5, using 2 MHz transverse angle probes at $\frac{1}{2}$ skip scanning positions, scanning through plate metal.

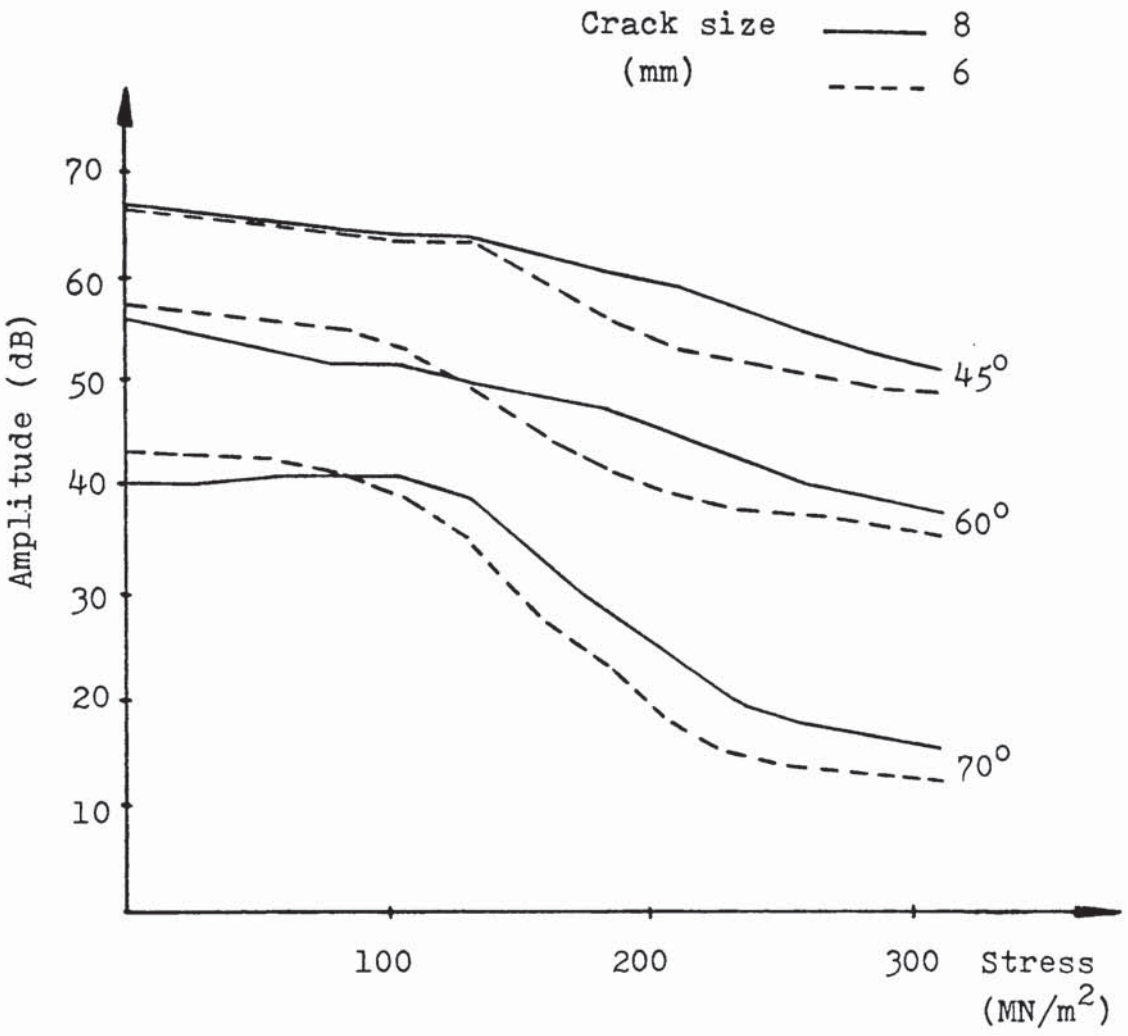

Figure 5.26 : Responses from corrosion-fatigue cracks in specimen S_5, using 2 MHz transverse angle probes at $\frac{1}{2}$ skip scanning positions, scanning through plate metal.

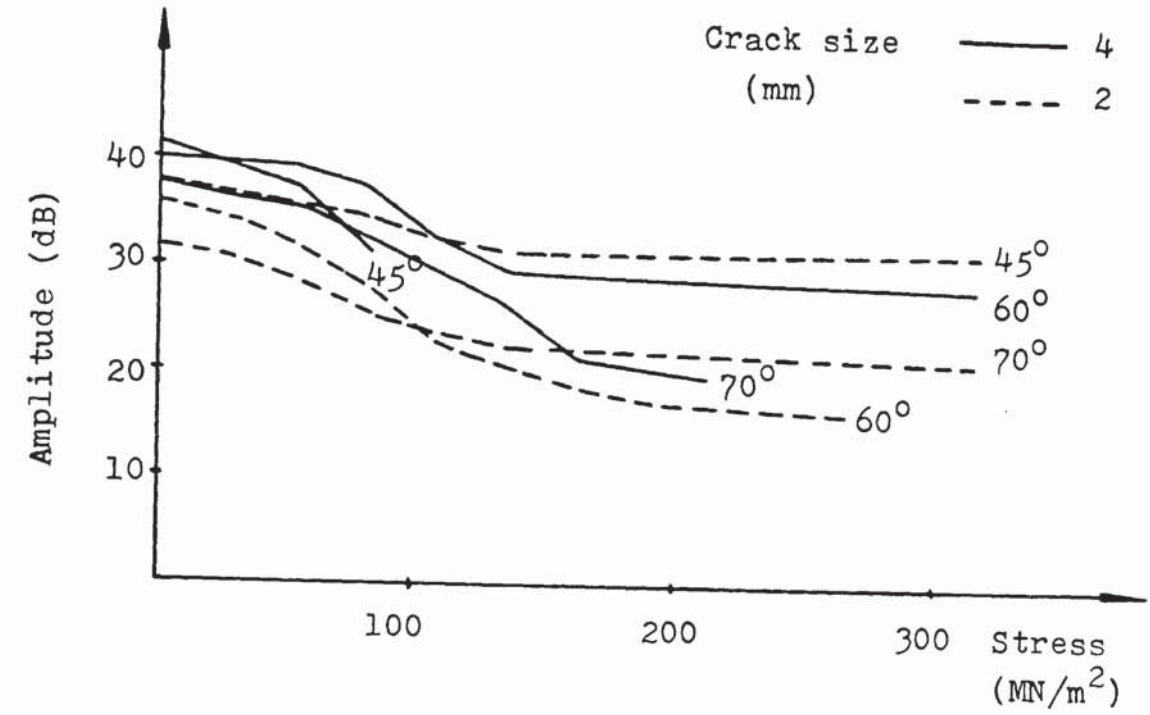

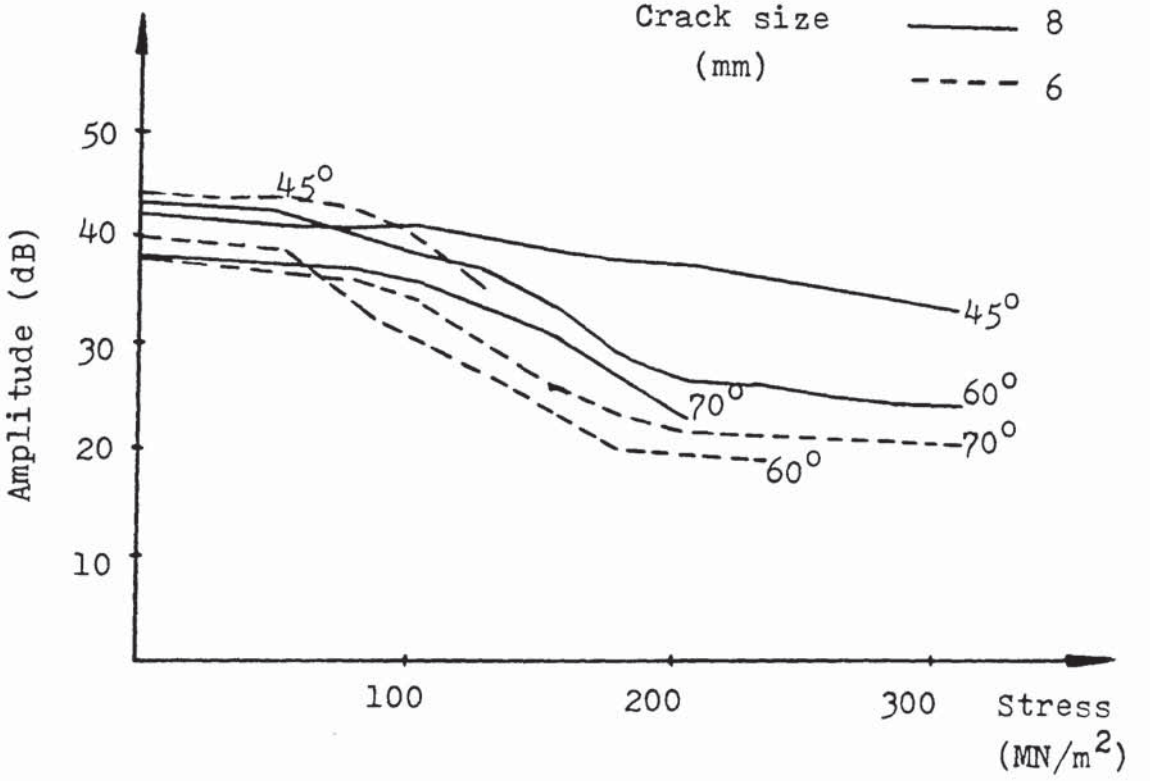

Figure 5.27 : Responses to corrosion-fatigue cracks in specimen S_5, using 2 MHz transverse angle probes scanning through weld metal at $\frac{1}{2}$ skip positions.

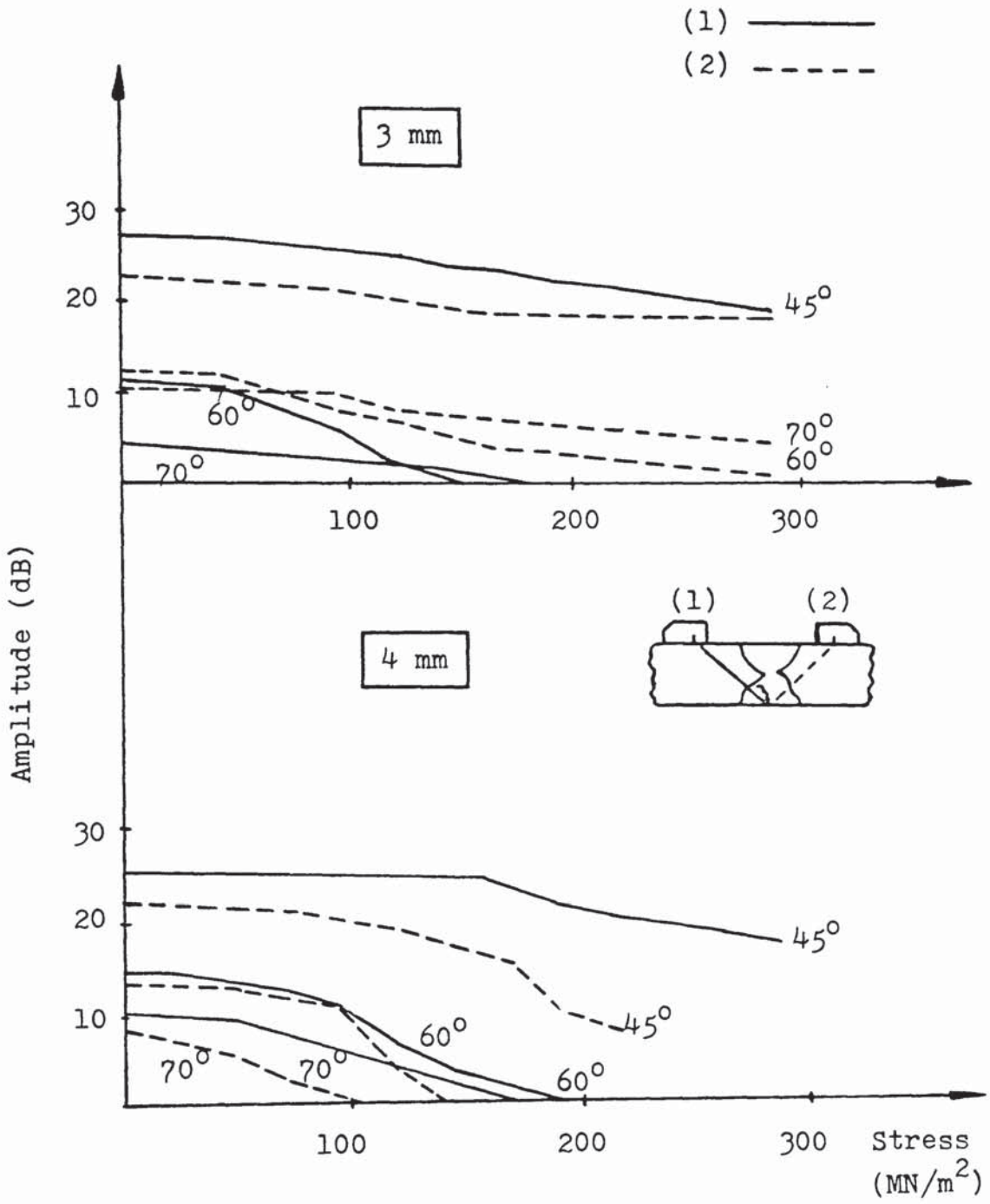

Figure 5.28 : Signal amplitude responses from fatigue cracks in specimen S_6, using 4 MHz longitudinal angle probes at ½ skip scanning positions.

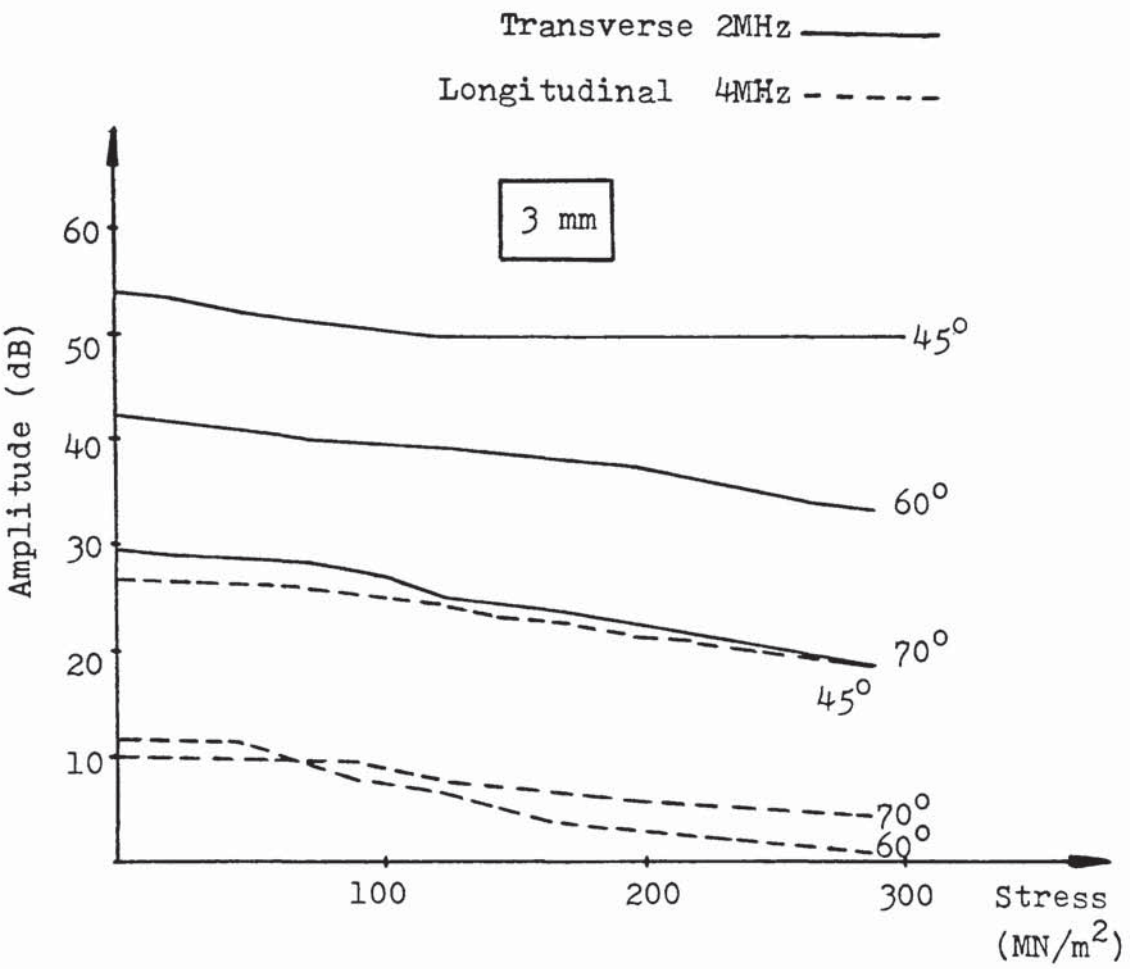

Figure 5.29 : Responses from fatigue crack in specimen S_6, using transverse and longitudinal angle probes at $\frac{1}{2}$ skip scanning positions.

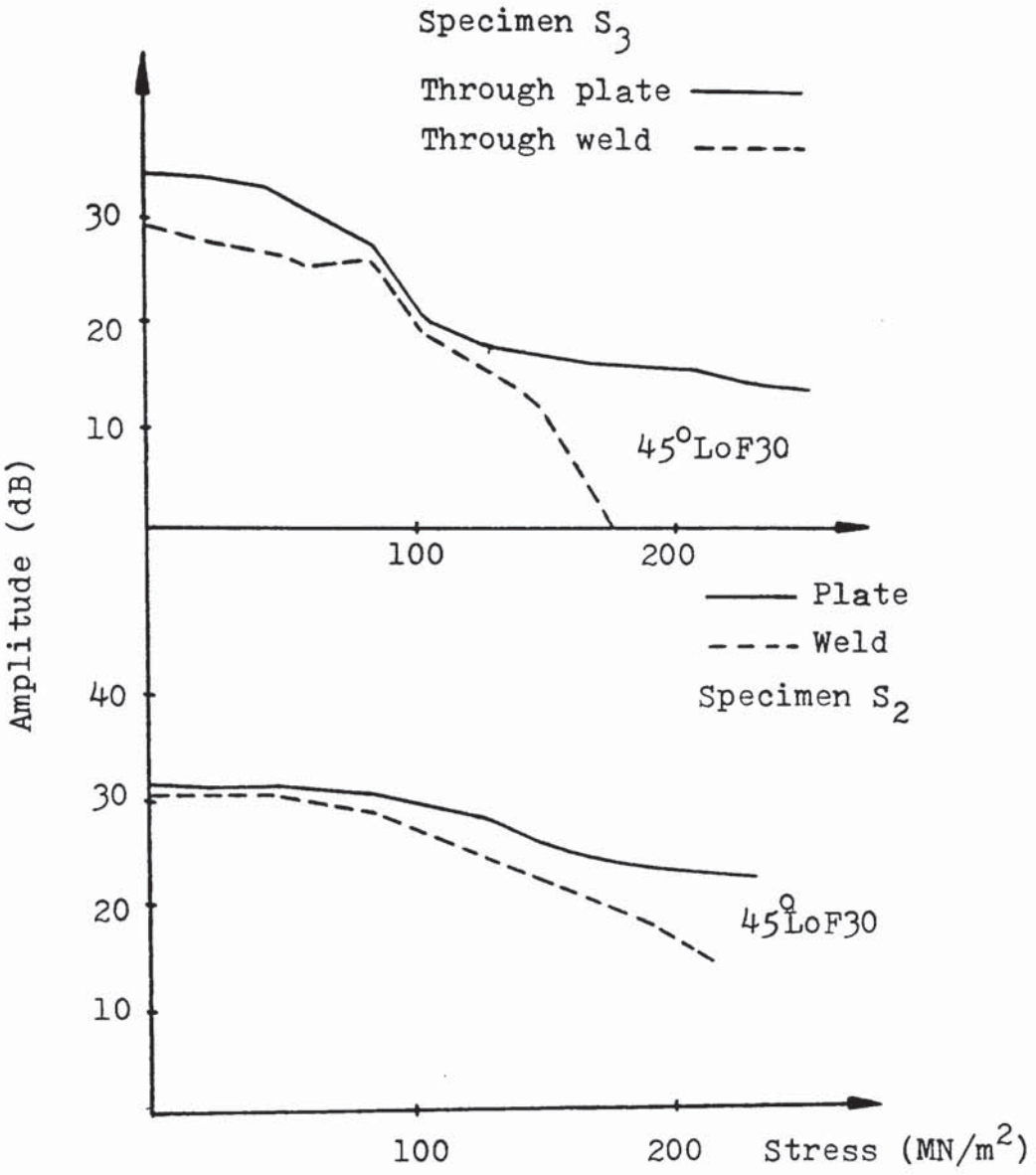

Figure 5.30 : Signal amplitude responses from 8 mm fatigue cracks in specimens S_2 and S_3, using a 2 MHz longitudinal focussed 45° angle probe at $\frac{1}{2}$ skip scanning positions.

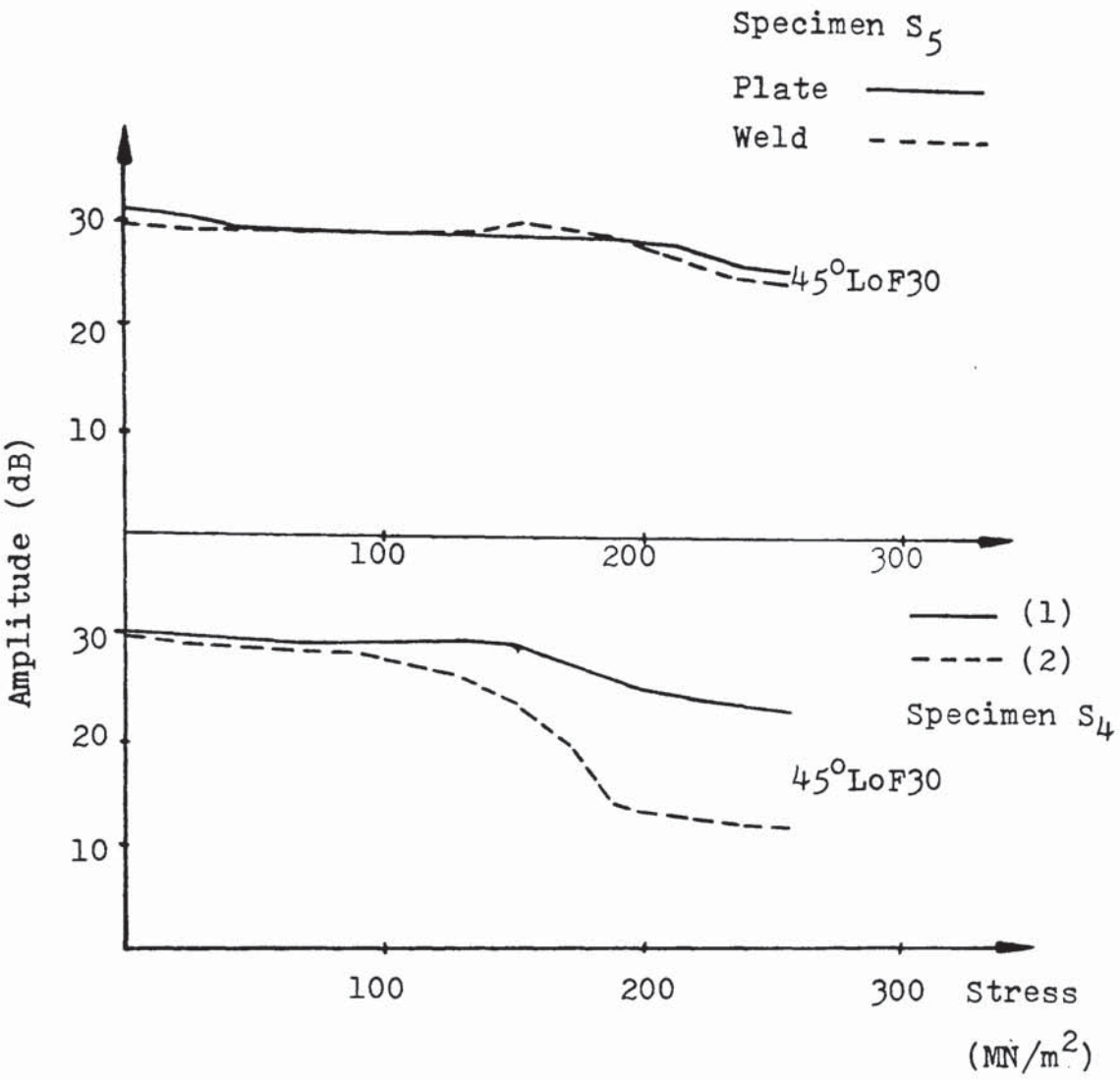

Figure 5.31 : Responses from 8 mm cracks in specimens S_4 and S_5, using a 2 MHz 45° focussed longitudinal angle probe at $\frac{1}{2}$ skip scanning positions.

6. DISCUSSION

In recent years considerable use has been made of austenitic stainless steel welds and castings, particularly in the chemical and in nuclear power plants. Such components have always been regarded as uninspectable by ultrasonics and have merely been radiographically examined. There is now a need, however, to demonstrate that such welds and castings are free of significant defects, as determined by fracture mechanics. For welds in these materials the situation is particularly bad because the preferential grain alignment along the thermal gradients during welding makes the completed weld elastically anisotropic. When this happens, the ultrasonic beam may be grossly distorted and skewed away from the normal direction. Until recently there has been no basic appreciation of precisely which aspects of the structure are responsible for the problems. Recent work in the CEGB[21,22,43], however, has considerably deepened our understanding and shown that it is possible, by careful attention to the welding process, to control the nature of the elastic anisotropy and hence fabricate austenitic welds in a way which permits inspection.

At present, therefore, it appears that a combination of control of the metallurgical structure and developments in special techniques for inspection and signal processing can produce improvements in the ultrasonic inspection of austenitic welds. Progress in understanding ultrasonic propagation and defect detection in these materials is discussed in the following sections.

6.1 The propagation of ultrasound in austenitic weldments

Considering the results of section 4.3, it has been shown that there is a cyclic variation in the velocity of ultrasonic waves with respect to the angle (θ) made by the direction of wave propagation and the axes of the elongated grains existing in MMA welds of 316 austenitic materials.

This velocity variation was observed to be between 4,930 to 5870 ms^{-1} for the 316 double-U welded specimens, and 5000 to 6500 ms^{-1} for the 316 single-V welded specimens.

It can be seen that the minimum values for both weld configurations used are quite close (less than 2 % difference), but in the case of the maximum observed values the difference is of the order of 10 %. There was evidence that the length of the samples cut from the double-U weldment was insufficient for those samples (strip resonators) which made angles of 22^{o}, 45^{o} and 67^{o} with the grain axes. This limitation could not be overcome, due to the physical size of the weld metal itself and by the difficulties involved in manufacturing samples of that size. In the case where the grains were running at 0^{o} and 90^{o} directions (parallel and perpendicular to the length direction), the specimens were sufficiently long for accurate results to be obtained and there was agreement in the results from both weld configurations, showing two minima occurring at 0^{o} and 90^{o}.

This result supports the proposition that the weld region of the 316 austenitic stainless steel is "orthotropic" rather than cubic, in which case the ultrasonic velocity would pass

through identical minimum values at 0^{o} and 90^{o}.

The experimental evidence (Figure 4.7) showed that the sound velocity in each sample varied with respect to the resonant frequency modes, but this variation was small compared with the large velocity variations observed with respect to different angles of propagation direction relative to the columnar grain axes.

The observation of two separate velocity minima at 0^{o} and 90^{o} (i.e. wave propagation direction parallel and perpendicular to the grain axes direction), and the fact that the values of the former were slightly lower, are in agreement with the only similar work to be published[21,22] concerning velocity variations in 316 austenitic welds made by the MMA process (Figures 4.8 and 4.9). On the same lines, experimental work on Inconel-182 weld metal[42] showed that the velocity and attenuation of ultrasound depends upon the propagation direction relative to the columnar grains.

It is safe to assume therefore that the velocity variations taking place in austenitic weldments constitute a property of these weldments, and that the magnitude of the variations are directly dependent on the amount of grain alignment existing in such welds.

Based on the experimental observations, it was felt that by using velocity variation values after "averaging" values obtained for the samples V_1, V_2, U_1, and U_2 would allow a wider spectrum of austenitic materials to be covered.

Using the "average" values for velocity variations in accordance with equations (12), (14) and (15), the elastic constants given in Table 4.8 were obtained. The elastic constants thus obtained for the austenitic weld metal, compare quite favourably with existing data on 316 austenitic weld metal[30], and 316 single crystals[110].

The elastic anisotropy factor for 316 austenitic welds, obtained when the "average" elastic constants are substituted in equation (16) was found to be $A = 3.66$, comparing favourably with $A = 3.63$ obtained by Silk[30] for 316 austenitic weld metal, and $A = 3.7$ obtained by Juva and Lenkkeri[110] for 316 single crystals.

Once the constants of Table 4.8 were obtained, it was decided to adopt the approach outlined by Gillan[98] in order to establish data on the three modes of propagation possible in austenitic weld metal. The decision to follow this approach was taken because, contrary to other approaches[30,109], there is no assumption regarding the position of the maximum velocity as a function of propagation direction. In the case of obtaining the elastic constants using specified points on the velocity curve (i.e. at 0°, 45° and 90°), it has been found that the resulting values of the elastic constants were rather sensitive to the position of the velocity maximum. Considering the resulting velocity values for longitudinal waves computed using the elastic constants obtained by the above technique (Figure 4.16) it can be seen that the maximum

velocity occurs at around 49°, in good agreement with the experimental values.

It should be made clear of course, that the grains existing in the austenitic welds have been assumed to be straight and parallel, with their <100> axes aligned in the vertical direction as shown in Figure 6.1.

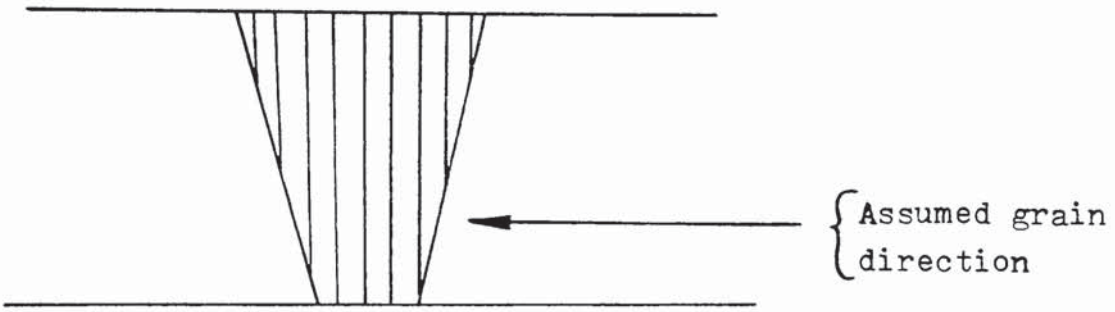

Figure 6.1 : Austenitic weld model

In reality, not all grains have their <100> axes parallel to the vertical direction (Figure 6.2), but as it was established by the Selected Area Electron Channelling Patterns there is a probability of more than 80 % that they would.

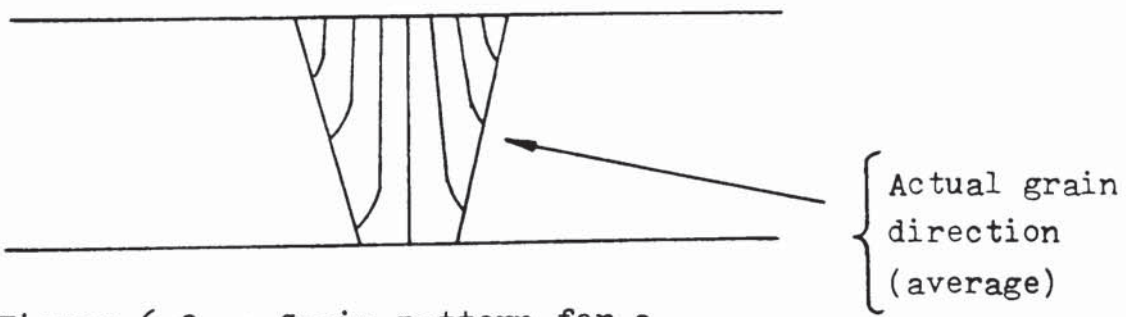

Figure 6.2 : Grain pattern for a single-V austenitic weld

Following Gillan[98], the elastic constants given in Table 4.10 were obtained for the transversely isotropic model assumed. Substituting the "average" elastic constants of Table 4.10 into equations (17), (18) and (19), the velocity variations relative to propagation direction for the three propagational wave modes (Longitudinal V_L, horizontally V_{T_1} and vertically V_{T_2} polarized transverse) were obtained as shown in Figures 4.16, 4.17 and 4.18. These results compare favourably with results obtained by Gillan[98] using data by Baikie et al[21].

In a similar manner, results for the group velocities (S_L, S_{T_1}, S_{T_2}), skewing angles (Δ_L, Δ_{T_1}, Δ_{T_2}) and the angles between group and phase velocities (θ_{g_L}, $\theta_{g_{T_1}}$, $\theta_{g_{T_2}}$) were obtained, Figures 4.19 to 4.23.

Interpreting these results, it can be seen that ray skewing for longitudinal waves leads to focussing at around 49°, and defocussing at 0° and 90°. For vertically polarized transverse waves (V_{T_2}), focussing should take place around 45°, whilst for horizontally polarized transverse waves (V_{T_1}), focussing should be important at 0°, with a steady decrease up to the region of 45°, beyond which the beam is focussed steadily to 90°. These theoretical results are in agreement with experimental results by Hudgell and Seed[37], using longitudinal waves propagating through austenitic welds. They have reported that angled longitudinal waves follow preferred paths through austenitic welds at 45° beam to grain angles. They also demonstrated, that the beam skewing effect is zero at beam to

grain angles of 0^{o} and 90^{o}, but large skewing effects take place at angles of only a few degrees either side of these values. For beam to grain angles of between 0^{o} and 15^{o}, there is a positive wavefront deviation which increases with beam angle, resulting in wide beams and poor signal to noise ratios. For angles between 46^{o} and 90^{o} the deviation is negative and decreasing, producing similar effects. At 45^{o} the deviation is zero, and in effect the beamwidths are narrow with higher signal to noise ratios. All these findings are consistent with the theoretical results obtained, and with experimental results described in section 3.5 and shown in Figure 3.13. It is also self-evident by the results of Figure 4.19, that transverse waves vertically polarized, (V_{T_2}) exhibit more distortion due to skewing than either of the other two modes. In practice[37], the skewing of vertically polarized transverse waves has been observed to be so severe, that their propagation direction in the weld region was changed by as much as 50^{o}, in good agreement with the maximum value of 48^{o} obtained using the theoretical approach (Table 4.12). It is considered appropriate that an illustration of beam focussing and defocussing should be given, see Figure 6.3.

These effects of focussing and defocussing of the ultrasonic beams propagating in austenitic weldments, could be used to explain the experimentally observed phenomenon of cyclic variations of attenuation.

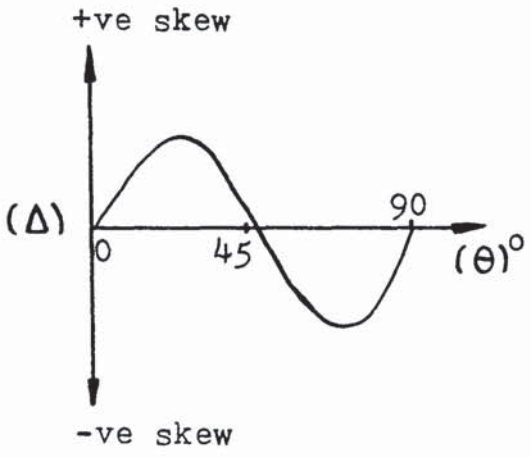

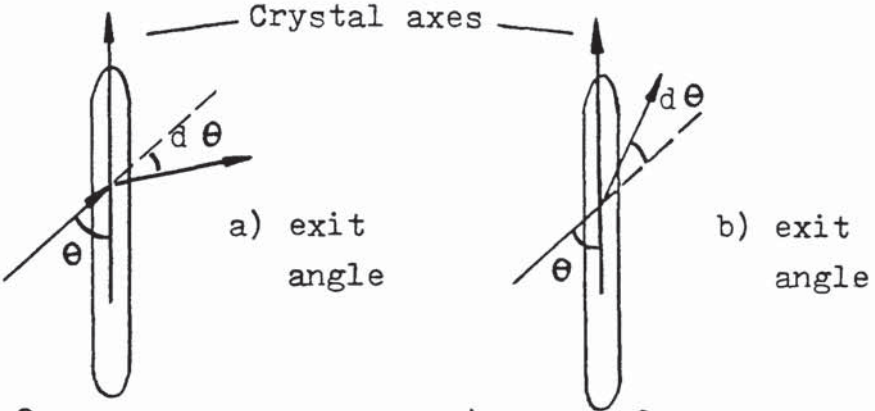

a) angle $\theta + d\theta$, +ve skew

b) angle $\theta - d\theta$, -ve skew

Considering a 50° diverging beam with the crystal axis :

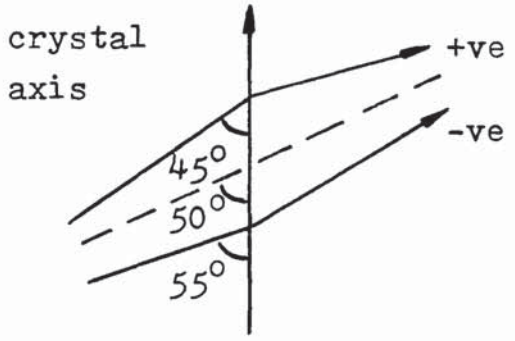

Focussing effect

Considering a 90° diverging beam with the crystal axis :

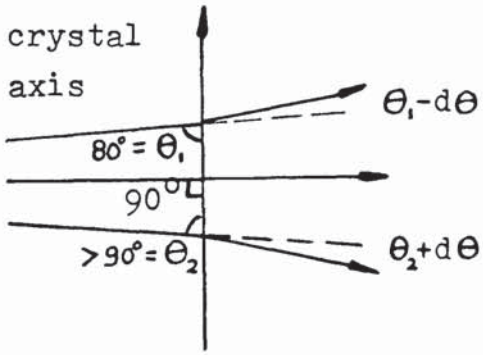

Defocussing effect

Figure 6.3 : Beam skewing

As reported in the literature[21,22,29] the attenuation in austenitic welds is found to be a maximum along the 0° and 90°, and minimum at 45° beam to grain angles. These values tie up with the intense focussing at 45° (hence less attenuation) and severe defocussing at 0° and 90° (higher attenuation), with increasing values in between.

The skewing of beams to be expected in austenitic welds (according to Figure 4.19), can give rise to false indications, because if a short-cut path is taken by the waves (due to skewing) when the beam is believed to have followed the path of an ordinary angled beam, this would lead to erroneous interpretations, and as shown in Figures 2.4 and 3.11, to false indications.

It has been recently demonstrated in the literature[29,30], that transverse waves horizontally polarized, can be less attenuated than longitudinal waves of equal wavelength. This has been attributed to the fact that horizontally polarized transverse waves cannot give rise to longitudinal waves by mode conversion[30].

Although the concept of horizontally polarized transverse waves providing a mode of propagation free of mode conversion is attractive, they still remain a laboratory curiosity, because practical difficulties in coupling these waves directly into a testpiece present a problem, a solution to which has not been found as yet.

The discussion above suggests that the problems of austenitic inspection may be ameliorated if the direction of the beam

axis is suitably chosen so as to coincide with an optimum direction (depending on wave mode). For longitudinal waves, both theory and experiment suggest that these optimum directions are at an angle of about 45° to 50° with respect to the axes of the columnar grains. At first sight this appears as an elegant solution to the problem, but it should be appreciated that the optimum beam direction for low attenuation will not in general coincide with the optimum angles for inspection. Baikie et al[21] have offered a solution by tailoring the weld metal structure in such a way that the optimum inspection direction and the direction of least attenuation coincide. Tomlinson et al[22] describe a successful use of this approach. It could be envisaged, however, that situations where these requirements will be in conflict with arguments based on cost or strength , and appart from that there are many welds already in existence that will require inspection. Therefore a universally accepted solution has not yet been found.

During the past few years, work carried out at the Harwell NDT Centre has aimed at the development of time-domain approaches to defect sizing[77,78]. An approach utilizing bulk longitudinal waves has been especially successful in ferritic materials and an accuracy of crack depth estimation better than $\pm$ 0.5 mm has been demonstrated[77]. Using the same technique, Silk[30] has demonstrated mean errors of $\pm$ 0.3 mm in sizing fatigue cracks in the centre line of a double-V weld preparation in 39 mm austenitic plate.

Although such accuracy is comendable, and deservedly has featured in the national press (Financial Times 24/3/81 "A body - scanner for big components"), the technique is essentially a sizing technique, and the basic problem is finding the defects before they can actually be sized.
On the theme of the "time of flight" sizing technique mentioned above, it is worth noting that polarized waves in a horizontal direction would provide a very useful alternative mode of propagation, bearing in mind the results discussed previously. Apart from the low attenuation and low degree of skewing, they provide the additional advantage, that being slower (almost half the speed of longitudinal waves) they can provide better resolution in time-domain analysis.
Although the possibility of "channelling" of ultrasonic beams travelling through the fibrous structure of the austenitic weld should not be ignored, it is more plausible that the spurious effects reported in the literature [42,44] and attributed to this trapping of ultrasonic energy within grains, are the result of the high degree of skewing of ultrasonic beams as predicted by Figures 5.19 and 5.24.
Comparing the "channelling" effect of ultrasound with optical channelling in light pipes (fibres), the latter requires total internal reflection of light whilst a comparable trapping of ultrasonic energy would only be acomplished under specialised conditions, i.e. in the case of individual crystallites being surrounded by a layer of

misaligned or isotropic material when a certain amount of ultrasonic energy could be genuinely trapped.

When crystallite to crystallite boundaries are assumed, the passage of ultrasonic energy should be perfectly efficient and no channelling effect can be envisaged affecting the ultrasound propagation.

During conventional transverse wave examination of austenitic weldments, large spurious indications have been reported[33, 38,46]. Using the same materials and inspection procedures, but utilizing longitudinal waves propagated at the same angles as the transverse waves, the effect of these spurious indications was lessened to a considerable degree. This result was attributed by Gray et al[33] to the acoustic impedance mismatch existing between austenitic plate and weld metals, e.g. quoting differences of up to 25 % in velocity of transverse waves between the metals constituting the austenitic "joint", with 5 % differences occurring for longitudinal waves.

Bearing in mind that a typical transducer used for ultrasonic inspection will respond to the soundwave pressure impinging on it, it is relatively easy to explain these spurious indications considering Figure 4.25. As it can be seen from Figure 4.25, the ratio of reflected to incident wave pressure from an austenitic weld/plate metal interface, is of the order of 21 % for conventional transverse waves travelling at an angle of around 45^{o} to the columnar grains existing in the weld metal; but only around 1 % for the longitudinal

and horizontally polarized transverse wave modes.
At 0^{o} beam to grain angles, all modes are comparable, and at 90^{o} longitudinal waves exhibit the lower (P_r/P_i) ratio followed by horizontally polarized and then by the conventional (vertically polarized) transverse wave modes.
A similar situation is portrayed by Figure 4.24 showing Reflection coefficients (%) for various beam to grain angles for the three propagational modes discussed above.
To assess the implications of these findings, on ultrasonic inspection in practice, it should be born in mind that longitudinal waves propagating at beam to grain angles around 45^{o} undergo focussing, resulting in less attenuation and therefore better signal to noise ratios. These waves seem to follow "preferred paths" at angles around 45^{o} exhibiting low degrees of skewing, and as it has been shown they are less prone to the impedance mismatch effect at these angles, reducing the risk of generating false indications.
Of course it would be rather oversimplistic to consider the case of longitudinal waves "closed", providing the solution to the designer's and inspector's nightmares, because with all the advantages just described there are also drawbacks that should be considered.
Therefore the proposition that has been maintained throughout this work still holds, i.e. each examination problem must be considered and tackled anew, and it is very important that in each case, calibration blocks should be made out of the

same materials as the object to be examined by ultrasonic methods, and reference blocks should contain similar weld metal as the welds to be examined.
The results discussed so far, do not provide a universal solution to the problem of ultrasound propagation in austenitic weldments, but they provide data, facilitating a better understanding and allowing sensible conclusions to be drawn when each case is considered on its merits.

6.2 Ultrasonic inspection of real defects in austenitic weldments

The recent emphasis on ultrasonics has served to point out a major defeciency in the system in its present form - the lack of a universally accepted set of physical reference standards. Even for something as seemingly straightforward as pulse-echo testing with longitudinal waves, the number of "standards" and standardizing procedures is surprisingly large. Flat-bottomed holes, side drilled holes, milled slots, saw cuts, V-notches, stepped blocks, all in either a simple geometrical form such as a cylinder or in shapes representing the part to be inspected are used.
Despite this plethora of reference standards for calibrating ultrasonic flaw detection systems, there is no acceptable "standard defect" that bears any resemblance to the defects most sought in in-service inspections, i.e. cracks.
There is a logical reason for this apparent omission.

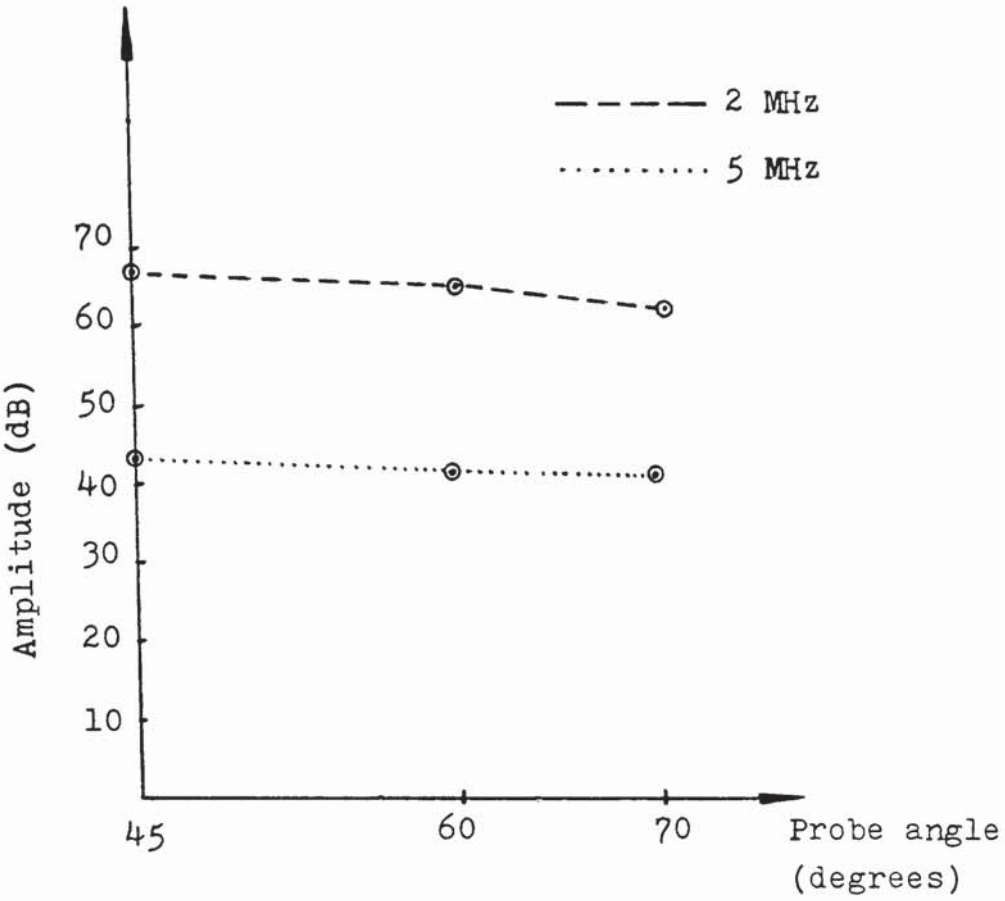

Figure 6.4 : Ultrasonic echo amplitude response of various transverse wave angle probes from the 100 mm quadrant of the IIW V_1 block

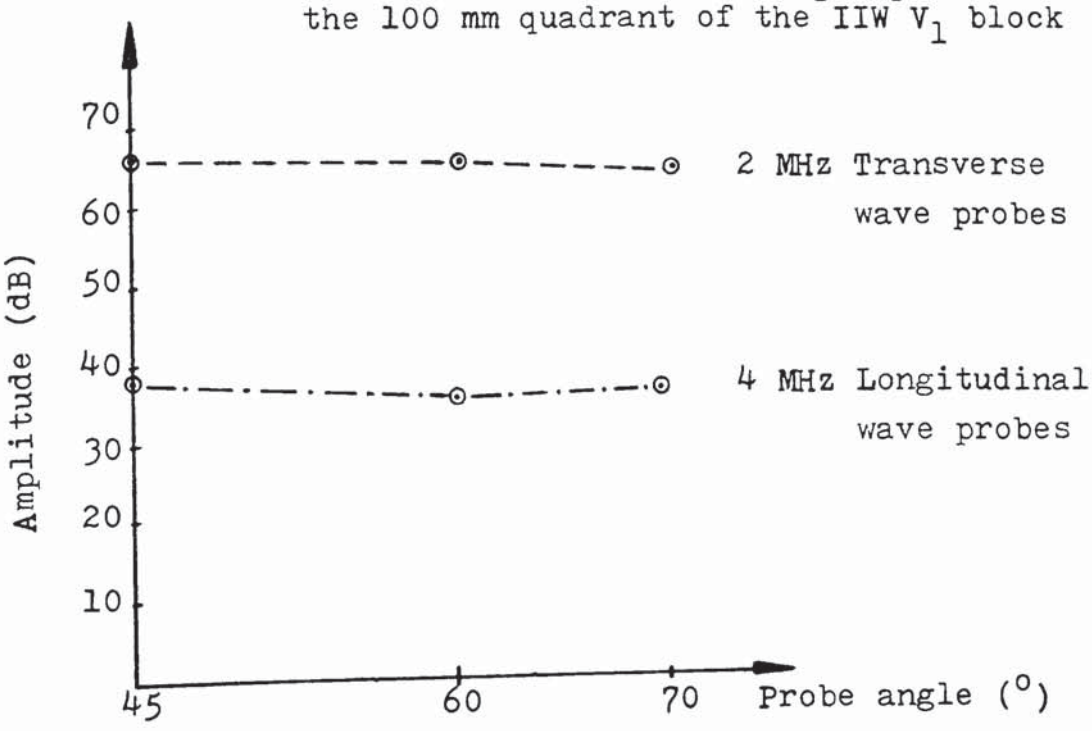

Figure 6.5 :Ultrasonic response of various angle probes from the 50 mm quadrant of the IIW V_2 block manufactured from 316 austenitic plate

The number of crack parameters that affect the ultrasonic response is quite large. Much work has been done in the recent past[111,112,113] to identify these parameters and to quantify their effects on ultrasonic response. Some of these parameters identified to date include crack size, shape and location, crack surface roughness, relative angle of incidence of ultrasonic beam on crack, type of defect, residual stress (crack closure), and applied stress (stress intensity).

For the traditional type of ultrasonic flaw detection system, in which only the peak amplitude and arrival time of the reflected signal are measured, "standard" cracks would still not permit quantitative flaw size determination because of the number of undefined variables in the "unknown" flaw.

Considering the results shown in Figures 6.4 and 6.5, it can be seen that the signal strength measured in terms of the maximum echo-amplitude, is of nearly the same intensity for all probes (45°, 60°, 70°) when using standard reflecting surfaces such as the 100 mm quadrant of the IIW V_1 block, or the 50 mm quadrant of the V_2 block. However, when real reflectors are considered, such as fatigue and corrosion-fatigue cracks, the ultrasonic response proved to be strongly influenced by the probe beam angle (Figures 5.7 to 5.15). It is striking that the 45° angle probes (both for longitudinal and transverse waves) provided the highest overall signal response, and it is possible that this could be related to

the reflecting properties of the cracks themselves, Figures 6.6 and 6.7 show surface topographies of the fatigue and corrosion-fatigue cracks investigated in sections 5.23 and 5.24.

In general these cracks tend to have jagged irregular surfaces oriented perpendicular to the testing surface. It has been demonstrated in the literature[113,114] that favourably oriented facets of a crack-like defect can give rise to echo signals of amplitude proportional to the projected area of a facet on the incident ultrasonic wave-front plane (Figure 5.2), thus suitably oriented facets could favour the reflection from a 45^{o} probe.

Recent work on surface open fatigue cracks in ferritic steel submerged arc welds, has shown that the optimum ultrasonic technique for detection of these cracks utilizes a 45^{o} 5 MHz probe at the half skip scanning position[122].

Comparing these results with this present work, it is clear that the performance of the angle probes has been reversed, in that the 2 MHz probes now give much higher response than the 5 MHz probes. In addition, unacceptable signal to noise ratios were achieved when the waves were propagated through the bulk of the weld metal (Figures 6.8 and 6.9). The 2 MHz probes, used at half skip scanning positions, proved to be the most efficient in detecting fatigue and corrosion-fatigue cracks of various sizes in the heat affected zones (HAZs) and in the weld metal itself of the austenitic weldments used.

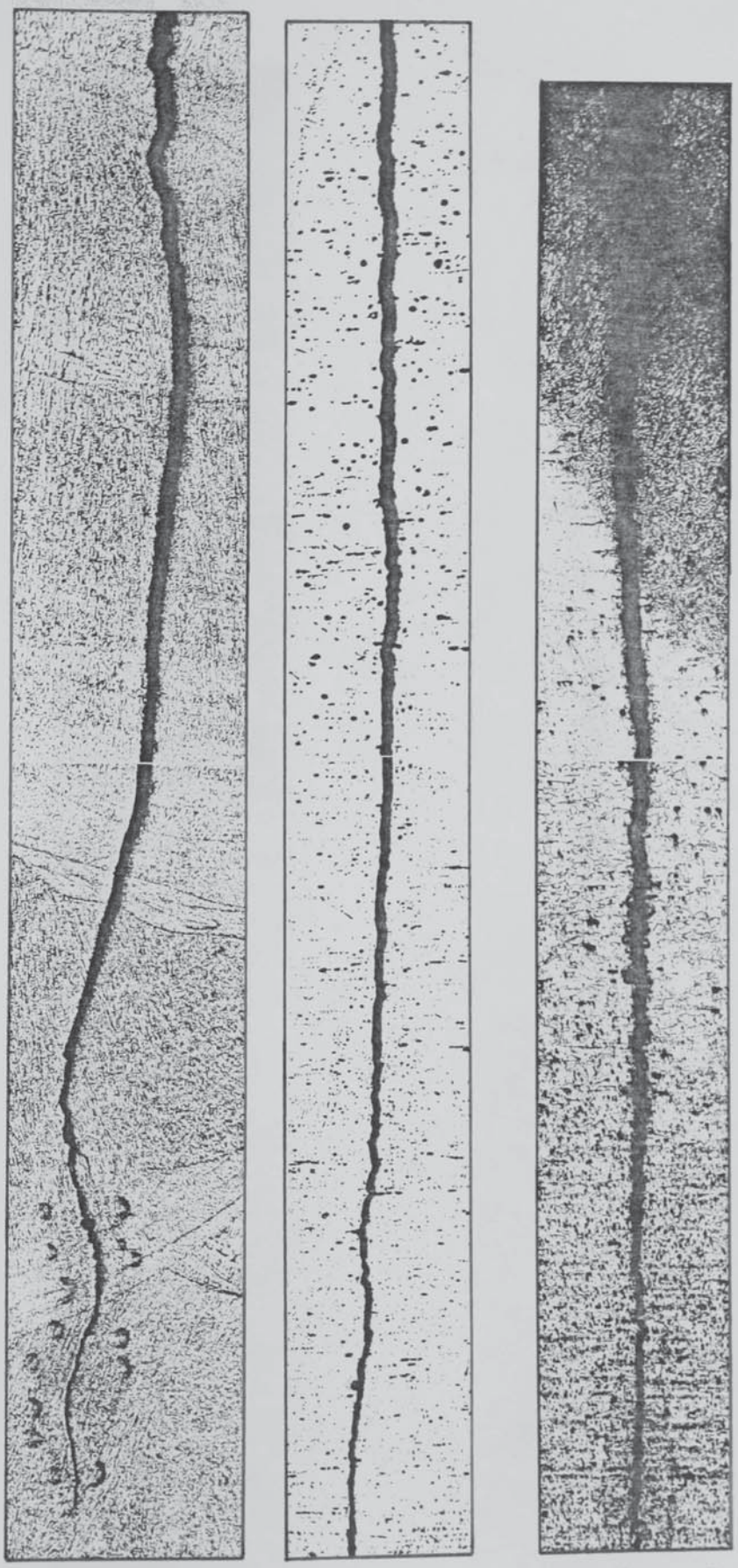

Specimen S_1 Specimen S_2 Specimen S_3

Figure 6.6 : Surface topography of fatigue cracks

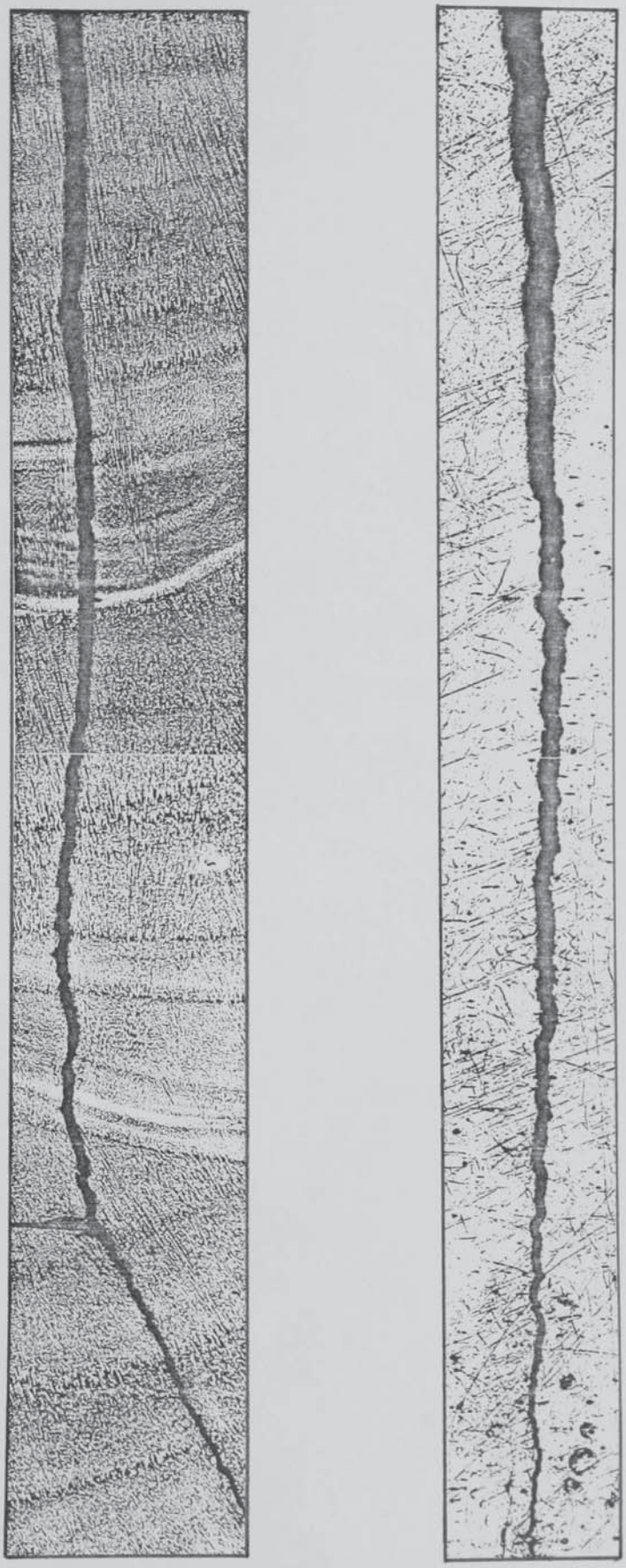

Specimen S_4 Specimen S_5

Figure 6.7 : Surface topography of corrosion-fatigue cracks

Figures 6.8 and 6.9, show CRT screen traces from an 8 mm fatigue crack in the HAZ of specimen S_2, when using 45^o, 60^o and 70^o transverse probes of 2 and 5 MHz frequencies, at half skip scanning positions. It can be deduced from these traces and their respective echo amplitudes that the 2 MHz 45^o probe appears to offer the best response from the 8 mm fatigue crack inspected from either side of the weld (i.e. with the sound propagating through plate metal only, and through plate and weld metal together). The traces also serve to demonstrate the difficulties of deciding which of the signals is coming from the crack itself, in the case of the 5 MHz probes when scanning with the beam propagating through the weld metal (Figure 6.9). The poor performance of the 5 MHz transverse probes is not unexpected, as already discussed in section 2.5.2.

Work carried out in the initial exploratory part of this research (section 3.4) using artificial reflectors in austenitic weldments, agrees with the above results in that the 45^o 2 MHz probe offers the best combination for detecting these reflectors in the parent metal/weld metal interfaces (HAZs), and again where the sound beam propagates through the weld metal.

During the investigations described in sections 5.23 and 5.24, it was observed that when the soundbeam was propagated through the weld metal, differences in the values of screen and geometrical ranges existed, with an overall increase in attenuation levels.

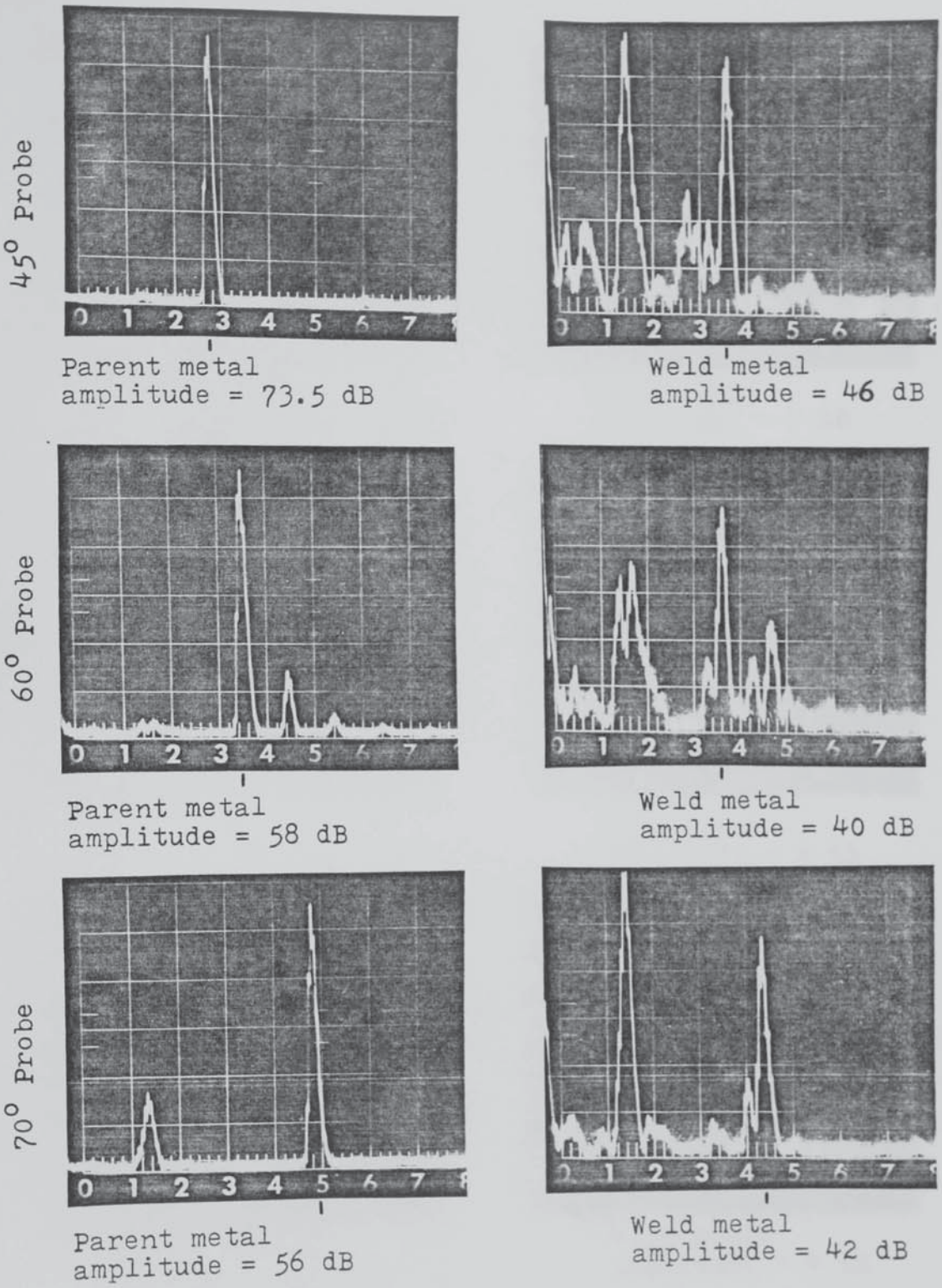

Figure 6.8 : Comparison between the screen traces from an 8 mm fatigue crack in the heat affected zone of specimen S_2, with the soundwaves propagating through plate metal or through weld metal, using transverse wave angle probes at half skip scanning position (2 MHz)

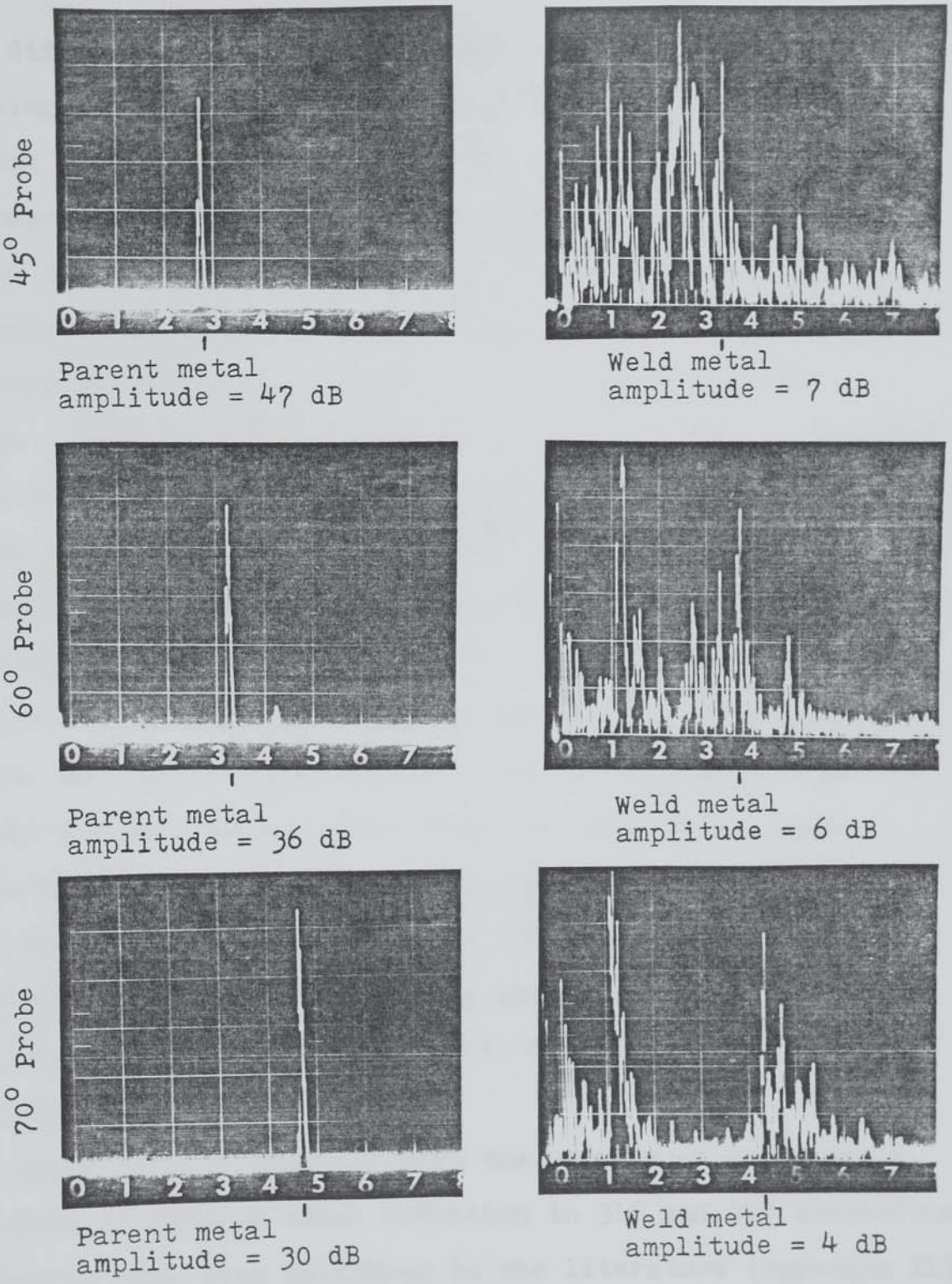

Figure 6.9 : Comparison between the screen traces from an 8 mm fatigue crack in the HAZ of specimen S_2, with the soundwaves propagating through plate metal or through weld metal, using 5 MHz transverse wave angle probes at half skip scanning position

The differences in the range values are a result of beam skewing taking place when the soundbeam reaches the parent metal/weld metal interface. This skewing (bending) is dependent on the angle of approach of the soundbeam, since the velocity of ultrasound inside the weld metal depends strongly on the angle between the weld grain axes and the soundbeam direction of propagation. Table 6.1, gives values for the geometrical and screen ranges observed when scanning the 8 mm crack in specimen S_2, through parent metal and through weld metal. When the beam propagates through the weld metal, it can be seen that the 45^{o} probes produced the largest differences in geometrical and screen ranges. This could be explained by the fact that when either 60^{o} or 70^{o} were employed, the velocities in the parent and weld metals were closer to each other, thus reducing the skewing effect (see Appendix 10 for example). Beam skewing, mode conversion at grain boundaries, and the impedance mismatch between plate and weld metals, are considered to be the main contributory factors to the high attenuation levels.

The above results together with the effects of compressive stresses on fatigue crack detection in 316 and 347 austenitic weldments have been published in the literature (Appendix 11). The effect of beam skewing described above, is supported by calculations involving the velocity values obtained in section 4.5, and adopting a simple model for the austenitic weld structure (Figure 6.1), and applying Snell's law to the

	Probe angle (degrees)	Frequency (MHz)	Geometrical Range (mm)	Screen Range (mm)
Through plate metal	45	2	30.5	31
	60	2	39	40
	70	2	56	58
	45	5	31	33.5
	60	5	36	37.5
	70	5	55	57
Through weld metal	45	2	37	41
	60	2	44	47
	70	2	48.5	52
	45	5	36.5	38.5
	60	5	44	46
	70	5	52	52

Table 6.1 : Screen range/geometrical range values obtained from an 8 mm fatigue crack in the heat affected zone of specimen S_2, using transverse angle probes

welds and probe angles concerned (Appendix 10).

Comparing the performance of the different wave modes employed (i.e. longitudinal and transverse), it can be seen that the longitudinal waves exhibited lower echo amplitude responses from the same cracks as compared to the transverse waves (Figures 5.12 and 5.15). This could create a false image of the situation, because the lower response is not related to the energy returned to the transducer by the cracks surface, but rather to the less energy injected into the material under test when using longitudinal angle probes. Similarly, the clarity of signals (i.e. good signal to noise ratios) and resolution offered by the longitudinal probes is not demonstrated in these Figures.

As long as the inspection was carried out on weldments up to 25 mm, the 2 MHz transverse probes proved that they should be considered first when contemplating ultrasonic inspection of austenitic weldments. This situation changed drastically when thicknesses in excess of 25 mm were involved as demonstrated by Figure 6.10. Unfortunately, various reasons did not allow real reflectors in thick materials to be available for ultrasonic examination, and consequently the comparison of the two wave modes in thick sections was restricted in inspection of artificial reflectors (side drilled holes) as described in section 3.7. As outlined in section 5.7, all real reflectors (fatigue

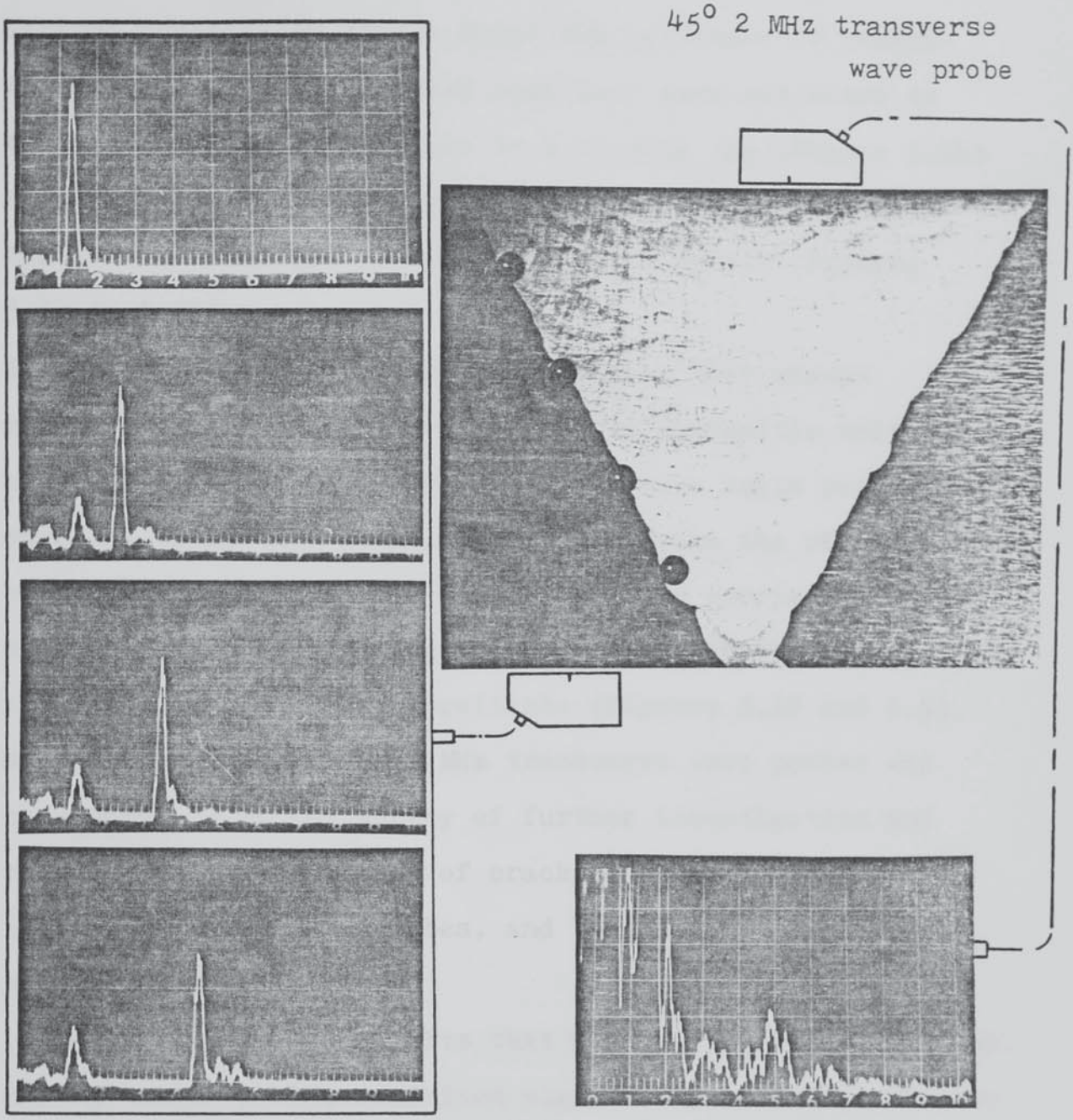

Figure 6.10 : Performance of transverse wave angle probes when inspecting thick austenitic weldments scanning through plate metal or through weld metal at half skip

and corrosion-fatigue cracks) were examined at their various propagation stages under the influence of compressive stresses. All cracked specimens were subjected to compressive elastic stresses in a bending jig (Figure 5.16) and the signal amplitude responses from the individual cracks were recorded for various stress levels (Figures 5.17 to 5.31).

It can be easily seen from these results that cracks existing in the heat affected zones of austenitic weldments could be detected by 5 MHz transverse wave angle probes when the ultrasonic beam propagated through the plate metal only. Once scanning with such probes was carried out with the ultrasonic beam propagating through the weld metal, the results were completely unreliable (Figures 5.19 and 6.9). Subsequently the use of 5 MHz transverse wave probes was considered to be not worthy of further investigation and the further interrogation of cracks took place using 2 MHz transverse angle wave probes, and longitudinal angle wave probes.

It is clear from the results that appart from few exceptions, the 45^{o} angle probes exhibited higher responses from various cracks, and also were less prone to crack closure at higher stress levels. Inspection of cracks situated in the centre of the weld metal (specimens S_1,S_4,S_6) showed different responses when scanned from opposite sides, both under zero load and under compressive stresses (Figures 5.17,5.23,5.24, and 5.28).

In the case of fatigue cracks (Figure 6.11) where the whole of the crack is almost at right angles to the specimen's surface, the difference in signal amplitude response could be attributed to the individual crack facets giving preference to stronger reflection on one side, but not on the other (Figure 6.12).
Work carried out by Haines[110], and Digiacomo et al[123], is in agreement with the idea that the reflected energy distribution depends on the geometry and reflectivity of a crack's surface.
In the case of the corrosion fatigue crack generated in the centre of the austenitic weld (specimen S_4), it can be seen that the crack although started at right angles to the specimen surface, on propagation it followed the columnar grains, therefore presenting two completely different surfaces to the ultrasonic beams (Figure 6.13). It is believed that although the individual facets still play a part in the way the ultrasound is reflected from the crack's surface, their contribution to reflectivity must be over-shadowed by the geometry of the crack itself. This particular crack geometry exhibited signal amplitude responses that did not follow the overall pattern (Figures 5.23,5.24), i.e. unusual loss of signals from the 45° and 60° probes, and lower signal to noise ratios.
Inspection of heat affected zone cracks (specimens S_2,S_5), followed the norm, with the 45° probes exhibiting the higher signal responses, followed by the 60° and 70° probes.

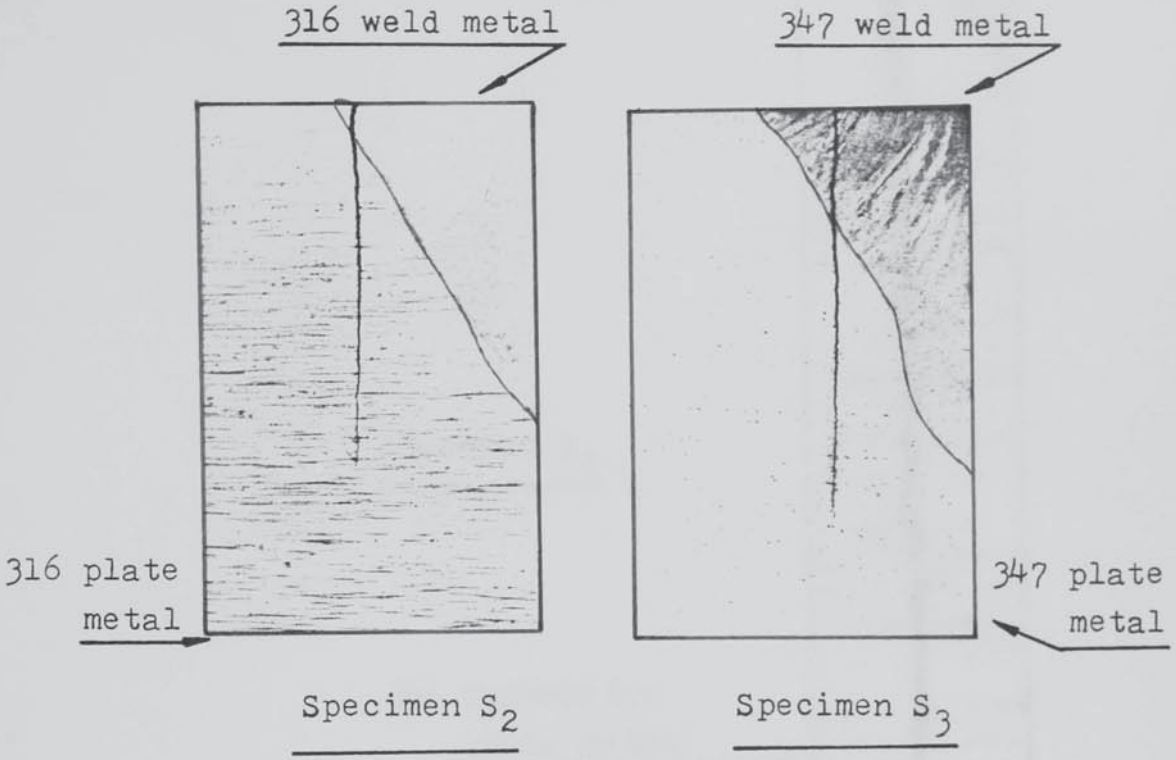

Figure 6.11 : Fatigue cracks in the heat affected zones of specimens S_2, S_3

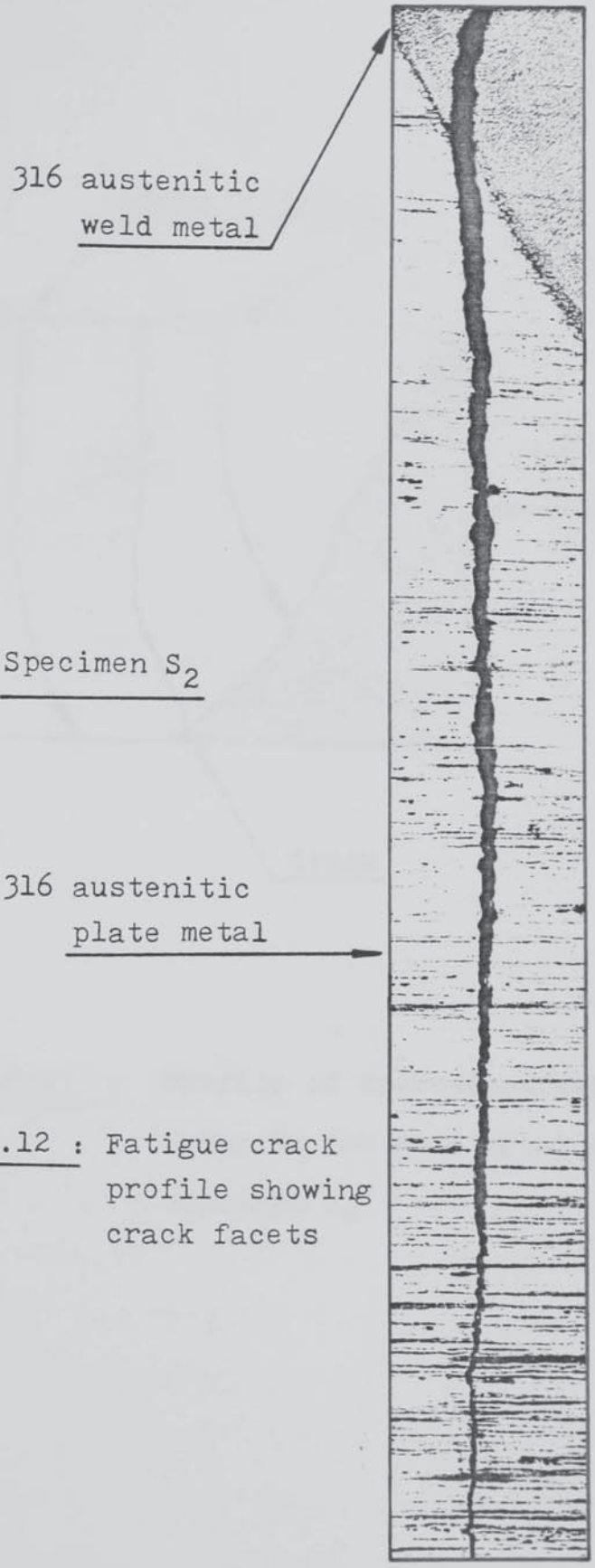

Figure 6.12 : Fatigue crack profile showing crack facets

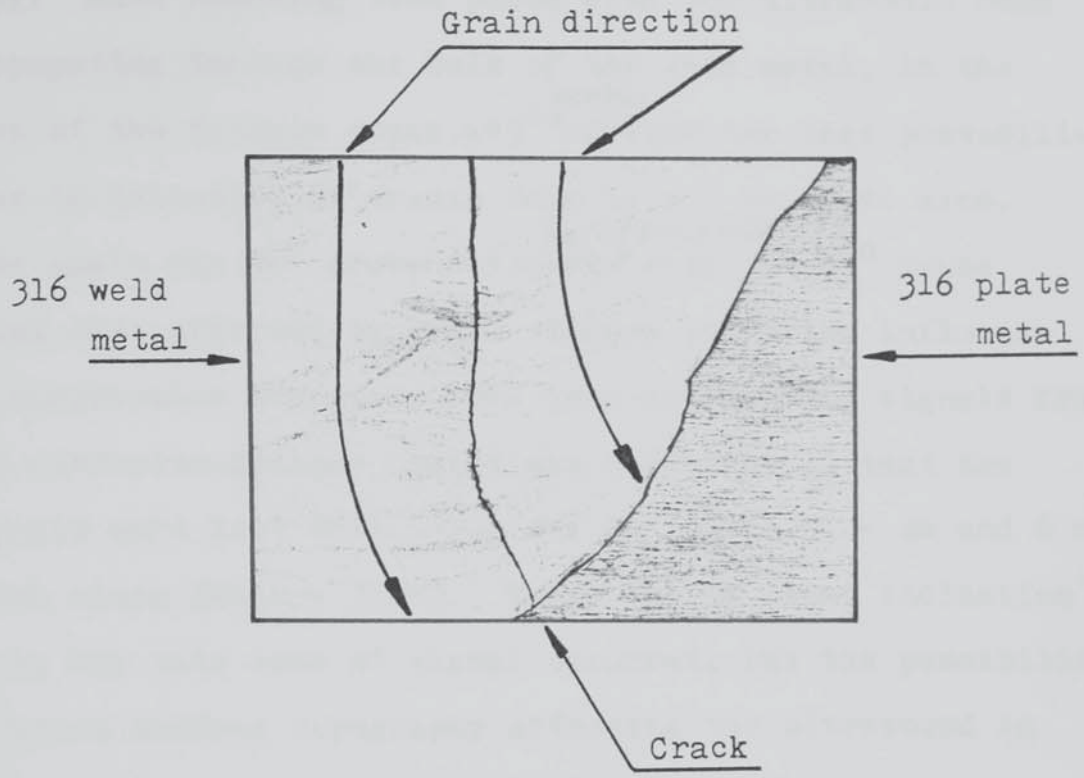

Figure 6.13 : Profile of corrosion-fatigue crack in the weld metal of specimen S_4

The 70° probes appeared to be prone to crack closure even when the ultrasonic beam propagated through plate metal only. When scanning took place with the ultrasonic beam propagating through the bulk of the weld metal, in the case of the fatigue crack, a 45° probe offered the best possibilities in detection of cracks down to a 2 mm depth size. Once again the 60° probe followed, in effectiveness with the 70° probe being most affected by crack closure under the influence of compressive stresses. The behaviour of the signals from the corrosion-fatigue cracks was different in that the signals were lost when using the 45° probe at 4 mm and 6 mm crack sizes (Figure 5.27). There was no clear indication as to why this loss of signal occurred, but the possibility of crack surface topography affecting the ultrasound in such a manner should not be excluded.

Due to reasons out of our control, the acquisition of longitudinal angle probes took place at a late stage of this work, and comparisons with transverse angle probes could be carried out in few cases only (Figures 5.28, 5.29, 5.30, 5.31). Overall the longitudinal angle probes exhibited lower signal amplitude responses, but this is an inherent problem due to their construction. Due to their lower signal amplitudes, the longitudinal angle probes appeared more affected by crack closure due to compressive stresses. On the other hand, when the ultrasonic beam propagated through the weld metal, they exhibited, in general, more acceptable signal to noise ratios than their transverse wave counterparts.

Comparing different angles of propagation, the 45° probes proved to be undoubtedly the most effective exhibiting twice the signal amplitude responses obtained by either the 60° or 70° probes. At the same time the 45° probes are not affected in general by crack closure due to the application of compressive stresses.

The longitudinal angle probes showed consistency when scanning through plate metal or through weld metal, the variations observed in signal amplitudes could be the result of the crack topography already discussed for transverse waves.

Difficulties expected in signal identification due to the transverse component generated simultaneously when using longitudinal angle probes, were experienced, but careful calibration using a V_2 block manufactured from 316 austenitic plate material, made the identification of signals less arduous.

During the initial stages in the experimental investigation of the influence of compressive stresses on the ultrasonic inspection of fatigue and corrosion-fatigue cracks, it was observed that some signals thought to be the result of ultrasonic energy reflected from the crack surfaces were not affected by the application of compressive stresses (Figure 6. 14). On further investigation, it was found that these signals were related to beam skewing and plate metal/weld metal interfaces. In the case of a signal resulting from a crack, on application of compressive stresses the crack

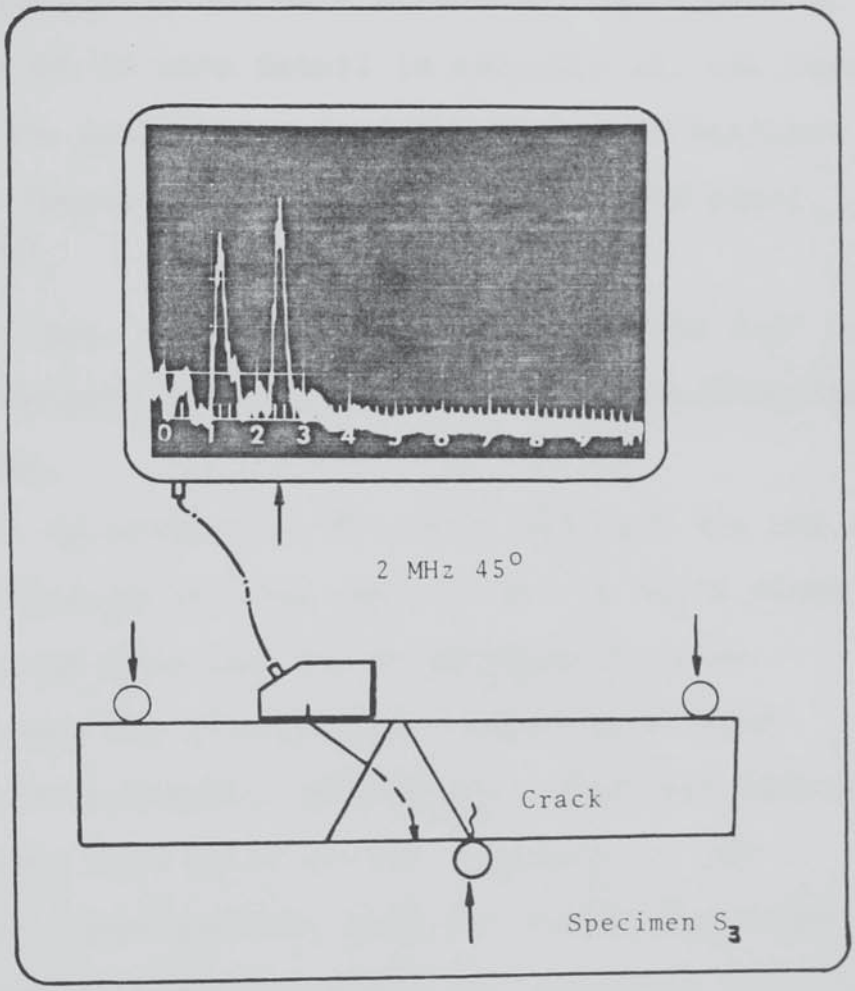

Figure 6.14 : Spurious indication, unaffected even at fairly high stress levels ($\geqslant$ 220 MNm^{-2})

undergoes partial progressive closure, thus presenting less and less reflecting surface available to the sound beam, producing an effective amplitude drop with increasing stresses (Figure 6.15). It then became easy to distinguish between "real" signals returning from the cracks, and "false" signals due to the weld structure. This part of the work is shown in more detail in Appendix 12, and forms the basis of the publication entitled "False indications in ultrasonic inspection of austenitic stainless steel weldments"[124].

Based on this idea, a small portable "Compression Jig" was manufactured (Figure 6.16), to be used as a demonstration or training aid.

Another useful by-product of this work was that the use of compressive stresses to ascertain whether or not a given signal originated from the cracks existing in these weldments allowed for a better understanding of beam behaviour in the austenitic weld metal. This was done by noting the probe exit point of the soundbeam on the specimen under investigation, when the signal was known to be 'real', and then using the values for angles in the plate metal already obtained to plot the beam path up to the fusion line. The angle of incidence to the grains was then noted and a simple calculation based on Snell's law was carried out. Assuming the weld model of Figure 6.1, it was possible to obtain quantitative estimates of the beam path in the weld metal, in agreement with expected beam behaviour

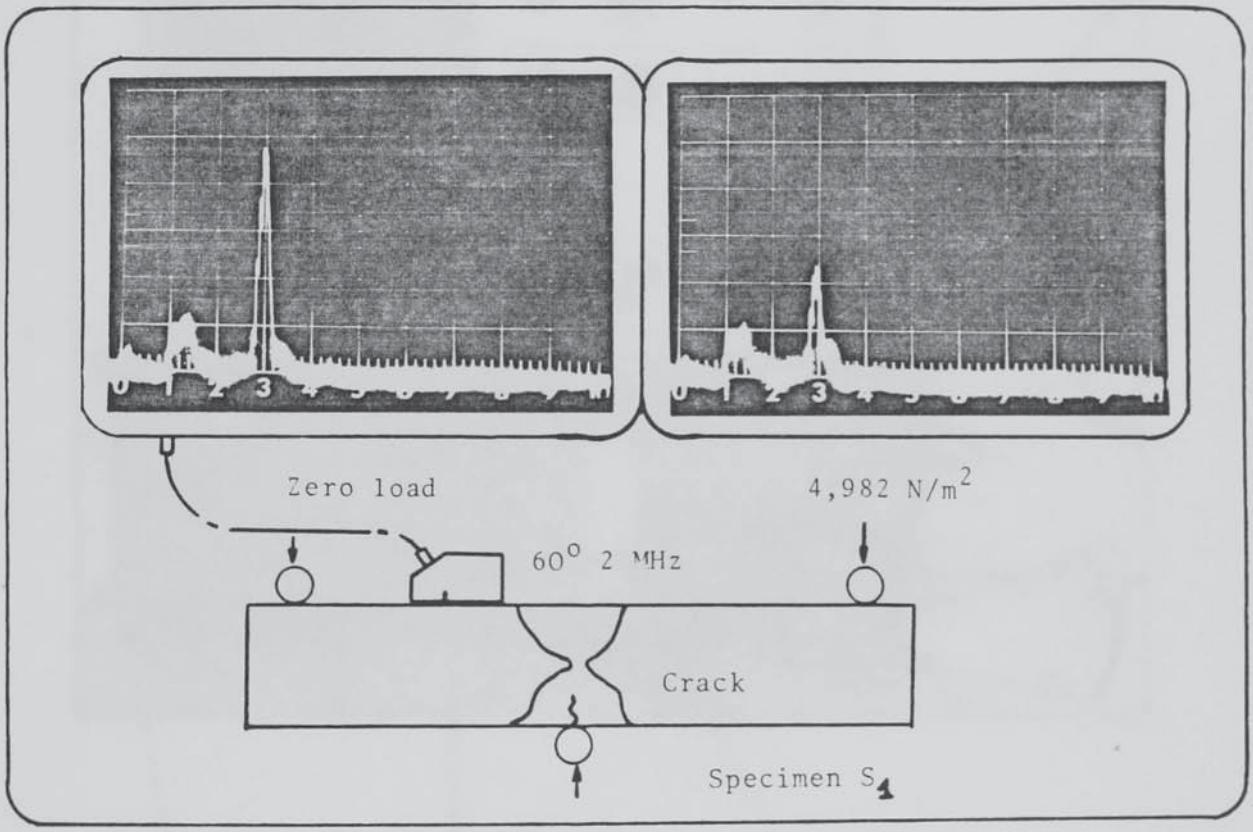

Figure 6.15 : Signals from fatigue crack in the weld metal of specimen S_1, at zero load, and at 4,982 Nm^{-2}, using a 60° transverse wave probe

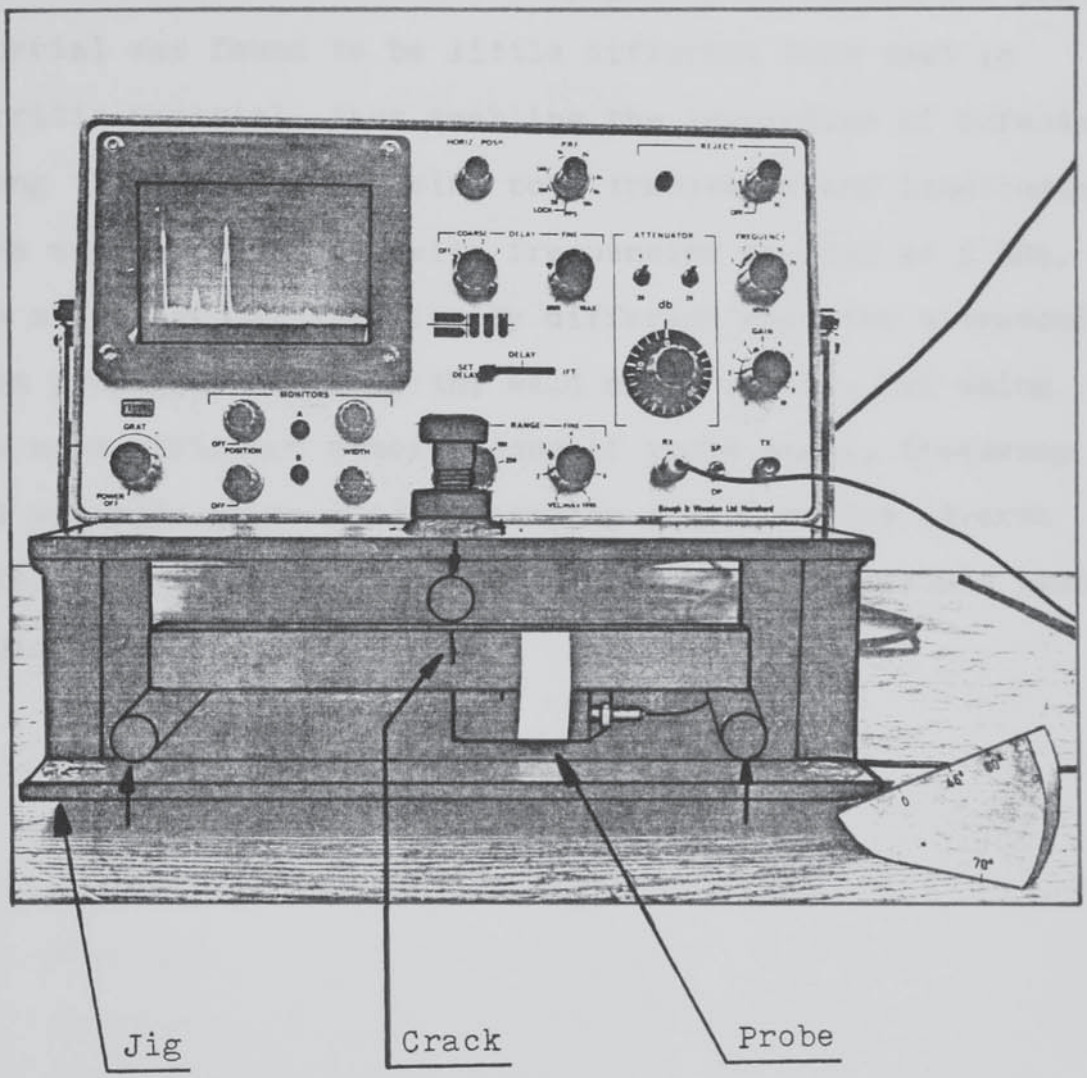

Figure 6.16 : "Compression Jig"

(beam skewing). Appendix 10, shows graphical representation of these effects based on quantitative estimates on velocity previously obtained.

The behaviour of ultrasound propagating in austenitic plate material was found to be little different from that in ferritic material, thus enabling the inspection of defects along the fusion line using both transverse and longitudinal wave angle probes even with frequencies as high as 5 MHz. The situation was drastically different when the ultrasonic beam propagated through the weld metal itself, but using the most efficient combinations of probe angle, frequency and wavemode at half skip scanning positions the adverse effects of the weld metal structure on the ultrasonic beam could be alleviated.

7. CONCLUSIONS

The results obtained by this study are considered to provide adequate ground for the following conclusions:

1. Austenitic welds contain long columnar grains with a major axis along a $\langle 100 \rangle$ crystallographic direction, and this structure leads to variations in ultrasonic velocity and attenuation.

2. Ultrasonic velocity is a function of the angle made by the direction of wave propagation and the axes of the columnar grains existing in austenitic stainless steel weldments.

3. There are two distinct velocity minima for longitudinal wave propagation, one when the direction of the waves is parallel to the grain axes and the other when perpendicular to them, the former being lower in value. This suggests that the weld region of the austenitic materials should be regarded as "orthotropic" in nature rather than cubic.

4. A slight velocity variation is observed at different resonant modes of frequency, but this is small compared with the large velocity variations occurring due to the different angles made by the direction of wave propagation and the columnar grain axes of these weldments.

5. In general, due to the velocity variations, erratic behaviour of the ultrasound in austenitic weldments is to be expected, resulting in focussing and defocussing, which depends on wave mode of propagation, and on the angle sustained between the direction of ultrasound propagation and the axes of the columnar grains in the austenitic welds.

6. Transverse wave inspection is a viable technique for austenitic weldments up to 25 mm thick, and 45^{o} 2 MHz transverse wave probes will detect fatigue and corrosion-fatigue cracks as small as 2 mm depth, located in the weld metal.

7. Fatigue and corrosion-fatigue cracks existing in the heat affected zones (HAZs) of austenitic weldments will be readily detected using transverse or longitudinal angle probes with frequencies up to 5 MHz, provided that the soundwaves propagate through the austenitic plate material only.

8. When the sound beam propagates through the austenitic weld metal itself, the 5 MHz transverse probes are rendered unsuitable for ultrasonic inspection of defects. A 45^{o} 2 MHz transverse wave probe at half skip scanning position offers an effective alternative, followed by 60^{o} and 70^{o} probes. Longitudinal wave angle probes provide a very useful "tool" in ultrasonic inspection of defects when the soundbeam propagates

through the weld metal, exhibiting acceptable signal to noise ratios.

9. For weld thicknesses over 25 mm, the transverse wave inspection is completely ineffective, and consideration should be given to various longitudinal angle probes. In thick weldments, a choice has to be made in the use of single crystal and double crystal (focussed) longitudinal angle probes, but this depends on factors such as weld geometry, component geometry, cost of inspection, and type of inspection.

10. The reflection of the ultrasound from fatigue and corrosion-fatigue cracks is a function of probe angle, frequency and mode. Under compressive stresses, 45^{o} probes produced, in general, the best responses, followed by 60^{o} probes. The 70^{o} probes were the most sensitive to "crack closure".

11. Examination of cracks from both sides showed variations in ultrasonic response. This is attributed to crack topography and crack geometry.

12. "False" indications may exist in austenitic weldments when ultrasound propagates through the weld metal. The use of compressive stresses provides a criterion for establishing the nature of an indication, offering possibilities of predicting beam paths inside austenitic welds.

8. FUTURE WORK

Although this study has improved the understanding of ultrasound behaviour in austenitic weldments, it is felt that work on the following areas is necessary:

1. Ultrasonic velocity measurements in a wider variety of weld metals of various austenitic types, including Inconel.

2. Ultrasonic inspection of other forms of weld defects such as lack of penetration, inclusions, lack of fusion and stress-corrosion cracks, should be carried out in austenitic weldments.

3. Work on the effect of weld "tailoring" on ultrasonic inspection of such welds should be encouraged.

4. A study on the effectiveness of defect sizing using various angles and different wave modes should be carried out using pulse-echo techniques as compared to diffraction time-of-flight techniques.

5. The effect of liquid absorption by various forms of cracks on ultrasonic response should be considered, with particular applications water, sea water and sodium.

6. A statistical analysis of the probability of :
a) detecting, b) locating accurately, and c) sizing of cracks, should be carried out.

9. REFERENCES

1. Brock, D., "Elementary Engineering Fracture Mechanics", Noordhoft International Publishing Company , Leyden, 1974.

2. Rolfe, S.T., "Use of fracture mechanics in design", Int. Met. Rev., 19,1974, 183-197.

3. Cherepanov, G.P., "Mechanics of brittle fracture", McGraw-Hill, 1st Edit. Translated from Russian, 1979.

4. Knott, J.F., "Fundamentals of fracture mechanics", J. Wiley & Sons, N.Y., 1973.

5. Irwin, G.R., "Fracture", Encyclopedia of Physics, Vol. VI, J. Springer, Heidelberg, 1958.

6. Allen, T.L., Trigilio, R.F., Whiting, A.R., "Automatic data recording during manual ultrasonic inspection", Periodic inspection of pressurized components, I.Mech. Eng. Conference Publications, 1979-4, pp. 117-126.

7. Dobbeni, D., Van Melsen, C., "Experience from the in-service inspections of the PWR steam generators", Periodic inspection of pressurized components, I. Mech. E. Conference Publications, 1979-4, 73-82.

8. Frederic, J.R., Ganapthy, S., Vanden Broek, C., Elzinga, M., "Improved characterization of discontinuities in thick walled pressure vessels", Periodic inspection of pressurized components, I. Mech. E. Conference Publications, 1979-4, 163-174.

9. Truman, J.E., "Stainless steel - A survey", The Metallurgist and the Materials Technologist, Part 1 Jan. 1980/ Part 2 Febr. 1980.

10. Castro, R., and De Cadenet, J.J., "Welding Metallurgy of stainless steels and heat resisting steels", Cambridge University Press, 1975.

11. Linnert, G.E., "Welding characteristics of stainless steels", Metals Engineering Quarterly, Section : VI, Nov. 1976, pp.226.

12. Haddrill, D.M., "The influence of carbon content on the weldability of cast austenitic alloys",Proc. of Conf. on Welding Creep-Resisting Steels, The Welding Inst., 17-18 Feb. 1970.

13. Gooch, T.G., Howard, R.D., McKeown, D., and Widgery, D.J., "Assessment of weldability of high temperature austenitic materials", Welding Research related to Power Plant, Proc. of Int. Conf. University of Southampton, 17-21 September 1972.

14. Folkhard, E., Schabereiter, H., Ornig, H., and Neff, F., "Problems related to the welding of austenitic steel in construction of atomic reactors", Welding Research related to Power Plant, Proc. Int. Conf. Univ. Southamton, 17-21 Sept. 1972.

15. Dickinson, F.S., and Watkins, B., "Cracking in welded joints - Occurence and Prevention in Nuclear Plant- 2", Welding and Metal Fabrication, Oct. 1973.

16. Ritter, J.C., and McPherson, R., "Embrittlement of the weld heat affected zone in a Mn-Cr-Mo-V steel", Metals Technology, 1 , 11 , 1974 , 506-511.

17. "Welding Creep-Resisting Steels", The Welding Inst. Proc. Conf. February 1970.

18. "Welding in the World", 7 , 4 , 1969 , 200-210.

19. Whit aker, J.S., and Jessop, T.J., "Ultrasonic detection and measurement of defects in stainless steel- A literature survey", Brit. J. NDT, 23, 6 , 1981, 293-303.

20. Proctor, E.S., Proc. 7th Symp. on NDE of Components and Materials in Aerospace Weapons Systems and Nuclear Applications, San Antonio, Texas , April 23-25, 1969, 180-187.

21. Baikie, B.L., Wagg, A.R., Whittle, M.J., and Yapp,D., "Ultrasonic Inspection of austenitic welds", J. of Brit. Nuc. Energy Soc., 3 , 1976 , 257-261.

22. Tomlinson, J.R., Wagg, A.R., and Whittle, M.J., "Ultrasonic inspection of austenitic welds", Brit.J. NDT , 22 , 3 , 1980 , 119-127.

23. Kupperman, D.S., Reimann, K.J., and Fiore, N.F., "Role of microstructure in ultrasonic inspectability of austenitic stainless steel welds", Mat. Eval., 36, 4 , 1978 , 70-74.

24. Bradfield, G., "The physical examination of metals", 2nd Edition, Arnold, London, 1960, pp.559.

25. Musgrave, M.J.P., "Calculations relating to the propagation of elastic waves in anisotropic media", NPL Report BP R7 / 61, 1961.

26. Winternheimer, C.G., and McCurdy, A. K., "Phenon-focusing and phenon-conduction in orthorombic and tetragonal crystals in the boundary-scattering regime", Phys. Rev. B , 18 , 12 , 1978.

27. Ratcliffe, B.J., "A review of the techniques using ultrasonic waves for the measurement of stress within materials", Brit. J. NDT, 11 , 5 , 1969, 48-58.

28. Firestone, F.A., and Frederick, J.R., J. Acoust. Soc. Amer., 18 , 1946 , pp.200.

29. Kupperman, D.S., and Reimann, K.J., "Effect of shear wave polarization on defect detection in stainless steel weld metal", Ultrasonics, 16, 1, 1978, 21-27.

30. Silk, M.G., "Inspecting austenitic welds", Research Techniques in NDT, Vol. 4, Academic Press, 1980, pp. 393-449.

31. Wilson, R., Sheet Metal Ind., 30, 1953, pp.146.

32. Juva, A., and Lenkkeri,J., "The effects of anisotropy on the propagation of ultrasonic waves in austenitic stainless steel", OECD CSNI Specialists meeting on Reliability of Ultrasonic Inspection of austenitic stainless steel components, Brussels, Belgium, May 29-30, 1980.

33. Gray, B.S., Hudgell, R.J., and Seed, H., "Longitudinal wave inspection of austenitic weldments", OECD CSNI Specialists meeting on reliability of ultrasonic inspection of austenitic stainless steel components, Brussels, Belgium, May 29-30, 1980.

34. Herberg,G., Müller, W., and Ganglbauer, O., "Preliminary results for practical ultrasonic testing of austenitic steel welds", NDT Int., 9, 5, 1976, 239-241.

35. Neumann, E., Wustenberg, H., Nabel, E., Leisner, W., "The ultrasonic testing of welds in austenitic steels", Int. Conf. on Quality Control and NDT in welding, London, The Welding Inst., Nov. 1974.

36. Edelman, X., "The practical application of ultrasonic testing of austenitic welded joints", Mat. Eval., 37, 9, 1979, 47-51.

37. Hudgell, R.J., and Seed, H., "Ultrasonic longitudinal examination of austenitic welds", Brit. J. NDT, 22, 3, 1980, 78-85.

38. Lack, B.J., "Ultrasonic testing of welds in high alloy steels and austenitic steels", NEI John Thompson Ltd., Private communication.

39. Papadakis, E.P., "Revised grain-scattering formulas and tables", J. Acoust. Soc. Amer., 37, 1965, 703-717.

40. Holmes, E., "Ultrasonic behaviour in austenitic stainless steel", App. Mat. Res., July 1963, 181-184.

41. Caussin, P. and Cermac, J., "Performances of the ultrasonic examination of austenitic steel components", Periodic inspection of pressurized components, I. Mech. E. Conference Publications, 1979-4, 207-218.

42. Holmes, E., and Beasley, D., "The influence of microstructure in the ultrasonic examination of stainless steel welds", J. of Iron and Steel Inst. April 1962.

43. Whittle, M.J., "Advances in ultrasonic flaw detection", CEGB Research, Nov. 1979, pp. 33-44.

44. Rose, J.L., and Singh, G.P., "A pattern recognition reflector classification feasibility study in ultrasonic inspection of stainless steel pipe welds", Brit. J. NDT, 21, 6, 1979, 308-311.

45. Yoneyama, H., Shibata, S., Kishigami, M., "Ultrasonic testing of austenitic stainless steel welds-False indications and the cause of their occurence", NDT Int., 11, 1, 1978, 3-8.

46. Pelseneer, J.P., and Louis, G., "Ultrasonic testing of austenitic steel castings and welds", Brit. J. NDT, 16, 4, 1974, 107-113.

47. Juva, A., and Haarvisto, M., "On the effects of microstructure on the attenuation of ultrasonic waves in austenitic stainless steels", Brit. J. NDT, 19, 6, 1977, 293-297.

48. Davies, G.J., "Solidification and casting", Applied Science Publishers, London, 1973, Chapter 6.

49. Morchan, B.A., and Kushnirenko, B.N., Automatic Welding (USSR), Vol. 13, 1960, pp. 89.

50. Autonets, O.P., and Psaras, G.G., ibid, Vol. 19, 1968, pp. 54.

51. Matreev, Y.M., Weld. Prod. (USSR), Vol. 15, 1968.

52. Gapchenko, M.N., Aut. Weld. (USSR), 23, 36, 1970.

53. Lucey, J.A., and Boughton,P., Brit. Weld. J., 1965, 12, pp. 159.

54. Needham, J.C., and Carter, A.W., ibid, 12, 1965, pp. 229.

55. Garland, J.G., Metal Construction, 1974, 6, pp. 121.

56. "Welding in the 1980's", Eng. Mat. and Design, Oct. 1980.

57. De Altamer, A., "Submerged arc narrow gap welding", Met. Constr., 12, 10, 1980, 520-523.

58. Grebennicov, V.V., and Sotinchenko, A.L., "Influence of ultrasonic frequency and focussing on the conditions for flaw detection in austenitic welds", Welding Production, 18, 12, 1971.

59. Seiger, H., and Engl, G., "Ultrasonic inspection of spherically shaped perforated areas of light water pressure vessels", NDT Int., 10, 6, 1977, 293-296.

60. Neumann, E, et al, "Development and improvement of ultrasonic testing techniques for austenitic nuclear components", BAM Federal Institute for Materials Testing, Report.

61. Juva, A. and Lieto, J., "The ultrasonic examination of thin austenitic stainless steel butt welds", Brit. J. NDT, 22, 4, 1980, 191-195.

62. Reinhart, E.R., "Program to improve nuclear code inspection methods", Mat. Eval., 36, 6, 1978, 36-42.

63. Abrahams, C.J., "Tube-to-tube butt-welds in thin austenitic steel, their ultrasonic examination using assisted hand scanning methods", Brit. J. NDT, 14, 3, 1972, 66-72.

64. Edelmann, X., "Application of ultrasonic testing techniques on austenitic welds for fabrication and in-service inspection", NDT Int., 14, 3, 1981, 125-133.

65. Krautkrämer J., and Krautkrämer, H., "Ultrasonic Testing of Materials", 2nd Edition, Springer-Verlag, N.Y., 1977.

66. Ermolov, N., and Pilin, B.P., "Possible ways of improving the sensitivity of ultrasonic inspection of parts with a large-grain structure", Translated from Defektoskopiya, No. 1, 1969, pp. 53-57.

67. Saitoh, T., and Takahashi, S., "Measuring the depth of cracks in austenitic stainless steel overlays by ultrasonic testing", Int. Advances in NDT, Vol. 7, 1981, pp. 375-394.

68. RTD commercial literature booklet, "Probes for inspection of austenitic material, mainly welds".

69. Krautkrämer GmbH, commercial literature booklet, "Probes for austenite".

70. Ermolov I.N., and Pilin, B.P., "Ultrasonic inspection of materials with coarse grain anisotropic structures", NDT Int., 9, 6, 1976, 275-280.

71. Bradfield, G., "Ultrasonic flaw detection in metals", The Physical Examination of Metals, 2nd Ed., 1960, Edward-Arnold, pp. 605-693.

72. Sproule, D.O., "Ultrasonic testing of welds", Brit. Weld. H., 6, 10, 1959, 470-479.

73. Mech, S.J., and Michaels, T.E., "Development of Ultrasonic Examination Methods for Austenitic Stainless Steel Weld Inspection", Mat. Eval., 35, 7, pp. 81-88, July 1977.

74. Kay, L., Whipp, E., and Bishop, M.J., Brit. J. Inst. Radio Engr., 23, 5, 1962, 373-380.

75. U.S. Patent No. 3 309 914, 1967.

76. Crostack, H.A., Deutsch, V., and Vogt, M., "Improvements in ultrasonic testing by means of narrow-band transmitter pulses of continuously variable frequency", Brit. J. NDT, 22, 4, 1980, 166-171.

77. Lidington, B.H., Silk, M.G., Montgomery, P., Hammond, G.C., "Ultrasonic measurement of the depth of fatigue cracks", Brit. J. NDT, 18, 1976, pp. 165.

78. Silk, M.G., and Lidington, B.H., "Defect sizing using an ultrasonic time delay approach", Brit. J. NDT, 17, 2, 1975.

79. Coffey, J.M., "Quantitative assessment of the reliability of ultrasonics for detecting and measuring defects in thick section welds", I. Mech. E. Conf. 1978, Tolerance of flaws in pressurized components.

80. Aldridge, E.E., "Ultrasonic holography and nondestructive testing", Materials Research and standards, 12, 12, 1972, 13-22.

81. Harper, H., "Improved displays for ultrasonic testing", CEGB Digest, Nov. 1974.

82. Bottcher, B., Schultz, E., and Wustenburgh, H., "A new method for crack depth determination in ultrasonic material testing", Proc. 7th World Conf. on NDT, Warsaw, 1973.

83. Silk, M.G., "Sizing crack-like-defects by ultrasonic means", Research techniques in NDT, Vol. 3, 1978, pp. 58.

84. Mucciardi, A.N., "ALN approach to defect characterisation", Review of quantitative NDE Rockwell Int. January 1976.

85. Orr, E.C., et al, "Application of non-linear signal processing to pipe and nozzle inspection", EPRI NP 964 project 1125 Interim report, January 1979.

86. Shankar, R., et al, "Feasibility of using ALN for eddy current signal analysis, EPRI NP_723, March 1978.

87. "Size Measurement and Characterisation of Weld Defects by Ultrasonic Testing", National Seminar, Coventry, 17th March 1981, The Welding Institute.

88. Nielsen, N., "P-scan system for ultrasonic weld inspection", Brit. J. NDT, 23, 2, 1981, 63-69.

89. Krautkrämer, J., "Interferometer Accessory", Gesellschaft für Electrophysic, Cologne, January 1961.

90. Hatherley, M., and Hutchinson, W.B., "An introduction to textures in metals", The Institute of Metallurgists Monograph, No.5, 1979.

91. Tchorzewski, R.M., and Hutchinson, W.B., "Anisotropy of fracture toughness in textured Titanium 6 Al-4V Alloy", Metallurgical Transactions, Vol. 9, 1978, 1113-1123.

92. Lloyd, G. E., and Hall, M.G., "Application of Scanning Electron Microscopy to the study of deformed rocks" , Centre for Materials Science, University of Birmingham, Internal Report.

93. Stott, D.E., Wise, M.L.H., Hutchinson W.B., "A distortion-free map for use with Electron Channelling Patterns", J. of Microscopy, Vol. 105, 3, 1975, 305-307.

94. Van Essen, C.G., Schulson, E.M., and Donaghay, R.H., "Electron Channelling Patterns from small (10μm) Selected Areas in the Scanning Electron Microscope", Nature, 225, pp. 847.

95. Joy, D.C., Booker, G.R., and Fearon, E.O., "Quantitative crystallographic orientation of microcrystals present in solid specimens using (SEM), ibid, 1971, pp. 497.

96. Davies, G.J., and Garland, J.G., "Solidification structures and properties of fusion welds", Int. Metallurgical Reviews, Vol. 20, No. 196, 1975.

97. Silk, M.G., "The propagation of ultrasound in austenitic weldments", UKAEA-Harwell, Report 9391, Feb. 1979.

98. Gillan, M.T., "Ultrasonic wave propagation in austenitic stainless steel weld metal", UKAEA-Harwell, Report TP 839, May 1980.

99. Adler, L., Cook, K.V., and Simpson, W.A., "Ultrasonic frequency analysis", Research Techniques in NDT, Vol. 3, Academic Press, London, 1977.

100. Bell, J.F.W.,"A solid acoustic thermometer", Ultrasonics, 6, 1968, 11-14.

101. Sharp, J.C.K., " A theoretical and experimental investigation into the spectra of selected resonators", Ph.D. thesis, University of Aston, May 1974.

102. Bell, J.F.W., and Sharp, J.C.K., "The precision measurement of the elastic constants of isotropic solids over wide temperature ranges", Rev. Int. Htes. Temp. et Refract., Vol. 12, 1975, 40-43.

103. Bell, J.F.W., Chen, J.Y.F., and Chaplain, K.R., "Ultrasonic characterisation of refractories at high temperatures", NDT Int., 13, 6, 301-304.

104. Kapranos, P.A., Al-Helaly, M.M.H., and Whittaker, V.N., "Ultrasonic velocity measurements in 316 austenitic weldments", Brit. J. NDT, 23, 6, 1981, 288-292.

105. Al-Helaly, M.M.H., "The vibration spectra of rectangular plates", Ph.D. Thesis, University of Aston, December 1981.

106. Chaplain, K.R., "Elasticity measurement at high temperatures", Ph.D. Thesis, University of Aston, August 1979.

107. Chen, J.Y.F., Ph.D. Thesis, University of Aston, 1978.

108. Miller, G.F., and Musgrave, M.J.P., "On the propagation of elastic waves in aeolotropic media-media of cubic symmetry", Proc. Roy. Soc. A 236, 1956, pp. 352.

109. Silk, M.G., Lidington, B.H., and Hammond, "A time domain approach to crack location and sizing in austenitic welds", Brit. J. NDT, 19, 2, 1980, 55-61.

110. Juva. A., and Lenkkeri, J., "The effects of anisotropy on the propagation of ultrasonic waves in austenitic stainless steel", Technical Research Inst. of Finland, Private communication.

111. Silk. M.G., "Estimates of the magnitude of some of the basic sources of error in ultrasonic defect sizing", AERE-R 9023, 1978.

112. Wustenberg, H., Kutzner, J., and Engl, G., "Dependence of echo amplitude on defect orientation in ultrasonic examination", Proc. 8th World Conf. on NDT, Cannes, France, September 1976.

113. Haines, N.F., and Langston, D.B., "The reflection of ultrasonic pulses from surfaces", CEGB/RD/B/N4115.

114. Haines, N.F.,"Reliability of ultrasonic inspection", Int. Symp. on Applications of reliability technology to nuclear power plants, Vienna, October 1977.

115. Birchak, J.R., and Gardner, C.G., "Comparative ultrasonic response of machined slots and fatigue cracks in 7075 Aluminium", Mat. Eval., Dec. 1976, pp. 275-280.

116. Golan, S., Adler, L., Cook, K.V., Nanstead, R.K., and Bulland, T.K., "Ultrasonic diffraction technique for characterisation of fatigue cracks", J. of Non-destructive evaluation, Vol. 1, 1, 1980, 11-19.

117. Wooldridge, A.B., "The effects of compressive stress on the ultrasonic response of steel-steel interfaces and of fatigue cracks", Brit. Inst. NDT, Symp. on Improving reliability of ultrasonic inspection, London, Nov. 1978.

118. Nabel, E., and Neumann, E., "Evaluation of flaw indications by ultrasonic pulse amplitude and phase spectroscopy", 8th World Conf. on NDT, Cannes, 1976.

119. Jessop, T.J., and Mudge, P.J., "Characterisation and size measurement of weld defects in ferritic steels by ultrasonic testing, Part 1.", Welding Inst. Symp., Leeds, March 1979.

120. Silk, M.G., "Developments in Inspection and Testing of pressurized components", Applied Science Publishers.

121. Blitz, J., "Fundamentals of Ultrasonics", 2nd. Edit., Butterworths, London, 1967.

122. Ibrahim, S.I., and Whittaker, V.N., "The influence of compressive stresses and other factors on the detection of fatigue cracks using ultrasonics", Brit. J. NDT ,22, 6, 1980, 286-290.

123. DiGiacomo, G., Crisci, J.R., and Goldspiel, S., "An ultrasonic method for measuring crack depth in structural weldments", Mat. Eval.,Sept. 1970, 189-202.

124. Kapranos, P.A., and Whittaker, V.N., "False Indications in ultrasonic inspection of austenitic stainless steel weldments", 1982, to be published in Nondestructive Testing Communications.

10. APPENDICES

Appendix 1. "Publication in the British Journal of NDT, as a result of the experimental work of section 4.3"

Aston University

Pageă removed for copyright restrictions.

Appendix 2. "Derivation of equation (5), Computation of constants A_0, A_2, A_4, A_6, and A_8, Polar representations of velocity variations from experimental results and computer programme entitled 'Experimental velocity variations'".

Appendix 2.

It is possible to express any periodic function f(x) as a series of circular functions (i.e. sines and cosines). It should be noted that the circular functions are periodic and hence it is necessary for f (x) to have the same periodic property.

The Fourier Series expressing these functions is :

$$f(x) = A_o + \sum_{1}^{\infty} \left(A_n \cos \frac{n\pi x}{T} + B_n \sin \frac{n\pi x}{T}\right)$$

Considering results already published[21,22,43], it follows that the velocity is a periodic function of the angle (θ) existing between soundwave propagation direction and the axis of the columnar grains.

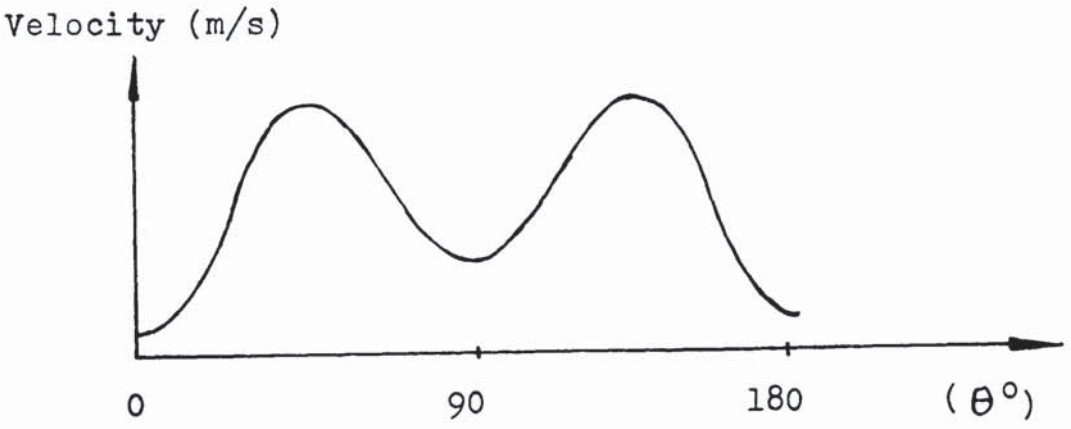

As it can be seen from the curve, there exists a symmetry about the vertical axis (0°), and also about $\Theta = 90^{\circ}$.

From these two considerations it follows :

(1) There are no sine terms in the Fourier Series representation of the function (i.e. the B terms are 0), and

(2) there are no odd harmonics in the F.S. representation (i.e. $A_1 = A_3 = A_5 = \ldots\ldots 0$),

therefore the Fourier Series representation becomes :

$$C_\theta = A_o + A_2\cos 2\theta + A_4\cos 4\theta + A_6\cos 6\theta + A_8\cos 8\theta + \ldots\ldots$$

where C_θ is the velocity of the ultrasonic waves as a function of (θ).

The values of the constants can be calculated by solving the above equation for the experimental values obtained for longitudinal velocity at 0°, 22°, 45°, 67°, and 90°:

	A_o	A_2	A_4	A_6	A_8
V_1	5891	-158	-700	58	-91.2
U_1	5508	39	-355	-106.4	-88
V_2	5824	-170	-563	75.3	-127
U_2	5560	-22	-319	-161	-9.2

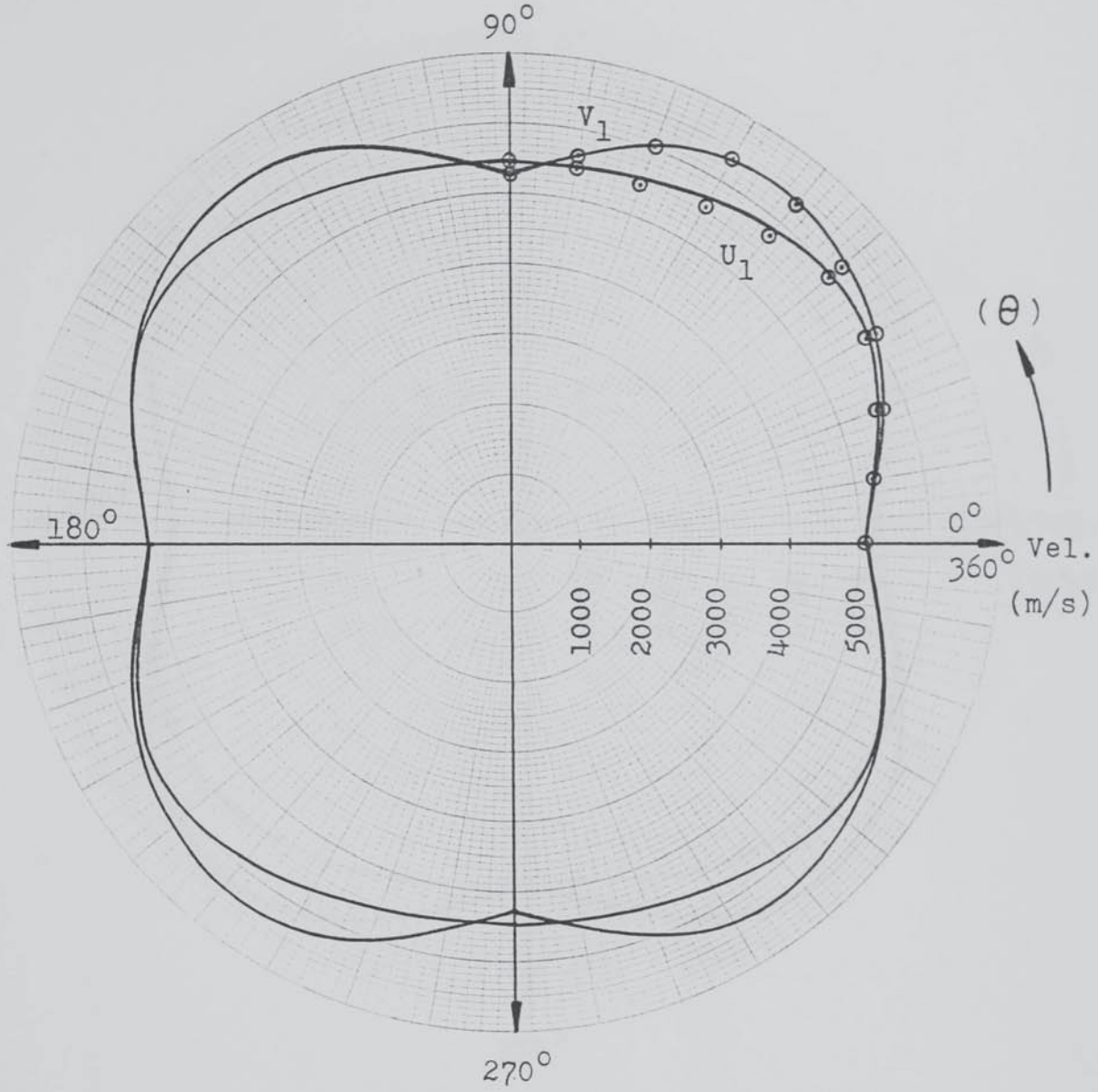

Experimental results for velocity variations in specimen V_1 and U_1, for longitudinal waves.

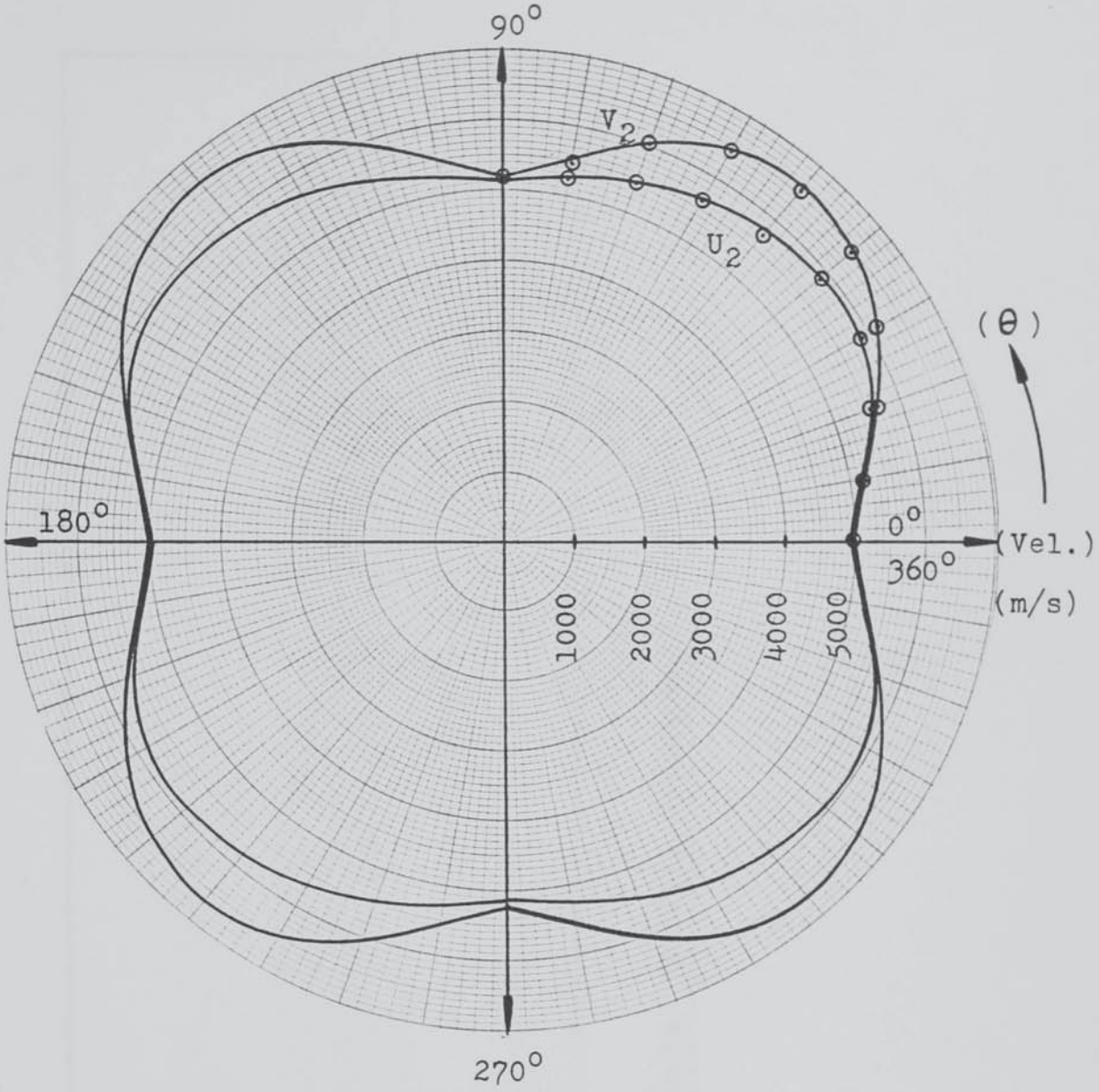

Experimental results for velocity variations in specimen V_2 and U_2, for longitudinal waves.

```
READY.

 10 PRINT "X","V1","U1","V2","U2"
 20 FOR I=0 TO 360 STEP 5
 30 X=(π*I)/180
 40 V1=5891.2-158*COS(2*X)-700*COS(4*X)+58*COS(6*X)-91.2*COS(8*X)
 50 U1=5507.9+38.9*COS(2*X)-355*COS(4*X)-106.4*COS(6*X)-37.9*COS(8*X)
 60 V2=5824.8-170.8*COS(2*X)-562.5*COS(4*X)+75.3*COS(6*X)-126.8*COS(8*X)
 70 U2=5560.4-21.7*COS(2*X)-318.75*COS(4*X)-160.8*COS(6*X)-9.15*COS(8*X)
 80 PRINT I,V1,U1,V2,U2
 90 NEXT I
 100 END
READY.
```

"Experimental Velocity Variations"

Appendix 3. "Computer programme for least squares curve fit, and resulting values of (C_o) ".

"Curve Fit "

```
READY.

 120 OPEN1,4:CMD1
 140 DIM N(20),X(100),Y(100)
 150 PRINT#1,SPC(1)"C1*X^2+C2*X+C3 FIT."
 160 PRINT#1,SPC(1)"------------------------------"
 162 PRINT#1
 164 PRINT#1
 170 PRINT#1,"X"SPC(24)"Y"
 180 PRINT#1,"------------------------------"
 182 PRINT#1
 190 READ N
 200 S1=0
 210 S2=0
 220 S3=0
 230 S4=0
 240 T0=0
 250 T1=0
 260 T2=0
 270 FOR I=1 TO N
 280 READ X(I),Y(I)
 290 PRINT#1,X(I)SPC(22)Y(I)
 300 S1=S1+X(I)
 310 S2=S2+X(I)^2
 320 S3=S3+X(I)^3
 330 S4=S4+X(I)^4
 340 T0=T0+Y(I)
 350 T1=T1+X(I)*Y(I)
 360 T2=T2+(X(I)^2)*Y(I)
 370 A=(N*S2-S1^2)
 380 B=(N*S3-S1*S2)
 390 D=(N*T1-S1*T0)
 400 F=(N*S4-S2^2)
 410 H=(N*T2-S2*T0)
 420 NEXT I
 430 C1=(D*B-A*H)/(B^2-A*F)
 440 C2=(D*H-F*D)/(B^2-A*F)
 450 C3=(T0-S1*C2-S2*C1)/N
 507 PRINT#1
 510 PRINT#1,"Y=";C1"X^2+";C2"X+";C3
 512 PRINT#1,
 514 PRINT#1,"------------------------------"
 520 DATA 7
 530 DATA 1,2
 540 DATA 2,5
 550 DATA 3,14
 560 DATA 4,29
 570 DATA 5,50
 580 DATA 6,77
 590 DATA 0,5
 600 END
READY.
```

Values of rod velocity (C_o) obtained using the Least Squares Curve Fit. for all resonators.

Angle (θ) (degrees)	Rod Velocity (m/s)			
	V_1	U_1	V_2	U_2
0	4308	4249	4784	4978
22	4806	5396	5058	4740
45	5605	5297	4719	4483
67	5299	4508	4667	4341
90	4481	4351	4802	4806

The values of the above table were obtained by substituting the experimental values for (C_ϕ) in the computer programme entitled "Curve Fit".

Appendix 4. "Computer programme used for obtaining theoretical values of velocity variations for the three propagational wave modes".

"Propagational Phase Velocities"

```
READY.

 2 OPEN 2,4
 4 CMD 2
 20 READ P
 21 READ  C1
 22 READ C2
 23 READ C3
 24 READ C4
 25 READ C5
 26 READ C6
 30 LET D=C3+C5
 35 LET M=C4-C5
 40 LET A=C1-C5
 45 PRINT "D","V1","V2","V3"
 50 FOR E=0 TO 360 STEP5
 55 LET B=(π*E)/180
 60 LET N=COS(B)
 70 LET M=SIN(B)
 80 LET D1=D*D
 90 LET H=1-N*N
 100 LET N1=N*N
 110 LET M1=M*M
 120 LET F=SQR((M1*A-N1*H)^2+4*M1*N1*D1)
 160 LET V1=SQR((M1*(C1+C5)+N1*(C4+C5)+F)/(2*P))
 170 LET V2=SQR((M1*(C1+C5)+N1*(C4+C5)-F)/(2*P))
 180 LET V3=SQR((2*M1*C6+N1*C5)/P)
 220 PRINT E,V1,V2,V3
 240 NEXT E
 250 DATA 7990,26.86E+10,10.93E+10,17.82E+10
 260 DATA 19.89E+10,14.85E+10,7.96E+10
 270 PRINT"V1"
 280 END
READY.
```

Appendix 5. "Computer programme used for obtaining the amount of skewing in austenitic weld metal for the three wavemodes".

"Skewing for the three wavemodes"

```
READY.

 2 OPEN 2,4
 4 CMD 2
 20 READ P
 21 READ C1
 22 READ C2
 23 READ C3
 24 READ C4
 25 READ C5
 26 READ C6
 30 LET D=C3+C5
 35 LET H=C4-C5
 40 LET A=C1-C5
 45 PRINT "B","L1","L2","L3"
 50 FOR E=0 TO 360 STEP5
 55 LET B=(π*E)/180
 60 LET N=COS(B)
 70 LET M=SIN(B)
 80 LET D1=2*D
 90 LET H1=H*H
 100 LET N1=N*N
 110 LET M1=M*M
 120 LET F=SQR((M1*A-N1*H)^2+4*M1*N1*D1)
 130 G=((A-H)*(A+N1*(H-A))-(A*H-D1)*(4*N1-2))
 140 I=SQR((A+N1*(H-A))^2-4*N1*(1-N1)*(A*H-D1))
 150 J=G/I
 160 LET V1=SQR((M1*(C1+C5)+N1*(C4+C5)+F)/(2*P))
 170 LET V2=SQR((M1*(C1+C5)+N1*(C4+C5)-F)/(2*P))
 180 LET V3=SQR((2*M1*C6+N1*C5)/F)
 185 L1=ATN(((M*N)/(2*P*V1^2))*(A-H+J))
 190 L2=ATN(((M*N)/(2*P*V2^2))*(A-H-J))
 195 L3=ATN(((M*N)/(P*V3^2))*(C6-C5))
 200 L1=((L1*180)/π)
 205 L2=((L2*180)/π)
 210 L3=((L3*180)/π)
 220 PRINT E,L1,L2,L3
 240 NEXT E
 250 DATA 7990,26.86E+10,10.93E+10,17.82E+10
 260 DATA 19.89E+10,14.85E+10,7.96E+10
 270 PRINT"V1"
 280 END
READY.
```

Appendix 6. "Computer programmes used for obtaining estimates of Group Velocities, and the magnitude of the angle existing between them and Phase Velocities".

"Propagational Group Velocities"

```
 2 OPEN 2,4
 4 CMD 2
 20 READ P
 21 READ C1
 22 READ C2
 23 READ C3
 24 READ C4
 25 READ C5
 26 READ C6
 30 LET D=C3-C5
 35 LET M=C4-C5
 40 LET A=C1-C5
 45 PRINT : "D","S1","S2","S3"
 50 FOR E=0 TO 360 STEP5
 55 LET D=(PI*E)/180
 60 LET N=COS(D)
 70 LET M=SIN(D)
 80 LET D1=D*D
 90 LET H=N*N
 100 LET N1=N*N
 110 LET M1=M*M
 120 LET F=SQR((M1*A-N1*H)^2+4*M1*N1*D1)
 130 B=((N1-M1)*(A+N1*(H-A))-(A*H-D1)*(4*N1-2))
 140 I=SQR((A-N1*(H-A))^2-4*N1*(1-N1)*(A*H-D1))
 150 J=B/I
 160 LET V1=SQR((M1*(C1-C5)+N1*(C4+C5)+F)/(2*P))
 170 LET V2=SQR((M1*(C1+C5)+N1*(C4+C5)-F)/(2*P))
 180 LET V3=SQR((2*M1*C6+N1*C5)/P)
 185 L1=ATN((M*N)/(2*P*V1^2))*(A-H+J))
 190 L2=ATN((M*N)/(2*P*V2^2))*(A-H-J))
 195 L3=ATN((M*N)/(P*V3^2))*(C6-C5))
 200 S1=(V1/COS(L1))
 205 S2=(V2/COS(L2))
 210 S3=(V3/COS(L3))
 220 PRINT E,S1,S2,S3
 240 NEXT E
 250 DATA 7900,26.86E+10,10.93E+10,17.82E+10
 260 DATA 19.89E+10,14.85E+10,7.96E+10
 270 PRINT"DY"
 280 END
READY.
```

"Angle between Phase and Group Velocities"

```
2 OPEN 2,4
4 CMD 2
20 READ P
21 READ  C1
22 READ C2
23 READ C3
24 READ C4
25 READ C5
26 READ C6
30 LET D=C3-C5
35 LET H=C4-C5
40 LET A=C1-C5
45 PRINT "B","K1","K2","K3"
50 FOR E=0 TO 360 STEP5
55 LET B=(π*E)/180
60 LET N=COS(B)
70 LET M=SIN(B)
80 LET D1=D*D
90 LET H1=H*H
100 LET N1=N*N
110 LET M1=M*M
120 LET F=SQR((M1*A-N1*H)^2+4*M1*N1*D1)
130 G=((A-D)*(A+N1*(H-A))-(A*H-D1)*(4*N1-2))
140 I=SQR((A+N1*(H-A))^2-4*N1*(1-N1)*(A*H-D1))
150 J=G/I
160 LET V1=SQR((M1*(C1+C5)+N1*(C4+C5)+F)/(2*P))
170 LET V2=SQR((M1*(C1+C5)+N1*(C4+C5)-F)/(2*P))
180 LET V3=SQR((2*M1*C6+N1*C5)/P)
185 L1=ATN(((M*N)/(2*P*V1^2))*(A-H+J))
190 L2=ATN(((M*N)/(2*P*V2^2))*(A-H-J))
195 L3=ATN(((M*N)/(P*V3^2))*(C6-C5))
200 L1=((L1*180)/π)
205 L2=((L2*180)/π)
210 L3=((L3*180)/π)
211 K1=E+L1
212 K2=E+L2
213 K3=E+L3
220 PRINT E,K1,K2,K3
240 NEXT E
250 DATA 7990,26.86E+10,10.93E+10,17.62E+10
260 DATA 19.89E+10,14.85E+10,7.96E+10
270 PRINT"V1"
280 END
READY.
```

Appendix 7. " Velocity variations for the three propagational modes in anisotropic 316 weld metal in polar form "

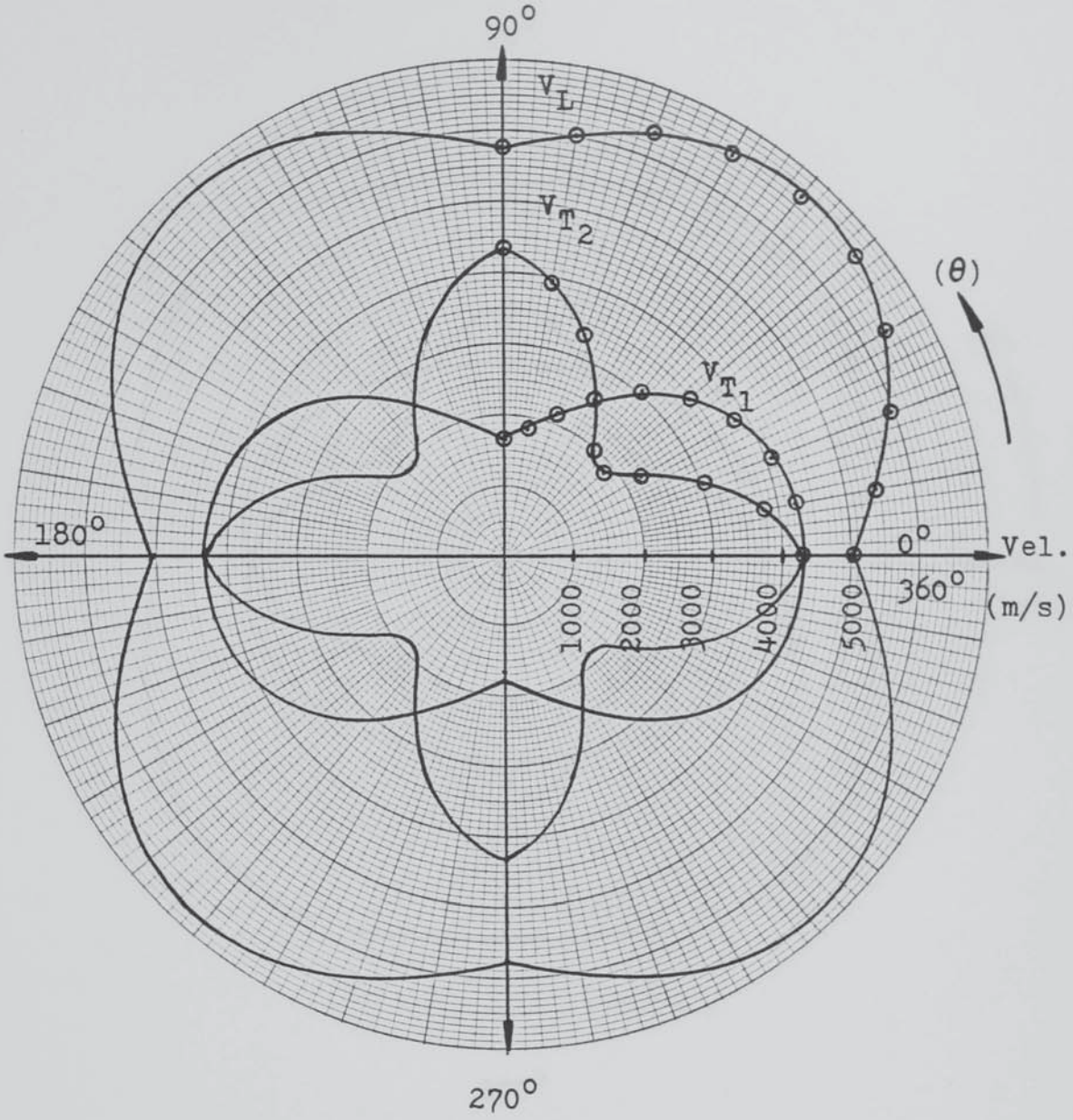

Computed velocity variations for all three propagational waves, using the V_1 elastic constants of Table 4.10.

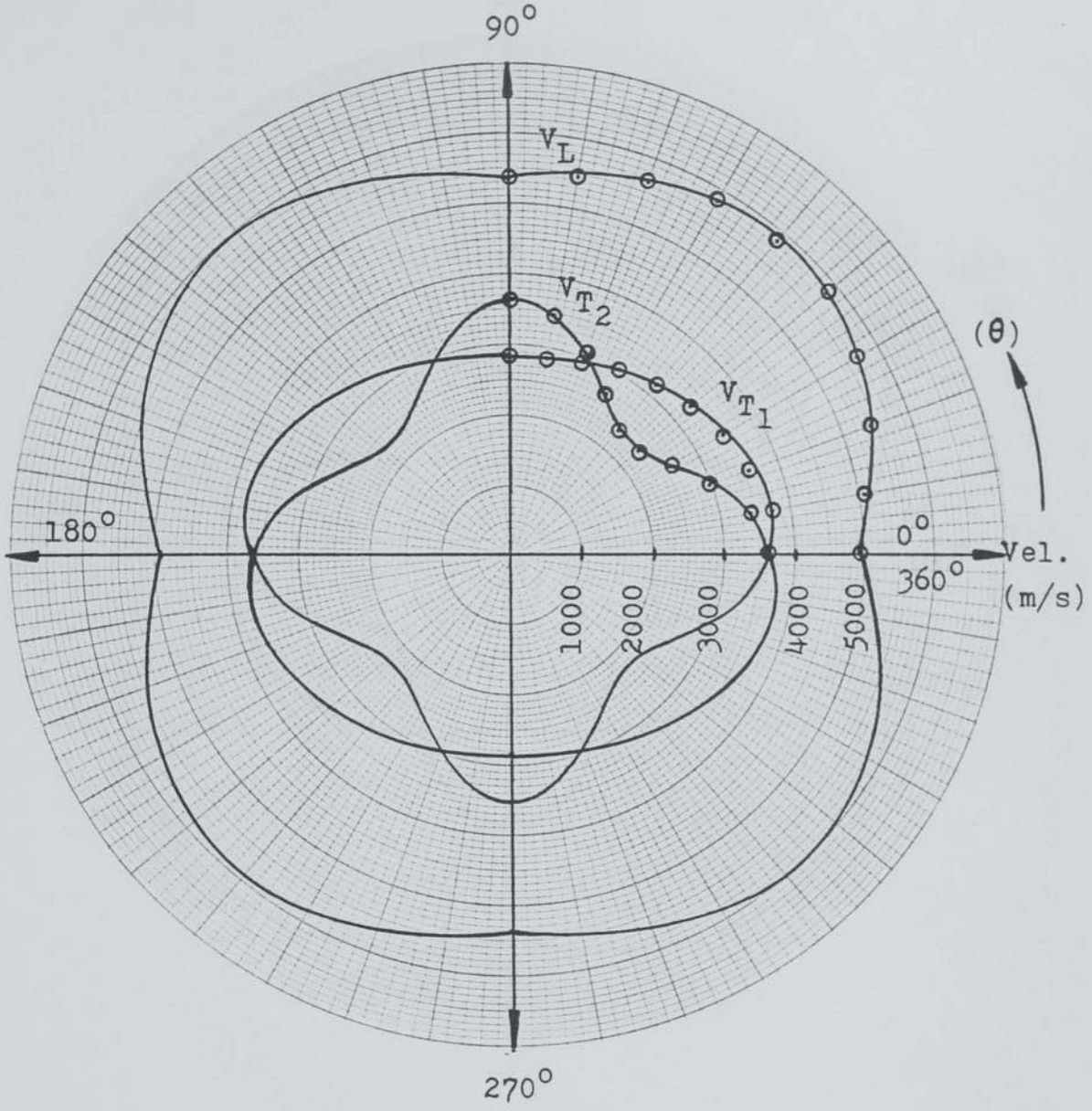

Computed velocity variations for all three propagational waves, using the U_1 elastic constants of Table 4.10.

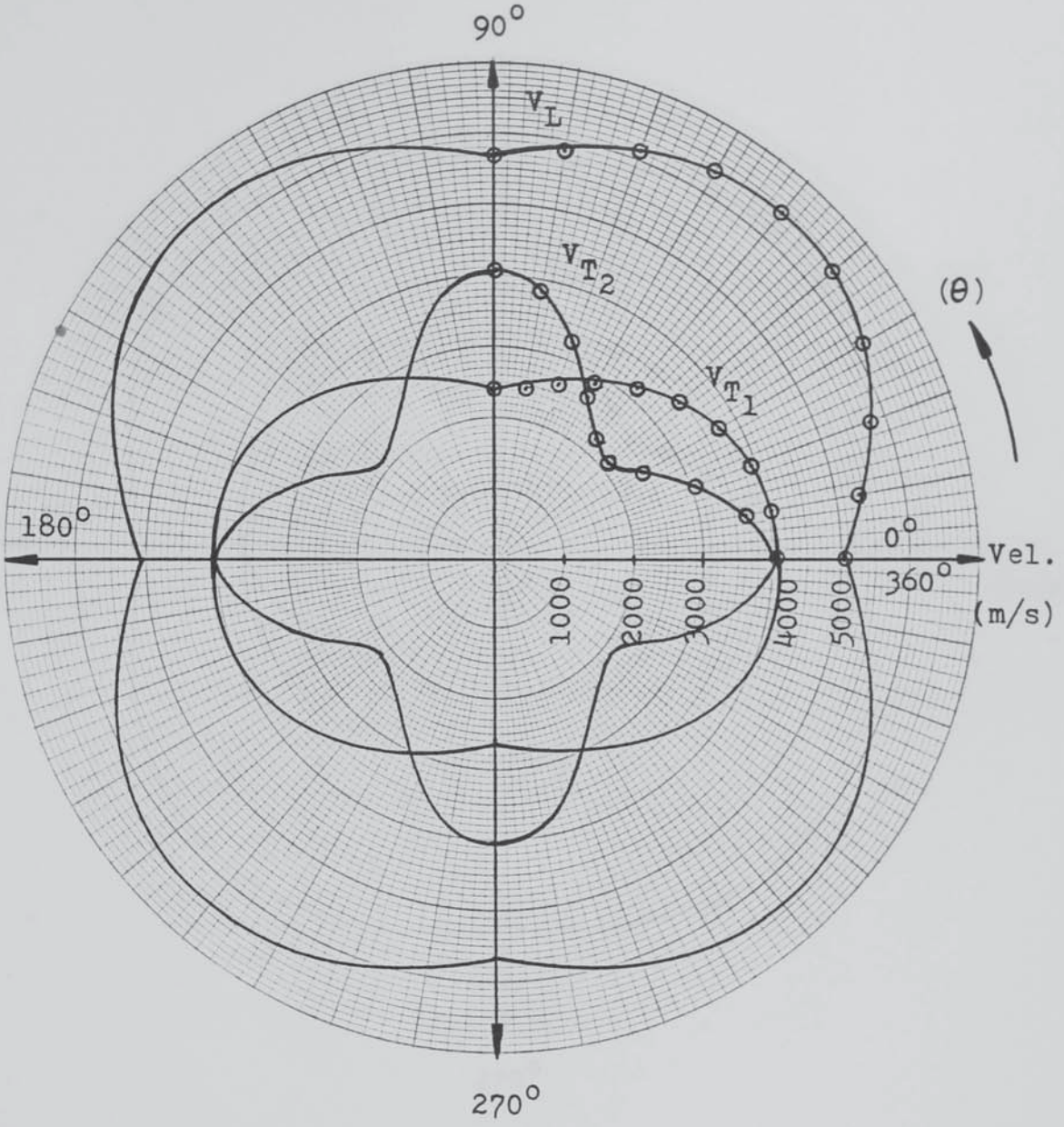

Computed velocity variations for all three propagational waves, using the V_2 elastic constants of Table 4.10.

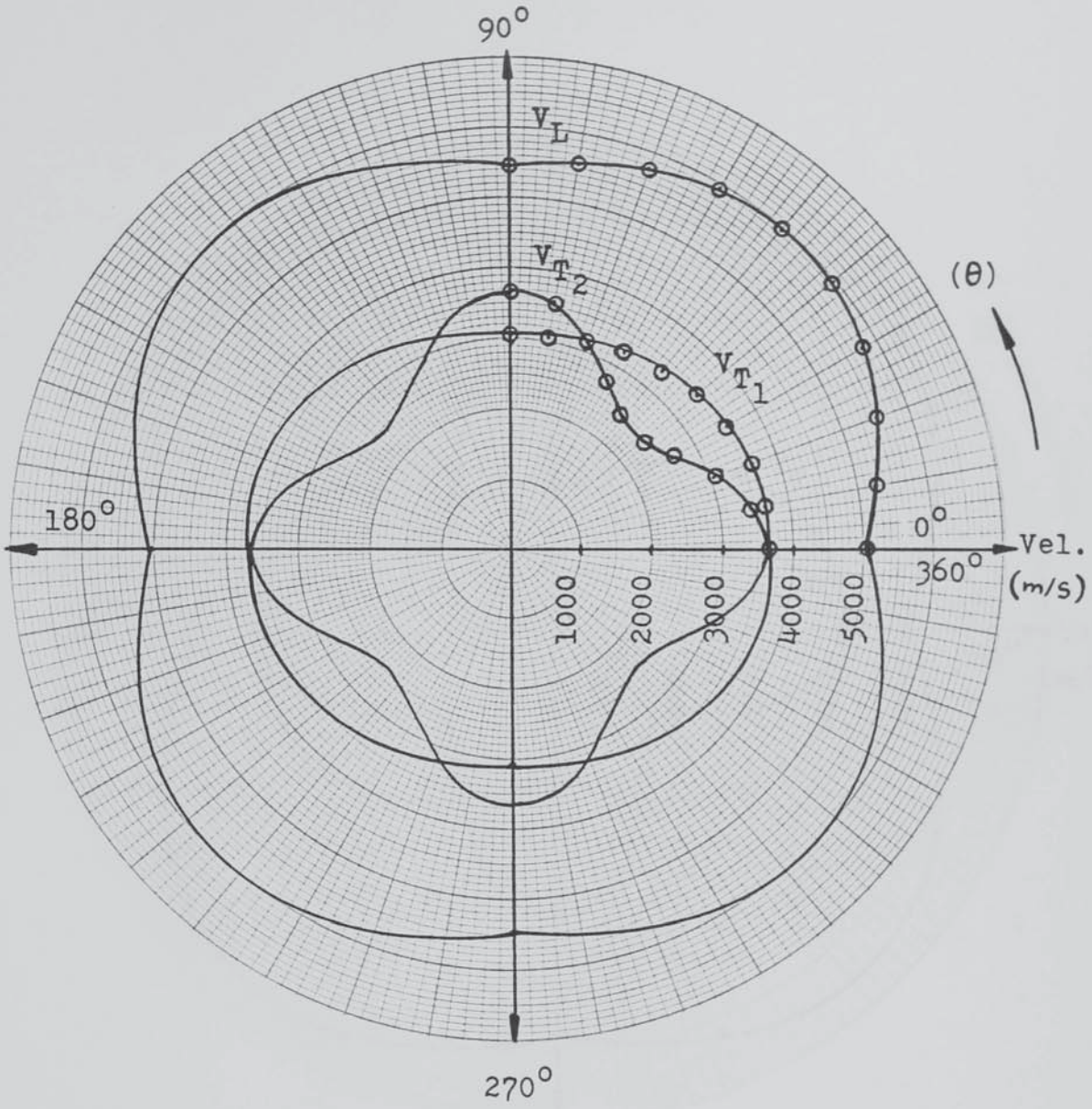

Computed velocity variations for all three propagational waves, using the U_2 elastic constants of Table 4.10.

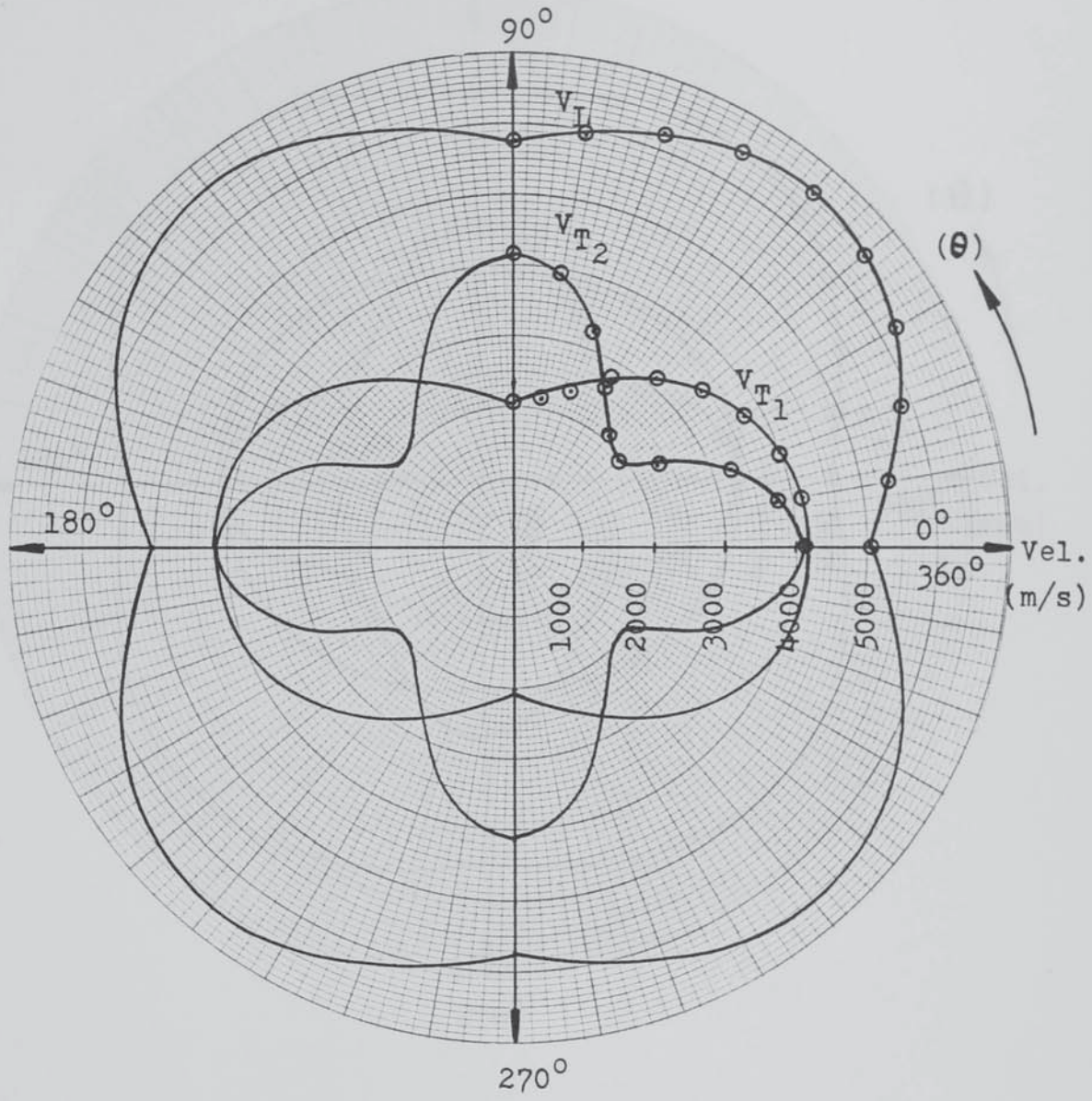

Computed values of velocity variations for all three propagational waves, using the V_1 and V_2 average elastic constants of Table 4.10.

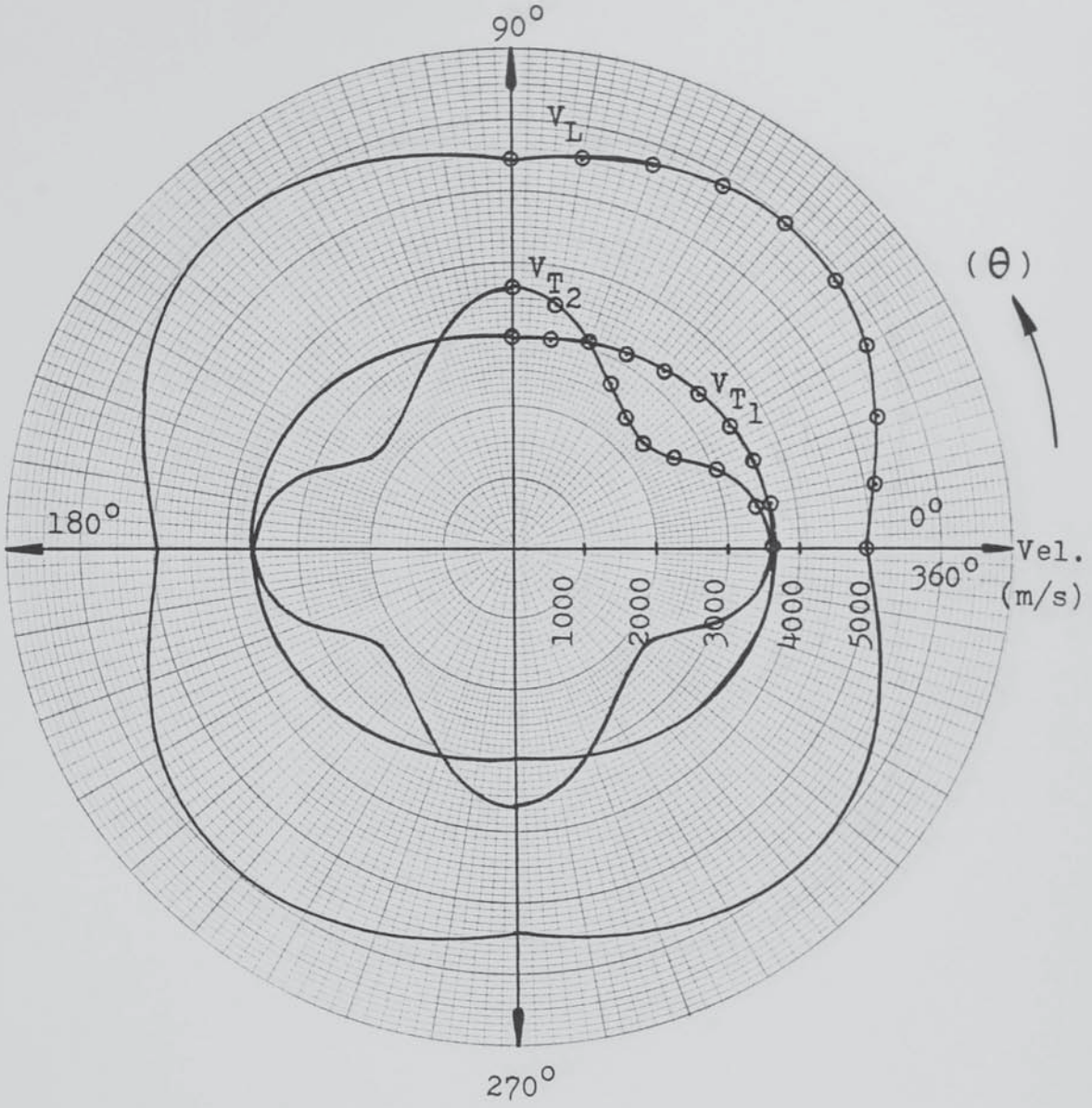

Computed values of velocity variations for all three propagational waves, using the U_1 and U_2 average elastic constants of Table 4.10.

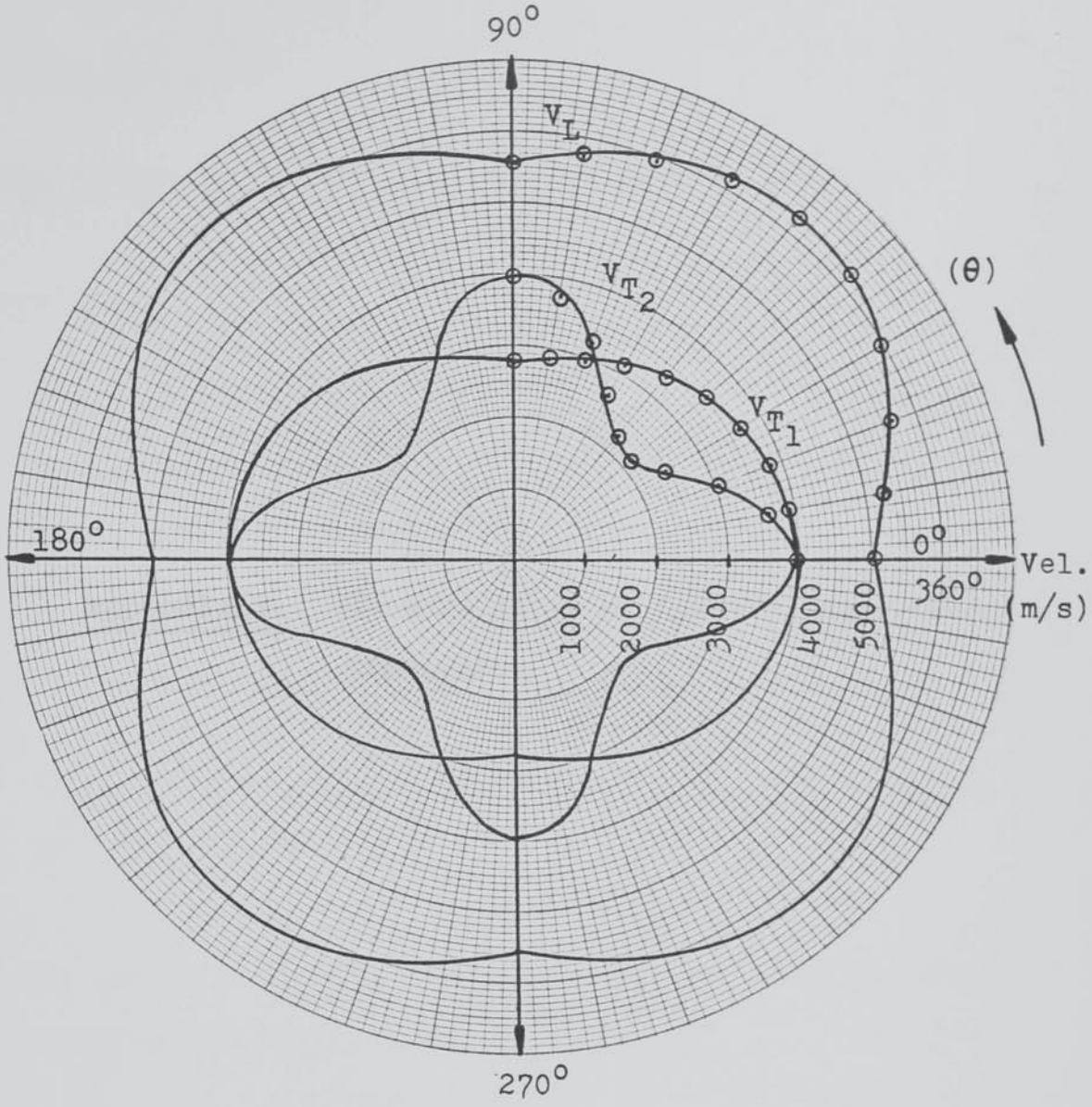

Computed values of velocity variations for all three propagational waves, using the "average" elastic constants of Table 4.10.

Appendix 8. "Determination of Elastic Compressive Stresses".

Appendix 8.

Determination of Elastic Compressive Bending Stresses

Assumptions :

1. The position of the neutral axis of the non-fatigued specimens is assumed to be the same after crack initiation and propagation at various depths.

2. The stress is assumed to be acting at the neck of the fatigue cracks and not at their tips.

3. The effect of plastic flow around the crack tips was not considered.

For the Amsler 2-ton high frequency fatigue machine, the bending stresses were calculated from :

Bending moment : $M = \frac{WL}{4}$,

Moment of Inertia : $I = \frac{bd^3}{12}$,

where : W = Load

L = Span (distance between supports)

b = Width of specimen

d = Thickness of specimen

From bending theory :

$$\frac{S}{Y} = \frac{M}{I}$$

where : S is the stress at a distance (Y) from the neutral axis.

$$\therefore \quad S = \frac{MY}{I}$$

Example

Specimen S_1

Dimensions : 20 x 35 x 300 (mm)

Span : 190 mm

Load (ton)	Load (N)	Bending Moment	Moment of Inertia	Stress (MN/m^2)
0.1	996.4	47239	23333.3	20.3
0.2	1992.8	94658	23333.3	40.6
0.3	2989.2	141987	23333.3	60.9
				etc.

Appendix 9. "Typical maximum amplitude data obtained from cracks under compressive loading".

Appendix 9.

Typical maximum echo amplitude measurements from fatigue cracks in austenitic stainless steel weldments under compressive loading.

Specimen S_1 , 45°, 60° and 70° 2 MHz probes at ½ skip.

Load (ton)	Stress (MN/m^2)	45° (dB)	60° (dB)	Stress (MN/m^2)	70° (dB)
0	0	49	41.8	0	34
0.1	20.3	49	41.8	21.3	33.8
0.2	40.6	49	41.8	42.6	34
0.3	60.9	48.5	41.5	63.9	34.3
0.4	81.2	48	40.5	85.2	34
0.5	101.5	47.8	39.8	106.5	33
0.6	121.8	47.3	38	127.8	31
0.7	142.1	46.3	36	149.1	29
0.8	162.4	46	34	170.4	27.5
0.9	182.7	45.8	33	191.7	26
1.0	203	45	32	213	25
1.1	223.3	44.8	31	234.3	24
1.2	243.6	44.5	30	255.6	23

Span = 190 mm for the 45° and 60° probes, and
= 200 mm for the 70°.

Note : The above values are obtained when scanning from one side of the crack.

Appendix 10. "Sample calculation and graphical representation on ultrasound propagation in austenitic 316 weld metal"

Using the average of longitudinal and transverse velocity values given in Table 4.5 for the 316 austenitic plate material, together with the computed velocities in the 316 austenitic weld metal for the three propagational wave modes of Table 4.11 in Snell's law, the following results were computed for three typical angle probes i.e. 45°, 60°, and 70°.

Beam to grain angle$^{\circ}$	Probe angle$^{\circ}$	Angle of refraction (r)$^{\circ}$		
		Wave mode		
		Longit.	Transv.Vert.	Tran.Hor.
45	45	46	28	48
60	60	60	46	56
70	70	66	68	58

Assuming the model of Figure 6.1, and considering an ultrasonic beam undergoing refraction according to Snell's law, the results outlined in the following page were obtained for typical conventional angle transverse wave probes.

Sample Calculation : 45° shear probe,

$$\frac{\sin 45}{\sin r} = \frac{3248}{2166} \quad \therefore \; r = 28^{\circ}$$

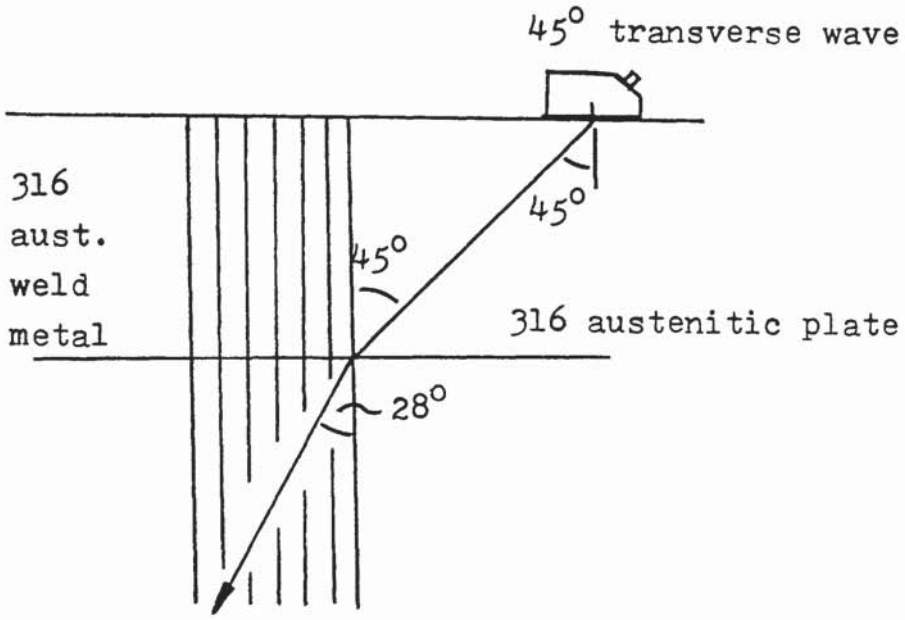
45° transverse wave probe
316
aust.
weld
metal
45°
45°
316 austenitic plate
28°

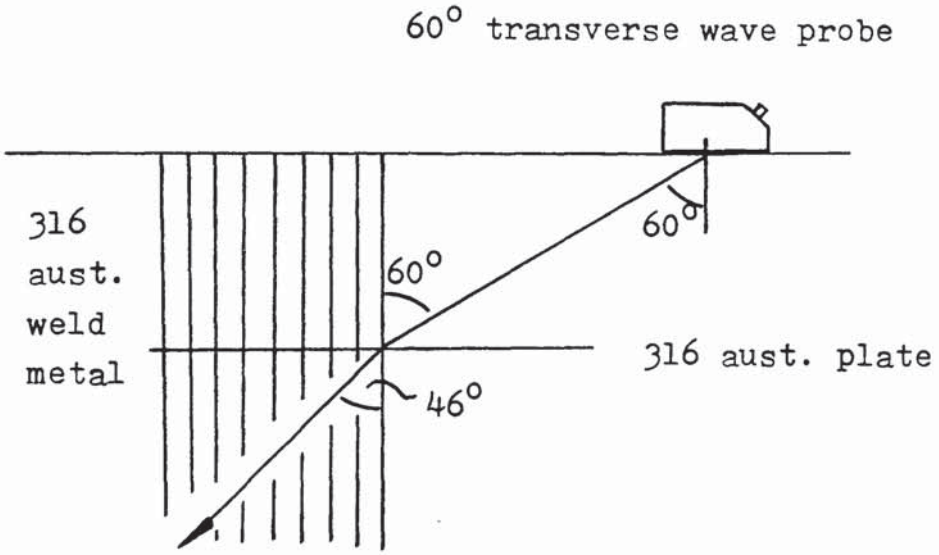
60° transverse wave probe
316
aust.
weld
metal
60°
60°
316 aust. plate
46°

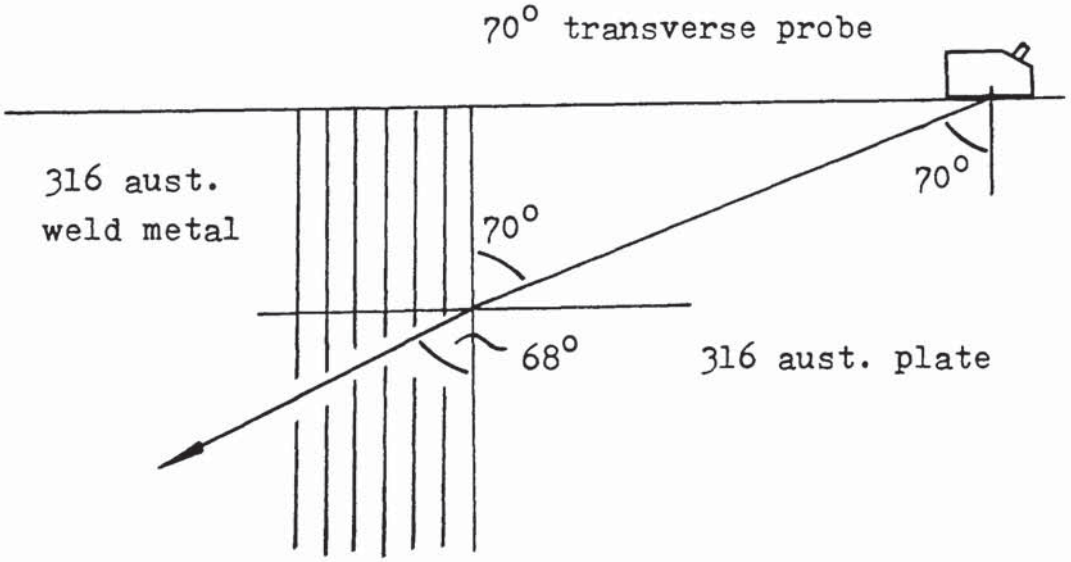
70° transverse probe
316 aust.
weld metal
70°
70°
68°
316 aust. plate

Appendix 11. "Publications in the British J. of NDT, as a result of the experimental work of section 5.2"

Aston University

Pageă removed for copyright restrictions.

Appendix 12. "Text of reference 124, to be published in Nondestructive Testing Communications"

Aston University

Pageă removed for copyright restrictions.